Investigating mechanisms of acquired resistance to AT13148, an AGC kinase inhibitor

Nathan David Breeds

January 2020

This thesis is submitted to the University of Kent for the degree of Doctor of Philosophy

Faculty of Sciences
School of Biosciences
University of Kent

Declaration

No part of this thesis has been submitted in support of an application for any degree or other qualification of the University of Kent, or any other University or Institution of learning.

Nathan David Breeds

January 2020

Abstract

The PI3K/AKT/mTOR (PAM) pathway is a major driver of cell growth, proliferation and survival, and is frequently dysregulated in cancer. AKT, a member of the AGC family of serine/threonine kinases, is a key signalling node within the PAM pathway, and as such, an attractive therapeutic target for the treatment of cancer. AT13148 is an ATP-competitive inhibitor of AKT, currently in phase 1 clinical trial, which also potently inhibits several other clinically relevant AGC kinases, such as ROCK1/2 and p70S6K. Acquired resistance to kinase inhibitors has been a barrier to their success, but resistance to AT13148 is yet to be defined. Therefore, the aim of this thesis was to investigate mechanisms of acquired AT13148 resistance, using preclinical cell line models.

Isogenic AT13148 resistant sub-clones were generated from the A2780 human ovarian carcinoma cell line, which harbours mutations in the PAM pathway. In these sub-clones, phosphorylation of S6RP (p70S6K substrate) and PRAS40 (AKT substrate) was refractory to AT13148 treatment, concurrent with increased ERK 1/2 phosphorylation, when compared to the parental A2780 cell line. Two of the resistant sub-clones were sensitised to AT13148 on exposure to the ERK inhibitor GDC-0994, with the combination of AT13148 and GDC-0994 shown to restore the inhibition of S6RP phosphorylation. This implicates ERK 1/2 as a driver of AT13148 resistance, potentially via the reactivation of the PAM pathway and suggests ERK inhibition as a strategy to overcome this resistance. A loss of DUSP6 expression, an ERK 1/2 phosphatase, was subsequently detected in AT13148 resistant sub-clones, but DUSP6 loss alone was not shown to cause a sustained increase in ERK 1/2 phosphorylation or confer AT13148 resistance, suggesting other factors are required for AT13148 resistance.

In conclusion, the results presented in this thesis identify ERK 1/2 as a driver of AT13148 resistance. This discovery has the potential to aid the ongoing clinical development of AT13148 and provide a therapeutic strategy to overcome AT13148 resistance.

Acknowledgements

Firstly, I'd like to thank the University of Kent for awarding me with a GTA scholarship and providing the resources that enabled me to conduct my PhD studies. I would also like to thank my supervisor, Professor Michelle Garrett, for placing her trust in me with this project. The support, advice and encouragement she has given me over the last four years has been instrumental in my development as a scientist and given me the firm foundations on which to build the rest of my career in science.

I am also grateful for the support of the members of the Garrett lab, past and present, especially Denis, Jasmine, Dan, Helen and Eithaar (honorary Garrett lab member). Even during the darkest times of my PhD, they managed to make the lab/office a pleasant and enjoyable environment to work in. However, a special thanks must go to Edith, our lab technician. To put it simply, the lab would not function without her, and my PhD would have been considerably more difficult without her presence. Not only has she been indispensable in the lab, but a true friend (more like family), and has always been there to offer me support with whatever was happening in my life. There are also many others within the School of Biosciences who I'd like to thank for their help and support throughout my PhD.

I would like to say a huge thank you to my wonderful and loving family, who have been a constant source of strength throughout my life, and especially during my PhD. To my mum, brother and Becca, my sister in law, I am especially thankful for the love and support that you have given me over the last year. I know that it has been a difficult time for all of us, but the submission of my PhD is just the start of what is bound to be a most cherished year for our family and a new beginning.

Finally, I'd like to dedicate this PhD thesis to my father, whom I miss dearly. The qualities that you instilled in me, and the unwavering love, support and encouragement that you provided, are the very reasons that led me to this PhD and endured me throughout. I hope I can live up to the example that you set for me and that I have made you proud.

Table of contents

List of Figures

List of Tables

Abbreviations

4E-BP	eIF4E-binding protein
ABL	abelson tyrosine-protein kinase
ADCY	adenylate cyclase
AGC	related to PKA, PKG and PKC
AKT	v-akt murine thymoma viral oncogene homolog
ALK	anaplastic lymphoma Kinase
ALK+	ALK fusion positive
ALL	acute lymphoblastic leukaemia
AMP	adenosine monophosphate
AP-1	activator protein 1
APC	adenomatous polyposis coli
APS	ammonium persulfate
ASCO	American Society of Clinical Oncology
ATP	adenosine triphosphate
BAD	Bcl-2 associated death promoter
BCA	bicinchoninic acid
BCI	2-benzylidene-3-(cyclohexylamino)-1-indanone hydrochloride
BCL-2	B-cell lymphoma 2
BCL-XL	B-cell lymphoma-extra large
BCR	breakpoint cluster region protein
BRCA1	breast cancer type 1 susceptibility protein
BRCA2	breast cancer type 2 susceptibility protein
BSA	bovine serum albumin
BSC	biological safety cabinet
cAMP	cyclic AMP
CBP	CREB binding protein
CD	common Docking
cdc25	cell Division cycle 25
CLL	chronic lymphocytic leukaemia
CREB	cAMP responsive element binding protein
CRISPR	clustered regularly interspaced short palindromic repeats
c-Src	proto-oncogene tyrosine-protein kinase Src
CST	cell signalling technology
ddH$_2$0	double distilled water
DMEM	Dulbecco's Modified Eagle Medium
DMSO	dimethyl sulfoxide
DNA	deoxyribonucleic acid
DTT	dithiothreitol
DUSP	dual-specificity phosphatase
ECL	enhanced chemiluminescence
EDTA	ethylenediamine tetra acetic acid
EGFR	epidermal growth factor receptor

eIF4E	eukaryotic initiation factor-4E
Elk-1	ETS transcription factor Elk-1
ERK	extracellular regulated kinase
ETS	E26 transformation specific
ETS-1	ETS proto-oncogene 1
ETS-2	ETS proto-oncogene 2
FBS	foetal bovine serum
FDA	U.S Food & Drug Administration
FGF	fibroblast growth factor
FGFR	fibroblast growth factor receptor
FISH	fluorescence *in situ* hybridisation
FoXO	forkhead Box O
FRS2	FGF receptor substrate 2
GAP	GTPase activating protein
GDP	guanosine diphosphate
GEF	guanine exchange factor
GIST	gastrointestinal stromal tumour
GRB2	growth factor receptor-bound protein 2
GSK3	glycogen synthase kinase 3
GTP	guanosine triphosphate
HEPES	4-(2-hydroxyethyl)-1-piperazineethanesulfonic acid
HER2	human epidermal growth factor receptor 2
HM	hydrophobic motif
HNSCC	head and neck squamous cell carcinoma
HRAS	harvey rat sarcoma viral oncogene homolog
HRP	horseradish peroxidase
ICR	Institute of Cancer Research
IEG	immediate early gene
IGF-1R	insulin like growth factor receptor 1
IRS1	insulin receptor substrate 1
KD	knockdown
KIM	kinase interaction motif
KRAS	Kirsten rat sarcoma viral oncogene homolog
LB	lysogeny broth
Lck	lymphocyte-specific protein tyrosine kinase
LIMK	LIM domain kinase
LOH	loss of heterozygosity
MAPK	mitogen activated protein kinase
MCL-1	induced myeloid cell differentiation protein
MEF	mouse embryonic fibroblast
MEK	mitogen-activated protein kinase kinase
MET	MET Proto-Oncogene, receptor tyrosine Kinase
MITF	melanocyte inducing transcription factor
MLC2	myosin regulatory light chain 2
MLCK	myosin light chain kinase

MLC-P	myosin light chain phosphatase
mTOR	mammalian target of rapamycin
mTORC1	mTOR complex 1
mTORC2	mTOR complex 2
Myc	MYC Proto-Oncogene, BHLH Transcription Factor
MYPT1	myosin phosphatase-targeting subunit 1
NDRG	N-Myc downstream regulated
NES	nuclear export sequence
NF1	neurofibromin 1
NFκB	nuclear factor-kappa B
NRAS	neuroblastoma RAS viral (v-ras) oncogene homolog
NSCLC	non-small cell lung carcinoma
NT	non-targeting siRNA
OD	optical density
ORF	open reading frame
p70S6K	p70 ribosomal S6 kinase
PAGE	polyacrylamide gel electrophoresis
PAH	polycyclic aromatic hydrocarbons
PAK	p21 activated kinase
PAM	PI3K/AKT/mTOR
PARP	poly-ADP ribose polymerase
PBS	phosphate-buffered saline
PDAC	pancreatic ductal adenocarcinoma
PDBu	phorbol 12,12-dibutyrate
PDGFR	platelet derived growth factor receptor
PDK1	phosphoinositide-dependent kinase-1
PEG	polyethylene glycol
PFS	progression free survival
PH	pleckstrin homology
ph+	Philadelphia chromosome positive
PI(3,4,5)P3	phosphatidylinositol-3,4,5-triphosphate
PI(4,5)P2	phosphatidylinositol-3,4-bisphosphate
PI3K	phosphoinositide-3-kinase
PIF	PDK1-interacting fragment
PIK3CA	phosphatidylinositol-4,5-bisphosphate 3-kinase catalytic subunit alpha
PKA	cAMP dependent protein kinase
PKC	protein kinase C
PKG	cGMP dependent protein kinase
PRAS40	proline rich substrate of AKT of 40 kDa
PTB	phosphotyrosine-binding domain
PTEN	phosphatase and tensin homolog
PTPase	protein tyrosine phosphatase
PVDF	polyvinylidene fluoride
RAF	v-raf murine sarcoma viral oncogene homolog

RAPTOR	regulatory associated protein of mTOR
RAS	rat sarcoma oncogene homolog
RAS regulated RAF-MEK-ERK pathway	MAPK pathway
Rb	retinoblastoma protein
RBD	Rho binding domain
RCC	renal cell carcinoma
RF	resistance factor
RHEB	RAS homolog enriched in brain
RNA	ribonucleic acid
ROCK	rho-associated coiled-coil containing kinase
ROS	reactive oxygen species
rpm	revolutions per minute
RSK	p90 ribosomal S6 kinase
RT	room temperature
RTK	receptor tyrosine kinase
RT-Q-PCR	reverse transcriptase quantitative polymerase chain reaction
S6RP	S6 ribosomal protein
SCLC	small cell lung carcinoma
SD	standard deviation
SDS	sodium dodecyl sulfate
SFK	Src family kinase
SGK	serum and glucocorticoid regulated kinase
SH2	Src homology-2 domain
shRNA	short hairpin RNA
siRNA	small interfering RNA
SOS	son of sevenless
SPRY	sprouty
SRB	sulforhodamine B
SS	synovial Sarcoma
TBS-T	Tris-buffered saline tween buffer
TCA	trichloroacetic acid
TCF	ternary complex factor
TE	Tris-EDTA buffer
TEMED	tetramethylethylenediamine
TKD	tyrosine kinase domain
TKI	tyrosine kinase inhibitor
TSC	tuberous sclerosis complex
TSG	tumour suppressor gene
VASP	vasodilator-stimulated phosphoprotein
VHL	von Hippel-Lindau
WHO	World Health Organisation
WT	wild type

Chapter 1

Introduction

1. Introduction

1.1. Introduction to cancer

Cancer is a major public health problem and is expected to rank as the leading cause of death and the most important barrier to increasing life expectancy in the 21st century (Bray *et al.*, 2018; Siegel *et al.*, 2019). According to the World Health Organisation (WHO) it is estimated that cancer is the 1st or 2nd leading causing of premature death (death before 70) in 91 out of 172 countries worldwide (Bray *et al.*, 2018). Furthermore, worldwide in 2018, it was estimated that there were 18.1 million new cancer cases and 9.6 million cancer deaths (Bray *et al.*, 2018). In the UK, it has been predicted that > 50% of adults under the age of 65 will be diagnosed with cancer at some point in their lifetimes (Ahmad *et al.*, 2015). Therefore, furthering our understanding of cancer; improving prevention, diagnosis and treatment, will be key to enhancing quality of life and increasing life expectancy in the 21st century.

Cancer cannot not be defined as a singular disease, but rather a collection of diseases that share a similar phenotype of uncontrolled cellular growth and proliferation, with invasion into surrounding local tissue, and in many cases, metastasis from primary sites to other organs. It is thought that normal cells become cancerous and gain the aforementioned phenotype, by the acquisition of several hallmarks of cancer, such as: sustained proliferative signalling, evading growth suppressors, resisting cell death, inducing angiogenesis and avoiding immune destruction (Hanahan and Weinberg, 2011; summarised in Figure 1.1). However, it is worth noting, that cancer cells need not acquire all these hallmarks, for example, whilst most tumours induce some form of angiogenesis, and require this for their growth, a minority of tumours grow in a purely non-angiogenic manner (Bridgeman *et al.*, 2017; Donnem *et al.*, 2018).

The process in which normal cells become cancerous, acquiring the hallmarks of cancer, is known as oncogenesis (also known as tumourigenesis or carcinogenesis). There are several theories has to how oncogenesis may occur, but the most prevalent, and widely accepted, is the somatic mutation theory (SMT), although other theories do exist such as the tissue organisation field theory of cancer, the metabolic theory of cancer and the cancer stem cell theory of cancer (Blagosklonny, 2005; Baker, 2015; Seyfried, 2015;

Tomasetti and Vogelstein, 2015; Afify and Seno, 2019). SMT states that cancer arises from a single somatic cell, from the stepwise accumulation of genetic and epigenetic alterations, which liberates cancer cells from the homeostatic mechanisms that govern normal cell proliferation (Blagosklonny, 2005). Thus, according to SMT, cancer can be described as a Darwinian process, in which oncogenesis is a succession of clonal expansions, each triggered by the chance acquisition of an enabling mutant phenotype (Hanahan and Weinberg, 2011). Inherited mutations, such as those in the *APC* and *BRCA1* genes, found in familial colorectal and breast cancer respectively, may also contribute to oncogenesis, in combination with somatic mutations (Stella *et al.*, 1992; Keisell *et al.*, 1993).
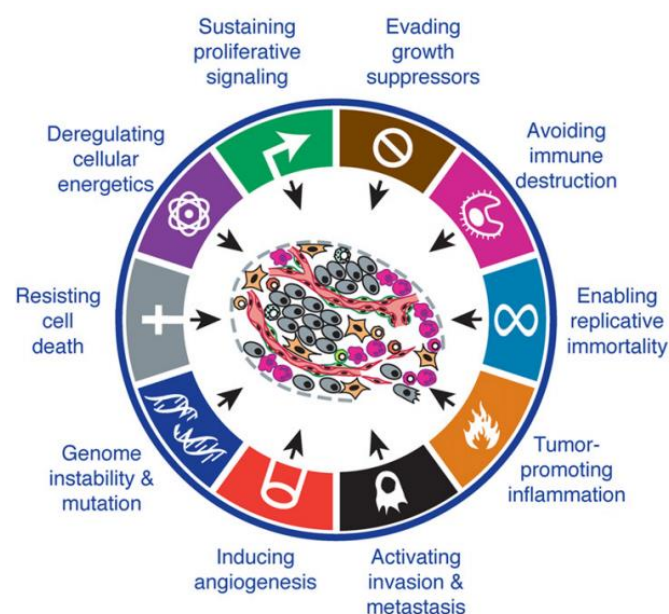
Figure 1.1: The hallmarks of cancer. Schematic diagram highlighting the "hallmarks of cancer". Taken from Hanahan and Weinberg, 2011

Due to the requirement of cancer cells to successively accumulate mutations, genomic instability (a hallmark of cancer, Figure 1.1) is seen in nearly all types of cancer, and is thought to be the main driver of the acquisition of the hallmarks of cancer (Negrini *et al.*, 2010; Hanahan and Weinberg, 2011; Seyfried, 2015). Genomic instability can exist in a number of different ways in a cell, including chromosomal instability, microsatellite DNA instability and increased frequency of base-pair mutations (Negrini *et al.*, 2010). However, normal healthy cells have a remarkably low rate of genetic mutation (approximately one mutation is introduced into the genome during each division cycle), due to the efficiency of DNA repair pathways in detecting and repairing DNA damage (Salk *et al.*, 2010; Hanahan and Weinberg, 2011). Therefore, in order for genomic

instability to arise, cancer cells often have an increased rate of DNA damage and genetic mutation (Negrini *et al.*, 2010; Salk *et al.*, 2010). This can be caused via exposure to mutagens, both internal and environmental, such as tobacco smoke, reactive oxygen species (ROS), polycyclic aromatic hydrocarbons (PAH) and ultraviolet light, which induce DNA damage (Anand *et al.*, 2008; Hanahan and Weinberg, 2011). As mentioned, there are cellular mechanisms to repair damaged DNA, but the increased mutational burden may prevent this damage from being repaired correctly, prior to cell division. Thus, an alteration to the DNA may become permanently fixed into the genome, potentially contributing to oncogenesis. Alternatively, defects within DNA repair pathways may also contribute to genomic instability, either alone or in combination with exposure to mutagens (Hanahan and Weinberg, 2011).

Mutations in cancer cells which provide a selective growth advantage, promoting oncogenesis, are known as driver mutations, whereas mutations that do not are known as passenger mutations (Pon and Marra, 2015). It is has been revealed that driver mutations are limited to subset of ~140 genes, with a typical tumour containing only two to eight "driver gene" mutations, thus the vast majority of mutations in tumours are passenger mutations (Vogelstein *et al.*, 2013). These driver gene mutations can be sub-categorised into oncogenes and tumour suppressor genes (TSGs). Oncogenes, which are referred to as proto-oncogenes in their non-mutated state, are genes which when activated by mutation confer a selective growth advantage to the cell, whereas TSGs, are genes which when inactivated by mutation confer a selective growth advantage (Vogelstein *et al.*, 2013). Oncogenes, tend be activated by focal amplifications, which increases protein expression, or by missense mutations, at a limited number of codons, which increases protein activity (Pon and Marra, 2015). For example, *RAS* is an oncogene which is activated in ~27% of cancers, often by a missense mutation (such as G12V and Q61K), which constitutively activate RAS by causing a loss of GTPase activity, leading to sustained proliferative signalling (Prior *et al.*, 2012; Hobbs *et al.*, 2016). In contrast, TSGs tend to be inactivated by focal deletions, and splice-site, nonsense and frameshift mutations across the entire length of the gene, which decrease protein expression or produce a truncated protein, but can also be inactivated by missense mutations that produce an inactive protein (Kern and Winter, 2006; Pon and Marra, 2015). For example, the TSG *TP53*, which is an important protein in sensing DNA

damage, is frequently mutated in cancer (~50% of cancers) by mutations which cause a loss of TP53 function (Rivlin *et al.*, 2011; Perri *et al.*, 2016). Additionally, it should be considered that epigenetic mechanisms may also contribute to the respective activation and inactivation of oncogenes and TSGs (Kwon and Shin, 2011). The stepwise accumulation of activated oncogenes and inactivated TSGs causes healthy somatic cells to gradually acquire the hallmarks of cancer (Figure 1.1), which leads to uncontrolled growth, invasion, metastasis, and ultimately, in many patients, death.

1.2. Oncogene addiction and targeted therapies

Despite the complexity of cancer, through the progressive accumulation of genetic and epigenetic abnormalities in genes with diverse functions, it has been observed that the removal of one or two of these abnormalities can drastically inhibit the growth of cancer cells (Weinstein and Joe, 2008). Much of the initial evidence for this came from cancer cell line models where, in many cases, the knockdown in the expression of a singular oncogene profoundly decreased cancer cell line growth. For example, Colomer and colleagues (Colomer *et al.*, 1994) demonstrated that the knockdown of the oncogene *ERBB2* caused up to a 60% decrease in the DNA synthesis and growth of *ERBB2* amplified breast cancer cell lines. A similar phenomenon was observed in pancreatic cancer; knockdown of the *KRAS* gene was shown to exclusively inhibit the growth of pancreatic cancer cell lines that expressed a mutated form of KRAS (Aoki *et al.*, 1997). Furthermore, the removal of a singular oncogene, via various techniques, was also shown to inhibit tumour growth in a number of mouse models (Weinstein and Joe, 2006).

This led to the concept of "oncogene addiction", a term created by Dr Bernard Weinstein in the early 21st century, which emphasises the apparent dependency of some cancers on one or two oncogenes for their growth and survival (Weinstein, 2000, 2002; Weinstein and Joe, 2006). The notion that cancers could be dependent on a singular oncogene was of immense therapeutic interest, as it suggested that an oncogene-targeted therapy (targeted therapy) could be used to successfully treat cancer. Furthermore, since normal healthy cells are not "oncogene addicted", it was considered that targeted therapies may have a greater therapeutic window, and much lower toxicity, when compared to traditional chemotherapeutic agents.

This therapeutic potential was realised with the small molecule tyrosine kinase inhibitor (TKI) imatinib, which was the first targeted therapy to be clinically approved (in 2001), initially used to treat Philadelphia chromosome positive (*ph+;* a 9:22 chromosomal translocation) chronic myeloid leukaemia (CML; Pagliarini, Shao and Sellers, 2015). The rationale for the use of imatinib in *ph+* CML was based upon pre-clinical data which showed that *ph+* CML cells were "addicted" to the oncogene BCR-ABL (a fusion protein in which the tyrosine kinase ABL is constitutively active), for their growth and survival (Daley *et al.*, 1990; Lugo *et al.*, 1990; Huettner *et al.*, 2000). Therefore, imatinib was developed to inhibit the tyrosine kinase activity of ABL, exploiting the oncogene addiction of *ph+* CML cells. Indeed, this proved a successful approach, as *ph+* CML patients treated with imatinib have an significant increase in survival, when compared to the previously established first-line therapy (interferon-α combined with low dose cytarabine; Henkes, van der Kuip and Aulitzky, 2008). Subsequently, many targeted therapies have now passed through clinical trials, and are currently used in the clinic to treat a number of different cancers (Pagliarini *et al.*, 2015).

In addition to imatinib, many of the targeted therapies that are used in the clinic or currently in clinical development, are also small molecule kinase inhibitors (Bhullar *et al.*, 2018). As of 2018, 37 kinase inhibitors had received FDA approval for the treatment of cancer and 150 kinase-targeted drugs were in clinical trials (Bhullar *et al.*, 2018). Kinases have been an attractive therapeutic target for cancer due the availability of ATP and co-factor binding pockets within kinases, which small molecule inhibitors can be designed to target with relative ease (Roskoski, 2016, 2019). Furthermore, many of the oncogenes that cancer cells become "addicted" to are kinases or function within signalling pathways which contain kinases (Weinstein and Joe, 2008; Gross *et al.*, 2015). The phosphoinositide 3-kinase (PI3K)/AKT/mammalian target of rapamycin (mTOR) pathway (PAM pathway), is one such pathway that is frequently implicated in oncogene addiction, and thus targeted by small molecule kinase inhibitors to treat cancer (Martini *et al.*, 2013; Fruman *et al.*, 2017; Revathidevi and Munirajan, 2019).

1.3. The PAM pathway

1.3.1. Function and regulation

As with other signalling pathways, the function of the PAM pathway is to respond to extracellular stimuli, and, through intracellular signalling, co-ordinate an adaptive cellular response to the external environment in which a cell is situated (Hassan *et al.*, 2013). Therefore, the PAM pathway is activated by range of extracellular stimuli including growth factors, integrins, hormones and neuropeptides, acting through their cognate receptors (e.g. receptor tyrosine kinases and G-protein coupled receptors ;Acosta-Martínez, 2012; Hassan *et al.*, 2013). In responding to extracellular stimuli the PAM pathway regulates a diverse array of biological functions such as cell metabolism, growth, proliferation, survival, angiogenesis and protein synthesis, many of which regulate the hallmarks of cancer (Liu, Cheng, Thomas M Roberts, *et al.*, 2009; Hanahan and Weinberg, 2011; Hassan *et al.*, 2013).

Within the context of cancer, the PAM pathway is often activated by receptor tyrosine kinases (RTKs) in response to growth factor stimulation (Liu, Cheng, Thomas M Roberts, *et al.*, 2009). Growth factors bind to extracellular regions of RTKs and stimulate RTK activation, by inducing RTK dimerization and trans-autophosphorylation of tyrosine residues within the intracellular tyrosine kinase domain (TKD) of RTKs (Du and Lovly, 2018). This facilitates the binding of class 1A phosphoinositide 3-kinases (PI3Ks) to activated RTK's, either directly or mediated via adapter proteins (e.g. insulin receptor substrate 1: IRS), inducing PI3K activation (Fruman *et al.*, 2017).

Class 1A PI3Ks are heterodimers, which consist of a p110 catalytic subunit, of which there are three isoforms (p110α, p110β, p110δ; respectively encoded by the genes *PIK3CA, PIK3CB* and *PIK3CD*) and a p85 regulatory subunit (encoded by the genes *PIK3R1, PIK3R2 and PIK3R3;* Liu *et al.*, 2009). The p85 subunit facilitates binding to phospho-tyrosine residues on activated RTKs (and adapter proteins) which is mediated by Src homology-2 (SH2) domains within p85 subunits. It is binding of p85 to activated RTKs that activates PI3K, by relieving inhibitory contacts between p85 and p110 subunits (Fruman *et al.*, 2017). Furthermore, p110 catalytic subunits all contain a RAS binding domain, which in p110α and p110δ facilitates binding to activated RAS, and in p110β,

the binding to activated RAC1/CDC42 (Gupta *et al.*, 2007; Fritsch *et al.*, 2013; Fruman *et al.*, 2017). This is thought to be required for the optimal activation of class 1A PI3Ks.

Upon activation by RTKs, PI3K is localised proximal to the plasma membrane, where it phosphorylates PI(4,5)P2 (phosphatidylinositol-3,4-bisphosphate) to PI(3,4,5)P3 (phosphatidylinositol-3,4,5-triphosphate), which acts as a 2nd messenger, facilitating the formation of membrane signalling complexes and activating multiple downstream signalling pathways (Figure 1.2; Liu, Cheng, Thomas M. Roberts, *et al.*, 2009; Fruman *et al.*, 2017). The phosphorylation of PI(4,5)P2 to PI(3,4,5)P3 can be reversed by the phosphatase and tensin homolog (PTEN), which dephosphorylates PI(3,4,5)P3 to PI(4,5)P2, thus acting as a major negative regulator of the PAM pathway and a tumour suppressor (Figure 1.2; Chen *et al.*, 2018).

Crucially, the formation of PI(3,4,5)P3 induces the activation of the serine/threonine kinase AKT (of which there are three isoforms: *AKT1, AKT2, AKT3*), a major signalling node within the PAM pathway; AKT contains a pleckstrin homology (PH) domain which facilitates binding to PI(3,4,5)P3 and recruitment to the plasma membrane (Manning and Toker, 2017). Once localised to the plasma membrane, AKT is phosphorylated by phosphoinositide-dependent kinase-1 (PDK1) and mTOR complex 2 (mTORC2), inducing the full activation of AKT (Figure 1.2). Upon activation, AKT can phosphorylate over 100 substrates, regulating much of the functional output of the PAM pathway (Manning and Cantley, 2007; Fruman *et al.*, 2017; Manning and Toker, 2017). Examples of AKT substrates include: glycogen synthase kinase 3β (GSK3β) which regulates cell cycle progression and metabolism; the Forkhead Box O (FoXO) family of transcription factors, Bcl-2 associated death promoter (BAD), and nuclear factor-kappa B (NFκB), which regulate cell survival; and the proline rich AKT substrate of 40 kDa (PRAS40) and tuberous sclerosis complex 2 (TSC2), which regulate protein synthesis (Figure 1.2; Manning and Cantley, 2007; Liu, Cheng, Thomas M Roberts, *et al.*, 2009; Fruman *et al.*, 2017; Manning and Toker, 2017).
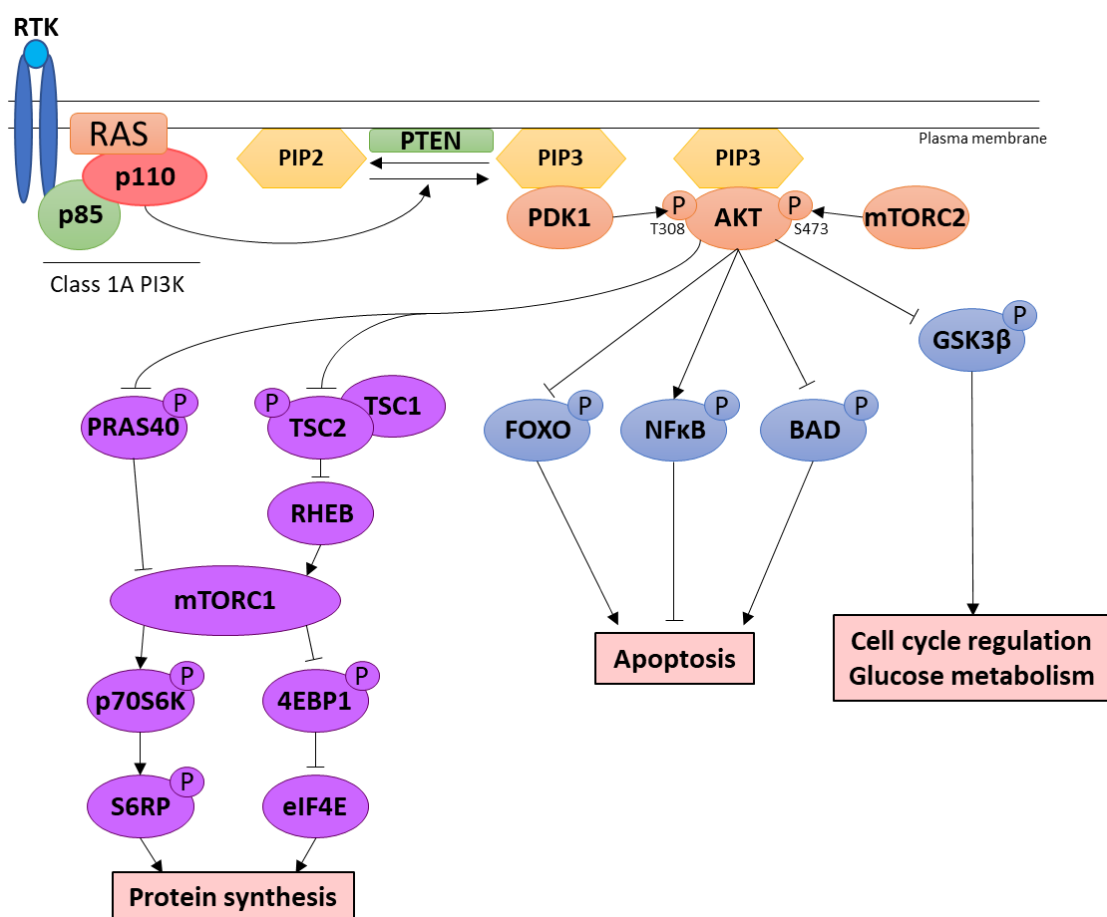
Figure 1.2: The PAM pathway. Diagram highlights some the key components of the PAM pathway and the cellular functions that they regulate. Black arrows represent positive regulation and block-headed arrows represent negative regulation. Image adapted from Liu *et al.*, 2009.

AKT also induces the activation of mTOR complex 1 (mTORC1), which is mediated by the inhibitory phosphorylation of PRAS40 and TSC2; PRAS40 functions as an inhibitory subunit of mTORC1 and TSC2 forms a complex with TSC1 (the tuberous sclerosis complex), which functions as a GTPase activating protein (GAP) of RAS homolog enriched in brain (RHEB), a positive regulator of mTORC1 activation (Figure 1.2; Inoki *et al.*, 2002, 2003; Sancak *et al.*, 2007). mTORC1 is a multi-subunit protein, in which kinase activity is derived from its mTOR serine/threonine kinase subunit (Laplante and Sabatini, 2012). Upon activation, mTORC1 phosphorylates numerous substrates that promote anabolic metabolism, such as protein synthesis, supporting cell growth and proliferation (Fruman *et al.*, 2017). The phosphorylation of p70 ribosomal S6 kinase (p70S6K) and the eukaryotic initiation factor-4E (eIF4E)-binding proteins (4E-BPs), by mTORC1, play an important role in the regulation of protein synthesis by mTORC1 (Roux and Topisirovic, 2018). Upon phosphorylation and activation by mTORC1, p70S6K can phosphorylate and regulate multiple components of the translational machinery, such as S6 ribosomal

protein (S6RP; Figure 1.2; Fenton and Gout, 2011). The phosphorylation of 4E-BPs, by mTORC1, prevents 4E-BPs binding to eIF4E, enabling eIF4E to bind to eIF4G and eIF4A, forming a cap-binding translation initiation complex (Figure 1.2; Fruman *et al.*, 2017; Roux and Topisirovic, 2018).

1.3.2. PAM pathway activation in cancer

Due to the role of the PAM pathway in regulating growth, proliferation and survival (as well as other hallmarks of cancer), mutations in this pathway are common in cancer, and it is considered to be one of the most frequently mutated pathways in cancer (Sanchez-Vega *et al.*, 2018). Indeed, it was revealed in a meta-analysis of cancer genome studies, that *PIK3CA* and *PTEN* were respectively the 2nd and 3rd most highly mutated genes in human cancers (Lawrence *et al.*, 2014). In general, these mutations act to hyperactivate the PAM pathway, liberating it from homeostatic/feedback control mechanisms, driving oncogenesis.

The majority of mutations in *PIK3CA (*which encodes the catalytic subunit p110α) occur within two mutational hotspots: E542K/E454K and H1047R, which act to cause a constitutive increase in kinase activity (Liu *et al.*, 2014). E542K/E454K mutations disrupts the inhibitory interface between p110α and p85 regulatory subunits, whereas H1047R enhances the interaction of p110α with the plasma membrane, independent of association with RAS (Liu *et al.*, 2014; Fruman *et al.*, 2017). *PIK3CA* mutations are particularly common in breast and endometrial cancers, where it is mutated in ~27% and ~24% of patients respectively (Liu, Cheng, Thomas M Roberts, *et al.*, 2009). Mutations in regulatory subunits and other catalytic subunits, which increase PI3K activity and hyperactivate the PAM pathway, also occur, albeit to a lesser extent (Liu, Cheng, Thomas M. Roberts, *et al.*, 2009; Fruman *et al.*, 2017). Alternatively, p110 catalytic subunits may be amplified in cancer, promoting hyperactivation of the PAM pathway. For example, the *PIK3CA* gene has been shown to be amplified in 69% of cervical cancer patients (Liu, Cheng, Thomas M Roberts, *et al.*, 2009).

Since PTEN functions as a major tumour suppressor of the PAM pathway, cancer-associated mutations of *PTEN* usually cause a loss of function/expression of PTEN. In many cancers there is a loss of heterozygosity (LOH) of *PTEN,* for example in prostate cancer and glioblastoma, where ~30% patients have LOH of *PTEN* (Liu, Cheng, Thomas

M Roberts, *et al.*, 2009)*.* It has also been shown that missense mutations, such as C124S and G129E mutations, can abrogate the lipid phosphatase activity of PTEN (Molinari and Frattini, 2014). However, it should be noted that PTEN expression is frequently shown to be downregulated in cancer in the absence of genetic loss or mutation, suggesting that epigenetic, transcriptional and post-transcriptional regulation of PTEN expression is involved in loss of PTEN expression, and thus hyperactivation of the PAM pathway (Carracedo *et al.*, 2011).

Hyperactivation of RTKs can also contribute to induction of PAM pathway activity in cancer, since, as discussed in section 1.3.1, RTKs are well-known regulators of the PAM pathway. A diverse array of mutations can cause RTK hyperactivation, including RTK amplification, amplification of growth factor genes (which act as ligands of RTKs) and gain-of-function missense mutations in RTKs. For example, the gene *ERBB2,* which encodes human epidermal growth factor receptor 2 (HER2), has been shown to be amplified in a number of different cancers including breast and ovarian cancer, where 15-30% of patients have an *ERBB2* amplification (Iqbal and Iqbal, 2014). In addition, the epidermal growth factor receptor (EGFR) has been shown to be mutated in ~32% of non-small cell lung carcinoma (NSCLC) patients, often by gain-of-function mutations (Prabhakar, 2015; Zhang *et al.*, 2016). However, the hyperactivation of RTKs does not exclusively cause an increase in PAM pathway activity, as RTKs are known to regulate a number of signalling pathways, such as the RAS regulated RAF-MEK-ERK pathway (the mitogen activated protein kinase [MAPK] pathway) (Kirouac *et al.*, 2016; Du and Lovly, 2018)

Mutations that cause the hyperactivation of RTKs and PI3K, or loss of PTEN function, all act to hyperactivate the PAM pathway by increasing the cellular pool of PI(3,4,5)P3, thus causing an increase in the activation of downstream effector kinases. However, mutations may also occur in downstream kinases of the PAM pathway, albeit to a lesser extent than upstream regulators (Fruman *et al.*, 2017). For example, *AKT1-3* have been shown to be mutated in approximately 3-5% of cancers, with the most common being an E17K missense mutation (Carpten *et al.*, 2007; Davies *et al.*, 2008; Yi and Lauring, 2016). This mutation occurs in the PH domain of *AKT* and causes constitutive localisation to the plasma membrane, therefore constitutive phosphorylation and activation, independent of PI3K activation (Carpten *et al.*, 2007; Davies *et al.*, 2008; Yi and Lauring,

2016). *AKT1-3* have also been shown to be amplified in cancer, particularly *AKT2*, which is amplified in ~30% of patients with head and neck squamous cell carcinoma (HNSCC; Pedrero *et al.*, 2005). In addition, gain of function missense mutations have also been reported in the mTOR gene, *MTOR*, inducing hyperactive mTORC1 and mTORC2, but these mutations are very rare (Grabiner *et al.*, 2014; Murugan *et al.*, 2019).

Whilst mutations are much rarer in *MTOR* and *AKT*, when compared to upstream PAM pathway components (e.g. *PIK3CA* mutations), mTOR and AKT are still found to be frequently hyperactivated in tumours. Increased AKT activity has been reported in ~40% of breast, ovarian, prostate and gastric cancers, and mTORC1 signalling is thought to be deregulated in ~80% of human cancers (Menon and Manning, 2008; Cargnello *et al.*, 2015; Revathidevi and Munirajan, 2019). This contrast between hyperactivation and rarity of activating mutations, is due the aforementioned alterations in upstream regulators of the PAM pathway and reflects how AKT and mTORC1 are important effector kinases of the PAM pathway. Furthermore, the strikingly high incidence of deregulated mTORC1 signalling, also reflects that mTORC1 can integrate non-PAM pathway signalling, which is also often deregulated in cancer (Laplante and Sabatini, 2012).

1.3.3. Targeting the PAM pathway

Due to the frequency by which it is mutated and hyperactivated in cancer, the PAM pathway has proven to be an attractive therapeutic target in cancer. There are currently several PAM pathway inhibitors that have been clinically approved to treat patients, and many more that are in clinical trials, most of which are kinase inhibitors (Alzahrani, 2019; Yang *et al.*, 2019). In general, PAM pathway inhibitors can be categorised into four groups: PI3K inhibitors, dual PI3K/mTOR inhibitors, mTOR inhibitors and AKT inhibitors (Alzahrani, 2019; Yang *et al.*, 2019).

Many of the initial first-generation PI3K inhibitors, such as wortmannin and LY294002, were pan-PI3K inhibitors; they showed no selectivity for individual PI3K isoforms, inhibiting all class 1 (1A and 1B) PI3Ks (Liu, Cheng, Thomas M Roberts, *et al.*, 2009)**.** Whilst these inhibitors helped gain invaluable insight into signalling mediated by PI3K, they demonstrated considerable toxicity in animals, thought to be caused by their lack

of selectivity for PI3K isoforms and other off-target effects (Marone *et al.*, 2008; Liu, Cheng, Thomas M Roberts, *et al.*, 2009). Subsequently, much of the focus, in the development of PI3K inhibitors, has been to synthesise isoform specific PI3K inhibitors. Indeed, of the four PI3K inhibitors have been clinically approved to treat cancer, two are isoform specific, with the other two shown to be dual-isoform specific (Alzahrani, 2019; André *et al.*, 2019; Yang *et al.*, 2019). For example, alpelisib, a PI3K-α specific inhibitor, has been approved to treat *PI3KCA* mutated, hormone receptor positive, HER2 negative breast cancer patients, in combination with fulvestrant, an estrogen receptor targeted therapy (André *et al.*, 2019). In these patients, it was demonstrated in a phase 3 clinical trial, that the combination of alpelisib-fulvestrant improved progression free survival (PFS) from 5.7 months to 11.0 months, when compared to fulvestrant-placebo (André *et al.*, 2019). The other clinically approved PI3K inhibitors are idelalisib: a PI3K-δ inhibitor, approved to treat chronic lymphocytic leukaemia (CLL) in combination with rituximab; copanlisib, which predominantly targets PI3K-α & δ, and is approved to treat adult patients with relapsed follicular lymphoma; and duvelisib, a dual PI3K-δ & γ inhibitor, approved to treat adult patients with relapsed CLL (Furman *et al.*, 2014; Flinn *et al.*, 2018; Alzahrani, 2019). All clinically approved PI3K inhibitors function as ATP-competitive kinase inhibitors.

Due to the importance of both mTORC1 in regulating the PAM pathway, as highlighted by 80% of cancers displaying dysregulated mTORC1 signalling, a number of mTOR inhibitors have also been developed that selectively target mTORC1. The 1st generation of mTOR inhibitors were rapamycin and its analogues (known as rapalogs), which function as allosteric inhibitors of mTORC1, by binding to FKBP12 (a subunit specific to mTORC1) and forming a ternary complex with mTOR, preventing substrate recruitment by steric hindrance (Meng and Zheng, 2015). The rapalogs, temsirolimus and everolimus, were both initially clinically approved for the treatment of metastatic renal cell carcinoma (RCC), with everolimus subsequently approved for use in HER2 negative breast cancer and pancreatic neuroendocrine tumours (Meng and Zheng, 2015; Roskoski, 2019). However, the clinical efficacy of temsirolimus and everolimus has been shown to be limited, and as such, both are usually only used as a 2nd or 3rd line therapy when treating cancer (Motzer *et al.*, 2010; Meng and Zheng, 2015). In addition, ATP-competitive mTOR inhibitors are also being developed and currently undergoing clinical

trials (Hua *et al.*, 2019). In directly inhibiting mTOR kinase activity, these inhibitors inhibit both mTORC1 and mTORC2, which is hoped will lead to greater therapeutic efficacy (Laplante and Sabatini, 2012).

Since PI3K and mTOR share a similar sequence homology in their catalytic cleft (ATP-binding site), many ATP-competitive PI3K inhibitors that were initially developed, such as PI-103, were also found to inhibit mTOR kinase (Schenone *et al.*, 2011). This opened up a new avenue in the search for effective inhibitors of the PAM pathway, as it was envisaged that the dual targeting of PI3K/mTOR, thus targeting both mTORC1 and mTORC2, might provide a greater therapeutic effect, when compared to other PAM pathway inhibitors. Indeed, several dual PI3K/mTOR inhibitors have been developed, many of which were shown in pre-clinical studies to elicit a greater apoptotic response, when compared to rapamycin/rapalogs (Chiarini *et al.*, 2015). As such, several dual PI3K/mTOR inhibitors are currently undergoing clinical phase trials including: dactolisib, apitolisib and gedatolisib (Yang *et al.*, 2019).

As discussed in section 1.3.1, AKT is major signalling node within the PAM pathway, regulating much of the pathway's functional output, such as proliferation and survival, and is therefore a major effector of the PAM pathway in driving oncogenesis. The critical function of AKT within the PAM pathway has made it an attractive therapeutic target, with several AKT inhibitors currently going through clinical trials (Revathidevi and Munirajan, 2019). One such example is MK-2206, which is an allosteric pan-AKT inhibitor, although MK2206 does display ~5-fold greater potency for AKT1 and 2, when compared to AKT3 (Hirai *et al.*, 2010). The exact mechanism in which MK-2206 functions as an allosteric AKT inhibitor is not fully understood, but it is thought that MK-2206 binding to AKT induces a closed conformation, that occludes binding sites for activating kinases (mTORC2 and PDK1) and AKT substrates (Cherrin *et al.*, 2010). MK-2206 is currently in several phase 2 clinical trials, either as a monotherapy or in combination with other cancer drugs, to treat a variety of cancers such as advanced breast cancers with PAM pathway mutations and advanced colorectal cancers (Prêtre and Wicki, 2018; Xing *et al.*, 2019; *clinicaltrials.gov*). Several other allosteric AKT inhibitors have also been developed, which inhibit AKT by disrupting the interaction between PI(3,4,5)P3 and the PH domain of AKT (Revathidevi and Munirajan, 2019). Perifosine is an allosteric inhibitor which inhibits AKT in this manner and is currently in a phase 3 clinical trial for the

treatment of advanced colorectal cancer (Revathidevi and Munirajan, 2019; *clinicaltrials.gov - identifier: NCT1097018*).

In addition, several ATP-competitive pan-AKT inhibitors have also been developed which have progressed to clinical trials (Revathidevi and Munirajan, 2019). Of these, capivasertib (AZD5363) and ipatasertib (GDC-0068) are the most advanced, with several phase 3 clinical trials currently being conducted with ipatasertib (*clinicaltrials.gov – identifier: NCT0307228, NCT04060862, NCT04177108, NCT03337724)*, and a phase 3 clinical trial recently initiated to treat advanced triple negative breast cancer patients with capivasertib in combination with paclitaxel (*clinicaltrials.gov – identifier: NCT03997123*). It should be noted, that due to the similarity of the ATP-binding pocket amongst the AGC protein kinase family (of which AKT is a member), ATP-competitive AKT inhibitors are prone to also inhibit other AGC kinases. This can be seen with capivasertib, which is equipotent against AKT1-3, cAMP dependent protein kinase (PKA) and p70S6K, all of which are AGC kinases (Davies *et al.*, 2012). However, the lack of selectivity does not seem to have hindered the progression of ATP-competitive AKT inhibitors through clinical development, and may actually improve efficacy, since many AGC kinases are also involved in oncogenesis (Pearce *et al.*, 2010a; Prêtre and Wicki, 2018).

1.4. AGC kinases

1.4.1. Structure, function and regulation

The AGC (related to PKA, cGMP-dependent protein kinase [PKG] and protein kinase C [PKC]) protein kinase family is family of serine/threonine protein kinases, which comprises 60 of the 518 protein kinases which make up the human kinome (Manning *et al.*, 2002; Pearce *et al.*, 2010a). As the name suggests, the family is defined as protein kinases which share sequence homology in their catalytic domains with PKA, PKC and PKG. The AGC protein kinase family mediate a number of diverse and important cellular functions, regulating many of the hallmarks of cancer, and as such, their mutation or dysregulation can contribute to oncogenesis (Pearce *et al.*, 2010a; Prêtre and Wicki, 2018). Therefore, many AGC kinases are an attractive therapeutic target, with several

inhibitors of AGC kinases (such as AKT inhibitors), currently in clinical phase trials (Prêtre and Wicki, 2018).

AGC kinases all share a similar structure within their catalytic domains, which is that of a prototypical kinase fold, consisting of a small amino-terminal lobe (N-lobe) containing a conserved β-sheet, and a large mainly α-helical carboxyl-terminal lobe (C-lobe; highlighted in Figure 1.3). Between these two lobes is a connecting polypeptide hinge region, which forms a binding pocket for one molecule of ATP, the phosphate donor. In addition to sharing a similar structure, most AGC kinases share a similar mechanism of activation involving the phosphorylation of two highly conserved motifs: the activation loop (also known as the activation segment or T-loop) and hydrophobic motif (HM). The activation loop, located within the C-lobe, adjacent to the ATP-binding site and connected to the N-lobe via an αC helix, contains important catalytic elements, such as the DFG (aspartate-phenylalanine-glycine) motif, which positions ATP for phosphoryl transfer. The phosphorylation of the activation loop is necessary for catalytic activation, as it leads to conformational changes within the αC helix, coordinating a network of hydrogen bonds between a Glu residue on the αC helix, a Lys residue on the N-lobe, and the phosphates of ATP. This network of hydrogen bonds is required for the catalytic activity of AGC kinases. The HM is located within the C-terminal tail of the C-lobe, and upon phosphorylation, wraps around the N-lobe to insert two aromatic residues into the hydrophobic pocket formed between the N-lobe and αC helix, stabilizing the active confirmation of the αC helix. In addition, the turn motif, also located within the C-terminal tail of the C-lobe, can also be phosphorylated, which stabilises the aforementioned interaction between the HM and hydrophobic pocket. The phosphorylation of these sites, within AGC kinases, collectively induces kinase activity by positioning the αC helix in an active confirmation, enabling efficient catalysis (Figure 1.3; Pearce *et al.,* 2010a; Taylor and Kornev, 2011; Arencibia *et al.*, 2013).
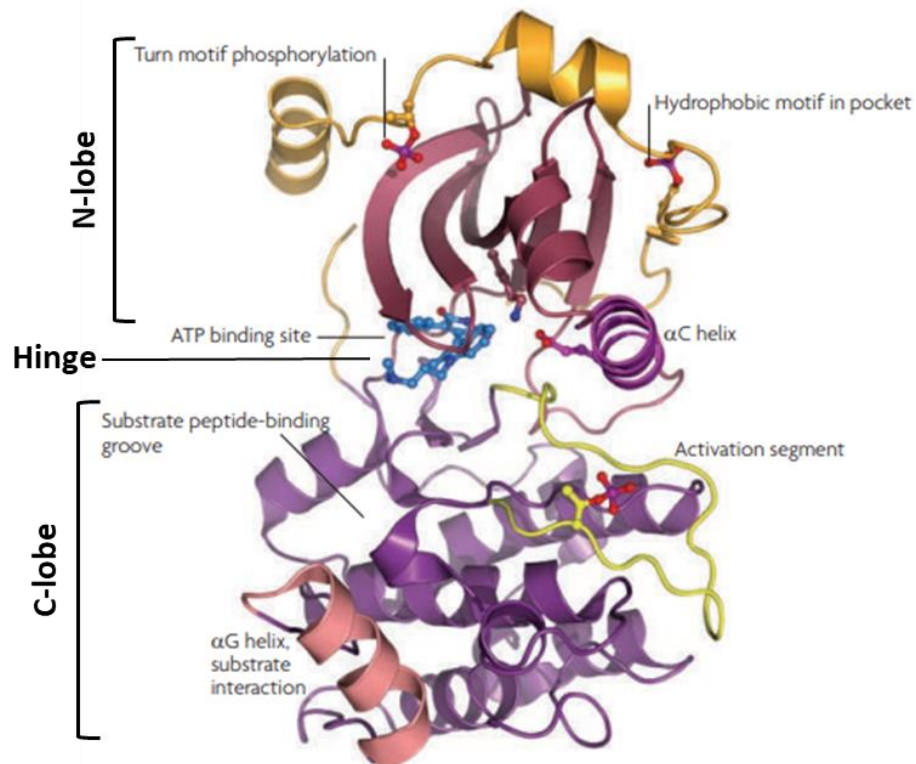
Figure 1.3: Conserved structure of the catalytic domain of AGC kinases. Crystal structure of the catalytic domain of PKCβ2 bound to a competitive inhibitor of ATP, with turn motif (T641), hydrophobic motif (S660) and activation segment (T500) phosphorylation. Key conserved structures and features of AGC kinases are highlighted. Image adapted and taken from Pearce *et al.,* 2010a.

Another common feature amongst AGC kinases, is the phosphorylation of their activation loop by PDK1; this is known to occur in 23 AGC kinases including AKT, p70S6K, serum and glucocorticoid regulated kinase (SGK) and p90 ribosomal S6 kinase (RSK) (Pearce *et al.*, 2010a). Through this extensive phosphorylation and activation of AGC kinases, PDK1 is known as a master regulator of AGC kinases, regulating a diverse array of cellular functions (Mora *et al.*, 2004). Interestingly, PDK1 is also an AGC kinase, and is constitutively active, due to the intrinsic ability of PDK1 to trans-autophosphorylate its own activation loop at Ser241 (Casamayor *et al.*, 1999; Pearce *et al.*, 2010a). PDK1 also contains a PH domain which helps regulate the phosphorylation of some of its targets, by co-localising to the plasma membrane in response to PI3K activation and the formation of PI(3,4,5)P3 (Arencibia *et al.*, 2013). However, most PDK1 substrates do not contain a PH domain, therefore phosphorylation by PDK1 is also regulated by another mechanism; PDK1 is thought to regulate the phosphorylation of most of its AGC kinase substrates through a region in its catalytic domain called the PDK1-interacting fragment (PIF) pocket (Balendran *et al.*, 1999; Pearce *et al.*, 2010a). The PIF pocket enables PDK1 to bind to phosphorylated HMs of AGC kinases, where upon binding it can phosphorylate

the activation loop (Arencibia *et al.*, 2013). Therefore, many AGC kinases have a similar mechanism of activation, whereby they are initially phosphorylated at their HM, which enables PDK1 to then bind via its PIF pocket to the target substrate kinase and phosphorylate the activation loop, inducing AGC kinase activation.

1.4.2. AKT and p70S6K

AKT and p70S6K are amongst the most well-characterised AGC kinases, and due to their role within the PAM pathway (see section 1.3), heavily implicated in oncogenesis, particularly AKT. Whilst their function and regulation were discussed in section 1.3.1, it is worth considering them in more detail. Both AKT and p70S6K are phosphorylated at their activation loop by PDK1, in common with many other AGC kinases, however the mechanism by which this process is regulated is distinct between AKT and p70S6K, as is HM phosphorylation.

The binding of AKT to PI(3,4,5)P3 in PI3K activated cells, mediated by the PH domain of AKT, is thought to be important for AKT phosphorylation by PDK1 for two reasons: 1) when AKT is an unbound state, its PH domain blocks the activation loop of AKT, but when bound to PI(3,4,5)P3 a conformational change takes place, making the activation loop accessible; 2) PDK1 also has a PH domain, so it can co-localize with AKT at the plasma membrane, upon PI3K activation (Stokoe *et al.*, 1997; Arencibia *et al.*, 2013). Therefore, by both binding to PI(3,4,5)P3, PDK1 can phosphorylate the activation loop of AKT (in AKT1, PDK1 phosphorylates Thr308 in the activation loop). Whilst the PDK1-mediated phosphorylation of the activation loop of AKT is required for activation, this only causes a partial activation of AKT, with HM phosphorylation necessary for full activation (Pearce *et al.*, 2010a). The exact mechanism by which AKT is phosphorylated at its HM is not fully understood, but it is generally accepted that mTORC2 phosphorylates the HM of AKT (Ser473 in AKT1), in a PI3K dependent manner. Recently, it has been suggested that this might be mediated by mTORC2 also binding to PI(3,4,5)P3, via the mammalian stress-activated MAP kinase-interacting protein 1 (mSin1) subunit of mTORC2, which contains a PH domain (Liu *et al.*, 2015; Yuan and Guan, 2015).

The phosphorylation of the activation loop of p70S6K requires the prior phosphorylation of the HM motif of p70S6K by mTORC1. Once phosphorylated, PDK1 can bind to the HM of p70S6K via its PIF pocket domain, and subsequently phosphorylate the activation loop

of p70S6K, inducing its activation (Biondi *et al.*, 2001; Arencibia *et al.*, 2013). This mechanism, in which prior HM phosphorylation is required for activation loop phosphorylation by PDK1, is known as the "PIF pocket mechanism" of AGC kinase activation, and is the mechanism by which most of the 23 AGC kinases, phosphorylated by PDK1, become activated (Balzano *et al.*, 2015). Interestingly, it has also been suggested that AKT can be activated via the PIF pocket mechanism, although the circumstances, and precise mechanism, in which AKT is activated in this manner, is yet to be fully established (Bozulic *et al.*, 2008; Arencibia *et al.*, 2013; Balzano *et al.*, 2015).

Both AKT and p70S6K play a key role in regulating the functional output of the PAM signalling pathway, much of which is linked to the hallmarks of cancer. In particular, AKT has been shown to regulate proliferation, growth, survival, angiogenesis and metabolism (Revathidevi and Munirajan, 2019). This is mediated through the phosphorylation of a reported ≥ 100 substrates by AKT, although only 20 of these have been comprehensively validated (Cole *et al.*, 2019). For example, AKT phosphorylates GSK3α and GSK3β at a conserved amino-terminal motif, at Ser21 and Ser9 respectively, which inhibits GSK3 by creating an intramolecular pseudosubstrate, preventing substrate accessibility to GSK3 (Manning and Toker, 2017). Many GSK3 phospho-targets are pro-survival factors or cell cycle regulators; such as induced myeloid cell differentiation protein (MCL-1), c-Myc and cyclin D1; which upon phosphorylation by GSK3, are targeted for proteasomal degradation (Diehl *et al.*, 1998; Manning and Toker, 2017). Therefore, activated AKT can stabilise the expression of these proteins, via inhibition of GSK3, mediating survival and cell cycle progression (Manning and Toker, 2017). Another key substrate of AKT, is the FoXO family of transcription factors; the phosphorylation of FoXO proteins by AKT sequesters FoXO proteins in the cytoplasm, preventing the transcription of FoXO-induced genes, most of which are involved in the negative regulation of survival, proliferation and growth (Zhang *et al.*, 2011; Manning and Toker, 2017).

The role of p70S6K within the PAM pathway is not quite as extensive as AKT. But as mentioned in section 1.3.1, p70S6K is a key substrate of mTORC1, regulating multiple components of the translational machinery, playing a crucial role in regulating protein synthesis, thus supporting cell growth and survival. However, p70S6K can also

phosphorylate other substrates, in addition to components of the translational machinery, some of which are shared substrates with AKT (Fenton and Gout, 2011; Mendoza *et al.*, 2011). For example, p70S6K can impart an inhibitory phosphorylation of GSK3β, in similar manner to AKT (Sutherland *et al.*, 1993; Mendoza *et al.*, 2011). In addition, p70S6K can phosphorylate the pro-apoptotic protein BAD, which results in BAD being sequestered by 14-3-3 (Harada *et al.*, 2001; Mendoza *et al.*, 2011). Hypo-phosphorylated BAD binds and neutralizes pro-survival B-cell lymphoma 2 (BCL-2) family proteins, such as BCL-2 and BCL-X$_L$, thus the phosphorylation of BAD by p70S6K (and AKT) liberates pro-survival BCL-2 family proteins, preventing apoptosis (Yang *et al.*, 1995; Harada *et al.*, 2001). Furthermore, p70S6K can impart inhibitory phosphorylation on insulin receptor substrate 1 (IRS1), rapamycin insensitive companion of mTOR (RICTOR) and mTOR, components of the PAM pathway upstream from p70S6K, thus playing an important role in feedback regulation of the PAM pathway (Fenton and Gout, 2011).

1.4.3. SGK

Another example of an AGC kinase that linked to cancer is SGK, of which there are three isoforms: SGK1-3. SGK's share a significant degree of homology with AKT, particularly within their kinase domains, where they share 55% identity in primary amino acid sequence with AKT (Tessier and Woodgett, 2006). As such, SGK and AKT have overlapping substrate specificity and have been shown to phosphorylate many of the same substrates, such as GSK3β, BAD, FoXO3a and TSC2 (Bruhn *et al.*, 2010). Furthermore, in a similar manner to AKT, all isoforms of SGK have been shown to require PI3K activation, and activation loop phosphorylation by PDK1, for their activation and function (Tessier and Woodgett, 2006). However, unlike AKT, isoforms of SGK do not possess a PH domain, and are therefore activated via the "PIF pocket mechanism", in a similar manner to p70S6K; the HM of SGK is initially phosphorylated, which provides a docking site for PDK1 to bind to SGK and phosphorylate the activation loop of SGK (Biondi *et al.*, 2001; Pearce *et al.*, 2010a). As with AKT, mTORC2 has been shown to be responsible for HM phosphorylation in SGK1, and considering the significant homology within the HM amongst SGK isoforms, is likely to be responsible for HM phosphorylation in SGK2 and SGK3 (García-Martínez and Alessi, 2008; Bruhn *et al.*, 2010). It is through these similarities to AKT, both in substrate specificity and mechanism of activation, that

SGK has been linked to the hallmarks of cancer. Interestingly, it has been shown that some *PIK3CA*-mutant cancer cell lines are independent of AKT for their growth and survival, but dependent upon SGK3, suggesting that there might be some functional redundancy amongst AKT and SGK in PAM pathway driven cancers (Gagliardi *et al.*, 2012).

1.4.4. ROCK and ROCK pathway signalling

The Rho-associated coiled-coil containing kinases (ROCK) are also AGC kinases, and act as crucial regulators of the actin-myosin cytoskeleton. There are two isoforms of ROCK, ROCK1 and ROCK2, which share a very similar structure consisting of an N-terminal kinase, a coiled-coil region, a Rho binding domain (RBD) and a C-terminal split PH domain, bisected by a C1 domain (Rath and Olson, 2012). Furthermore, ROCK1 and 2 share 64% identity in their primary amino acid sequence, with the greatest degree of homology (92%) seen within their kinase domains (Julian and Olson, 2014). Whilst a few studies have shown some isoform specific functions of ROCK1 and 2, they are mostly considered to be functionally redundant to one another (Thumkeo *et al.*, 2005; Kümper *et al.*, 2016).

Unlike other AGC kinases, ROCK1 and 2 do not require the phosphorylation of their activation loop or HM to induce activation (Pearce *et al.*, 2010a). Instead, ROCK1 and 2 are activated by the binding of GTP-bound RhoA, RhoB and RhoC, members of the RAS superfamily of GTPases (Rath and Olson, 2012). The exact mechanism in which the binding of Rho activates ROCK1 and 2 is unknown, but it is thought that Rho binds to the RBD of ROCK, causing conformational changes, which disrupts the negative regulatory interactions between the N-terminal kinase domain and auto-inhibitory C-terminal region of ROCK (Rath and Olson, 2012; Julian and Olson, 2014). However, in contrast to RhoA-C, the binding of GTP-bound RhoE to ROCK1, has been shown to negatively regulate ROCK1 activation (Riento *et al.*, 2003). Interestingly, PDK1 has also been shown to competitively bind to ROCK1 in a similar region to RhoE, antagonizing the negative regulation of ROCK1 by RhoE, in a kinase-independent manner (Pinner and Sahai, 2008).

Furthermore, there is evidence to suggest that ROCK can be activated independently of Rho, for example, by caspase-3 or granzyme B mediated cleavage of the auto-inhibitory C-terminal of ROCK during apoptosis, or via the binding of arachidonic acid to the PH

domain of ROCK (Feng *et al.*, 1999; Sebbagh *et al.*, 2001, 2005; Wen *et al.*, 2008). In addition, the activity of ROCK1 and 2 is also known to be modulated by phosphorylation, such as the phosphorylation of Tyr722 ROCK2 by Src, which inhibits ROCK2 activation by preventing the binding of Rho (Lee *et al.*, 2010; Julian and Olson, 2014).

As mentioned, upon activation ROCK predominantly regulates the actin-myosin cytoskeleton, which is primarily achieved by the phosphorylation of a few key substrates. ROCK phosphorylates myosin regulatory light chain 2 (MLC2), a subunit of myosin, at Thr18/Ser19, which causes increased actin-myosin contractility by activating myosin ATPase, thus promoting the interaction of myosin and F-actin to generate contractile force (Figure 1.4; Julian and Olson, 2014). ROCK also acts to increase the phosphorylation of MLC2 by negatively regulating MLC phosphatase (MLC-P), a phosphatase of MLC2. MLC-P is composed of three subunits, a catalytic protein phosphatase 1 subunit and two non-catalytic subunits: myosin phosphatase-targeting subunit 1 (MYPT1), a myosin binding subunit; and M20, the function of which is currently unknown (Matsumura and Hartshorne, 2008). ROCK negatively regulates MLC-P by phosphorylating MYPT1, inhibiting the binding of MLC-P to myosin, therefore preventing the dephosphorylation of MLC2 by MLC-P (Figure 1.4; Julian and Olson, 2014). ROCK also can promote actin polymerisation, by phosphorylating and activating LIM domain kinases (LIMK), which in turn phosphorylate and inactivate the actin severing protein cofilin (Figure 1.4; Ohashi *et al.*, 2000; Prunier *et al.*, 2017). In addition, ROCK can phosphorylate several other substrates which facilitate regulation of the actin-myosin cytoskeleton (e.g. adducin & ezrin/radixin/moesin proteins), as well other substrates which regulate the functional output of ROCK independently of the actin-myosin cytoskeleton (e.g. beclin1 & PTEN), although these are less well characterised (Riento and Ridley, 2003; Amano *et al.*, 2010; Amin *et al.*, 2013; Gurkar *et al.*, 2013).
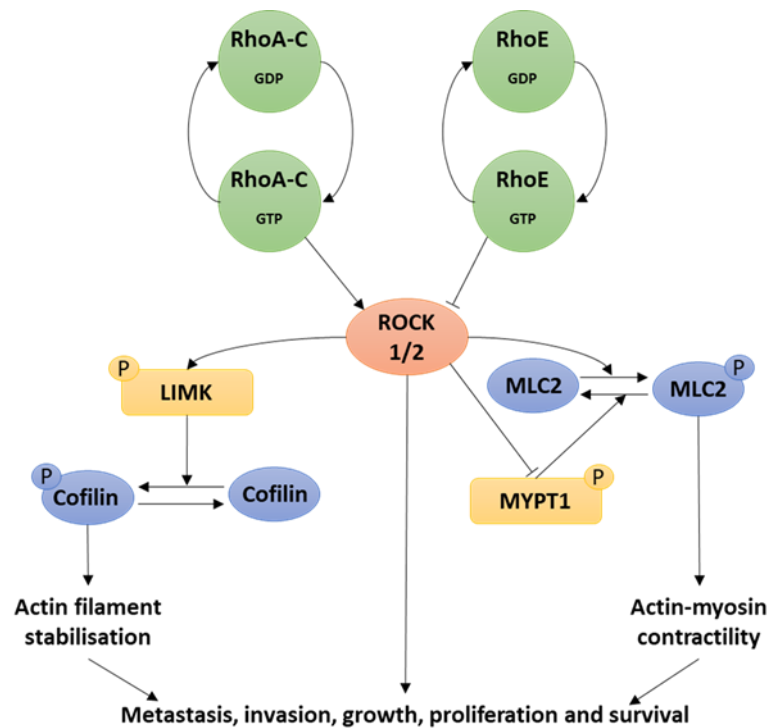
Figure 1.4: The Rho/ROCK pathway. Diagram depicts the Rho/ROCK pathway, its regulation of the actin-myosin cytoskeleton, and its functional output within the context of cancer. ROCK is predominantly associated with cancer by its regulation of the actin-myosin cytoskeleton, but phosphorylation of other substrates (outside the actin-myosin cytoskeleton) may also contribute to cancer.

Through the regulation of actin-myosin contractility, ROCK has been shown to regulate several cellular functions, many of which are associated with the hallmarks of cancer, particularly tumour cell invasion and metastasis (Julian and Olson, 2014; Pandya *et al.*, 2017). For example, ROCK induced actin-myosin contractility has been shown to regulate amoeboid migration, a particularly rapid form of cell migration, which is often used by cancer cells to invade surrounding tissues (Wyckoff *et al.*, 2006; Krakhmal *et al.*, 2015). Moreover, ROCK has also been shown to regulate cancer cell extravasation, an important step of the metastatic cascade (Stoletov *et al.*, 2010).

In addition to tumour cell invasion and metastasis, ROCK is being increasingly linked to regulation of the cell cycle and proliferation (Street and Bryan, 2011; Rath and Olson, 2012). Olson and Croft (Croft and Olson, 2006) demonstrated that the activation of ROCK in mouse embryonic fibroblasts (MEF) increased cell cycle progression and proliferation, and that this was due to modulation in the expression of several cell cycle regulators, such as cyclin D1 and cyclin A, both of which were increased by ROCK activation. This regulation of the cell cycle, by ROCK activation, was shown to be dependent upon increased actin-myosin contractility (Croft and Olson, 2006). A similar phenomenon was seen by Kümper and colleagues (Kümper *et al.*, 2016), where MEF cells, in which both

ROCK1 and ROCK2 had been genetically deleted, were shown to be defective in proliferation, due to cell cycle arrest and the induction of senescence. Using *in vivo* mouse models of melanoma and NSCLC, Kümper and colleagues (Kümper *et al.*, 2016) also showed that the expression of ROCK1 and 2 is essential for tumour formation, i.e. cancer cells in which ROCK1 and 2 had been genetically deleted could not form tumours (Kümper *et al.*, 2016). Furthermore, ROCK1 and 2 have also been implicated in providing the contractile strength required for cytokinesis (the physical act of cell division, dividing one parental cell into two daughter cells, which occurs at the end of mitosis), with genetic depletion of *ROCK1 and ROCK2* shown to increase the number of binucleate cells, a marker of failed cytokinesis (Matsumura, 2005; Kümper *et al.*, 2016).

1.4.5. PKA

In addition to ROCK, other AGC kinases also have a distinctive mechanism of activation, such as PKA; PKA is activated by the 2nd messenger cAMP, which is generated by the enzyme adenylate cyclase, downstream of G-protein coupled receptors (GPCRs), which are stimulated by extracellular stimuli such as cytokines and hormones (Pearce *et al.*, 2010a). PKA is maintained in an inactive state by the formation of an heterotetrameric complex consisting of two catalytic subunits (of which there are three isoforms) and two regulatory subunits (of which there are four isoforms), which act as pseudosubstrates to the catalytic domains suppressing activity (Pearce *et al.*, 2010a; Sapio *et al.*, 2014). The binding of cAMP to these regulatory subunits induces a conformational change that releases the catalytic subunits, freeing them to phosphorylate substrates. Additionally, PKA also requires activation loop phosphorylation to induce activation, which in common with other AGC kinases is mediated by PDK1, although PKA autophosphorylation may also contribute (Cheng *et al.*, 1998; Moore *et al.*, 2002). Upon activation, PKA regulates a diverse array of cellular functions, such as proliferation, survival and migration (Sakamoto and Frank, 2009; Caretta and Mucignat-Caretta, 2011; Sapio *et al.*, 2014).

1.5. AT13148, an AGC kinase inhibitor

As discussed in section 1.3, the PAM pathway is frequently dysregulated in cancer and is an attractive therapeutic target for cancer therapy. In recent years, there has been an increasing focus on developing small molecule inhibitors of AKT, due to the importance of AKT within the PAM pathway. Subsequent to the crystal structure of AKT2 being resolved in 2002 at the Institute of Cancer Research (ICR) by David Barford and co-workers, a collaboration was established between the ICR, Cancer Research Technology and Astex Pharmaceuticals, to discover and develop potent and selective ATP-competitive AKT inhibitors, using fragment and structure-based design (Yang *et al.*, 2002). This led to the discovery of AT13148, which was shown to potently inhibit AKT1 and AKT3, with weaker inhibition of AKT2 (Figure 1.5 Yap *et al.*, 2012). However, AT13148 was also found to inhibit several related AGC kinases: PKA, ROCK1, ROCK2, p70S6K, SGK3 & RSK1; some of which were more potently inhibited by AT13148 than AKT1 and AKT3. Specifically, AT13148 displayed moderate potency (IC_{50} = 10 - 100 nM in *in vitro* kinase assays) against AKT1, AKT3, SGK3 and RSK1, but potently inhibited ($\leq$ 10 nM IC_{50} in *in vitro* kinase assays) PKA, ROCK1, ROCK2 and p70S6K (Figure 1.5; Yap *et al.*, 2012). In a pre-clinical study, AT13148 was shown have efficacy in a number of human cancer cell lines with PAM pathway mutations (e.g. *PIK3CA* and *PTEN)*, where AT13148 was shown to induce a pro-apoptotic response, as well as efficacy being seen in several *in vivo* mouse human tumour xenograft models (Yap *et al.*, 2012).
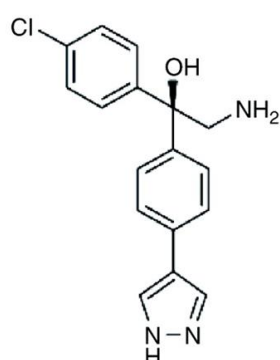
AT13148 target	IC_{50} (nM)
AKT1	38
AKT2	402
AKT3	50
p70S6K	8
PKA	3
ROCK1	6
ROCK2	4
SGK3	63
RSK1	85

Figure 1.5: Structure and targets of AT13148. Chemical structure of AT13148 and the IC_{50} of AT13148 against its targets, as determined via *in vitro* kinase assays. Adapted from yap *et al.,* 2012.

Despite the lack of selectivity for AKT, AT13148 was taken forward for further clinical development due to its pro-apoptotic cellular phenotype and because many of the additional AGC kinases targeted by AT13148 are of therapeutic interest in the treatment

of cancer, as discussed in section 1.5 (Yap *et al.*, 2012). In addition, most selective AKT inhibitors (selective in comparison to AT13148) have shown limited efficacy in clinical trials when used as a monotherapy (Prêtre and Wicki, 2018; Xing *et al.*, 2019). A similar phenomenon has been observed with other PAM pathway inhibitors, for example the rapalogs temsirolimus and everolimus, which whilst clinically approved, have been shown to have limited efficacy when used as monotherapies (Motzer *et al.*, 2010; Meng and Zheng, 2015). It has been suggested that PAM pathway inhibitors may have limited efficacy, when used as a monotherapy, due to the relief of negative feedback within the PAM pathway, which causes reactivation of the PAM pathway (O'Reilly *et al.*, 2006; Prêtre and Wicki, 2018; Wang *et al.*, 2019). In targeting several components of the PAM pathway (AKT, p70S6K and SGK3), AT13148 may be able to overcome this, causing a stronger more durable decrease in PAM pathway activation, thus improving efficacy, when compared to more selective PAM pathway inhibitors. It should also be considered that targeting kinases outside the PAM pathway (e.g. ROCK and PKA), which are clinically relevant in the treatment of cancer, could also contribute to the efficacy of AT13148.

AT13148 has recently completed a phase 1 clinical trial in patients with advanced solid tumours with the full publication of results from this trial currently awaited (*clinicaltrials.gov – identifier: NCT01585701*). However, the results from the initial first in human/dose-escalation study (part of the phase 1 clinical trial) were presented at the American Society of Clinical Oncology (ASCO) annual meeting in 2015 (the abstract of which is publicly available: Papadatos-Pastos *et al.*, 2015), where AT13148 was shown to have favourable pharmacokinetics/pharmacodynamics, as well as acceptable toxicities. Currently, a specific clinical indication for the use of AT13148, which could be evaluated should AT13148 progress to a phase 2 clinical trial, has not been identified, but several have been suggested and are currently under investigation.

Based upon pre-clinical data, in which the efficacy of AT13148 was shown in human cancer cell lines with PAM pathway mutations, AT13148 could be used to treat cancers in which the PAM pathway is dysregulated. Breast cancers in particular have a high rate of *PI3KCA* and *PTEN* mutations (27% and 25% of patients respectively), thus breast cancer patients could benefit from treatment with AT13148 (Liu, Cheng, Thomas M Roberts, *et al.*, 2009). However, a phase 2 clinical trial in which advanced breast cancer

patients with PAM pathway mutations were treated with the allosteric AKT inhibitor MK2206, showed limited clinical efficacy due the inability of MK2206 to sufficiently inhibit PAM pathway signalling (Xing *et al.*, 2019). Nonetheless, as previously discussed, in targeting several kinases of the PAM pathway, AT13148 could potentially have improved efficacy in treating breast cancer patients, when compared to more selective AKT inhibitors such as MK2206.

It should also be considered that in targeting other clinically relevant AGC kinases, AT13148 could potentially be used in treating cancers in which the PAM pathway is not dysregulated. For example, since AT13148 can potently inhibit ROCK1 and 2 it has also been investigated as an anti-invasive/metastatic drug. Rath and colleagues (Rath *et al.*, 2018) showed that AT13148 was able to block the invasion of PDAC cells into surrounding healthy pancreatic tissue in an *in vivo* mouse model. They suggested that AT13148 could be used in the adjuvant setting to enable surgical resection by maintaining separation between tumour and healthy tissue (Rath *et al.*, 2018). Moreover, AT13148 has been shown to inhibit melanoma cell motility *in vitro* and in an *in vivo* mouse model, further highlighting the potential for AT13148 to be used as an anti-invasive/metastatic drug (Sadok *et al.*, 2015).

In addition, the use of other ROCK inhibitors, either as a monotherapy or in combination with other cancer therapies, is currently being investigated and showing great promise. Smit and colleagues (Smit *et al.*, 2014) used a functional short hairpin RNA (shRNA) screen to identify ROCK1 as a potential combinatorial drug target for BRAF mutant melanoma. The combination of a ROCK inhibitor with a proteasomal inhibitor (such as bortezimib) has also been suggested as a therapy for mutant *KRAS* NSCLC (Kumar *et al.*, 2012). Furthermore, the inhibition of ROCK has been shown to be synthetically lethal with loss of von Hippel-Lindau (VHL) in renal cell carcinoma (RCC) (Thompson *et al.*, 2017). Since there currently aren't any ROCK inhibitors in clinical trial for the treatment of cancer, AT13148 could fill this void, and potentially have additional efficacy by the targeting of other AGC kinases.

However, despite the clinical potential of AT13148, the history of targeted therapies and other drugs in the treatment of cancer, informs us that, should AT13148 progress to

clinical approval, resistance to AT13148 is almost inevitable. Resistance to targeted cancer therapies will be focused upon in the following sections.

1.6. Resistance to targeted cancer therapies

1.6.1. The challenge of drug resistance

Drug resistance to targeted therapies, as well as other cancer therapies, is a major barrier to the successful treatment of cancer, with drug resistance continuing to be the principle limiting factor to achieving cures within cancer patients (Vasan *et al.*, 2019). Unfortunately, most patients with advanced cancer ultimately die because some or all their cancer cells exhibit or develop resistance to all available therapeutic avenues (Garraway and Jänne, 2012). It is thought that the inherent genomic instability and heterogeneity within cancer, as well as the plasticity of oncogenic signalling pathways, contribute to the near-universality of resistance to cancer therapies (Garraway and Jänne, 2012; Konieczkowski *et al.*, 2018).

Drug resistance can be categorised as intrinsic drug resistance or acquired drug resistance. Intrinsic resistance (also known as *de novo* resistance) can be defined as when a tumour shows no initial response to a therapy that should have been effective based upon the underlying biology or genetics of the tumour (Garraway and Jänne, 2012). For example, 10-20% of patients with mutant *BRAF* V600E melanoma and ~95% of patients with mutant *BRAF* V600E colorectal cancer, show no response to the BRAF V600E inhibitor vemurafenib (Flaherty *et al.*, 2010; Chapman *et al.*, 2011; Kopetz *et al.*, 2015; Griffin *et al.*, 2017). In contrast, acquired resistance can be defined as tumour progression in the face of ongoing treatment to which the tumour was initially sensitive (Garraway and Jänne, 2012). An example of this can be seen in *ph+* CML patients treated with imatinib; 20-25% of these patients stop responding to imatinib after initially undergoing a complete haematological and/or cytogenic response (Milojkovic and Apperley, 2009).

Due to the prevalence of resistance to targeted therapies, both intrinsic and acquired, understanding the molecular mechanisms of resistance may provide opportunities to improve patient outcome. For example, in many cases, understanding the molecular mechanism of resistance has led to the identification of novel therapeutic strategies to

overcome resistance, increasing the magnitude or duration of clinical response. This can be seen in imatinib resistant *ph+* CML, where the discovery that resistance is often driven by secondary mutations in BCR-ABL, has led to the development of 2nd and 3rd generation inhibitors that can overcome resistance and increase the duration of clinical response (Jabbour *et al.*, 2015). Furthermore, understanding the molecular mechanisms of resistance may enable the identification of predictive biomarkers to clinically stratify patients, based upon their likelihood of responding to a particular therapy (Cree and Charlton, 2017).

Despite the complexity in the mechanisms of resistance to targeted therapies, it has been suggested that they converge on three recognizable patterns of resistance: 1) pathway re-activation, 2) pathway by-pass, 3) pathway indifference (Highlighted in Figure 1.6; Konieczkowski, Johannessen and Garraway, 2018). These are discussed in the following subsections.
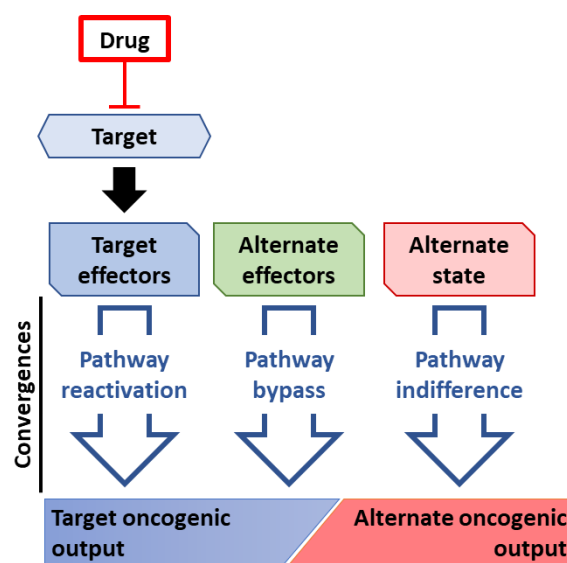
Figure 1.6: Converging mechanisms of resistance. Schematic diagram highlights how mechanisms of resistance converge on three recognisable patterns, based upon their relationship between drug target and downstream pathways: pathway reactivation, pathway bypass and pathway indifference. These are discussed in section 1.6.2. Figure adapted from Konieczkowski *et al.,* 2018.

1.6.2.   Mechanisms of drug resistance to targeted therapies

1.6.2.1.   Pathway reactivation

As discussed in section 1.2, most targeted therapies target oncogenes, and their downstream effector pathways, which cancer cells have become dependent on for their growth and survival (oncogene addiction). The most common convergent pattern of

resistance is pathway re-activation; a process in which the core downstream effector pathways, downstream of the drug target, become re-engaged/reactivated, causing sustained growth and survival in the presence of a targeted therapy (Konieczkowski *et al.*, 2018). For example, approximately 70% of BRAF mutant melanoma's that clinically progress after RAF and/or MEK inhibitor treatment, show sustained ERK 1/2 phosphorylation, indicating re-activation of the MAPK pathway (Konieczkowski *et al.*, 2018). In general, there are three distinct mechanisms in which pathway reactivation can occur: Drug target alterations, activation of parallel effectors, and alterations in upstream and downstream effectors.

Many of the initially identified mechanisms of resistance to targeted therapies entailed alterations in the drug target which render the protein target insensitive to the drug itself, thus rendering downstream effector pathways refractory to inhibition (Konieczkowski *et al.*, 2018). Within the context of kinase inhibitors, especially TKIs, this is frequently caused by mutations in the kinase domain, within contact points crucial for kinase-inhibitor interaction. Often these mutations are gatekeeper mutations; gatekeeper refers to a conserved amino acid residue found in the catalytic cleft of tyrosine kinases which is crucial for the binding of many TKI's (Garraway and Jänne, 2012; Roskoski, 2016). For example, threonine 315 is the gatekeeper residue of the ABL tyrosine kinase domain and is frequently mutated to isoleucine (T315I mutation) in imatinib resistance. This mutation has been detected in 13% of imatinib resistant *ph+* CML patients and 37% of *ph+* acute lymphoblastic leukaemia (ALL) patients, and prevents imatinib from inhibiting the BCR-ABL fusion protein (Soverini *et al.*, 2014; Ursan *et al.*, 2015). Other examples, of gatekeeper mutations, include erlotinib-resistant *EGFR* mutant NSCLC (T790M mutation) and crizotinib-resistant anaplastic lymphoma kinase (ALK) rearranged NSCLC (ALK[L1169M]; Garraway and Jänne, 2012). The knowledge that gatekeeper mutations frequently generate resistance to TKIs has led to the development of novel TKIs which can bind and inhibit gatekeeper mutated tyrosine kinases, such as ponatinib and osimertinib, which are respectively used to treat *ABL[T315I]* positive *ph+* CML/ALL patients and *EGFR[T790M]* positive NSCLC patients (Garnock-Jones, 2016; Pavlovsky *et al.*, 2019).

In addition, other alterations in the drug target may also confer resistance to a targeted therapy such as mutations in non-contact residues which lead to an altered confirmation. This has been observed in resistance to type 2 kinase inhibitors, inhibitors which bind kinases in their inactive confirmation outside the ATP-site, such as imatinib and sunitinib (Garraway and Jänne, 2012; Klug *et al.*, 2018). Many of these mutations occur in the activation loop of kinases, inducing a constitutively active confirmation, preventing the binding of type 2 inhibitors (Klug *et al.*, 2018). Furthermore, amplification of drug target can also confer resistance to targeted therapies, such as amplification of *BCR-ABL*, which has been shown to cause resistance to imatinib in *ph+* CML (Gorre *et al.*, 2001; Campbell *et al.*, 2002; Garraway and Jänne, 2012).

Pathway reactivation can also be achieved by effector proteins which act in parallel to the targeted protein (Garraway and Jänne, 2012; Konieczkowski *et al.*, 2018). This is a common mechanism of resistance to RTK inhibitors, as most RTKs regulate the same downstream effector pathways, predominantly the MAPK and PAM pathways, therefore gain-of-function mutations in RTKs can compensate for the inhibition of other RTKs, by re-engaging the appropiate effector pathways. A study by Yu and colleagues (Yu *et al.*, 2013), in patients with *EGFR*-mutant NSCLC with acquired resistance to EGFR TKI therapies, demonstrated that *MET* and *HER2* (both RTKs) amplification was seen in 5% and 13% of pateints respectively. This has led to the rationale that the combination of EGFR TKI with a MET or HER2 inhibitor could be an effective therapeutic strategy to treat *EGFR*-mutant NSCLC patients with acquired resistance to EGFR TKI therapies. Recently, a phase 1b/2 clinical trial was conducted, in which capmatinib (a MET TKI) was used in combination with gefitinib (EGFR TKI) to treat pateints with EGFR-mutated, MET-dysregulated NSCLC, which showed promising results (Wu *et al.*, 2018). Interestingly, in the case of *MET* amplification, it has been shown that resistance occurs due to re-activation of the PAM pathway in an ERBB3-dependent manner (Engelman *et al.*, 2007). Since the amplification/activation of other RTKs might also induce EGFR TKI resistance in this manner, co-targetting the PAM pathway could also be a potential therapeutic avenue.

Another notable example of pathway reactivation mediated by parallel effectors can be found in mutant *BRAF* melanoma; a small percentage of BRAF inhibitor resistant patients have been shown to have gain-of-function mutations in *MAP3K8*, a gene which encodes

COT kinase (Lehmann *et al.*, 2019). As a MAP3K, COT kinase functions in parallel with BRAF within the MAPK pathway, phosphorylating and activating MEK 1/2 which subsequently phosphorylates and activates ERK 1/2 (Dasi *et al.*, 2005; Johannessen *et al.*, 2010). As such, gain-of-function mutations in *MAP3K,* in mutant *BRAF* melanoma, can re-engage the MAPK pathway in the presence of BRAF inhibition, driving resistance (Figure 1.7A; Johannessen *et al.*, 2010; Lehmann *et al.*, 2019).

In addition, alterations in upstream and downstream effectors of the target protein can cause pathway re-activation. Alterations in both upstream and downstream effectors are frequent in mutant *BRAF* melanomas resistant to BRAF inhibition. For example, *NRAS* and *KRAS,* upstream effectors of BRAF, have been shown to have gain-of-function resistance mutations in 20% of mutant *BRAF* melanoma patients with acquired resistance to BRAF inhibition (Johnson *et al.*, 2015). Gain-of-function resistance mutations in *NRAS* and *KRAS* (e.g. a Q61K or G12V substitution) can re-engage MAPK signalling, by activating CRAF and ARAF (alternate RAF isoforms), leading to sustained ERK 1/2 phosphorylation in the presence of BRAF inhibition (Figure 1.7; Nazarian *et al.*, 2010; Dumaz, 2011; Dorard *et al.*, 2017). Furthermore, gain-of-function resistance conferring mutations have been idenitifed in MEK 1/2 (e.g. C121S/C125S substitution), a downstream effector of BRAF, in 7% of mutant *BRAF* melanoma patients with acquired resistance to BRAF inhibition, which again, drives resistance against BRAF inhibition by causing a sustained phosphorylation of ERK 1/2 (Figure 1.7B; Wagle *et al.*, 2011; Van Allen *et al.*, 2014; Johnson *et al.*, 2015). Alterations in downstream effectors also contributes to resistance to EGFR therapies (cetuximab & panitumumab) in colorectal cancer, with resistance-conferring mutations frequently found in *KRAS* and *BRAF,* which enable sustained MAPK pathway activation in the presence of anti-EGFR therapy (Zhao *et al.*, 2017).

Since 70% of resistance mutations in mutant *BRAF* melanoma's converge upon MAPK pathway re-activation (including the aformentioned mutations in *NRAS, KRAS, MEK 1/2* and *MAP3K8)*, the combination of BRAF and MEK inhibitors is now used as a 1st line therapy in treatment naïve patients with mutant *BRAF* melanoma's, to circumvent the acquisition of resistance via re-activation of the MAPK pathway (Arozarena and Wellbrock, 2017). This has proven to be a successful aproach with phase 3 clincial trials

demonstrating improved efficacy when compared to BRAF inhibitor monotherapy (Ascierto *et al.*, 2016; Trojaniello *et al.*, 2019).
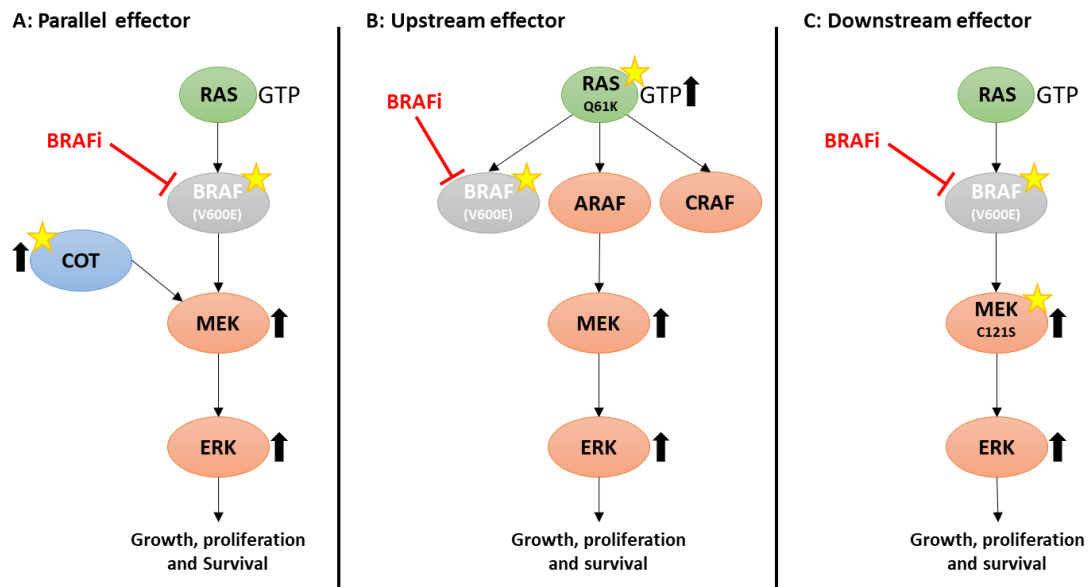
Figure 1.7: Mechanisms of MAPK pathway re-activation in resistance to BRAF inhibition in melanoma. The MAPK pathway is frequently re-activated in resistance to BRAF inhibition in *BRAF* mutant melanoma, and provides an instructive example of the mechanisms which drive pathway reactivation in resistance to targeted therapies: **(A)** activation of a parallel effector, such as COT kinase; **(B)** activation of an upstream effector, such as RAS; **(C)** activation of a downstream effector, such as MEK 1/2. Gain-of-function mutations are highlighted with a yellow star.

1.6.2.2. *Pathway bypass*

Whilst many resistance mechanisms to targeted therapies converge upon pathway re-activation, in a minority of cases resistance occurs in the absence of pathway re-activation; i.e. despite resistance, the targeted pathway is still robustly inhibited in the presence of drug (Konieczkowski *et al.*, 2018). However, one must consider that for a targeted therapy to be effective, not only is it required that downstream effector pathways must be robustly inhibited, so must the oncogenic output regulated by downstream effector pathways (e.g. transcriptional or translational output). Within cancer there is a significant degree of redundancy amongst signalling pathways that control cell proliferation, survival, and many of the other hallmarks of cancer, with these pathways shown to engage many of the same oncogenic outputs (Kaelin, 2006; Kitano, 2007; Konieczkowski *et al.*, 2018). Therefore, one of the ways in which resistance can occur to targeted therapies, in the absence of pathway re-activation, is by pathway bypass, a process in which targeted oncogenic output is re-engaged via an alternative signalling pathway, independent from the downstream effector pathways initially targeted (Konieczkowski *et al.*, 2018).
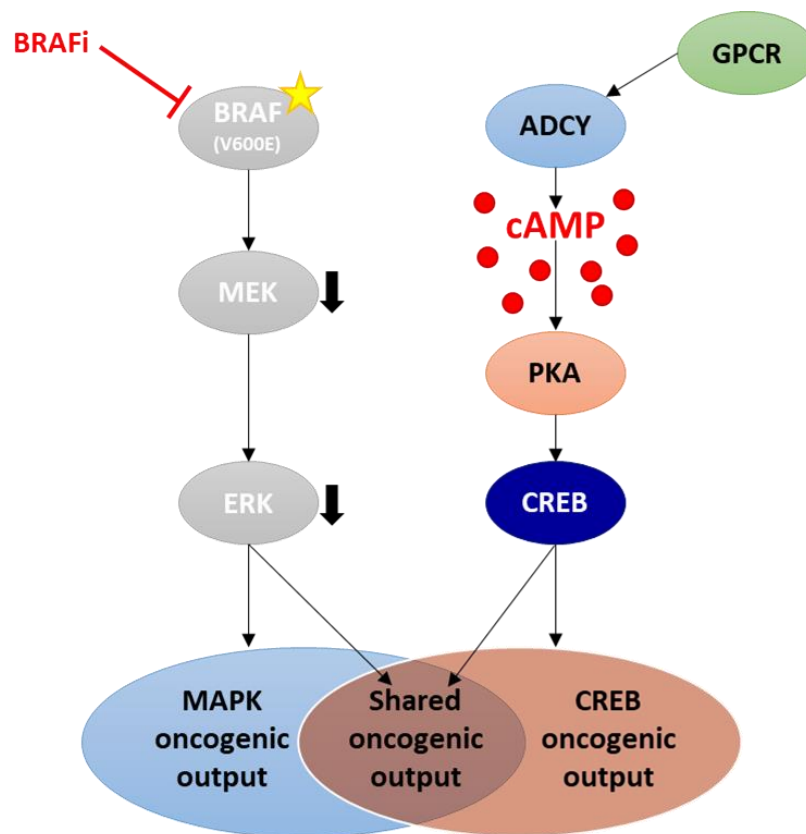
Figure 1.8: Pathway bypass of the MAPK pathway in BRAF inhibitor resistance in melanoma. Diagram summarises how activation of GPCR/cAMP/CREB signalling can drive resistance to BRAF inhibition in *BRAF* mutant melanoma, by bypass of the MAPK pathway. The MAPK pathway and GPCR/cAMP/CREB signalling axis have shared oncogenic output, such as the transcription factors MITF and ETV, therefore activation of the GPCR/cAMP/CREB signalling axis can compensate for the inhibition of the MAPK pathway. ADCY: adenylate cyclase. Figure adapted from Johannessen *et al.,* 2013.

Pathway bypass has been observed in mutant *BRAF* melanoma, where a functional genetic screen in mutant *BRAF* melanoma cell lines, by Johannessen and colleagues (Johannessen *et al.*, 2013), demonstrated that resistance against MAPK pathway inhibitors (e.g. BRAF inhibitor) can be mediated by MAPK pathway bypass. Specifically, they showed that overexpression of genes within the GPCR/cAMP/cAMP responsive element binding protein (CREB) signalling axis were able to confer resistance, including numerous *GPCR* genes; *ADCY9*, an adenylate cyclase gene; and *PRKACA*, a catalytic subunit of PKA. They hypothesised that as the MAPK pathway and GPCR/cAMP/CREB signalling axis converge upon a core set of transcriptional outputs, such as the transcription factors ETV1 and melanoma inducing transcription factor (MITF), GPCR/cAMP/CREB signalling could compensate for MAPK pathway inhibition (Figure 1.8). In other words, GPCR/cAMP/CREB signalling can engage the same oncogenic outputs as the MAPK pathway, therefore drive resistance against MAPK pathway inhibitors in a MAPK pathway independent manner. A similar approach (functional

genetic screen) also revealed that purinergic P2Y receptors (a family of GPCRs) can drive resistance against ALK (an RTK) inhibition in ALK-dependent NSCLC cells, independently of downstream effectors of ALK, such as the MAPK and PAM pathways. Furthermore, it was shown that there was an overlap between the gene signature associated with P2Y driven resistance and pathway reactivation-based resistance mechanisms, thus it was hypothesised that P2Y receptors induced resistance against ALK inhibition by re-engaging transcriptional outputs regulated by downstream effectors of ALK.

1.6.2.3. Pathway indifference

Pathway re-activation and pathway by-pass represent distinct patterns of resistance to targeted therapies, but they nonetheless converge, driving resistance by re-engaging the targeted oncogenic output. However, there are some examples of resistance in which both targeted downstream effector pathways and oncogenic output continue to be robustly inhibited despite the acquisition of resistance. Often, in these circumstances, cancer cells have transcended into an alternative malignant cell state (transcriptional or otherwise), in which growth, proliferation and survival are completely independent of the initially targeted oncogenic dependencies. This is referred to as pathway indifference (Konieczkowski *et al.*, 2018).

Perhaps the best example of resistance caused by pathway indifference is in breast cancer patients treated with poly-ADP ribose polymerase (PARP) inhibitors. PARP inhibitors (e.g. olaparib) are predominantly used to treat ovarian and breast cancer patients with loss-of-function germline mutations in *BRCA1* or *BRCA2* (proteins critical in the repair of double strand DNA breaks), based on the synthetic lethal relationship between BRCA1/2 and PARP (Lord and Ashworth, 2017). Remarkably, it has been shown that resistance to PARP inhibitors can be mediated by secondary mutations in *BRCA1/2*, which restore the function of BRCA1/2, abolishing the synthetic lethal relationship between BRCA1/2 and PARP (Barber *et al.*, 2013; ter Brugge *et al.*, 2016; Gogola *et al.*, 2019). In effect, due to the importance of BRCA1/2 in DNA repair, the restoration of BRCA1/2 function shifts cancer cells from a genome-unstable state to a genome-stable state (Konieczkowski *et al.*, 2018).

Another notable example of pathway-indifferent resistance can be found in *EGFR*-mutant NSCLC patients treated with EGFR inhibitors. In a minority of these patients,

acquired resistance to EGFR inhibitors is mediated via a histological transformation consistent with that of small cell lung carcinoma (SCLC), whilst still maintaining expression of mutant *EGFR* (Sequist *et al.*, 2011; Yu *et al.*, 2013; Piotrowska *et al.*, 2015). In these patients, resistance against EGFR inhibitors seems to have occurred via the transformation of their lung cancer from NSCLC to SCLC. Accordingly, a study by Piotrowska and colleagues (Piotrowska *et al.*, 2015) demonstrated that three out of four *EGFR*-mutant NSCLC patients that underwent a SCLC transformation, had a marked therapeutic response to platinum-etoposide-based chemotherapy, a classic SCLC treatment, highlighting the acquisition of an alternate SCLC-associated oncogenic output.

1.7. Overview and aims of this thesis

The PAM pathway is a key regulator of many of the hallmarks of cancer such as growth, proliferation and survival, and as such is an attractive therapeutic target for the treatment of cancer. Due to the importance of AKT within the PAM pathway, efforts have been made to discover and develop small-molecule AKT inhibitors as a novel targeted cancer therapy, of which several are currently in clinical trials for the treatment of cancer, showing promising results (Kim *et al.*, 2017; Schmid *et al.*, 2018; Revathidevi and Munirajan, 2019). AT13148 is distinct amongst AKT inhibitors as it potently inhibits several AGC kinases, both within the PAM pathway (p70S6K and SGK3) and outside (ROCK and PKA), that are of therapeutic relevance in the treatment of cancer (Yap *et al.*, 2012). Therefore, AT13148 may have improved efficacy in treating cancers with dysregulated PAM pathway signalling, as well as having a potential clinical use in cancers in which the PAM pathway is not dysregulated but in which other AT13148 targets may be important such as ROCK1/2 (e.g. PDAC, see section 1.5).

Despite the clinical potential of AT13148, the history of kinase inhibitors and other drugs in the treatment of cancer, informs us that acquired drug resistance is very likely to occur in the clinic to AT13148, if not inevitable (Garraway and Jänne, 2012). As was highlighted in section 1.6.2, understanding the mechanisms of acquired drug resistance to targeted therapies in the clinic, has led to the identification of therapeutic strategies to overcome resistance, increasing the magnitude or duration of clinical response. In many of these cases, the use of pre-clinical cell line models has enabled the identification of clinically

relevant mechanisms of acquired drug resistance, and have been instrumental in identifying and validating therapeutic strategies to overcome resistance (Johannessen *et al.*, 2010; Nazarian *et al.*, 2010; Garraway and Jänne, 2012). Therefore, pre-clinical cell line models provide an effective means of studying acquired drug resistance whilst a drug is still in clinical development, such as AT13148.

With this in mind, a project was instigated to generate resistance to AKT inhibitors, including AT13148, in pre-clinical cell line models (Akan, 2015). During this project an AT13148 resistance sub-line (A2780-148R) was derived from the human ovarian carcinoma cell line A2780, a cell line with dysregulated PAM pathway signalling. The aims of this thesis were therefore to investigate the acquired mechanisms of resistance to AT13148, using A2780-148R as a pre-clinical cell line model, and identify therapeutic strategies to overcome AT13148 resistance.

Aims and objectives

- Investigate the mechanisms(s) of resistance to AT13148 in the A2780-148R cell line by:
  - Cross-resistance profiling using a range of targeted inhibitors
  - Evaluating the baseline activation of the PAM pathway and other AT13148 targeted pathways.
  - Examining the response of the PAM pathway and other AT13148 targeted pathways to AT13148.
- Validate identified AT13148 resistance mechanisms using a range of *in vitro* techniques.
- Devise and validate therapeutic strategies to overcome identified mechanisms of AT13148 resistance.

Chapter 2

Materials and Methods

2. Materials and Methods

2.1. Compounds and Materials

Compounds used on cultured cells, shown in Table 2.1, were prepared and diluted in dimethly sulfoxide (DMSO; Sigma-Aldrich, Germany) under sterile conditions and stored at -80°C. Unless otherwise stated, all other chemicals and reagents were purchased from Sigma-Aldrich (Germany).

Table 2.1: Summary of compounds used for cell-based experiments. Table lists compounds used for cell-based experiments, such as SRB cell viability assays.

Inhibitor/drug	Target(s)	[Stock]	Supplier
AT13148	AGC kinases	20 mM	Astex pharmaceuticals, UK
AZD4547	FGFR1-3	10 mM	Selleck chemicals, USA
Capiversatib (AZD5363)	AKT	20 mM	Selleck chemicals, USA
Selumetinib (AZD6244)	MEK 1/2	10 mM	Selleck chemicals, USA
BCI	DUSP6	50 mM	Sigma-Aldrich, Germany
GDC-0994	ERK 1/2	20 mM	Adooq, USA
GSK269962	ROCK	20 mM	Tocris Bioscience, USA
GSK429286A	ROCK	10 mM	Tocris Bioscience, USA
KX2-391	Src	20 mM	Selleck chemicals, USA
MK2206	AKT	20 mM	Selleck chemicals, USA
NVP-AEW541	IGF-1R	10 mM	Selleck chemicals, USA
PD0325901	MEK 1/2	10 mM	Selleck chemicals, USA
PF4708671	p70S6K	20 mM	Tocris Bioscience, USA
SCH772984	ERK 1/2	1 mM	Adooq, USA
SU6656	Src family kinases	20 mM	Selleck chemicals, USA
WH-4-023	Lck and Src	10 mM	Selleck chemicals, USA

2.2. General cell culture

2.2.1. Cell lines and culture

A2780 human ovarian carcinoma cells were originally obtained from the health protection agency (Salisbury, UK). A2780-148R, an AT13148 resistance sub-line derived from A2780 cells, were generated by Dr Denis Akan, whilst in the Garrett laboratory (Institute of Cancer Research, London, UK; Akan, 2015). HEK293T cells were a kind gift from Dr Tim Fenton (University of Kent, UK), and were provided at passage number 20. All cell lines were cultured in Dulbecco's Modified Eagle Medium (DMEM; Gibco, UK), containing 3.7 g/L Glucose and 4 mM L-glutamine, supplemented with 10% (v/v) foetal

bovine serum (FBS; Gibco, UK). DMEM supplemented with 10% (v/v) FBS is hereafter referred to as complete DMEM. All cell culture was performed under sterile conditions in a class II biological safety cabinet (BSC), and cells grown at 37°C in a humidified 5% CO_2 incubator, henceforth referred to as standard growth conditions.

Passaging of cells (sub-culture) was undertaken when cells were approximately 70-90% confluent. In T25 flasks, cell culture medium was aspirated off cells and cells rinsed in 2ml of phosphate-buffered saline (PBS; Oxoid, UK). 0.5ml of 0.25% Trypsin-EDTA (ThermoFisher Scientific, USA) was subsequently added to cells and flasks placed in an incubator, under standard growth conditions, until cells had detached. If required, flasks were gently agitated to ensure that cells had sufficiently detached. Cells were then re-suspended in complete DMEM, and depending on the split (usually between 1:10 and 1:40), an appropriate volume added to a new flask. Additional complete DMEM was then added to the new flask for a final volume of 5ml. Complete DMEM was also added to the remaining cells in the trypsinised flask, to a final volume of 5ml, to keep as a backup. For passaging cells in T75 or T175 flasks, the aforementioned volumes were multiplied 3 and 7-fold respectively. Cell lines were routinely tested for *mycoplasma* contamination using the VenorGeM® *mycoplasma* PCR-based detection kit (Minerva labs, UK)

When counting cells to plate for an assay, cells were trypsinised and re-suspended in complete DMEM. Re-suspended cells were then diluted between 1:2 – 1:5 in trypan blue and 10 µl added to the chambers of a BRAND® haemocytometer, to count the number of cells. After counting, re-suspended cells were diluted accordingly in complete DMEM, then plated as required for the desired assay.

In order to prevent genetic drift, cells were passaged for a maximum of 6 months, and regularly cryo-preserved and stored in liquid nitrogen. To cryo-preserve, cells were routinely cultured in a T75 flask and allowed to grow to 70% confluence. Cells were then trypsinised and re-suspended in complete DMEM (as per section 2.2.1), prior to centrifugation at X 270g for 5 minutes to generate a cell pellet. Cell culture medium was subsequently aspirated from the cell pellet, and cells re-suspended in 3ml of freeze-down media (complete DMEM + 10% [v/v] DMSO). Cells were then equally aliquoted into three cryovials, which were transferred to a Nalgene® Mr frosty container

(containing propan-2-ol) and left overnight in a -80°C freezer. The following day, cryovials were transferred to a liquid nitrogen container, for long-term storage.

When required, cryo-preserved cells were thawed by placing cryovials (containing cells) in a 37°C water-bath for 2-3 minutes. Once thawed, cells were mixed with a total volume of 5ml complete DMEM in a falcon tube, then centrifuged at 270 x g for 5 minutes, to generate a cell pellet. Subsequently, cell culture medium was aspirated from the cell pellet, and cells re-suspended in 5ml of fresh complete DMEM. Re-suspended cells were then transferred into a T25 flask and allowed to grow under standard growth conditions. Within 3-5 passages, cells were expanded to grow in a T75 flask and cryo-preserved as previously described.

2.2.2. Generation of AT13148 resistant cell lines

As mentioned in section 2.2.1, A2780-148R, an AT13148 resistant sub-line derived from A2780 cells, was generated by Dr Denis Akan (Akan, 2015). This was accomplished by performing AT13148 dose-escalation on A2780 cells. Briefly, A2780 cells were grown under standard growth conditions in their half maximal growth inhibitory concentration (GI_{50}) of AT13148. Upon reaching ~70% confluency, A2780 cells were passaged and the concentration of AT13148 increased by 1x AT13148 GI_{50} value in A2780 cells. This process was repeated over a period of 6-months, from which the A2780-148R cell line was generated. A2780-148R cells were routinely sub-cultured in 5.2 µM AT13148 (x 13 the GI_{50} of A2780 cells), as described in section 2.2.1.

Isogenic sub-clones (148R clones) were derived from A2780-148R cells by limiting dilution. A2780-148R cells were seeded at 0.5 cells per well in a 96-well plate in 200 µl complete DMEM and grown under standard growth conditions. After plating, wells were inspected every day under light microscopy to check for visible colonies of cells; single colonies were visible 5-15 days after plating. When colonies became visible to the naked eye, cell culture medium was carefully aspirated and colonies were incubated with 40 µl trypsin-EDTA at 37°C until cells had detached, then resuspended in 200 µl complete DMEM and grown under standard growth conditions. This was to evenly to distribute cells across each well, to facilitate further growth in a 96-well plate. Upon reaching ~70-90% confluency, cells were again trypsinised, as previously described, and re-suspended

in complete DMEM to a final volume of 200 µl. Re-suspended cells were then transferred to a 24-well plate and additional complete DMEM added for a total volume of 500 µl per well. Upon reaching ~70-90% confluency, cells were rinsed with 400 µl PBS, prior to being incubated in 200 µl trypsin-EDTA at 37°C until cells had detached, then re-suspended in 800 µl complete DMEM. Re-suspended cells were then transferred to a 6-well dish and additional complete DMEM added for total volume of 2ml per well. This process was repeated to expand cells from a 6-well plate to a T25 flask, using 2 x the volumes described for trypsinising cells in 24-well plates. 148R clones were subsequently routinely sub-cultured in T25 flasks, as described in section 2.2.1, in complete DMEM containing 5.2 µM AT13148.

A2780-148R cells and 148R clones were removed from AT13148 one week prior to plating for an assay into drug-free complete DMEM, unless otherwise stated. Furthermore, when A2780-148R cells and 148R clones were thawed from cryopreservation (as described in section 2.2.1), cells were initially sub-cultured in drug-free complete DMEM for 2-3 passages, prior to being routinely sub-cultured in complete DMEM containing 5.2 µM AT13148.

2.3. Cell line growth characterisation

Cells were plated in seven 96-well plates in 200 µl of complete DMEM at multiple densities, as indicated in the text, and allowed to grow under standard growth conditions. Over the course of a week, one plate was fixed per day by the addition of 70 µl 10% (w/v) trichloroacetic acid (TCA), prior to being stained and analysed as described for the sulforhodamine B (SRB) cell viability assay (see section 2.4). Cell line growth characterisation assays were used to identify optimal seeding densities for subsequent SRB cell viability assays.

2.4. Sulforhodamine B cell viability assay

The sulforhodamine B (SRB) dye binds to basic to amino acids residues, so therefore can provide an estimation of cellular density and be used to measure cell viability (Skehan *et al.*, 1990). Cells were plated in a 96-well plate, in 160 µl complete DMEM, at the seeding densities indicated in the text, and allowed to grow under standard growth

conditions for 48 hours. Cells were not plated in the outer wells of 96-well plates; 200 µl per well of PBS was added instead. For screening response to compounds, drugs were serially diluted and added to cells in 40 µl of complete DMEM per well, at the concentrations indicated in the text. For untreated and DMSO-vehicle control wells, 40 µl per well of complete DMEM alone, or complete DMEM containing DMSO at the maximum concentration used for compound serial dilution, was respectively added. Cells were then grown under standard growth conditions for 96-hours, prior to being fixed with 70 µl per well of 10% (w/v) TCA for 30 minutes and then washed three times in water. After fixation, cells were then stained with 70 µl per well of 0.4% (w/v) SRB solubilised in 1% (v/v) acetic acid (ThermoFisher Scientific, USA) for 30 minutes and then washed three times in 1% (v/v) acetic acid to remove any excess SRB. Plates were subsequently dried in a 37°C oven for at least three hours, followed by addition of 100 µl per well of 10 mM Tris-base (ThermoFisher Scientific, USA) and then placed on a microplate shaker for 10 minutes to solubilise protein-bound SRB. Absorbances were read at a wavelength of 490 nm using a Victor X4 multi-label plate reader (PerkinElmer Life Sciences, USA). Raw absorbances were blank adjusted by subtracting the mean absorbance of the outer wells (in which no cells were plated) containing 100 µl Tris-base. These values were percentage normalised to the mean absorbance of the untreated control wells and GI_{50} values determined using non-linear regression on GraphPad Prism 6 (GraphPad Software Inc, USA).

An adapted SRB cell viability assay was performed in 24-well plates when analysing the response of cells to targeted knockdown of gene expression by small interfering RNAs (siRNAs; see section 2.6). When performing these assays, cells were fixed, stained and solubilized as described, but the volumes were adjusted as follows: 500 µl 10% (w/v) TCA, 500 µl 0.4% (w/v) SRB solubilised in 1% (v/v) acetic acid, and 250 µl 10 mM Tris-base. Raw absorbance values were read, and data analysed, as described for a 96-well plate.

2.5. Cell lysis and western blotting

2.5.1. Cell lysis

Lysis buffer (Table 2.2) was prepared in advance and stored in aliquots at -80°C.

Table 2.2: Components of lysis buffer. Lysis buffer components, concentrations used in lysis buffer, and manufacturer are given. HEPES: 4-(2-hydroxyethyl)-1-piperazineethanesulfonic acid, DTT: Dithiothreitol.

Component	Concentration	Manufacturer
HEPES pH 7.4	50 mM	Sigma-Aldrich, Germany
NaCl	250 mM	Sigma-Aldrich, Germany
Nonidet-P40 substitute	0.1% (v/v)	Roche, Switzerland
DTT	1 mM	Melford labs, UK
EDTA	1 mM	FisherScientific, UK
NaF	1 mM	Sigma-Aldrich, Germany
β-Glycerophosphate	10 mM	Sigma-Aldrich, Germany
Sodium orthovanadate	0.1 mM	Sigma-Aldrich, Germany
Complete™ protease inhibitor cocktail	1 tablet per 50 ml	Roche, Switzerland

Cells were plated in 10 cm dishes, 7 cm dishes, 6-well plates or 24-well plates in complete DMEM (seeding densities indicated in the text) and allowed to grow for up to 72 hours under standard growth conditions. If drug treatment was required, cell culture medium was removed after 48 hours and replenished with fresh complete DMEM containing drug (concentrations indicated in the text), and cells allowed to grow under standard growth conditions for an additional 4 hours, unless otherwise stated. To lyse cells, cell culture medium was removed and cells washed twice with ice-cold PBS, prior to the addition of ice-cold lysis buffer (components shown in Table 2.2). The volume of ice-cold lysis buffer added depended on the tissue culture plasticware used: for 10 cm dishes 100 μl was added; for 7 cm dishes 50 μl was added; for 6-well plates 20 μl was added; and for 24-well plates 10 μl was added. After ice-cold lysis buffer was added, cells were immediately manually scraped into lysis buffer, then transferred to pre-chilled microcentrifuge tubes and incubated on ice for 30 mins for cell lysis to occur. Lysates were then centrifuged at 14,000 x g for 10 mins at 4°C, to clear any insoluble material, and cleared lysate transferred to a clean microcentrifuge tube, which was either kept on ice for immediate use or snap-frozen on dry ice and stored at -80°C for future use.

2.5.2. Determination of protein concentration

To determine the total protein concentration of cell lysates, a BCA (Bicinchoninic acid) assay was performed using a Pierce™ BCA protein assay kit (ThermoFisher Scientific, UK; Smith *et al.*, 1985). Cleared lysates (from section 2.5.1) were diluted 10 to 20-fold in ddH$_2$0 (double distilled water) and 10 µl added in triplicate to a 96-well plate. On each plate, 10 µl of bovine serum albumin (BSA) protein standards (diluted 0.1 – 1.0 mg/ml) and ddH$_2$O blanks were also added in triplicate. A copper (II) sulfate solution was then diluted 1:50 in BCA and 200 µl added to each well. Plates were then placed on a microplate shaker for 30 seconds, prior to being incubated at 37 °C for 30 minutes. After incubation, absorbances were measured at a wavelength of 560 nm using a Victor X4 multi-label plate reader (PerkinElmer Life Sciences, USA). Raw absorbances were blank subtracted using the mean absorbance of ddH$_2$O blanks, and total protein concentration determined by generating a standard curve from BSA protein standards.

If the total protein concentration of cell lysate was predicted to be low (< 0.1 mg/ml in diluted cell lysate), a modified BCA assay was performed, in which BSA standards were diluted 5 – 500 µg/ml and 96-well plates were incubated in a 60 °C oven for 30 minutes. All data analysis was performed using Microsoft Excel 2016 (Microsoft, USA).

2.5.3. SDS-PAGE and western blotting

Protein expression and protein phosphorylation at specific sites was detected using sodium dodecyl sulphate-polyacrylamide gel electrophoresis (SDS-PAGE) followed by western blot analysis (Towbin *et al.*, 1979; Burnette, 1981). Cell lysates were thawed on ice and then normalised to the same protein concentration in lysis buffer and 5x sample buffer (0.3M Tris pH6.8, 50% [v/v] glycerol [ThermoFisher Scientific, UK] 25% [v/v] β-mercaptoethanol, 10% [w/v] SDS [ThermoFisher Scientific, UK] and 0.05% [v/v] bromophenol blue). Subsequently, to denature and reduce proteins, samples were heated at 95 °C for 5 minutes in a heat block and then briefly centrifuged.

After sample preparation, proteins were separated by molecular weight using SDS-PAGE under denaturing conditions (Laemmli, 1970). Equal amounts of protein (5 – 80 µg) were loaded into the wells of an 8%, 10% or 12% Tris-glycine gel (resolving gel), depending on the molecular weight of target proteins, containing a 4% stacking gel (components of

resolving and stacking gels are shown in Table 2.3). In addition, 7 μl of dual-coloured pre-stained protein standards (Bio-Rad, USA) were also loaded to monitor protein resolution across Tris-glycine gels. Gel electrophoresis was undertaken using a Hoefer SE250 electrophoresis unit (Hoefer, USA) with a Tris-glycine running buffer (25 mM Tris-base, 192 mM glycine, 0.1% [w/v] SDS) under a constant voltage of 150V. Gel electrophoresis was performed until the dye front was approximately 1 cm from the bottom edge of the Tris-glycine gel.

Table 2.3: Summary of the components of Tris-glycine gels. Table lists the concentrations and manufacturer of the components used to make Tris-glycine gels. TEMED: Tetramethylethylenediamine, APS: Ammonium persulfate.

Component	Resolving gel concentration	Stacking gel concentration	Manufacturer
Acrylamide/Bis (29:1)	8-12% (v/v)	4%	Bio-Rad, USA
Tris-HCl pH 8.8	0.375 M	N/A	Sigma-Aldrich, Germany
Tris-HCl pH 6.8	N/A	0.125 M	Sigma-Aldrich, Germany
SDS	0.1% (v/v)	0.1% (v/v)	Sigma-Aldrich, Germany
TEMED	0.05% (v/v)	0.1% (v/v)	Sigma-Aldrich, Germany
APS	0.05% (w/v)	0.05% (w/v)	Bio-Rad, USA

After protein electrophoresis, separated proteins were transferred to a methanol-activated 0.2 μm pore Immobilon-P polyvinylidene fluoride (PVDF) membrane (Millipore, USA), using a wet transfer system. Proteins were transferred for 75 minutes in pre-chilled transfer buffer (25 mM Tris-base, 192 mM glycine, 10% [v/v] methanol [ThermoFisher Scientific, USA]) under a constant voltage of 100V. After transfer, membranes were re-activated in methanol and briefly incubated in a ponceau S solution (0.1% [w/v] ponceau S in 5% [v/v] acetic acid), to check for efficient transfer of proteins and to aid in cutting PVDF membranes according to the molecular weight of target proteins. Membranes were then blocked for one hour in Tris-buffered-saline Tween buffer (TBS-T; 50 mM Tris pH 8.0, 150 mM NaCl, 0.1% [v/v] Tween-20) containing 5% (w/v) milk (Marvel, UK), on an orbital shaker. TBS-T containing 5% milk is henceforth referred to as blocking buffer and all subsequent antibody incubations and wash steps were performed using an orbital shaker.

Table 2.4: List of antibodies used for western blot analysis. CST: cell signalling technology

Primary Antibody	Supplier	Catalogue number	Species	Dilution
AKT	CST, USA	4691	Rabbit	1:5000
AKT pS473	CST, USA	4060	Rabbit	1:5000
DUSP 4	Santa Cruz, USA	sc-17821	Mouse	1:200
DUSP 5	Santa Cruz, USA	sc-393801	Mouse	1:100
DUSP 6	Santa Cruz, USA	sc-377070	Mouse	1:500
Elk-1	Santa Cruz, USA	sc-365876	Mouse	1:1000
Elk-1 pS383	Santa Cruz, USA	sc-8406	Mouse	1:200
ERK 1/2 pThr202/Tyr204	CST, USA	4370	Rabbit	1:4000
ERK1/2	CST, USA	4696	Mouse	1:8000
FGFR2	CST, USA	11835	Rabbit	1:1000
GAPDH	Chemicon, USA	MAB374	Mouse	1:200000
GSK3β	CST, USA	9315	Rabbit	1:2000
GSK3β pS9	CST, USA	5558	Rabbit	1:2000
IGF-1R β	CST, USA	3027	Rabbit	1:1000
MEK 1/2	CST, USA	9122	Rabbit	1:2000
MEK 1/2 pS217/221	CST, USA	9154	Rabbit	1:4000
MYPT1	CST, USA	8574	Rabbit	1:2000
MYPT1 pT696	CST, USA	5163	Rabbit	1:500
PRAS40	CST, USA	2691	Rabbit	1:10000
PRAS40 pT246	CST, USA	2640	Rabbit	1:2000
ROCK 1	CST, USA	4035	Rabbit	1:1000
ROCK 2	CST, USA	9029	Rabbit	1:1000
S6RP	CST, USA	2217	Rabbit	1:10000
S6RP pS235/236	CST, USA	2211	Rabbit	1:8000
Tubulin α 1B	Bio-Rad, USA	VPA00172	Rabbit	1:1000
β-Actin	Santa Cruz, USA	sc-47778	Mouse	1:4000
Secondary Antibody				
Anti-mouse HRP conjugate	Bio-Rad, USA	170-6516	Goat	1:10000
Anti-Rabbit HRP conjugate	Bio-Rad, USA	170-6515	Goat	1:10000

After blocking, membranes were incubated overnight at 4°C in blocking buffer containing diluted primary antibody (Table 2.4). The next day, membranes were washed twice for 10 minutes in TBS-T, prior to incubation for one hour at room temperature (RT) with goat anti-rabbit or goat anti-mouse horseradish peroxidase (HRP)-conjugated secondary antibody in blocking buffer (Bio-Rad, USA; Table 2.4). Membranes were then washed four times for five minutes in TBS-T and detection performed using Clarity™ western enhanced chemiluminescence (ECL) substrate (Bio-Rad, USA), according to

manufacturer's instructions. Bands were visualised by exposure to Hyperfilm ECL (GE healthcare, UK) and processed using an Optimax™ 2010 film processor (Protec, Germany).

2.5.4. Membrane stripping

Antibodies for phosphorylated proteins were stripped from membranes by incubation with stripping buffer (50 mM glycine, 1% [w/v] SDS, pH 2.0) for five minutes and then twice washed with TBS-T for five minutes. Membranes were then re-blocked in blocking buffer for 30 minutes and incubated with primary antibody for total protein overnight, as previously described (section 2.5.3). If required, this process was repeated to re-probe membranes with primary antibodies for loading controls (Table 2.4).

2.6. Knockdown of gene expression with small interfering RNA

Small interfering RNAs (siRNAs) were used for the transient knockdown of target gene expression in cells, using reverse transfection with Lipofectamine 2000 (ThermoFisher Scientific, USA), a lipid-based transfection reagent. Lipofectamine 2000 and siRNA oligonucleotides were used at the concentrations indicated in the text. Non-targeting control and death control siRNA oligonucleotides were used to establish transfection efficiency and toxicity. The sequences of siRNA oligonucleotides and manufacturers are shown in Table 2.5.

Lipofectamine 2000 and siRNA oligonucleotides were appropriately diluted and mixed together in Opti-MEM™ reduced serum medium (ThermoFisher Scientific, USA), then incubated for 15 minutes at RT to complex. In the meantime, cells were trypsinised, counted (as per section 2.2.1), and appropriately diluted in complete DMEM, depending on the seeding density required.

For 96-well SRB assays, 50 µl of lipid/oligonucleotide complex was added per well followed by 110 µl of cells in complete DMEM per well (at the seeding densities indicated in the text) and allowed to grow for 24 hours under standard growth conditions, prior to treatment with inhibitors in 40 µl of complete DMEM (at the concentrations indicated in the text). After treatment, cells were grown for an additional 72 hours under standard growth conditions, and cell viability analysed by SRB assay (as per section 2.4).

Table 2.5: List of siRNA oligonucleotides used

siRNA	Target gene	Target sequence (5'-3')	Manufacturer
D-003964-01	DUSP6	GAACUGUGGUGUCUUGGUA	Dharmacon, USA
D-003964-03	DUSP6	UGGGUUACCUUAUGCAGAA	Dharmacon, USA
D-003964-04	DUSP6	GACUGUGGCUUACCUUAUG	Dharmacon, USA
D-003964-05	DUSP6	GCGACUGGAACGAGAAUAC	Dharmacon, USA
SMARTpool	DUSP6	pool of individual DUSP6 siRNAs	Dharmacon, USA
AllStars negative control	Non-targeting	Sequence validated by QIAGEN	QIAGEN, Germany
AllStars Hs cell death control	Death control	Sequence validated by QIAGEN	QIAGEN, Germany

To assess knockdown of target gene expression by siRNA, western blot analysis was performed, in parallel with SRB cell viability assays. Lipid/oligonucleotide complexes and cells were prepared as described, and after complexing, 500 µl of lipid/oligonucleotide complex was added per well of a 6-well plate, followed by the addition of 1.1 ml of cells, at the seeding densities indicated in the text. Cells were then allowed to grow under standard growth conditions for 24-96 hours, depending on the timepoint being analysed, prior to cell lysis and western blot analysis (see section 2.5).

A modified 2-day SRB cell viability was also performed in a 24-well plate, in which western blot analysis was performed in parallel in a separate 24-well plate. Lipid/oligonucleotide complexes and cells were prepared as described, and after complexing, 125 µl of lipid/oligonucleotide complex was added to each well of a 24-well plate, prior to the addition of cells at 275 µl per well, at the seeding densities indicated in the text. Cells were then incubated for 4 hours under standard growth conditions, then treated with inhibitors in 100 µl of complete DMEM, at the concentrations indicated in the text, followed by an additional incubation for 48 hours under standard growth conditions. Cell viability was subsequently analysed using an SRB assay (see section 2.4). For western blot analysis, after the addition of lipid/oligonucleotide complex and cells, cells were incubated for 4-52 hours, depending on the timepoint being analysed, prior to cell lysis and western blot analysis (see section 2.5).

2.7. Plasmid DNA preparation

2.7.1. Plasmid recovery

The lentiviral plasmid pLenti-DUSP6-C-Myc-DDK, was a kind gift from Dr Osamu Tetsu (University of California, San Francisco, USA; orginal publiation: Phuchareon *et al.*, 2015), which was provided spotted on a piece of filter paper. Spotted plasmid DNA was cut out of the filter paper and placed in a microcentrifuge tube with 200 µl Tris-EDTA buffer (TE; 10 mM Tris pH 8.0, 1 mM EDTA), briefly vortexed, and allowed to incubate at RT for 10 minutes. Subsequently, 1 µl of recovered plasmid DNA was used to transform competent *E.coli* (see section 2.7.2). The lentiviral plasmids pCMV-dR8.91 and pMD2.G were both kind gifts from Dr Tim Fenton (University of Kent, UK) and were provided as glycerol stocks of transformed *E.coli*. These were streaked on lysogeny broth (LB) agar plates (1% [w/v] bacto-tryptone, 0.05% [w/v] yeast extract, 0.05% [w/v] NaCl and 1.5% [w/v] agar) containing 125 µg/ml ampicillin, and incubated overnight at 37°C. Colonies were subsequently picked for overnight growth in LB (see section 2.7.2).

2.7.2. Transformation of plasmid DNA

Plasmid DNA was amplified by the transformation of calcium competent DH5α *E. coli* cells (a kind gift from Dr Mark Shepherd, University of Kent). 1 µl of recovered plasmid DNA was added to a 50 µl aliquot of freshly thawed competent cells and allowed to incubate on ice for 30 minutes. To heat shock competent cells the DNA/*E. coli* mixture was heated in a 42°C water-bath for one minute, prior to being cooled on ice for two minutes, followed by addition of 950 µl of lysogeny broth (LB; 1% [w/v] bacto-tryptone, 0.05% [w/v] yeast extract, 0.05% [w/v] NaCl) and incubation in a 37°C water-bath at 180 rpm for 45 minutes. Transformed *E.coli* was then spread on LB agar plates (1% [w/v] bacto-tryptone, 0.05% [w/v] yeast extract, 0.05% [w/v] NaCl and 1.5% [w/v] agar), containing 125 µg/ml of ampicillin or 34 µg/ml of chloramphenicol, depending on the on the antibiotic resistance gene present on plasmids, and incubated overnight in a 37°C incubator. Subsequently, colonies were picked and used to inoculate 10 ml or 30 ml of LB, containing 125 µg/ml of ampicillin or 34 µg/ml of chloramphenicol, and incubated at 37°C overnight in a water-bath at 180 rpm. After overnight culture, glycerol stocks were prepared by mixing 500 µl of transformed *E. coli* (from overnight culture) with 500 µl 50% (v/v) glycerol in a cryovial, which was then stored at -80°C for future use.

2.7.3. Extraction of plasmid DNA

For small-scale purification of plasmid DNA, 1.5 ml of overnight culture from transformed *E. coli* was used (see section 2.7.2). *E. coli* cells were pelleted by centrifugation at 16,000 x g for 30 seconds followed by extraction of plasmid DNA from the cell pellet using a Monarch plasmid miniprep kit, according to manufactures instructions (New England Biolabs, USA). Plasmid DNA was eluted in a final volume of 40 µl TE buffer. For mid-scale purification of plasmid DNA, 30ml of overnight culture from transformed *E. coli* was used (see section 2.7.2). *E.coli* cells were pelleted by centrifugation at 4000 x g for 15 minutes followed by extraction of plasmid DNA from the cell pellet using a QIAGEN plasmid plus midi kit, according to the manufacturer's instructions (QIAGEN, Germany), plasmid DNA was eluted in a final volume of 200 µl TE buffer. Plasmid DNA concentration was determined using a Nanodrop ND-1000 UV/Vis spectrophotometer (Nanodrop, USA).

2.8. Generation of DUSP6 expressing lentivirus

2.8.1. Co-transfection of lentiviral plasmids into HEK293T cells

HEK293T cells were plated in complete DMEM at a density of 3.5×10^6 cells per 10 cm dish and allowed to adhere and grow overnight under standard growth conditions. After overnight growth, cells were between 50-80% confluent and ready for transfection using Lipofectamine 2000. A 50µl Opti-MEM™ solution was prepared containing the following amount of lentiviral plasmids: 2 µg pLenti-DUSP6-C-Myc-DDK, 1.5 µg pCMV-dR8.91 and 1.5 µg pMD2.G. This was mixed 1:1 with a 48% (v/v) Lipofectamine 2000 solution (in Opti-MEM™) and incubated at room temperature for 20-30 minutes to allow plasmid DNA and Lipofectamine 2000 to complex. Cell culture medium was then removed from HEK293T cells, replaced with 8ml Opti-MEM™, and 100µl of complexed plasmid DNA/lipid added dropwise. Dishes were then gently agitated to ensure equal distribution of the complexed plasmid DNA/Lipid, prior to being incubated for 5 hours under standard growth conditions, to allow transfection to proceed. After transfection, Opti-MEM™ was aspirated and replaced with complete DMEM and cells grown for a further 48 hours under standard growth conditions. Cell culture medium containing lentivirus (viral supernatant) was then removed from HEK293T cells, transferred to a

50ml falcon and centrifuged at 3000 x g for 1 min, to pellet any cells/cell debris. Viral supernatant was subsequently removed from any cells/cell debris that had pelleted and passed through a 0.44 μM filter using a syringe, then aliquoted and frozen at -80°C, or if supernatant was to be purified, stored overnight at 4°C prior to purification the following day.

2.8.2. Polyethylene glycol purification of lentivirus

For purification of lentivirus, polyethylene glycol (PEG) purification was performed, using a protocol adapted from Kutner and colleagues (Kutner *et al.*, 2009). In order to purify lentivirus, the following solution was prepared: 40.8ml crude viral supernatant, 13.9ml 36.5% (w/v) PEG 6000, 4.3ml 4M NaCl and 1ml of PBS, which resulted in final concentration of 8.5% PEG 6000 and 0.3M NaCl in a total volume of 60ml. The solution was incubated at 4°C for 1.5 hours, being mixed by gentle inversion every 20-30 minutes. After incubation, the solution was aliquoted into two 50 ml tubes and centrifuged at 7000 x g for 10 minutes at 4°C, to pellet precipitated lentivirus. Supernatant was subsequently removed and the pellet, containing purified lentivirus, re-suspended in a total volume of 480 μl of 50 mM Tris-HCl pH 7.4. Purified lentiviral vector was then vortexed for 20-30 seconds, snap-frozen on dry-ice and stored at -80°C for future use.

2.9. Generation of transient over-expressing cell lines using lentiviral transduction

Cells were plated in a 6-well plate at 5×10^5 cells per well and allowed to grow overnight under standard growth conditions. The next day, cells were 50-80% confluent and ready for lentiviral transduction. Lentivirus was diluted, as shown in the text, in complete DMEM supplemented with 5-10 μg/ml of hexadimethrine bromide (polybrene; Merck, USA). Cell culture medium was then removed from 6-well plates and replaced with 1 ml per well of diluted lentivirus, or complete DMEM supplemented with 5-10 μg/ml of polybrene to use as a control. Plates were then gently agitated, to ensure an even distribution of lentiviral particles, and grown under standard growth conditions for 24 hours. Cell culture medium was then aspirated off and cells washed in PBS, prior to being trypsinised and re-suspended in complete DMEM. Cells were then either plated in 6-

well plates, for western blot time point analysis (see section 2.5), or in 96-cell plates for SRB cell viability assays (see section 2.4), at the densities indicated in the text.

Chapter 3

**Investigating AT13148 resistance
in A2780-148R**

3. Investigating AT13148 resistance in A2780-148R

3.1. Introduction

In 2012, a project was initiated to identify potential mechanisms of acquired resistance to AKT inhibitors, including AT13148. This project was conducted at both the ICR and University of Kent, the results of which are currently un-published or published as part of a doctoral thesis (Akan, 2015). In this project, resistance was generated against AT13148 in the human ovarian carcinoma cell line A2780. A2780 was selected as this cell line harbours a loss of function *PTEN* mutation (383-391 deletion), decreasing PTEN lipid phosphatase activity, and a gain of function *PIK3CA* mutation (E365K substitution), increasing p110α PI3K activity (Saito *et al.*, 2000; Wee *et al.*, 2008; Hanrahan *et al.*, 2012; cancer.sanger.ac.uk - COSMIC: the cataologue of samatic mutations in cancer). Together, these mutations cause hyperactive PAM pathway signalling in A2780, a potential clinical indication for use of AT13148 (section 1.5).

Resistance to AT13148 was generated by dose-escalation, a process whereby the concentration of AT13148 that A2780 cells were exposed to was incrementally increased over a 6-month period. At the end of this process, an A2780 derived AT13148 resistant cell line was generated, A2780-148R, which was routinely sub-cultured in 5.2 µM AT13148, 13x the GI_{50} of parental A2780 cells against AT13148 (0.40 µM, Table 3.1). A2780-148R was subsequently used as model to investigate mechanisms of acquired resistance to AT13148.

As part of the project extensive cross-resistance profiling was conducted on A2780-148R, the results of which are summarised in Table 3.1. One of the most interesting findings of cross-resistance profiling was that A2780-148R cells were sensitive to linsitinib and NVP-AEW541, both inhibitors of IGF-1R. In addition, IGF-1R was found to be over-expressed via microarray analysis, which was later validated at the protein level using western blotting. The over-expression of IGF-1R was subsequently investigated as a mechanism of resistance to AT13148.

To this end, A2780 cell line clones stably expressing IGF-1R were generated to assess if over-expression of IGF-1R alone could confer resistance to AT13148. However, the level

of IGF-1R over-expression was not found to correlate with resistance to AT13148, thus suggesting that the over-expression of IGF-1R alone was not sufficient to confer the AT13148-resistant phenotype. In addition, the inverse experiment was performed, whereby IGF-1R was knocked-down in A2780-148R cells using siRNA. Whilst knockdown of IGF-1R did not sensitize A2780-148R cells to AT13148, it did significantly reduce viability in untreated A2780-148R cells, but not A2780 cells, pheno-copying the effect of IGF-1R inhibition. Together, these data suggested that the over-expression IGF-1R alone does not confer resistance AT13148, but that A2780-148R cells have an increased dependency on IGF-1R for their growth and survival. Therefore, IGF-1R inhibition may still be a valid therapeutic strategy in AT13148 resistant tumours over-expressing IGF-1R.

The over-expression of IGF-1R was the only candidate mechanism of resistance that was identified and investigated in A2780-148R. However, cross-resistance profiling did reveal other notable changes, which could be implicated in resistance. Perhaps the most striking was that A2780-148R cells were found to be cross-resistant to two ROCK inhibitors: Y-27632 and GSK429286A (Table 3.1). This was of particular interest since ROCK1 and 2 are potently inhibited by AT13148 and clinically relevant targets. Cross-resistance profiling also demonstrated that A2780-148R cells were sensitive to AZD4547, an FGFR inhibitor (Table 3.1). This was in parallel with upregulation in the gene expression of fibroblast growth factor receptor 1 & 2 (FGFR1 and FGFR2) in A2780-148R, which was identified by microarray analysis (Akan, 2015).

However, whilst the cross-resistance profiling previously performed had been extensive, some important targets had been overlooked (Table 3.1). One such target was the Src family of kinases (SFKs), a family of non-receptor tyrosine kinases renowned for being pleiotropic, interacting with several different pathways (Bromann *et al.*, 2004). In particular, SFKs are known to interact with a number of receptor tyrosine kinases (RTKs), for example, Src, the founding member of SFK's, has been shown to phosphorylate autophosphorylation sites on IGF-1R, inducing its activation (Peterson *et al.*, 1996; Bromann *et al.*, 2004). In addition, Src has also been shown to regulate ROCK signalling via its activating tyrosine phosphorylation of p190RhoGAP (GAP: GTPase activating protein), which potentiates hydrolysis of GTP to GDP, inactivating Rho and therefore its

downstream effectors ROCK1 & 2 (Fincham *et al.*, 1999). Since A2780-148R has been shown to have increased sensitivity to IGF-1R inhibition, as well as increased IGF-1R expression, and cross-resistance to ROCK inhibition, SFK's are a worthwhile target for cross-resistance profiling.

In summary, the previous work conducted on acquired resistance to AT13148 in A2780-148R has helped gain clinically relevant insight into AT13148 resistance, however, a bona fide mechanism of resistance has not been identified. Therefore, the aim of this chapter was to further investigate mechanisms of acquired resistance to AT13148 using A2780-148R as a model. Initially, to ensure A2780-148R was behaving as previously described, key findings, such as IGF-1R over-expression and sensitivity to IGF-1R inhibition, were validated. In addition, cross-resistance to ROCK inhibition and sensitivity to FGFR inhibition were investigated, and cross-resistance profiling extended to include SFK inhibitors. Furthermore, the potential contribution of the MAPK pathway to AT13148 resistance was also investigated.

Table 3.1: Summary of previous cross-resistance profiling conducted on A2780-148R. Table summarises GI$_{50}$ and resistance factor (RF; A2780-148R GI$_{50}$/A2780 GI$_{50}$) data from cross-resistance profiling. Data points are the mean ± SD of all experiments conducted. Cross-resistance (RF ≥ 2.00) was highlighted in red and sensitivity (RF ≤ 0.50) in green. Statistical significance calculated using a student's t-test, * $p ≤ 0.05$, ** $p ≤ 0.01$, *** $p ≤ 0.001$. n ≥ 3 independent experiments. Data adapted from a doctoral thesis (Akan, 2015) and unpublished data.

		A2780	A2780-148R	
Drug	**Target**	**GI$_{50}$**	**GI$_{50}$**	**RF**
5 FdU (nM)	Pyrimidine analogue	51.10 ± 17.00	36.10 ± 3.90	0.71
AT13148 (µM)	AGC kinases	0.40 ± 0.17	3.71 ± 0.68 *	9.25
AUY-922 (nM)	HSP90	5.50 ± 1.00	4.7 ± 0.40	0.85
AZD2014 (µM)	mTORC1/2	0.03 ± 0.03	0.05 ± 0.04*	1.67
AZD4547 (µM)	FGFR 1-3	0.09 ± 0.05	0.02 ± 0.01*	0.22
Capiverasertib (µM)	AKT	0.72 ± 0.21	0.77 ± 0.19	1.07
BI-D1870 (µM)	p90RSK	2.02 ± 0.19	1.20 ± 0.07**	0.59
Bleomycin (IU ml-1)	DNA	0.10 ± 0.04	0.05 ± 0.02	0.50
Cisplatin (µM)	DNA	1.09 ± 0.42	1.19 ± 0.32	1.09
Crizotinib (µM)	ALK/MET/ROS1	0.24 ± 0.02	0.19 ± 0.02*	0.79
Doxorubicin (nM)	DNA	8.66 ± 2.86	8.14 ± 3.94	0.94
Everolimus (nM)	mTORC1	1.43 ± 0.49	3.23 ± 0.99*	2.26
GDC-0879 (µM)	B-RAF	7.19 ± 3.53	5.49 ± 2.93	0.76
GDC-0941 (µM)	PI3K	0.10 ± 0.03	0.10 ± 0.03	1.00
GSK2334470 (µM)	PDK1	1.01 ± 0.08	0.98 ± 0.38	0.97
GSK429286A (µM)	ROCK	3.98 ± 1.10	40.30 ± 5.70***	10.13
H1152 (µM)	ROCK	0.78 ± 0.15	1.24 ± 0.45	1.59
INCB018424 (µM)	JAK1/2	15.10 ± 1.20	14.40 ± 1.40	0.95
Lapatinib (µM)	EGFR/HER2	4.71 ± 0.48	6.04 ± 0.16*	1.28
Linsitinib (µM)	InsR/IGF-1R	5.91 ± 2.61	0.75 ± 0.57*	0.13
Mitomycin C (nM)	DNA	13.4 ± 6.0	9.8 ± 5.6	0.73
MK2206 (µM)	AKT	0.30 ± 0.25	0.29 ± 0.21	0.97
Nintedanib (µM)	VEGFR/FGFR/PDGFR	0.40 ± 0.11	0.47 ± 0.15	1.18
NVP-AEW541 (µM)	IGF1R	3.05 ± 0.35	0.18 ± 0.03***	0.06
Paclitaxel (nM)	Tubulin	1.19 ± 0.50	1.95 ± 0.82	1.63
PD0325901 (µM)	MEK	0.069 ± 0.030	0.098 ± 0.049	1.42
PF4708671 (µM)	p70S6K	8.30 ± 1.96	16.70 ± 3.20*	2.01
PI-103 (µM)	PI3K/mTOR/DNA-PK	0.11 ± 0.04	0.12 ± 0.03	1.09
PP242 (µM)	mTORC1/2	0.12 ± 0.02	0.12 ± 0.03	1.00
SB203580 (µM)	p38 MAPK	32.3 ± 4.6	37.1 ± 4.6	1.15
SN38 (nM)	Topoisomerase I	2.30 ± 0.01	1.88 ± 0.13**	0.82
Y-27632 (µM)	ROCK	19.00 ± 3.00	58.70 ± 4.50***	3.09

3.2. Results

3.2.1. Growth characterisation of A2780 and A2780-148R cells

Before SRB cell viability assays could be performed, the optimal seeding densities for A2780 and A2780-148R cells in a 96-well plate were established. This was to ensure that both cell lines were in log phase growth and had similar growth kinetics during the 96-hour drug treatment window of a standard 6-day SRB cell viability. Therefore, one could be confident that results obtained from SRB cell viability assays were due to genuine differences in how the cells responded to a drug, rather than an artefact caused by a difference in growth kinetics.

Cells were plated at various densities in 96-well plates, and one plate fixed per day, and analysed via SRB assay. Figure 3.1 shows that the optimal seeding density for A2780 and A2780-148R was 800 and 1600 cells per well respectively. At these densities, cells were at log phase growth between 48 hours and 144 hours, the 96-hour drug treatment window in a standard 6-day SRB cell viability assay. In addition, when the optimal seeding densities were superimposed on one another, it was shown that they had near identical growth (Figure 3.1). The doubling times for A2780 and A2780-148R, when plated at their optimal seeding density, was also calculated using the following equation (OD: optical density):

$$Doubling\ time = \frac{96\ hours * \log(2)}{\log(OD\ at\ 144\ hours) - \log(OD\ at\ 48\ hours)}$$

The doubling times were found to be very similar with A2780 having a doubling time of 23.6 hours and A2780-148R 26.5 hours (Figure 3.1). Taken together, optimal seeding densities for A2780 and A2780-148R were established that enabled near-identical growth kinetics over the course of a standard 6-day SRB cell viability assay.
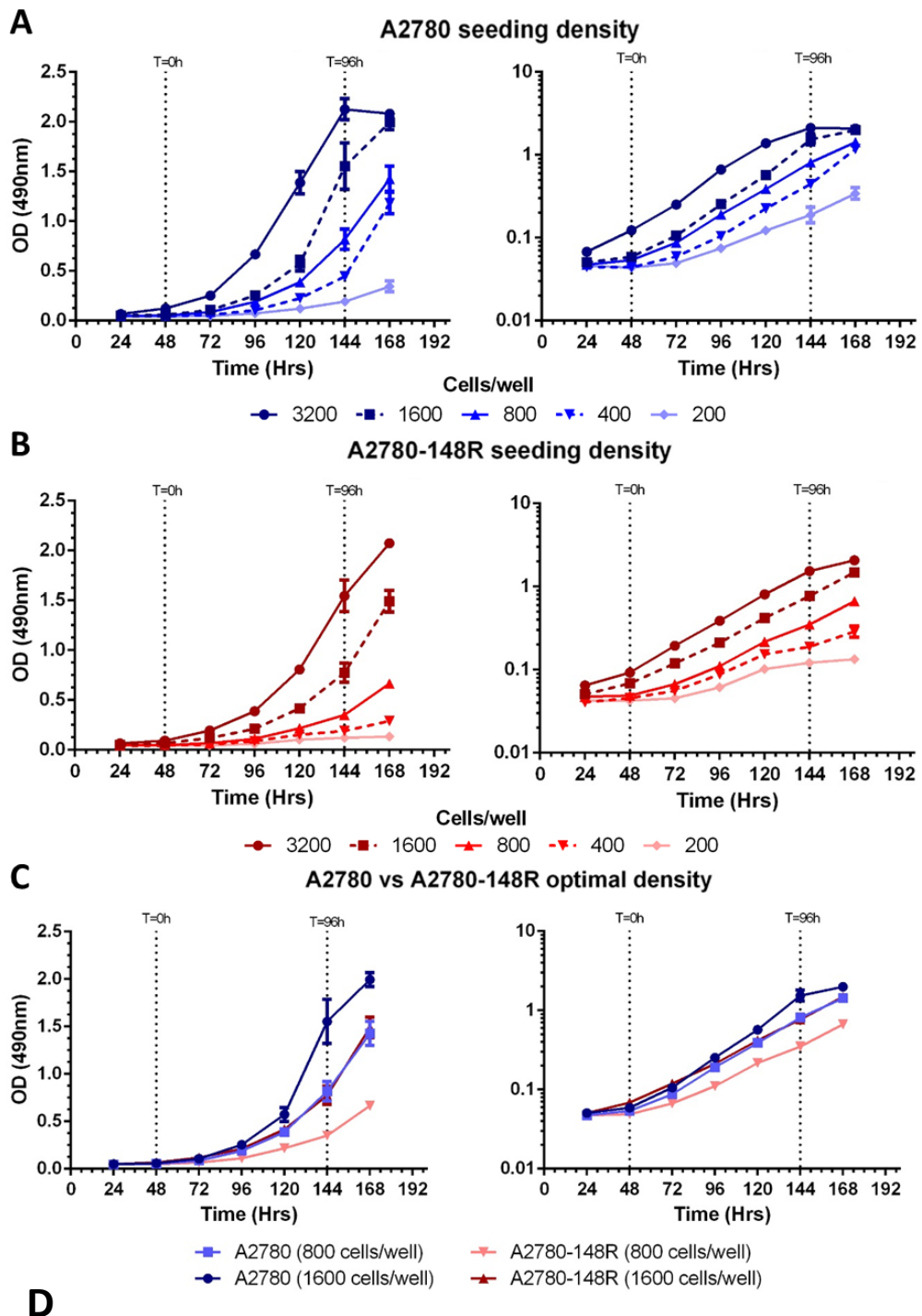
Figure 3.1: Characterisation of A2780 and A2780-148R cell line growth in a 96-well plate. Cells were plated at the densities indicated, with 6 replicates per density, in 96-well plates. A plate was fixed every 24 hours and analysed via SRB assay. Growth curves were generated using GraphPad Prism 6 for **(A)** A2780 **(B)** A2780-148R **(C)** over-lay of selected optimal seeding densities for A2780 and A2780-148R. T=0h and T=96h highlight the 96-hour time period in which cells would be treated with drug in a standard 6-day SRB cell viability assay. Data points represent the mean ± SD of one representative experiment. **(D)** Table summarises the doubling times of A2780 and A2780-148R in a 96-well plate at their optimal seeding densities. Data points represent the mean ± SD from n = 3 independent experiments.

3.2.2. Response of A2780 and A2780-148R to AT13148 and DMSO

After their optimal seeding densities had been established, A2780 and A2780-148R could be further characterised by SRB cell viability assays. This was used to generate dose-response curves to drugs/tool compounds and identify GI_{50} values, the concentration of drug required to cause a 50% reduction in cell viability in a standard 6-day SRB cell viability assay. The GI_{50} values could then be used to calculate a resistance factor (RF, equation shown below), a ratio of resistant cell line GI_{50} to parental cell line GI_{50}, a measure of resistance/sensitivity. E.g. an RF value of 2 would indicate 2-fold resistance to a drug, whereas an RF value of 0.5 would indicate 2-fold sensitivity.

$$Resistance\ factor\ (RF) = \frac{Mean\ Resistant\ GI_{50}}{Mean\ Parental\ GI_{50}}$$

At first, it was crucial to validate the resistance of A2780-148R against AT13148. Figure 3.2A & C shows that A2780-148R was resistant to AT13148; the GI_{50} for parental A2780 cells was 0.27μM, whereas A2780-148R had a GI_{50} of 1.36μM. This was shown to be statistically significant and equated to an RF value of 5.04 (Figure 3.2A & C). This was lower than what has been previously described for AT13148 (RF = 9.25, Table 3.1), but nonetheless validated the resistance of A2780-148R against AT13148 and its use as a model to identify acquired mechanisms of resistance to AT13148.

Since all the drugs used in chapter 3 were dissolved in DMSO, a polar aprotic solvent which can be toxic to cells (Jamalzadeh *et al.*, 2016), DMSO toxicity was assessed in a standard 6-day SRB cell viability assay. Figure 3.2B shows that A2780 and A2780-148R responded in a similar manner to DMSO. From the dose-response curves it was determined that 0.2% was the maximum concentration of DMSO that could be used without significantly effecting cell viability in this assay format. Therefore, where possible, the highest concentration of DMSO to be used in SRB cell viability assays was 0.2%.

A

B

C

	A2780	A2780-148R	
Drug	**GI_{50}**	**GI_{50}**	**RF**
AT13148 (µM)	0.27 ± 0.15	$1.36 \pm 0.77{***}$	5.04
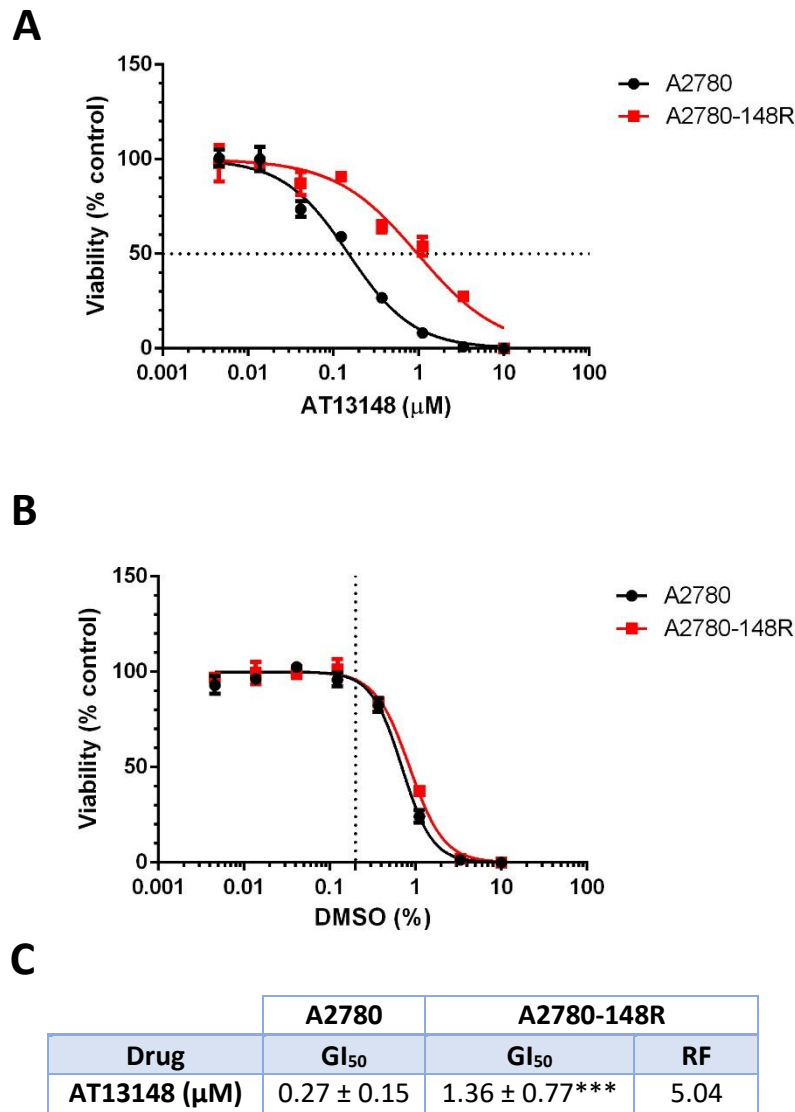
Figure 3.2: Dose-response curves for AT13148 and DMSO, and GI_{50} determination for AT13148, in A2780 and A2780-148R cells. Cells were plated in triplicate in a 96-well plate and allowed to grow under standard growth conditions for 48 hours. They were then treated with a serial dilution of AT13148 or DMSO for 96-hours, prior to being analysed by an SRB assay. Dose-response graphs were generated for **(A)** AT13148 and **(B)** DMSO using GraphPad Prism 6, curves were fitted using non-linear regression. Dotted line marks the GI_{50} of AT13148 or effect of 0.2% DMSO. Data points represent the mean ± SD from one representative experiment. **(C)** Table summarises AT13148 GI_{50} and RF, data points are the mean ± SD of all experiments conducted. Statistical significance was calculated using a student's t-test, *** *p ≤ 0.001*. n = 17 (AT13148) or 4 (DMSO) independent experiments.

3.2.3. Light microscopy of A2780 and A2780-148R

Cancer cells exhibit a wide variety of morphologies which are related to their tissue of origin, adaptive changes during tumorigenesis, and can also be altered during therapy resistance. Therefore, the morphology of A2780 and A2780-148R was investigated under light microscopy, to see if any insight could be gained into their response to AT13148 and possibly resistance. Figure 3.3 shows that A2780 cells had a similar morphology to what has been previously described (Haslehurst *et al.*, 2012); they grew as compact 'pebble-like' clusters, with cells having a rounded/polygonal morphology, consistent with an epithelial phenotype. A2780-148R had a similar morphology, displaying an epithelial phenotype, however they appeared slightly larger and grew in a less compact manner; growing as large branches of inter-connected cells (Figure 3.3). Both A2780 and A2780-148R didn't appear to undergo contact-inhibition; cells grew on top of one another, particularly with A2780 cells (Figure 3.3)

Cells were also treated with 5.2 µM of AT13148, the concentration that A2780-148R is routinely cultured in (maintenance dose of AT13148) and allowed to grow for 48 hours. In response to AT13148, A2780 and A2780-148R both developed a "spindle-like morphology", with cells becoming long and thin (Figure 3.3). However, it should be noted that the spindle-like morphology was only seen in a subset of the total population of cells. A2780 cells also appeared to be undergoing membrane blebbing, suggesting an apoptotic response to AT13148, which was not apparent in A2780-148R, both treated and untreated, or untreated A2780 cells (Figure 3.3).
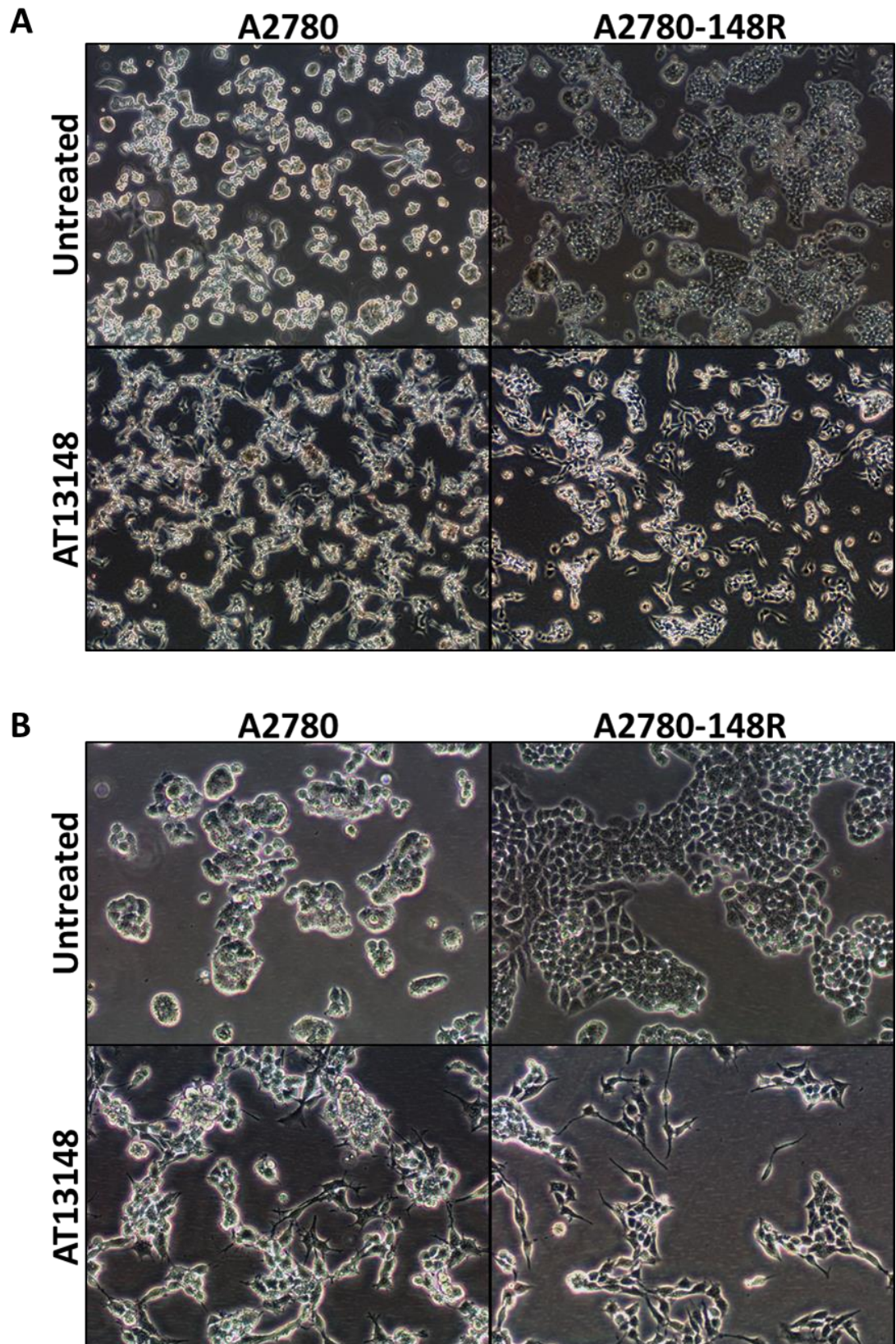
Figure 3.3: Images of untreated and AT13148 treated A2780 and A2780-148R cells under light microscopy. Cells were split into T25 flasks to allow 2-3 days growth, and either left untreated or treated with 5.2μM AT13148. After 48 hours, when cells were ~70% confluent, cells were observed under a light microscope at **(A)** x40 or **(B)** x100 magnification, and images taken. Images representative of two independent experiments.

3.2.4. Cross-resistance profiling of A2780-148R

Cross-resistance profiling was undertaken by performing SRB cell viability assays using various drugs and tool compounds targeting several different signalling pathways. Identifying a differential response (resistance or sensitivity) of A2780-148R, when compared to A2780, may provide insight into mechanisms of resistance against AT13148.

3.2.4.1. AKT inhibition

AT13148 is known to target both AKT1 and AKT3 (Yap *et al.*, 2012), so it's possible that altered signalling within the PAM pathway could contribute towards resistance against AT13148. Therefore, A2780 and A2780-148R cells were profiled with the ATP-competitive pan-AKT inhibitor capiverasertib (AZD5363, Davies *et al.*, 2012). Figure 3.4 shows A2780 had a GI_{50} of 0.18 µM, whereas A2780-148R had GI_{50} of 0.55 µM. This difference was statistically significant, resulting in an RF value of 3.06, indicating low-level cross-resistance (Figure 3.4). However, it should be noted that this was not previously demonstrated (RF = 1.07, Table 3.1).
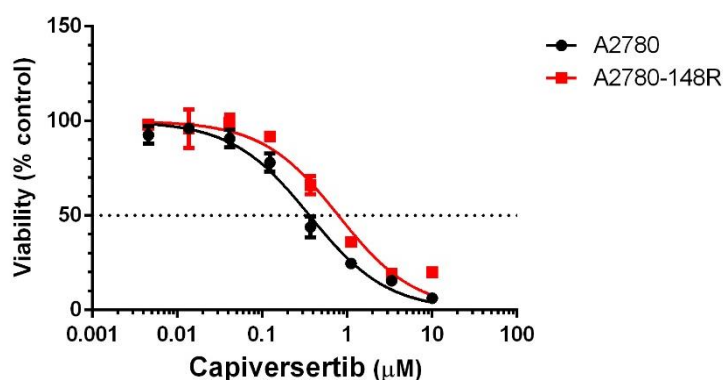
	A2780	A2780-148R	
Drug	GI_{50}	GI_{50}	RF
Capiverasertib (µM)	0.18 ± 0.02	0.55 ± 0.013*	3.06

Figure 3.4: Dose-response curves and GI_{50} determination for capiverasertib in A2780 and A2780-148R cells. Cells were plated in triplicate in a 96-well plate and allowed to grow under standard growth conditions for 48 hours. They were then treated with a serial dilution of capiverasertib for 96-hours, prior to being analysed by SRB assay. Dose-response graphs and non-linear regression curves were generated using GraphPad Prism 6. Dotted line marks 50% viability on the y-axis. Data points represent the mean ± SD from one representative experiment. Table summarises capiverasertib GI_{50} and RF, data points represent the mean ± SD of all experiments conducted. Statistical significance was calculated using a student's t-test, * *p ≤ 0.05*. n = 3 independent experiments.

3.2.4.2. ROCK inhibition

Previous work had demonstrated that A2780-148R cells were cross-resistant to ROCK inhibition (Table 3.1). In order to validate this, cross-resistance to ROCK inhibition was investigated using two ROCK inhibitors: GSK429286A, which A2780-148R had previously been shown to be cross-resistant to (Table 3.1), and GSK269962, a more potent ROCK inhibitor (Lotz-Jenne *et al.*, 2016). Figure 3.5A & C shows that there was a statistically significant difference in the response to GSK429286A; A2780 had a GI_{50} of 1.89 μM and A2780-148R had a GI_{50} of 40.43 μM. This resulted in an RF value of 21.39, indicating a high level of cross-resistance to GSK429286A (Figure 3.5C), and ~2-fold increase compared to what had been shown previously (RF = 10.13, Table 3.1). However, the cross-resistance to GSK269962 was shown to be even greater; the GI_{50} of A2780 was 0.02 μM compared to 1.72 μM in A2780-148R (Figure 3.5B & C). This difference was also statistically significant, resulting in an RF value of 86.00, demonstrating a strong level of cross-resistance to GSK269962 (Figure 3.5C). Taken together, these data validate cross-resistance to ROCK inhibition, perhaps suggesting altered ROCK signalling in AT13148 resistance, which warrants further investigation.

A

B

C

	A2780	A2780-148R	
Drug	**GI_{50}**	**GI_{50}**	**RF**
GSK429286A (µM)	1.89 ± 1.10	40.43 ± 20.96*	21.39
GSK269962 (µM)	0.02 ± 0.01	1.72 ± 1.07***	86.00
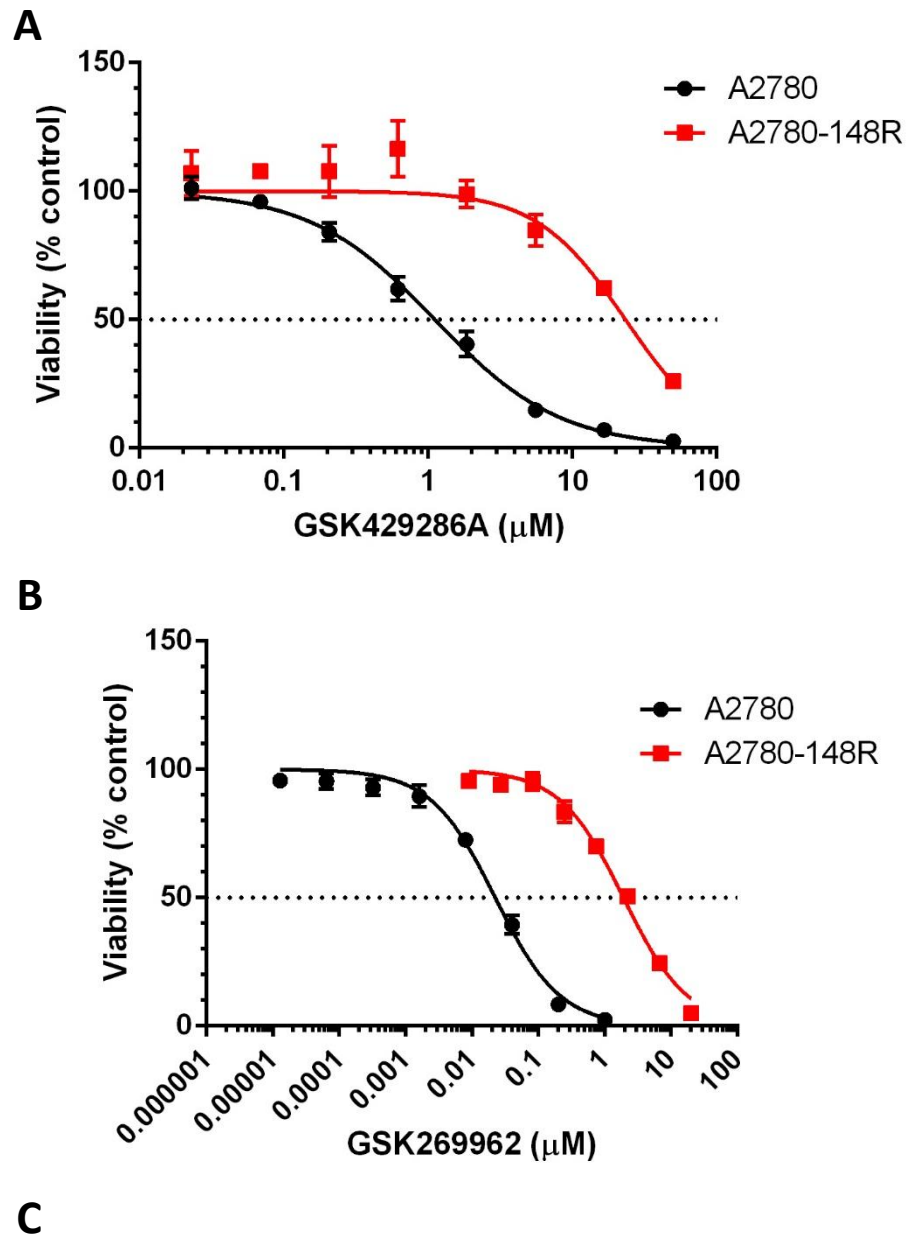
Figure 3.5: Dose-response curves and GI_{50} determinations for GSK429286A and GSK269962 in A2780 and A2780-148R cells. Cells were plated in triplicate in a 96-well plate and allowed to grow under standard growth conditions for 48 hours. They were then treated with a serial dilution of GSK429286A or GSK269962 for 96-hours, prior to being analysed by SRB assay. Dose-response graphs and non-linear regression curves were generated for **(A)** GSK429286A or **(B)** GSK269962 using GraphPad Prism 6. Dotted lines mark 50% viability on the y-axis. Data points represent the mean ± SD from one representative experiment. **(C)** Table summarises GI_{50} and RF values, data points represent the mean ± SD of all experiments conducted. Statistical significance was calculated using a student's t-test, * *p ≤ 0.05*, *** *p ≤ 0.001.* n = 5 (GSK429286A) or 9 (GSK269962) independent experiments.

3.2.4.3. IGF-1R and FGFR inhibition

One of the most remarkable findings of the previous work conducted on A2780-148R was the overexpression of IGF-1R and sensitivity to IGF-1R inhibition. In addition, A2780-148R was also found to show some sensitivity to FGFR inhibition. This apparent dependency on some RTKs was investigated using NVP-AEW541 and AZD4547, IGF-1R and FGFR inhibitors respectively.

Just as was observed previously it was found that A2780-148R was sensitive to both NVP-AEW541 and AZD4547 (Figure 3.6A-C). Figure 3.6A, C shows that A2780-148R was ~7-fold more sensitive to NVP-AEW541 than parental A2780 cells (RF = 0.14); A2780 had a GI_{50} of 1.56 µM compared to 0.22 µM for A2780-148R. However, A2780-148R cells were even more sensitive to AZD4547; A2780 had a GI_{50} of 0.52 µM whereas the GI_{50} for A2780-148R was 0.03 µM, which meant that A2780-148R was ~17-fold more sensitive (RF = 0.06) to AZD4547 (Figure 3.6B). The sensitivity to both NVP-AEW541 and AZD4547 was statistically significant (Figure 3.6A, B). It should be noted that whilst sensitivity to NVP-AEW541 and AZD4547 was consistent with previous results (Table 3.1), there were some differences in RF values, particularly for AZD4547 (previous RF value in Table 3.1: 0.22 vs 0.06 in Figure 3.6C)

A

B

C

		A2780	**A2780-148R**	
Drug	**Target**	**GI$_{50}$**	**GI$_{50}$**	**RF**
NVP-AEW541 (μM)	IGF-1R	1.56 ± 0.22	0.22 ± 0.04**	0.14
AZD4547 (μM)	FGFR 1/2/3	0.52 ± 0.11	0.03 ± 0.01***	0.06
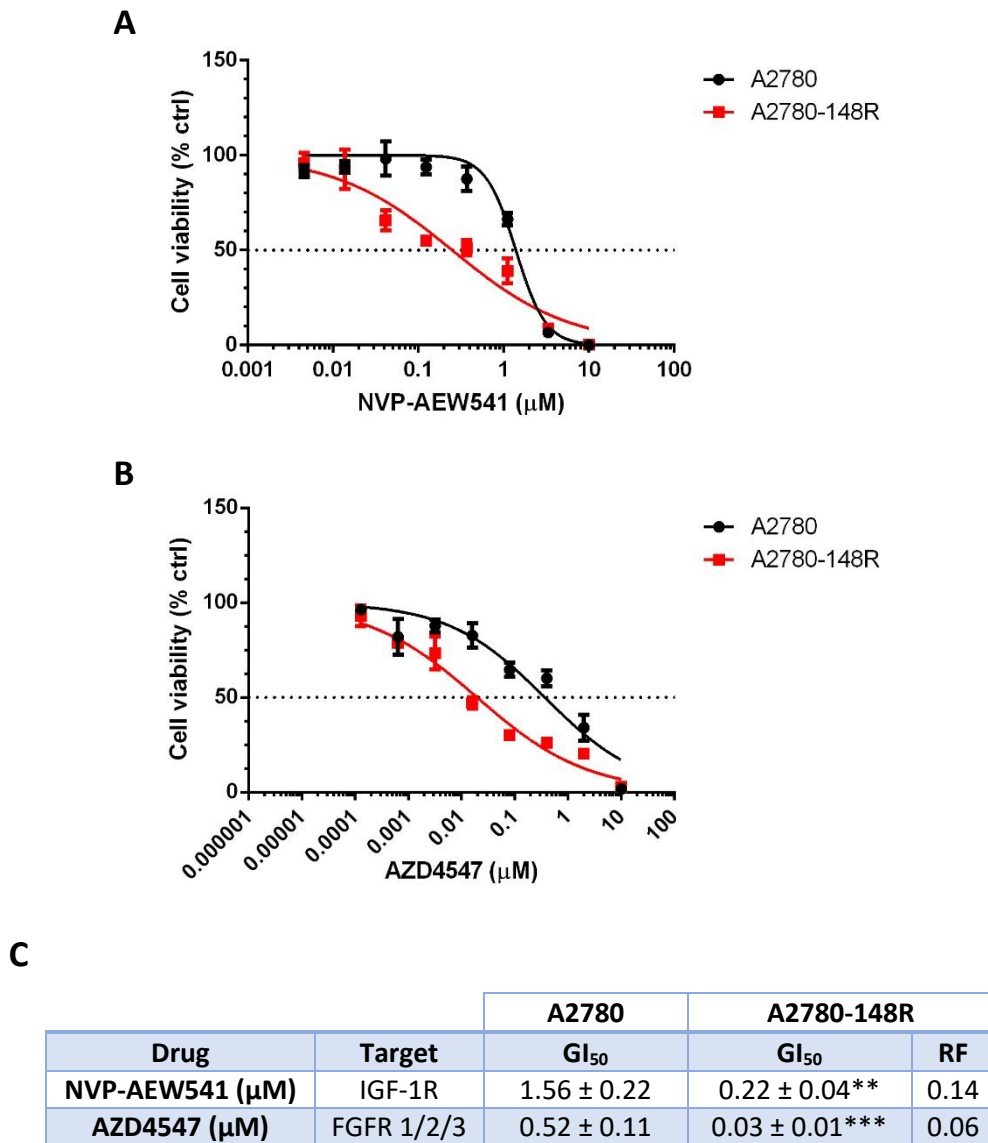
Figure 3.6: Dose-response curves and GI$_{50}$ determinations for NVP-AEW541 and AZD4547 in A2780 and A2780-148R cells. Cells were plated in triplicate in a 96-well plate and allowed to grow under standard growth conditions for 48 hours. They were then treated with a serial dilution of NVP-AEW541 and AZD4547 for 96-hours, prior to being analysed by SRB assay. Dose-response graphs and non-linear regression curve fits were generated for **(A)** NVP-AEW541 or **(B)** AZD4547 using GraphPad Prism 6. Dotted lines mark 50% viability on the y-axis. Data points represent the mean ± SD from one representative experiment. **(C)** Table summarising GI$_{50}$ and RF, data points are the mean ± SD of all experiments conducted. Statistical significance was calculated using a student's t-test, ** *p ≤ 0.01*, *** *p ≤ 0.001.* n = 4 (NVP-AEW541) or 8 (AZD4547) independent experiments.

3.2.4.4. SFK inhibitors

Together, the cross-resistance profiling previously conducted (Table 3.1), and undertaken thus far in this chapter (Figure 3.4-Figure 3.6), had provided a broad overview of the responsiveness of A2780 and A2780-148R cells to a broad range of drugs and tool compounds. However, inhibitors had not been used against SFKs, a family of non-receptor tyrosine kinases, which are pleiotropic and known to interact with IGF-1R and the ROCK pathway (Peterson *et al.*, 1996; Fincham *et al.*, 1999). As such, cross-resistance profiling was performed using several inhibitors of the SFK's.

Figure 3.7 shows that there was low-level of cross-resistance to WH-4-023, an inhibitor of c-Src and lymphocyte-specific protein tyrosine kinase (Lck). A2780 had a GI_{50} of 0.85 µM against WH-4-023, compared to a GI_{50} of 1.82 µM in A2780-148R, a statistically significant difference, equating to an RF value of 2.14 (Figure 3.7). In contrast, A2780-148R was shown to be slightly sensitive to KX2-391, a peptidomimetic c-Src-specific inhibitor; A2780-148R had a GI_{50} of 17.70 µM compared to 25.24 µM in A2780, representing an RF value of 0.70, but this was not statistically significant (Figure 3.7). SU6656, a broad SFK inhibitor, was also used, but there was no difference in response; both A2780 and A2780-148R had a GI_{50} of 0.66 µM (Figure 3.7). In summary, cross-resistance profiling using inhibitors of SFK's did not reveal any substantial differences between A2780 and A2780-148R.
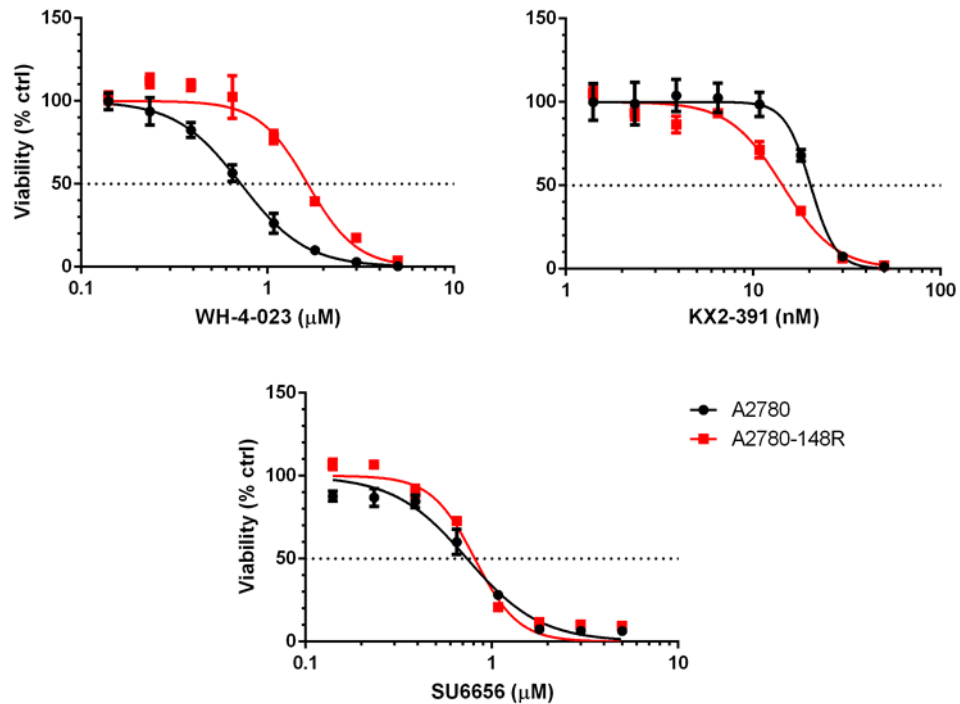
		A2780	A2780-148R	
Drug	**Target(s)**	**GI_{50}**	**GI_{50}**	**RF**
WH-4-023 (µM)	Lck & Src	0.85 ± 0.11	1.82 ± 0.20**	2.14
KX2-391 (nM)	Src	25.24 ± 3.97	17.70 ± 4.48	0.70
SU-6656 (µM)	SFK	0.66 ± 0.22	0.66 ± 0.20	1.00

Figure 3.7: Dose-response curves and GI_{50} determinations for SFK inhibitors in A2780 and A2780-148R cells. Cells were plated in triplicate in a 96-well plate and allowed to grow under standard growth conditions for 48 hours. They were then treated with a serial dilution of SFK inhibitors for 96-hours, prior to being analysed by SRB assay. Dose-response graphs and non-linear regression curve fits were generated for using GraphPad Prism 6. Dotted lines show the GI_{50}. Data points represent the mean ± SD from one representative experiment. Table summarising GI_{50} and RF, data points are the mean ± SD of all experiments conducted. Statistical significance was calculated using a student's t-test, * *p ≤ 0.05*, ** *p ≤ 0.01.* n = 3 (WH-4-023), 4 (KX2-391 &SU-6656) independent experiments.

3.2.5. Analysis of basal signalling in A2780 and A2780-148R

3.2.5.1. Markers of PAM pathway signalling

AT13148 is known to target both AKT and p70S6K, both of which act within the PAM pathway. It was therefore important to understand how this pathway was functioning in A2780-148R, compared to parental A2780 cells, as differences could contribute towards AT13148 resistance. As such, the expression of markers of the PAM pathway were assessed at the basal level. A2780-148R cells were released from AT13148 for one week prior to assaying or maintained in 5.2 µM of AT13148 (maintenance dose).

Figure 3.8 shows that the phosphorylation of S473 AKT was similar between parental A2780 cells and released A2780-148R cells. However, there was a marked increase in S473 AKT phosphorylation in maintained A2780-148R cells, consistent with what has previously been described for ATP-competitive AKT inhibitors (Figure 3.8, Okuzumi *et al.*, 2009). The phosphorylation of two direct substrates of AKT, T246 PRAS40 and S9 GSK3β, was also assessed. T246 PRAS40 phosphorylation was similar in released A2780-148R cells, when compared to parental A2780 cells, but the phosphorylation of S9 GSK3β was slightly reduced (Figure 3.8). In maintained A2780-148R cells, the phosphorylation of both T246 PRAS40 and S9 GSK3β was decreased, consistent with inhibition of AKT by AT13148 (Figure 3.8). Further down the pathway, the phosphorylation of S235/236 S6RP, a p70S6K substrate, was also shown to be unchanged in released A2780-148R cells, but as expected, substantially lowered in maintained A2780-148R cells (Figure 3.8). The total expression of the aforementioned proteins was found to be consistent across all cell lines/conditions (Figure 3.8). Taken together, these data show that the PAM pathway was mostly unchanged in A2780-148R, at basal level, and that AT13148 was still able to reduce PAM pathway activation.
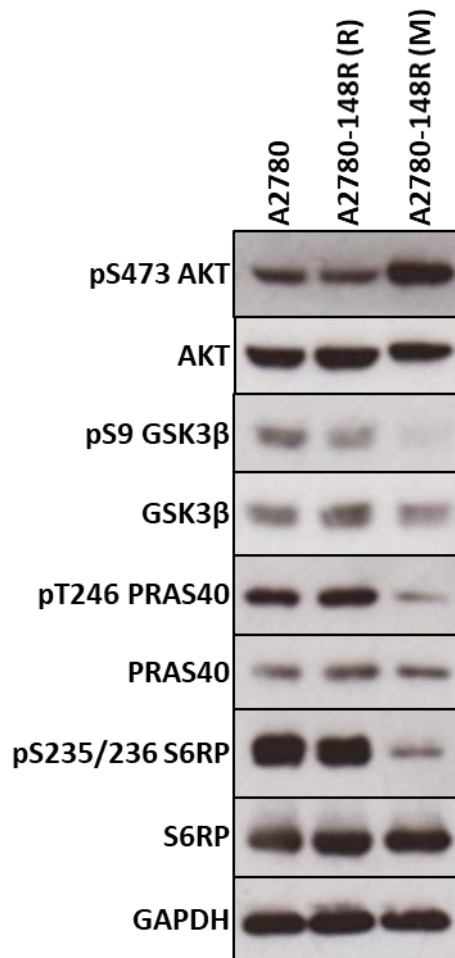
Figure 3.8: Analysis of the basal expression of markers of the PAM pathway in A2780 and A2780-148R. A2780-148R cells were either released (R) from AT13148 one week prior to plating or maintained (M) in 5.2 µM AT13148. Cells were plated at 0.5 x 10^6 (A2780) or 1 x 10^6 (A2780-148R) cells per 10 cm dish and allowed to grow for 72 hours under standard growth conditions, with maintained A2780-148R cells grown in the presence of 5.2 µM AT13148. Cells were then lysed prior to western blot analysis. Western blot membranes were probed with antibodies for phospho-proteins, stripped, and then re-probed with antibodies for total proteins and loading control (GAPDH). Data are representative of four independent experiments.

3.2.5.2. Markers of ROCK pathway signalling

Since both isoforms of ROCK are targeted by AT13148 and cross-resistance to ROCK inhibitors was shown (Figure 3.5), basal signalling of the ROCK pathway was assessed in parental A2780 cells and released A2780-148R cells. Figure 3.9 shows that the total expression of ROCK1 and ROCK2 remained unchanged between A2780 and A2780-148R cells. Conversely, there appeared to be a slight reduction in phosphorylation of T696 MYPT1, a substrate of ROCK, in A2780-148R, whilst the total expression of MYPT1 remained the same (Figure 3.9). This could indicate lower ROCK pathway activity in A2780-148R and possibly a lower dependency on ROCK signalling, which could

contribute towards AT13148 resistance. However, this change was only small, and investigating the response of the ROCK pathway to AT13148 would provide a much better understanding of the pathway's contribution to AT13148 resistance.
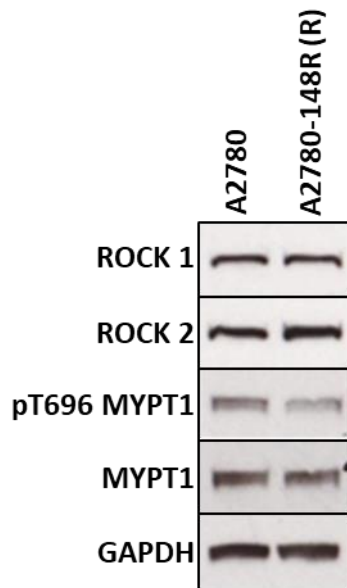
Figure 3.9: Analysis of the basal expression of markers of the ROCK pathway in A2780 and A2780-148R. A2780-148R cells were released (R) from AT13148 one week prior to plating**.** A2780 and A2780-148R cells were plated at either 0.5 x 10^6 (A2780) or 1 x 10^6 (A2780-148R) cells per 10 cm dish and allowed to grow for 48 hours under standard growth conditions. Cells were then lysed prior to western blot analysis. Western blot membranes were probed with antibodies for phospho-proteins, stripped, and then re-probed with antibodies for total proteins and loading control (GAPDH). Data are representative of four (ROCK1 & 2) or six (MYPT1) independent experiments.

3.2.5.3. IGF-1R and FGFR2 expression

The expression of IGF-1R and FGFR2 was assessed in order to investigate the sensitivity to IGF-1R and FGFR inhibition (Figure 3.6A, B). IGF-1R expression was assessed in both released and maintained A2780-148R cells, whereas FGFR2 expression was only assessed in released A2780-148R cells. As expected, IGF-1R was shown to be considerably over-expressed in both released and maintained A2780-148R cells (Figure 3.10A). However, IGF-1R was expressed at a greater level in maintained A2780-148R cells, when compared to released A2780-148R cells, which has previously not been identified (Figure 3.10A). Contrary to the previously described microarray data (section 3.1), FGFR2 was shown to be expressed at the same level both released A2780-148R cells and parental A2780 cells (Figure 3.10B).

Figure 3.10: Analysis of the basal expression of IGF-1R and FGFR2 in A2780 and A2780-148R. A2780-148R cells were either released (R) from AT13148, one week prior to the experiment, or maintained (M) in 5.2 µM AT13148. A2780 and A2780-148R cells were plated at either 0.5 x 10^6 (A2780) or 1 x 10^6 (A2780-148R) cells per 10 cm dish and allowed to grow for 72 hours under standard growth conditions, with maintained A2780-148R cells grown in the presence of 5.2 µM AT13148. Cells were then lysed prior to western blot analysis. Western blot membranes were probed with antibodies for **(A)** IGF-1R and **(B)** FGFR2, stripped, and then re-probed with an antibody for β-Actin (loading control). Data are representative of four (IGF-1R) or five (FGFR2) independent experiments.

3.2.5.4. Markers of the MAPK pathway

The MAPK pathway was also investigated in A2780 and released A2780-148R cells, as it is a major growth factor pathway commonly associated with resistance to a number of different cancer therapies (Garraway and Jänne, 2012). Figure 3.11 shows that there was a slight increase in the phosphorylation of ERK 1/2 at Thr202/Tyr204 in A2780-148R, however, in contrast, there was a small decrease in S217/221 MEK 1/2 phosphorylation in A2780-148R (Figure 3.11). Since ERK 1/2 is only known to be phosphorylated by MEK 1/2 this finding was unexpected; one would usually expect MEK 1/2 phosphorylation to be increased if ERK 1/2 phosphorylation was. The total protein expression of both ERK 1/2 and MEK 1/2 remained the same between parental A2780 cells and A2780-148R cells (Figure 3.11).
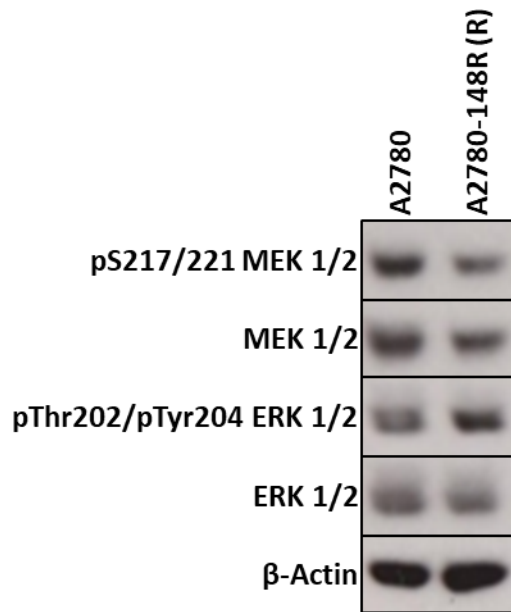
Figure 3.11: Analysis of the basal expression of markers of the MAPK pathway in A2780 and A2780-148R. A2780-148R cells were released (R) from AT13148 one week prior to plating**.** A2780 and A2780-148R cells were plated at either 0.5 x 10^6 (A2780) or 1 x 10^6 (A2780-148R) cells per 10 cm dish and allowed to grow for 72 hours under standard growth conditions. Cells were then lysed prior to western blot analysis. Western blot membranes were probed with antibodies for phospho-proteins, stripped, and then re-probed with antibodies for total proteins or loading control (β-Actin). Data are representative of four (MEK 1/2) or five (ERK 1/2) independent experiments.

3.2.6. Analysis of signalling pathway response to AT13148

The investigation into the basal activity of several key signalling pathways did not reveal any dramatic differences between A2780 and A2780-148R cells, especially in pathways targeted by AT13148 (PAM and ROCK pathways). Despite this, these pathways might have still exhibited a differential response to AT13148, which could have contributed towards AT13148 resistance. Therefore, A2780 and A2780-148R cells were treated with a range of AT13148 concentrations, between 0.1 μM – 10 μM, and the response of key signalling pathways assessed via western blot analysis.

3.2.6.1. Biomarkers of AT13148 target inhibition

Initially, the response of substrates downstream of AKT and p70S6K, targets of AT13148, was investigated, in order to assess if AT13148 was still able to effectively inhibit the PAM pathway in A2780-148R. Figure 3.12 shows that the phosphorylation of PRAS40 decreased in a similar manner in both A2780 and A2780-148R; T246 PRAS40 phosphorylation was unaffected at 0.1 μM – 1μM of AT13148, but almost completely lost at ≥ 5 μM (Figure 3.12). Phosphorylation of S6RP was similarly unchanged but

appeared to be more potently affected by AT13148 than PRAS40 phosphorylation; in both A2780 and A2780-148R, only 0.5-1 µM of AT13148 was required to cause a reduction in S235/236 S6RP phosphorylation, and at ≥ 5 µM there was little signal remaining (Figure 3.12). The total protein expression of PRAS40 and S6RP appeared to be unaffected by AT13148 in both A2780 and A2780-148R (Figure 3.12).

The response of the ROCK pathway to AT13148 was also evaluated by measuring the phosphorylation of MYPT1, a substrate of ROCK1 and 2. Just as with the PAM pathway, the ROCK pathway had a near-identical response to AT13148 in A2780 and A2780-148R (Figure 3.12). In both cell lines, 0.1 µM of AT13148 caused sharp reduction in the phosphorylation of MYPT1 at T696, however, increasing the concentration of AT13148 beyond 0.1 µM did not seem to have any additional affect (Figure 3.12). The total expression of MYPT1 also appeared to be mostly unaffected by AT13148 in both A2780 and A2780-148R (Figure 3.12). Taken together, these data show that the PAM and ROCK pathways responded in a similar manner to AT13148 in A2780 and A2780-148R.
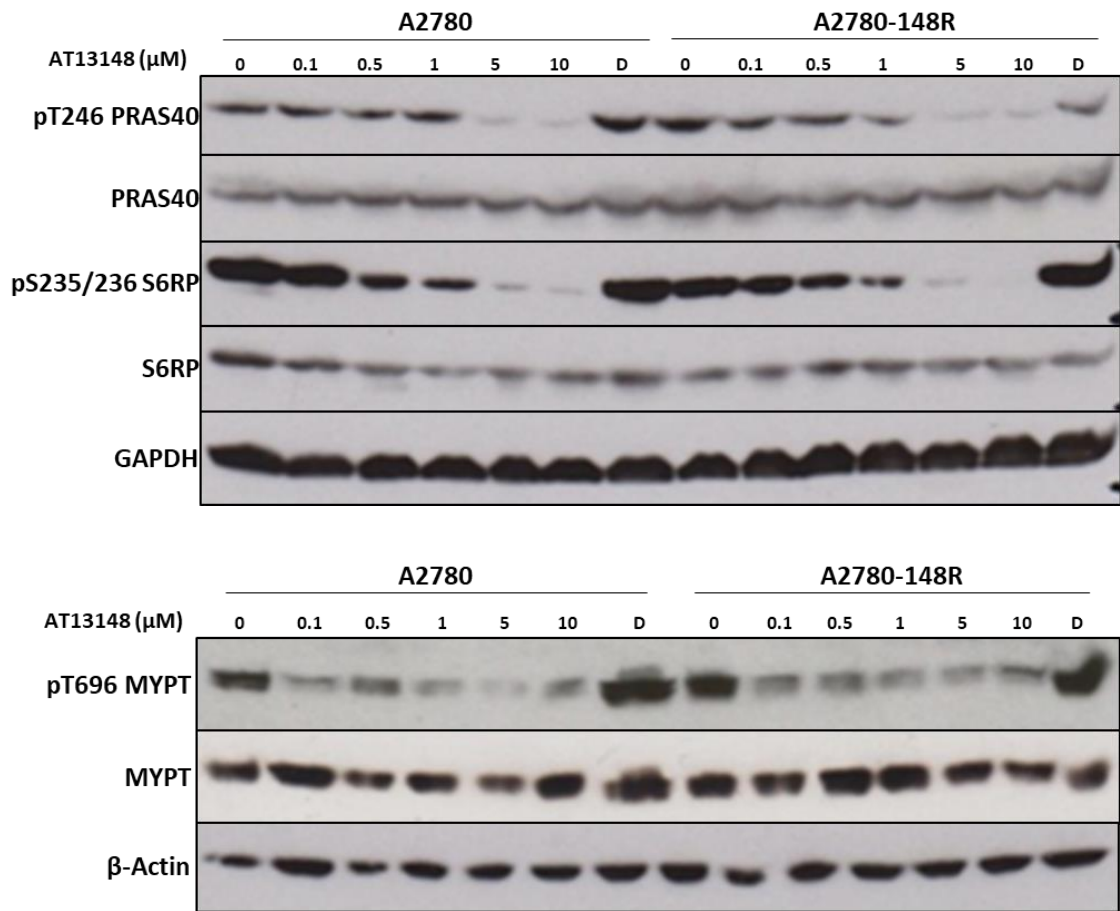
Figure 3.12: Analysis of markers of the PAM and ROCK pathways in response to AT13148. Cells were plated at either 0.5 x 10^6 (A2780) or 1 x 10^6 (A2780-148R) cells per 10 cm dish and allowed to grow for 48 hours under standard growth conditions. Cells were then treated with AT13148, as shown (0 µM = untreated), or D: DMSO vehicle control for 4 hours prior to being lysed for western blot analysis. Western blot membranes were probed with antibodies for phospho-proteins, stripped, and then re-probed with antibodies for total proteins or loading control (GAPDH or β-Actin) Data are representative of four (PRAS40 & S6RP) or three (MYPT1) independent experiments.

3.2.6.2. Markers of the MAPK pathway

AT13148 is not known to directly target the MAPK pathway, however, it was shown in Figure 3.11 that there was slight increase in ERK 1/2 phosphorylation in A2780-148R. This could possibly indicate that the MAPK pathway is affected by AT13148 and that it was altered in A2780-148R, contributing towards AT13148 resistance. The response of the MAPK pathway to AT13148 was therefore assessed, using ERK 1/2 phosphorylation as a biomarker of MAPK pathway activation. Figure 3.13 shows that the MAPK pathway responded to AT13148, in both A2780 and A2780-148R, but in a distinctive manner from one another. In A2780, the phosphorylation of ERK 1/2 at Thr202/Tyr204 was decreased with 0.1 µM AT13148, but there was an increase with ≥ 0.5 µM, with a peak in Thr202/Tyr204 ERK 1/2 phosphorylation at 5–10 µM AT13148 (Figure 3.13). In A2780-

148R, concentrations of AT13148 between 0.1 μM and 1 μM didn't have a great effect on Thr202/Tyr204 ERK 1/2 phosphorylation, although it did appear that there was a slight reduction (Figure 3.13). However, ≥ 5 μM AT13148 elevated the phosphorylation of Thr202/Tyr204 ERK 1/2 in A2780-148R cells (Figure 3.13). Interestingly, the phosphorylation of Thr202/Tyr202 ERK 1/2 was greater in A2780-148R, when compared to parental A2780 cells, both at a basal level (0 μM AT13148), to a much greater extent than in Figure 3.11, and across all AT13148 concentrations used (Figure 3.13). The response of the MAPK pathway to AT13148, in A2780 and A2780-148R, warrants further investigation as it has the potential to contribute towards resistance and to be exploited therapeutically.

Figure 3.13: Analysis of markers of the MAPK pathway in response to AT13148. Cells were plated at either 0.5 x 10^6 (A2780) or 1 x 10^6 (A2780-148R) cells per 10 cm dish and allowed to grow for 48 hours under standard growth conditions. Cells were then treated with AT13148, as shown (0 μM = untreated), or D: DMSO vehicle control for 4 hours prior to being lysed for western blot analysis. Western blot membranes were probed with antibodies for phospho-proteins, stripped, and then re-probed with antibodies for total proteins or loading control (β-Actin). (S): short exposure to hyperfilm, (L): long exposure to hyperfilm. Data are representative three independent experiments.

3.2.7. Analysis of the response of signalling pathways to ROCK inhibition

One of the main findings from cross-resistance profiling presented in this chapter, was cross-resistance to ROCK inhibition (Figure 3.5). Therefore, the response of the ROCK pathway to the ROCK inhibitor GSK269962 was assessed, in order to investigate the potential mechanism of ROCK cross-resistance. Figure 3.14 shows that GSK269962 was able to potently inhibit the ROCK pathway in A2780; 0.02 μM GSK269962 was able to cause a drastic decrease in the phosphorylation of T696 MYPT1. However, as was seen with AT13148 in Figure 3.12, increasing the concentration of GSK269962 beyond 0.02 μM did not cause any further reductions in T696 MYPT1 phosphorylation (Figure 3.14).

In comparison, the phosphorylation of T696 MYPT1 in A2780-148R was shown to be partially refractory to GSK269962; ≥ 2.5 µM GSK269962 was required to cause a substantial reduction in T696 MYPT1 phosphorylation (Figure 3.14). The total protein expression of MYPT1 did not show any response to GSK269962 in either cell line. Taken together, these data suggest that there was a partial maintenance of the ROCK pathway in response to GSK269962 in A2780-148R.
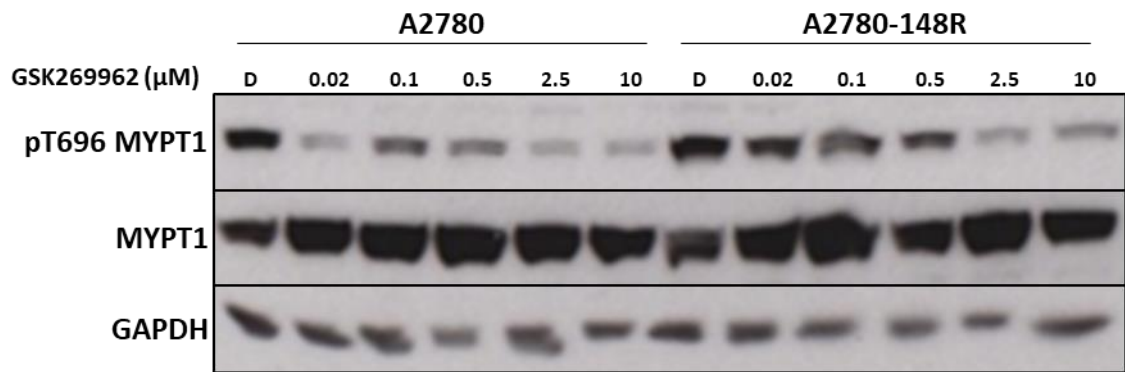
Figure 3.14: Analysis of markers of the ROCK pathway in response to GSK269962. Cells were plated at either 0.5 x 10^6 (A2780) or 1 x 10^6 (A2780-148R) cells per 10 cm dish and allowed to grow for 48 hours under standard growth conditions. Cells were then treated with GSK269962, as shown, or D: DMSO vehicle control for 4 hours prior to being lysed for western blot analysis. Western blot membranes were probed with antibodies for phospho-proteins, stripped, and then re-probed with antibodies for total proteins or loading control (GAPDH). Data are representative of three independent experiments.

The response of the MAPK pathway to GSK269962 was also assessed, to investigate if the inhibition of ROCK1 & 2 contributed to the MAPK pathway response to AT13148 seen in Figure 3.13. Figure 3.15 shows that the MAPK pathway did respond to GSK269962 in A2780 but not in A2780-148R. In A2780, 0.02 µM GSK269962 caused a decrease in Thr202/Tyr204 ERK 1/2 phosphorylation but increasing the GSK269962 concentration further did not cause any additional decreases (Figure 3.15). This was in stark contrast to what was seen in A2780-148R, where none of the concentrations of GSK269962 effected Thr202/Tyr204 ERK 1/2 phosphorylation (Figure 3.15). Whilst, in both A2780 and A2780-148R, ERK 1/2 total protein did not respond to GSK269962, there was a lower expression of total ERK 1/2 protein across all GSK269962 concentrations in A2780-148R, when compared to parental A2780 cells (Figure 3.15). In addition, Thr202/Tyr204 ERK 1/2 phosphorylation was greater in A2780-148R, when compared to A2780, across all concentrations of GSK269962 and in the DMSO vehicle control (Figure 3.15). In summary, these data show that the activation the MAPK pathway decreased in

response to ROCK inhibition in parental A2780 cells, but that this response was lost in A2780-148R.
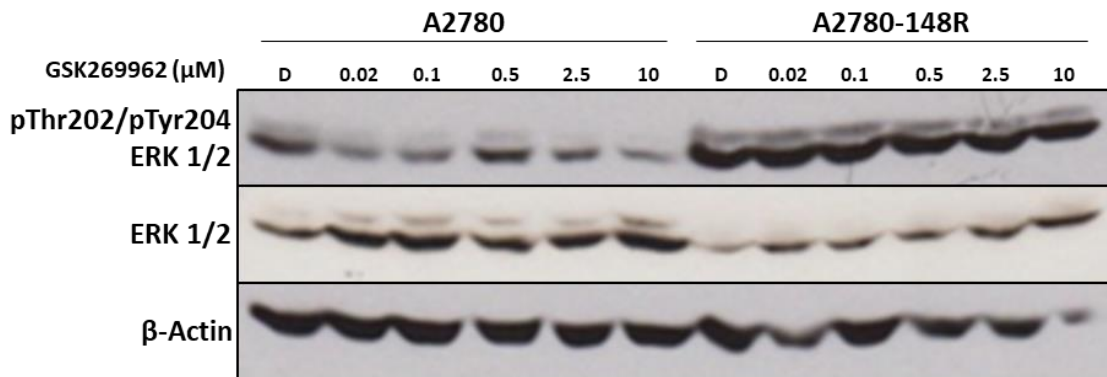
Figure 3.15: Analysis of markers of the MAPK pathway in response to GSK269962. Cells were plated at either 0.5×10^6 (A2780) or 1×10^6 (A2780-148R) cells per 10 cm dish and allowed to grow for 48 hours under standard growth conditions. Cells were then treated with GSK269962, as shown, or D: DMSO vehicle control for 4 hours prior to being lysed for western blot analysis. Western blot membranes were probed with antibodies for phospho-proteins, stripped, and then re-probed with antibodies for total proteins or loading control (β-Actin) Data are representative of two independent experiments.

3.3. Discussion

The main aim of this chapter was to investigate the mechanism of acquired resistance to AT13148 using A2780-148R as a model. Before this could be undertaken, the resistance of A2780-148R to AT13148 was validated. Reassuringly, A2780-148R was shown have ~5-fold resistance to AT13148 and could therefore be used as a model to investigate acquired mechanisms of AT13148 resistance (Figure 3.2). Subsequently, to try and gain insight into AT13148 resistance, the morphology of A2780 and A2780-148R was assessed in untreated cells and in response to AT13148 (Figure 3.3). Whilst there were some differences between untreated A2780 and A2780-148R cells, these weren't significant, with both morphologies consistent with an epithelial phenotype. In response to AT13148 both cell lines exhibited a similar response; cells developed a "spindle-like" morphology where they extended long-processes, making the cells become long and thin. This response is indicative of inhibition of ROCK1 and 2 and has been previously described; Kümper and colleagues (Kümper *et al.*, 2016) described this phenotype in mouse embryonic fibroblasts (MEF) with a conditional knockout of ROCK1 and 2, as well as in response to the ROCK inhibitor H1152. Furthermore, Rath and colleagues (Rath *et al.*, 2018) observed a similar response in PDAC cells treated with AT13148, and showed that, in regards to cell morphology, AT13148 pheno-copied ROCK-selective inhibitors. Therefore, this "spindle-like" morphology in response to AT13148 in A2780 and A2780-148R, is likely caused by the inhibition ROCK1 and 2 by AT13148, although the impact of the inhibition of other AT13148 targets can't be discounted. However, this response was not ubiquitous in A2780 and A2780-148R, only being observed in sub-set of the total population of cells, perhaps highlighting a heterogenous response to AT13148, at least in morphology.

It is also worth noting that some A2780 cells exhibited a morphology indicative of apoptosis (membrane blebbing) in response to AT13148 (Saraste and Pulkki, 2000). This response was less apparent in A2780-148R, which was interesting considering that AT13148 has previously been shown to induce an apoptotic phenotype in cancer cells (Yap *et al.*, 2012). It's possible that A2780-148R cells have been able to overcome this, although a more thorough investigation of the apoptotic response would be required to ascertain this.

In addition, cross-resistance profiling was performed on A2780-148R where it was shown that A2780-148R cells were cross-resistant to the AKT inhibitor capiversatib (Figure 3.4). Since capiversatib also inhibits p70S6K, as well as AKT, both members of the PAM pathway as well as targets of AT13148, this might suggest altered PAM pathway signalling in A2780-148R (Davies *et al.*, 2012; Yap *et al.*, 2012). However, the level of cross-resistance was relatively low (~3-fold), and capiversatib is also known to target kinases outside the PAM pathway, including PKA and ROCK2 (Davies *et al.*, 2012). Therefore, it's difficult to draw any strong conclusions from cross-resistance to capiversatib, perhaps a more selective AKT inhibitor, such as MK2206, could be used in future (Hirai *et al.*, 2010).

A2780-148R was also shown to have substantial cross-resistance to ROCK inhibition with cross-resistance seen against two ROCK inhibitors: GSK429286A and GSK269962 (Figure 3.5). Including the previously established cross-resistance to Y-27632, shown in Table 3.1, cross-resistance has now been observed with three ROCK inhibitors, where, as shown in Table 3.2, the level of cross-resistance appears to correlate with the potency against ROCK1 and 2, thus giving a high-level of confidence that ROCK cross-resistance is genuine. This cross-resistance to ROCK inhibition was of particular interest, since AT13148 potently targets ROCK1 & 2 and could potentially be used in the clinic as a ROCK inhibitor (Rath *et al.*, 2018). It suggests that the inhibition of ROCK1 & 2 is important for the effect of AT13148 in A2780 cells, and therefore, to become resistant to AT13148, A2780-148R cells have had to overcome this.

Table 3.2: Summary of the IC_{50} against ROCK1 and 2 for different ROCK inhibitors as determined from biochemical assays. Table adapted from Lotz-Jenne *et al.*, 2016; ROCK IC_{50} data was generated using *in vitro* kinase assays. RF values were obtained from [1]Table 3.1 and [2]Figure 3.5.

ROCK inhibitor	ROCK1 IC_{50}	ROCK2 IC_{50}	RF
Y-27632 (nM)	2273.0	1585.0	3.09[1]
GSK429286A (nM)	46.7	55.3	21.39[2]
GSK269962 (nM)	7.0	1.2	86.00[2]

Cross-resistance profiling also validated the previously identified sensitivity to NVP-AEW541, an IGF-1R inhibitor, and AZD4547, an FGFR inhibitor, in A2780-148R (Figure 3.6). However, the sensitivity to AZD4547 was much greater than what had been seen

previously: ~17-fold sensitivity in Figure 3.6 vs ~4.5-fold sensitivity in Table 3.1 (highlighted in Table 3.3). Whilst there were some differences between data in this chapter and that which has been shown previously, this was perhaps the most dramatic, warranting an explanation. One potential explanation is that a different batch of FBS would have been used, and that FBS is known to have batch to batch variation in the concentration of growth factors (Zheng *et al.*, 2008). If the FBS used in this chapter had more FGF's (fibroblast growth factors), than the FBS used previously, then it could lead to a greater activation of FGFR signalling and possibly increased dependency. However, one wouldn't expect batch to batch variation to cause such a notable difference, other factors should also be considered. Cancer cell lines are known to be heterogenous, due to the existence of pre-existing sub-populations, as well as inherent genomic instability (Ben-David *et al.*, 2018). Over time with continuous cell culture this can cause genetic and population drift, altering drug response, which could have played a role in the altered response to AZD4547. Nonetheless, in both datasets sensitivity was seen to IGF-1R and FGFR inhibition, and this could potentially be applied to patients with resistance to AT13148.

Table 3.3: Comparison of datasets generated for AZD4547 in A2780 and A2780-148R. [1]data generated in this chapter (Figure 3.6) [2]data from previous work (Table 3.1). Statistical significance was calculated using a student's t-test, * $p \leq 0.05$, *** $p \leq 0.001$, n $\geq$ 3.

	A2780	A2780-148R	
Drug	**GI_{50}**	**GI_{50}**	**RF**
AZD4547[1] (μM)	0.52 ± 0.11	0.03 ± 0.01***	0.06
AZD4547[2] (μM)	0.09 ± 0.05	0.02 ± 0.01*	0.22

A number of drugs/tool compounds targeting SFK's were also used in cross-resistance profiling, as they had previously not been screened for (Figure 3.7). As mentioned in section 3.1, SFK's are known to regulate the activation of IGF-1R as well as negatively regulating ROCK signalling, and as such one might expect an altered response to SFK inhibition in A2780-148R (Peterson *et al.*, 1996; Fincham *et al.*, 1999). Whilst there was low-level cross-resistance to the Src and Lck inhibitor WH-4-023 (~2-fold), none of the SFK inhibitors used showed any substantial cross-resistance or sensitivity in A2780-148R. This would seem to suggest that signalling via SFK's is unchanged between A2780 and A2780-148R, and that they are not responsible for IGF-1R sensitivity, ROCK cross-resistance, or resistance to AT13148.

To follow up on cross-resistance profiling, PAM pathway activation was investigated, initially at a basal level (Figure 3.8). The activation of the PAM pathway appeared to be similar across A2780 and A2780-148R cells, with the phosphorylation of AKT; its substrates, PRAS40 and GSK3β; and S6RP, a p70S6K substrate, all shown to be unchanged. A2780-148R was also maintained in 5.2 µM AT13148 (maintenance dose of AT13148), which was shown to cause a striking increase in the phosphorylation of AKT. Due to inhibition of AKT by AT13148, one would intuitively not expect this, but this has been previously established to occur in response to AT13148 and not affect the phosphorylation of AKT substrates (Yap *et al.*, 2012). This response is common in other ATP-competitive AKT inhibitors, such as capiversatib and A-443654, which again, despite inhibitor induced AKT phosphorylation, are still able to function as AKT inhibitors (Okuzumi *et al.*, 2009; Davies *et al.*, 2012). Okuzumi and colleagues (Okuzumi *et al.*, 2009) provided a mechanistic explanation for this by showing that A-443634 still induced phosphorylation of kinase-dead AKT, demonstrating that relief of negative feedback downstream of AKT is not a cause of inhibitor-induced AKT phosphorylation (Okuzumi *et al.*, 2009). They suggest a kinase intrinsic mechanism, such as a conformational change in AKT decreasing the access of AKT phosphatases (Okuzumi *et al.*, 2009). Therefore, as expected, maintained A2780-148R cells had decreased phosphorylation of substrates downstream of AKT and p70S6K, despite increased AKT phosphorylation. Thus, indicating that AT13148 was still able to inhibit the PAM pathway in A2780-148R, but dose-response assays were better able to evaluate this.

The activation of the ROCK pathway was also assessed at a basal level; as previously described, A2780-148R had significant cross-resistance to ROCK inhibition, and this could have possibly indicated altered signalling via ROCK1 and 2, targets of AT13148 (Figure 3.9). Indeed, whilst both isoforms of ROCK had similar expression in A2780 and A2780-148R, there was a slight reduction of the phosphorylation of the ROCK substrate MYPT1. In isolation, it is difficult to interpret the implication of a reduction in the phosphorylation of MYPT1 on the activation of the ROCK pathway. A more comprehensive analysis of the pathway would be required to assess this, looking at multiple substrates of ROCK. This was attempted by western blotting for the ROCK substrates MLC2 and LIMK, but they proved difficult to consistently detect (data not shown). However, the decrease in the phosphorylation of MYPT1 could indeed indicate

that there was reduced activation of the ROCK pathway in A2780-148R. This could explain the cross-resistance to ROCK inhibition; perhaps the ROCK pathway has been by-passed in A2780-148R.

The over-expression of IGF-1R was also observed in A2780-148R, validating previous results and re-affirming that IGF-1R expression could potentially be used as a biomarker for sensitivity to IGF-1R inhibition in AT13148 resistant patients (Figure 3.10A; Akan, 2015). However, there was a marked difference between A2780-148R released from AT13148 and A2780-148R maintained; IGF-1R expression was much greater in maintained A2780-148R, suggesting that AT13148, to a certain extent, induces the expression of IGF-1R. This could be caused by the relief of negative feedback in the PAM pathway, due to the inhibition of AKT by AT13148. Chandarlapaty and colleagues (Chandarlapaty *et al.*, 2011) showed that AKT inhibition increases the expression of IGF-1R in a FoXO dependent manner, in a number of cancer cell lines. A similar effect was also seen by Zorea and colleagues (Zorea *et al.*, 2018) in PI3K-driven ovarian cancer cells treated with the PI3K inhibitor taselisib. It would be interesting to see if the expression of IGF-1R is further decreased when released for a longer period from AT13148 and whether this impacts sensitivity to IGF-1R.

Despite sensitivity to FGFR inhibition, and previous microarray analysis showing an increase in FGFR2 mRNA expression, FGFR2 had a similar protein expression in A2780 and A2780-148R (Figure 3.10B). This was disappointing as it was hoped that FGFR2 could potentially be used as a biomarker for FGFR sensitivity in AT13148 resistant patients, and its overexpression a possible candidate driver of resistance. However, there are four isoforms of FGFR (three targeted by AZD4547, FGFR1-3) which could have altered expression in A2780-148R. In addition, it's also possible that FGFR expression was unchanged, but that phosphorylation and activation was increased, causing a dependency on FGFR signalling, thus increased sensitivity to AZD4547 and possibly resistance to AT13148. This has been seen in EGFR-dependent head and neck squamous cell carcinoma (HNSCC) and NSCLC cell lines, where a constitutively active FGFR3 fusion protein (FGFR3-TACC3) has been shown to cause resistance to combined EGFR/ERBB3 blockade, via the maintenance of MAPK signalling (Daly *et al.*, 2017). In addition, increased phosphorylation of FGFR signalling, has been shown to drive resistance to

BRAF (V600E) inhibition in BRAF mutant melanoma cell lines (Yadav *et al.*, 2012). Therefore, FGFR signalling warrants further investigation in A2780-148R.

The basal signalling of the MAPK pathway was also evaluated, where some changes were identified; the phosphorylation of ERK 1/2 shown to be slightly increased, but MEK 1/2 phosphorylation slightly decreased (Figure 3.11). Since MEK 1/2 is upstream of ERK 1/2 in the MAPK pathway one would usually expect the phosphorylation of ERK 1/2 to be decreased if MEK 1/2 phosphorylation was decreased. However, ERK 1/2 is known to impart inhibitory phosphorylations on RAF, the kinase upstream from MEK, and thus provides an explanation as to how increased phosphorylation of ERK 1/2 can lead to decreased MEK 1/2 phosphorylation (Dougherty *et al.*, 2005; Ritt *et al.*, 2010). It should also be noted that ERK1/2 phosphorylation was shown to be increased in untreated cells in dose-response assays; the phosphorylation of ERK 1/2 was greater in untreated A2780-148R cells than untreated A2780 cells in both AT13148 and GSK269962 dose-response western blots, however, to a much greater extent than was seen in basal western blots (Figure 3.13 & Figure 3.16). This difference, between basal and dose-response western blots, could be due to the presence of distinct sub-populations of cells in A2780-148R that were selected for over time/under different cell culture conditions.

Whilst investigating basal signalling provided a broad overview of the differences between A2780 and A2780-148R in several different pathways, it didn't provide any information on how these pathways responded in the presence of AT13148. To this end, dose-response western blot assays were performed with AT13148. Broadly speaking, these assays revealed that the PAM and ROCK pathways, two key pathways targeted by AT13148, were equally inhibited by AT13148 in A2780 and A2780-148R (Figure 3.12). By assessing these two pathways, the response of most AT13148 targets was evaluated including: AKT1, AKT3, ROCK1, ROCK2, p70S6K, and to a certain extent SGK3, since it has overlapping substrate specificity with AKT (Bruhn *et al.*, 2013). The only major AT13148 target for which inhibition was not assessed at all, was PKA. The PKA substrate vasodilator-stimulated phosphoprotein (VASP) was blotted for but proved difficult to detect (data not shown). Nonetheless, since the PAM pathway is hyperactivated in A2780 cells (due to *PTEN* and *PIK3CA* mutations), and A2780-148R cells have cross-resistance to ROCK inhibition, the fact that both the PAM and ROCK pathways responded

in a similar manner, in A2780 and A2780-148R, suggests that the mechanism of resistance to AT13148 was caused by the by-pass of these pathways (Figure 3.16). In other words, another pathway is compensating for the inhibition of PAM and ROCK signalling by AT13148, driving resistance (Figure 3.16). An example of this can been seen in BRAF mutant melanoma, where signalling through platelet-derived growth factor receptor (PDGFR) has been shown to by-pass the MAPK pathway, driving resistance to BRAF (V600E) inhibition (Nazarian *et al.*, 2010).
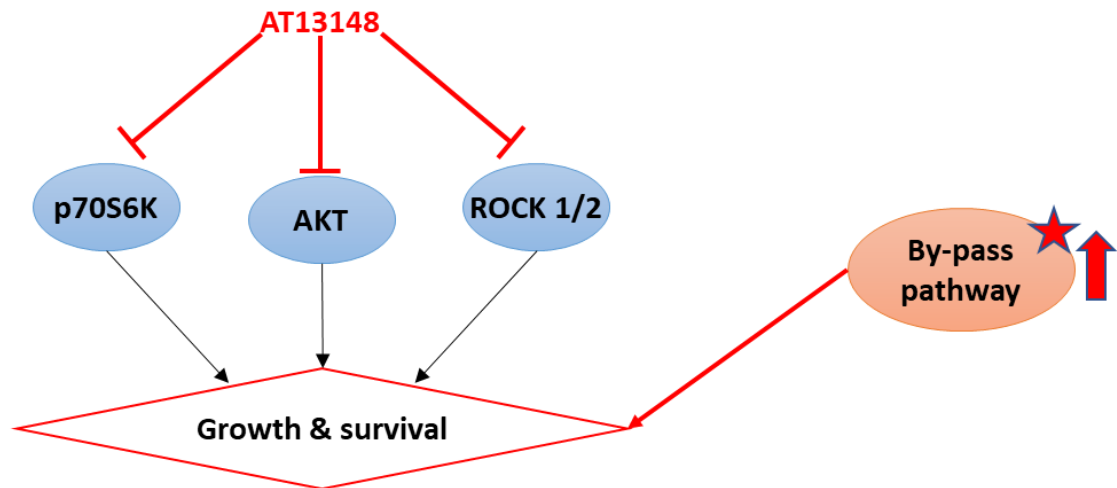
Figure 3.16: By-pass of AT13148 targets as a potential mechanism of resistance to AT13148. Resistance to AT13148 might be driven by the upregulation of a by-pass pathway, which circumvents the inhibition of the PAM (AKT and p70S6K) and ROCK (ROCK 1/2) pathways by AT13148, driving growth and survival independently of AT13148 targeted pathways.

Due to the differences identified in the MAPK pathway at a basal level, the response of the MAPK pathway to AT13148 was also investigated in A2780 and A2780-148R (Figure 3.13). In parental A2780 cells there was a remarkable response in the phosphorylation of ERK 1/2 to AT13148. Lower doses decreased ERK 1/2 phosphorylation, but higher doses increased phosphorylation, this can be characterised as a bi-directional dose-response. This response was present in A2780-148R, but to a lesser extent, and as mentioned earlier, the phosphorylation of ERK 1/2 was at a higher level when untreated, compared to A2780. This response was not anticipated as AT13148 is not known to inhibit any members of the MAPK pathway. However, several targets of AT13148 are known to regulate the MAPK pathway. For example, PKA and AKT are known to positively regulate the expression of dual-specificity MAPK phosphatases (MKP's or DUSP's), and both impart inhibitory phosphorylations on RAF proteins (Zimmermann and Moelling, 1999; Guan *et al.*, 2000; Pursiheimo *et al.*, 2002; Phuchareon *et al.*, 2015;

Figure 3.17A). Consequently, inhibition of PKA and AKT by AT13148 could increase the phosphorylation of ERK 1/2 (Figure 3.17A). In contrast, inhibition of ROCK has been shown to decrease the activation of the MAPK pathway, via an undefined mechanism which seems to be dependent upon the regulation of actin-myosin contractility by ROCK (Croft and Olson, 2006; Chang *et al.*, 2018; Figure 3.17B). Interestingly, as discussed below, in A2780 cells ERK 1/2 phosphorylation did decrease in response to inhibition of ROCK by GSK269962 (Figure 3.15). Therefore, the opposing effects of AT13148 targets on the MAPK pathway could explain the response of ERK 1/2 phosphorylation to AT13148 (Figure 3.17A & B).
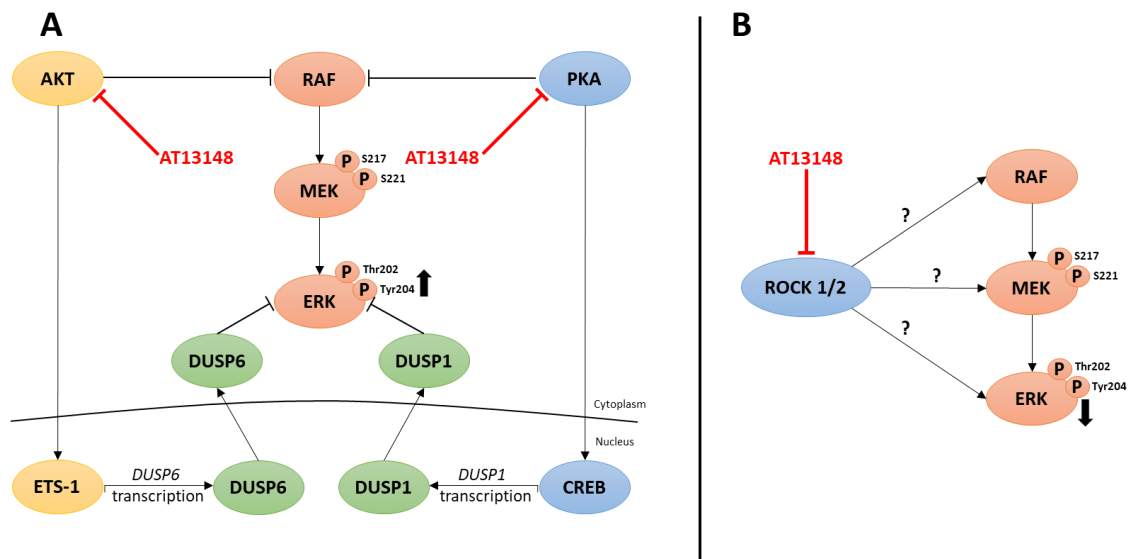
Figure 3.17: Potential mechanisms of AT13148 mediated regulation of the MAPK pathway. (A) Both AKT and PKA can negatively regulate the MAPK pathway by inhibitory phosphorylation's of RAF, or by mediating transcription of DUSP proteins, which de-phosphorylate ERK 1/2. Inhibition of AKT and PKA, by AT13148, might therefore be responsible for increased ERK 1/2 phosphorylation seen in response to some concentrations of AT13148. **(B)** ROCK has been shown to positively regulate MAPK pathway activation, by an undefined mechanism(s). Consequently, inhibition of ROCK1 & 2 by AT13148, may be responsible for decreased ERK 1/2 phosphorylation seen in response to some concentrations of AT13148.

To further investigate the response of the MAPK pathway to AT13148, in particular the contribution of ROCK1 and 2 inhibition by AT13148, the response of ERK 1/2 phosphorylation to the ROCK inhibitor GSK269962 was evaluated (Figure 3.15). Remarkably, GSK269962 was able to cause a decrease in the phosphorylation of ERK 1/2 in parental A2780 cells but had no effect in A2780-148R. Again, just as with AT13148, GSK269962 is not known to target the MAPK pathway, so this result was quite unexpected. However, as previously mentioned, it has been reported in the literature that ROCK inhibition can affect the MAPK pathway. In melanoma cell lines, Chang and colleagues (Chang *et al.*, 2018) showed that the inhibition of ROCK exhibited a variable

response on cell proliferation and the activation of the MAPK and PAM pathways, and that this seemed to correlate with *BRAF* status. In *BRAF* wild-type (WT) melanoma cells, ROCK inhibition decreased proliferation and ERK 1/2 phosphorylation, but AKT phosphorylation was mostly unaffected; whereas in mutant *BRAF* V600E melanoma cells, ROCK inhibition increased proliferation, whilst having little effect on ERK 1/2 phosphorylation (there was a slight increase), but induced a notable increase in AKT phosphorylation (Chang *et al.*, 2018).

This could explain the difference in response to GSK269962; A2780 cells had lower basal ERK 1/2 phosphorylation, which decreased in response to GSK269962, and were sensitive to GSK269962; therefore, parental A2780 cells pheno-copy *BRAF* WT melanoma cells. In contrast, A2780-148R cells pheno-copy *BRAF* V600E melanoma cells; they had increased basal ERK 1/2 phosphorylation, which was unaffected by GSK269962, and whilst GSK269962 did not increase proliferation, A2780-148R cells were shown to be cross-resistant. It would be interesting to see if AKT phosphorylation was also increased in A2780-148R cells, in response to GSK269962. This divergence in the response of the MAPK pathway to ROCK inhibition, between A2780 and A2780-148R cells, may explain why A2780-148R cells were cross-resistant to ROCK inhibition. It also suggests that the ability of lower concentrations of AT13148 to cause a decrease in ERK 1/2 phosphorylation might be due to the inhibition of ROCK1 and 2 by AT13148.

In addition, the response of the ROCK pathway to the ROCK inhibitor GSK269962 was also assessed. Interestingly, in A2780-148R the ROCK pathway was shown to be partially refractory to inhibition by GSK269962, shown by a maintenance in the phosphorylation of the ROCK substrate MYPT1. This could suggest that the ROCK pathway is altered in some way to maintain the activity of the pathway in the presence of a ROCK inhibitor, which, in addition to ERK 1/2 phosphorylation also being refractory to ROCK inhibition in A2780-148R, may contribute to ROCK cross-resistance. This is contrary to the AT13148 response where, as previously described, the ROCK pathway responded in a similar manner in A2780 and A2780-148R (Figure 3.12). However, GSK269962 is a far more selective ROCK inhibitor, so perhaps the broader activity of AT13148 means that it is able to overcome possible changes within the ROCK pathway in A2780-148R that make it partially refractory to GSK269962.

It is worth noting that there were some issues in using the phosphorylation of T696 MYPT1 as a marker of ROCK pathway inhibition in A2780 and A2780-148R; in response to both AT13148 and GSK269962 the phosphorylation of T696 MYPT1 was never completely abolished (Figure 3.12 & Figure 3.15). This is likely to be caused by another kinase, not targeted by AT13148 and GSK269962, phosphorylating MYPT1 T696. For example, it has been shown that both ROCK1 & 2 and myotonic dystrophy kinase-related CDC42-binding kinase (MRCK), a CDC42 effector kinase, are required for the phosphorylation of T696 MYPT1, and, to a certain extent, can compensate for one another (Wilkinson *et al.*, 2005). Consequently, the use of T696 MYPT1 phosphorylation alone may not give an accurate reflection of ROCK pathway inhibition, and the use of other ROCK substrates should be considered. However, Kumper and colleagues (Kümper *et al.*, 2016) showed that inhibition of ROCK only leads to transient reduction in the phosphorylation of its downstream substrates, indicating that alternative mechanisms of phosphorylation exist for many ROCK substrates. Therefore, other ROCK substrates would likely have similar issues to T696 MYPT1, when used as a marker of ROCK pathway inhibition.

In summary, the work conducted in this chapter has validated A2780-148R as a model of resistance to AT13148. A2780-148R cells have been shown to be sensitive to IGF-1R and FGFR inhibitors, which provides a potential therapeutic strategy in AT13148 resistant patients. In addition, ROCK and PAM pathways were shown to be equally responsive to AT13148 in A2780 and A2780-148R, highlighting the by-pass of AT13148 targets as a potential mechanism of resistance. By-pass of the ROCK pathway is likely to be of particular importance, due the strong cross-resistance exhibited to ROCK inhibitors in A2780-148R. Furthermore, ERK 1/2 phosphorylation was shown to respond to AT13148 and GSK269962 in A2780 and A2780-148R, as well as being increased at the basal level in A2780-148R cells, the extent of which varied across experiments, suggesting the existence of sub-populations within A2780-148R. The following chapters will investigate the possible contribution of the by-pass of AT13148 targets and increased ERK 1/2 phosphorylation to AT13148 resistance.

Chapter 4

**Identification of candidate drivers
of AT13148 resistance in A2780-
148R isogenic clones**

4. Identification of candidate drivers of AT13148 resistance in A2780-148R isogenic clones

4.1. Introduction

One of the defining features of cancer, as a disease, is the wide range of heterogeneity that it displays. This heterogeneity can be seen on a number of different levels (inter-patient, inter-tumour and intra-tumour) but for the purposes of the work presented here intra-tumour heterogeneity (ITH) is the most relevant. Perhaps the clearest definition of ITH in its modern usage is from Heppner (Heppner, 1984) who described ITH as where "tumour cell differences are believed to be due to differences in cell lineage, i.e. due to the presence of distinctly different sub-populations capable of breeding true". In other words, the differences are due to genetic or epigenetic alterations and are transmissible to daughter cells. These tumour cell differences encompass differences in proliferation, progression through the cell cycle, antigen expression, membrane composition and response to therapy, to name a few (Heppner, 1984). It should be noted that these differences can exist between cells of the same tumour but occur independently of differences in cell lineage. Factors such as oxygen concentration, growth factor concentration, matrix biophysical properties; which show spatial variation across a tumour, and stochastic variation can contribute towards cell to cell variation within a tumour, but are not considered to be ITH (Heppner, 1984; Welch, 2016).

Much of the initial work on ITH focused on isolating sub-populations (also referred to as sub-clones) within a tumour and subsequently culturing them as individual cell lines (Heppner, 1984). Whilst some insight was gained into ITH from these studies, differences between isolated sub-populations could not be reliably stated to be caused by ITH alone, as the process of isolation of cells from a population can be a stimuli for new phenotypes in itself (Heppner, 1984). It was not until the advent of new sequencing technologies, such as single cell sequencing and deep sequencing, that the full depth of ITH was able to be grasped (Navin *et al.*, 2011; Gerlinger *et al.*, 2012). These studies have shown the extent of ITH within tumours and enabled cancer to be understood as an

evolutionary process in which: individual variation exists across the population, this variability is heritable, and individual variation leads to differences in cell survival (Gerlinger and Swanton, 2010). Furthermore, several clinical implications of ITH have been identified such as tumour sampling bias, therapy induced ITH and the impact of ITH upon therapy response and resistance (Swanton, 2012).

With regards to therapy resistance, studies on ITH have made it increasingly clear that sub-populations harbouring resistance conferring mutations frequently exist in tumours prior to treatment and are subsequently positively selected for upon treatment, driving acquired drug resistance (Burrell and Swanton, 2014; highlighted in Figure 4.1). An example of this can be seen in lung cancers which are treated with EGFR TKIs, such as gefitinib and erlotinib, in which resistance is commonly caused by a secondary T790M mutation in EGFR. Several studies have shown that T790M mutated cells are present in treatment naïve tumours and are selected for during treatment, leading to the rapid generation of resistance, and poor clinical outcome (Su *et al.*, 2012; Burrell and Swanton, 2014). In contrast, resistant sub-populations are not always detected in pre-treatment samples, and whilst this could be a limitation of the current sequencing technologies, it is likely that some resistance conferring mutations arise *de novo* during treatment (Burrell and Swanton, 2014).

In addition, studies have shown that, whether resistance develops from pre-existing mutated resistant sub-populations, *de novo* mutations, or a combination of the two, resistance is often polyclonal (Burrell and Swanton, 2014, highlighted in Figure 4.1). This means that several sub-populations conferring distinct resistance mutations, to a single therapy, can co-exist within the same tumour. One such example can be seen in a study by Liegl and colleagues (Liegl *et al.*, 2008) on resistance mechanisms to KIT/PDGFR TKIs in gastrointestinal stromal tumours (GIST), where it was demonstrated that three patients had two distinct resistance conferring secondary mutations in *KIT,* within the same lesion. A similar phenomenon has also been seen in *BRAF* V600E mutant melanoma, where Van Allen and colleagues (Van Allen *et al.*, 2014) identified a patient with co-existing MEK1 and NRAS mutations, within the same tumour, that conferred resistance against BRAF inhibitors. These mutations represent two distinct mechanisms of resistance, as NRAS is upstream of BRAF and MEK1 is downstream.
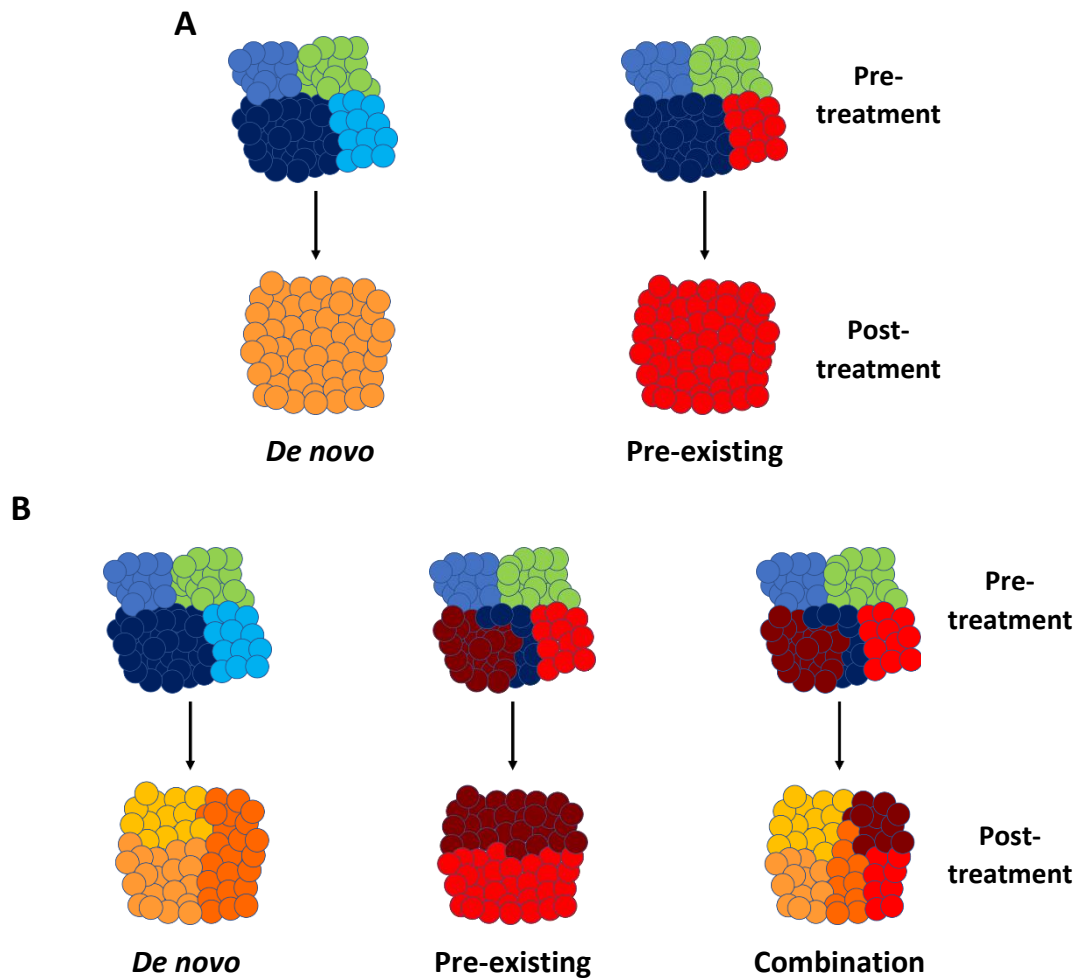
Figure 4.1: The impact of ITH upon the development of acquired polyclonal drug resistance. (A) Shows how resistance can develop via *de novo* mutations or by therapy induced selection of pre-existing mutated resistant sub-populations. **(B)** *De novo* resistance mutations, pre-existing resistant sub-populations, or combination of the two, can interact to generate polyclonal drug resistance. Figure adapted from Swanton, 2012.

As to be expected, since they are derived from singular tumours, human cancer cell lines have also been shown to have extensive heterogeneity. Much of the evidence for this seems to have come from isolating sub-populations from cancer cell lines, however, the use of modern sequencing technologies has also been used to map heterogeneity within cancer cell lines. For example, Ben-David and colleagues (Ben-David *et al.*, 2018) used deep sequencing to analyse 27 strains of the MCF-7 human breast cancer cell line, all of which were found to be sub-clonal, the extent of which varied across strains. In terms of the work conducted here, the heterogeneity within the A2780 human ovarian carcinoma cell line has not been mapped, but one can assume that it is heterogeneous

due to the near universality of ITH, which has been documented within ovarian cancer (Blagden, 2015). It is also possible that heterogeneity also exists within A2780-148R, and that resistance to AT13148 is polyclonal; i.e. there are two or more sub-populations within A2780-148R with distinct mechanisms of resistance to AT13148. There was some evidence of this shown in chapter 3, which was discussed in section 3.3, where the phosphorylation of ERK 1/2 in A2780-148R was shown to be increased at a basal level, however the extent of this was variable across experiments (Figure 3.11, Figure 3.13 & Figure 3.15). This variability could be caused by the presence of distinct sub-populations within A2780-148R which are selected for over time due subtle variations within cell culture conditions and experimental set-up.

Whilst the possibility of A2780-148R polyclonal resistance is interesting, as several distinct mechanisms of resistance to AT13148 could be identified, it does present some issues. Aside for the variability in results, polyclonal drug resistance may make it difficult to distinguish and validate mechanisms of resistance. For example, if a sub-population, that was present at a frequency of 5% of the total A2780-148R population, had attained resistance by direct re-activation of an AT13148 targeted pathway, this might be masked by the rest of the population that retained an AT13148 responsive pathway. Furthermore, when attempting to validate such a mechanism of resistance, by abolishing the resistance mechanism within A2780-148R (e.g. via pharmacological inhibition), the low frequency of the resistant sub-population would likely lead to a false-negative result.

To overcome these issues many studies on resistance to cancer therapies employ the use of isogenic sub-clones (Garraway and Jänne, 2012). This is often undertaken by using limiting dilution, where resistant cell lines are plated at ≤ 1 cell/well in a 96-well plate to isolate separate resistant sub-populations (isogenic sub-clones). Whilst, as previously mentioned, the effect of isolating sub-populations does have its limitations, the use of isogenic sub-clones has proved an effective way of identifying mechanisms of resistance, often with clinical relevance. Engelman and colleagues (Engelman *et al.*, 2007) generated resistance to the EGFR inhibitor gefitinib in the *EGFR* mutant NSCLC cell line HCC827 using dose-escalation and subsequent isogenic sub-cloning. They found that resistance was driven by increased MET expression (via an increase in copy number) and

that combination with PHA665752, a MET inhibitor, could re-sensitise resistant isogenic sub-clones to gefitinib. In addition, it was shown that MET amplification was present in tumours from resistant patients. It's interesting to note that the increase in MET copy number was not identified in the original 'polyclonal' resistant cell line (generated from dose-escalation alone, not isogenic sub-cloning), which highlights the importance of deriving resistant isogenic sub-clones; i.e. without isogenic sub-cloning it would have been difficult to identified MET amplification as a mechanism of resistance. Similar approaches have been used to identify mechanisms of resistance to vemurafenib & crizotinib, to name a few, many of which have been clinically validated (Nazarian *et al.*, 2010; Katayama *et al.*, 2011). Most studies employing the use of isogenic sub-clones tend to focus on one isogenic sub-clone, and therefore only identify one mechanism of resistance. However, Gowrishankar and colleagues (Gowrishankar *et al.*, 2012) used several isogenic sub-clones (derived from the same polyclonal resistant cell line) to identify distinct mechanisms of resistance to dabrafenib (a BRAF V600E inhibitor) in a *BRAF V600E* melanoma cell line, including activating *NRAS* mutations and increased expression of COT1 kinase. This highlights how the use of isogenic sub-clones can enable the identification of several distinct mechanisms of resistance to the same therapy.

Taking into account the likelihood of resistance to AT13148 within A2780-148R being polyclonal, the aim of this chapter was to generate isogenic sub-clones from A2780-148R to investigate AT13148 resistance. Initially, the focus was to screen these sub-clones based on the key findings of chapter 3, such as cross-resistance to ROCK inhibition and sensitivity to IGF-1R inhibition. The results from this were then used to select sub-clones for further characterisation to identify putative candidate drivers of resistance.

4.2. Results

4.2.1. Determination of AT13148 resistance and cross-resistance profiling in 148R clones

In total, 10 isogenic sub-clones (henceforth referred to as 148R clones) were derived from A2780-148R by limiting dilution that were able to undergo routine sub-culture (Figure 4.2). Subsequently, AT13148 resistance was determined, and cross-resistance profiling performed to compare 148R clones to A2780 and A2780-148R cells. This was conducted so that resistance to AT13148 could be validated, and 148R clones with the most unique phenotypes, which might be indicative of a distinct mechanism of resistance, could be identified and selected for further characterisation and investigation of AT13148 resistance. The drugs used in cross-resistance profiling were drugs that A2780-148R had been shown to have strong resistance or sensitivity to in chapter 3: GSK269962, NVP-AEW541 and AZD4547. It should be noted that 148R clones were originally plated at 1600 cells/well (the optimal seeding density for A2780-148R, Figure 3.1), but that this was changed for some clones based on observations during SRB assays. In addition, to maximise their chance of survival, 148R clones were initially cultured in the absence of 5.2 µM AT13148 (the maintenance dose of AT13148).

4.2.1.1. AT13148

Figure 4.2 shows that all 148R clones, except for 148R-I (RF = 1.86, not statistically significant), were shown to have greater than 2-fold resistance to AT13148 (RF ≥ 2.00), with this being statistically significant in all but two clones (148R-G and 148R-U). A2780-148R was also shown to be resistant to AT13148; the GI_{50} for A2780-148R was 0.94 µM compared to 0.22 µM in A2780, a statistically significant difference giving an RF value of 4.27, consistent with the result in chapter 3 (Figure 4.2, previous result Figure 3.2). However, 148R clones exhibited differing levels of resistance when compared to one another and A2780-148R (Figure 4.2). Some 148R clones exhibited lower resistance than what was seen in A2780-148R, such as 148R-K and 148R-P which had GI_{50} values of 0.76 µM and 0.62 µM respectively, resulting in an RF of ~3 (Figure 4.2). In contrast, 148R-J and 148R-N had GI_{50} values of 2.51 µM (RF = 11.41) and 2.04 µM (RF = 9.27) respectively,

much higher than was seen with A2780-148R (Figure 4.2). Taken together, the majority of 148R clones were shown to be resistant to AT13148, but there was variation in the level of resistance amongst 148R clones.
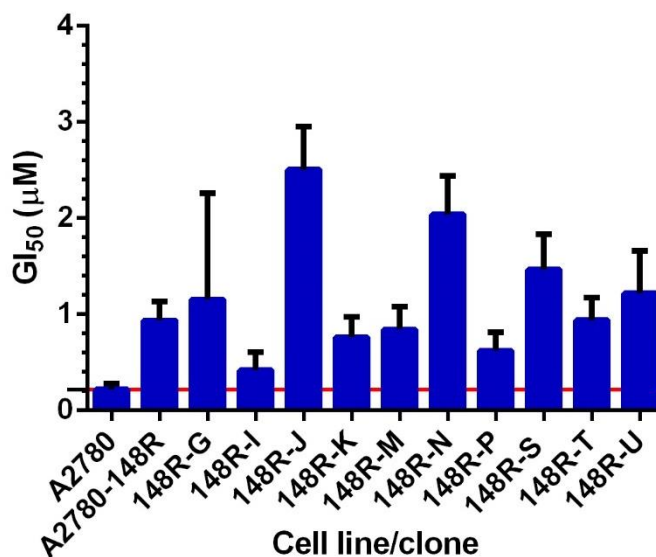
Cell line	GI_{50} (μM)	RF
A2780	0.22 ± 0.06	N/A
A2780-148R	0.94 ± 0.20***	4.27
148R-G	1.15 ± 1.11	5.23
148R-I	0.41 ± 0.19	1.86
148R-J	2.51 ± 0.45**	11.41
148R-K	0.76 ± 0.21**	3.45
148R-M	0.84 ± 0.24**	3.82
148R-N	2.04 ± 0.40*	9.27
148R-P	0.62 ± 0.19*	2.82
148R-S	1.46 ± 0.37**	6.64
148R-T	0.94 ± 0.23*	4.27
148R-U	1.22 ± 0.44	5.55

Figure 4.2: Summary of GI_{50} and RF values for AT13148 in A2780, A2780-148R and 148R clones. Graph and table summarise the GI_{50} and RF values for AT13148 in A2780, A2780-148R and 148R clones, as determined from a standard 6-day SRB cell viability assay. Graph was generated using GraphPad Prism 6. Bars and table data points depict the mean GI_{50} ± SD from all experiments conducted. The red line on the y-axis of the graph marks A2780 GI_{50}. Statistical significance was calculated using a student's t-test, * $p \leq 0.05$, ** $p \leq 0.01$, *** $p \geq 0.001$, n ≥ 3 independent experiments.

4.2.1.2. GSK269962

The response of 148R clones to the ROCK inhibitor GSK269962 was assessed to investigate if they were cross-resistant to ROCK inhibition, as was seen with A2780-148R in chapter 3 (Figure 3.5). All 148R clones had RF values of > 10.00, indicating strong cross-resistance to GSK269962 (Figure 4.3A). This was shown to be statistically significant in all 148R clones except 148R-G, T & U. Also, as previously shown in chapter 3, A2780-148R was cross-resistant to GSK269962; A2780-148R had GI_{50} of 1.310 µM compared to 0.026 µM in A2780, a statistically significant difference equating to a RF of 50.38 for A2780-148R, consistent with the previous result (Figure 4.3A, previous result Figure 3.5). As with AT13148, there was a large degree of variation in response to GSK269962 amongst 148R clones, with some clones having a lower GI_{50} than A2780-148R and some higher. The lowest GI_{50} was seen in 148R-I, which had a GI_{50} of 0.287 µM (RF = 11.42), substantially lower than the GI_{50} for A2780-148R (Figure 4.3A). Conversely, the highest GI_{50} was seen in 148R-J, which had a GI_{50} of 4.388 µM (RF = 168.77), which was greater than A2780-148R and 15-fold higher than 148R-I (Figure 4.3B). Other 148R clones, such as 148R-N (GI_{50}: 1.662, RF = 63.92), were not too dissimilar from A2780-148R (Figure 4.3A).

It was interesting to note that 148R clones with the highest and lowest GI_{50} for GSK269962, 148R-J and 148R-I respectively, corresponded to what was seen with AT13148, i.e. 148R-J had the highest AT13148 GI_{50} and 148R-I the lowest (Figure 4.2 & Figure 4.3). To investigate if there was any correlation between the GI_{50} of AT13148 and GSK269962 amongst 148R clones, A2780-148R, and A2780, Pearson correlation coefficient analysis was performed (Figure 4.3B). This gave a statistically significant R value of 0.89 and an R^2 value of 0.79, indicating that there was strong positive correlation between the GI_{50} values of AT13148 and GSK269962 in 148R clones, A2780-148R and A2780 (Figure 4.3B). In summary, the majority of 148R clones were cross-resistant to the ROCK inhibitor GSK269962, but there was large variation in the level of cross-resistance. In addition, the strong positive correlation between AT13148 and GSK269962 GI_{50} suggests AT13148 resistance is dependent upon overcoming the inhibition of ROCK by AT13148.
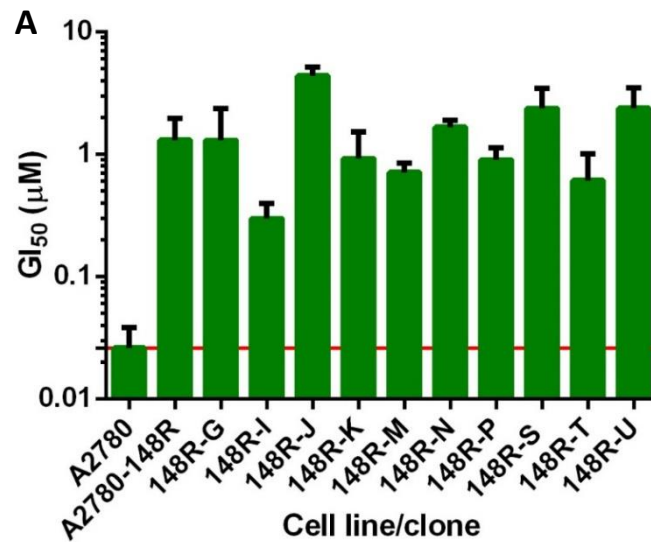
Cell line	GI$_{50}$ (μM)	RF
A2780	0.026 ± 0.012	N/A
A2780-148R	1.310 ± 0.655***	50.38
148R-G	1.301 ± 1.060	50.04
148R-I	0.297 ± 0.098*	11.42
148R-J	4.388 ± 0.746**	168.77
148R-K	0.918 ± 0.609*	35.31
148R-M	0.711 ± 0.138**	27.35
148R-N	1.662 ± 0.228***	63.92
148R-P	0.901 ± 0.226*	34.65
148R-S	2.363 ± 1.069*	90.88
148R-T	0.611 ± 0.393	23.50
148R-U	2.374 ± 1.106	91.31
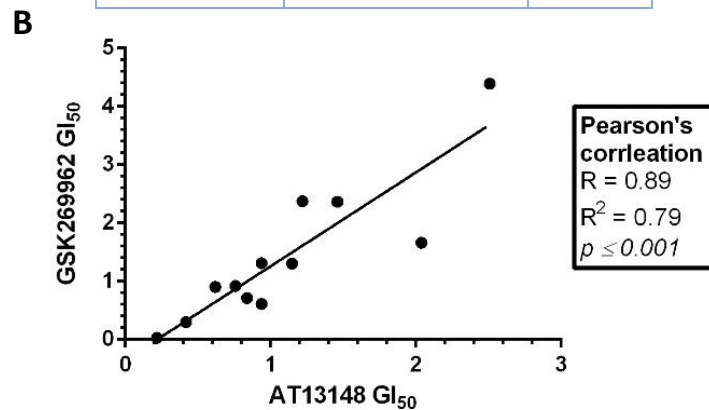
Figure 4.3: Summary of GI$_{50}$ and RF values for GSK269962 and correlation with AT13148 in A2780, A2780-148R and 148R clones. (A) Graph and table summarise the GI$_{50}$ and RF values for GSK269962 in A2780, A2780-148R and 148R clones, as determined from a standard 6-day SRB cell viability assay. Graph was generated using GraphPad Prism 6. Bars and table datapoints depict the mean GI$_{50}$ ± SD from all experiments conducted. The red line on the y-axis of the graph highlights A2780 GI$_{50}$. Statistical significance was calculated using a student's t-test, * $p \leq 0.05$, ** $p \leq 0.01$, *** $p \geq 0.001$, n ≥ 3 independent experiments. **(B)** Graph displays the correlation between AT13148 and GSK269962 GI$_{50}$ values. Data points represent the mean GI$_{50}$ for an individual cell line (A2780, A2780-148R or 148R clones). Pearson's correlation coefficient and statistical significance were calculated using GraphPad Prism 6. n ≥ 3 independent experiments.

4.2.1.3. NVP-AEW541

Since A2780-148R had been shown to be sensitive to the IGF-1R inhibitor NVP-AEW541 (Figure 3.6), when compared to parental A2780 cells, the response of 148R clones to NVP-AEW541 was investigated. The response amongst the 148R clones was again diverse, but remarkably none of them had a strong level of sensitivity to NVP-AEW541, with only three clones; 148R-I, P and S, shown to have a greater than 2-fold sensitivity (RF ≤ 0.50) to NVP-AEW541 (Figure 4.4A, B). A2780 had GI_{50} of 1.72 µM compared to 0.63 µM in 148R-I, 0.76 µM in 148R-P and 0.78 µM in 148R-S, equating to RF values of 0.37, 0.44 and 0.45 respectively, which were all statistically significant (Figure 4.4A, B). In contrast, 148R-N and 148R-U had statistically significant low-level cross-resistance against NVP-AEW541; 148R-N and 148R-U had GI_{50} values of 4.11 µM (RF = 2.39) and 3.87 µM (RF = 2.25) respectively (Figure 4.4A, B).

Unexpectedly, A2780-148R was not shown to be sensitive to NVP-AEW541; A2780-148R had a GI_{50} of 1.09 µM, which although statistically significant, only equated to an RF value of 0.63 (Figure 4.4A, B). This contradicts what was seen in chapter 3, where A2780-148R was shown to have an RF value of 0.14, indicating sensitivity to NVP-AEW541 (Figure 3.6). Upon closer inspection, the loss of sensitivity seemed to have been caused by an increase in the GI_{50} of A2780-148R (0.22 µM in Figure 3.6 vs 1.09 µM in Figure 4.4A, B), rather than a decrease in the GI_{50} of A2780 (1.56 µM in Figure 3.6 vs 1.72 µM in Figure 4.4A, B). This might explain why 148R clones did not have a high degree of sensitivity to NVP-AEW541; they were derived from A2780-148R cells that had already lost sensitivity/were in the process of losing sensitivity to NVP-AEW541. Indeed, Figure 4.4C shows the gradual increase in A2780-148R GI_{50} against NVP-AEW541 over the course of successive SRB assays that were conducted during the time in which 148R clones were isolated from A2780-148R and initially characterised. For example, the GI_{50} for NVP-AEW541 in A2780-148R cells increased from 0.25 µM on the 28Nov16, when A2780-148R cells were plated for limiting dilution, to 1.84 µM on 18Jan17 (Figure 4.4C). Taken together, these data suggest that 148R clones have lost most of their sensitivity to NVP-AEW541, with many clones showing no sensitivity and some even cross-resistance. This is likely to be explained by the loss of sensitivity to NVP-AEW541 in A2780-148R, from which 148R clones were derived.

A

B

Cell line	GI$_{50}$ (μM)	RF
A2780	1.72 ± 0.34	N/A
A2780-148R	1.09 ± 0.43**	0.63
148R-G	1.25 ± 0.55	0.73
148R-I	0.63 ± 0.13***	0.37
148R-J	1.21 ± 0.07*	0.70
148R-K	0.97 ± 0.28**	0.56
148R-M	1.34 ± 0.64	0.78
148R-N	4.11 ± 0.07***	2.39
148R-P	0.76 ± 0.37**	0.44
148R-S	0.78 ± 0.42*	0.45
148R-T	2.56 ± 0.67	1.49
148R-U	3.87 ± 0.17***	2.25

C

	A2780	A2780-148R	
Date	GI$_{50}$ (μM)	GI$_{50}$ (μM)	RF
28-Nov-16	1.39	0.25	0.18
18-Dec-16	1.41	0.51	0.36
10-Jan-17	1.30	0.62	0.48
11-Jan-17	2.16	0.99	0.46
17-Jan-17	1.64	1.31	0.80
18-Jan-17	1.58	1.84	1.16
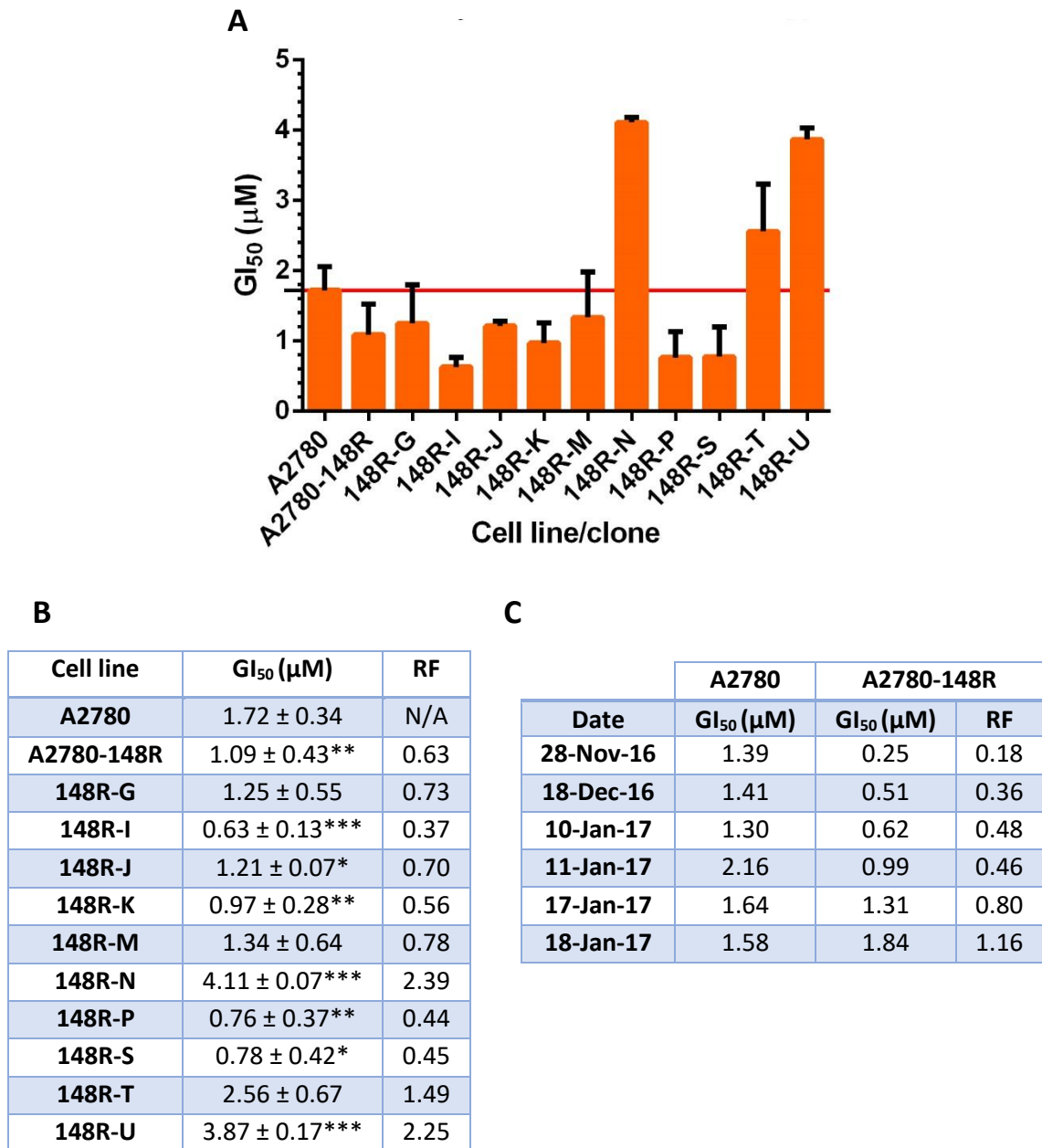
Figure 4.4: Summary of GI$_{50}$ and RF values for NVP-AEW541 in A2780, A2780-148R and 148R clones.
(A, B) Summary of the GI$_{50}$ and RF values for NVP-AEW541 in A2780, A2780-148R and 148R clones, as determined from a standard 6-day SRB cell viability assay. Graph was generated using GraphPad Prism 6. Bars depict the mean GI$_{50}$ ± SD of all experiments conducted. Red line on the y-axis of the graph highlights A2780 GI$_{50}$. Table summarises NVP-AEW541 GI$_{50}$ and RF, GI$_{50}$ data points represent the mean ± SD of all experiments conducted. Statistical significance was calculated using a student's t-test, * *p ≤ 0.05*, ** *p ≤ 0.01*, *** *p ≥ 0.001,* n ≥ 3 independent experiments. **(C)** Table summarises GI$_{50}$ and RF values for NVP-AEW541 in A2780 and A2780-148R over time. GI$_{50}$ and RF values were taken from individual experiments.

4.2.1.4. AZD4547

The response of 148R clones to the FGFR inhibitor AZD4547 was also assessed to see if they maintained sensitivity to AZD4547, which was shown in A2780-148R in chapter 3 (Figure 3.6). Figure 4.5 shows that A2780-148R had statistically significant sensitivity to AZD4547, compared to parental A2780 cells; A2780-148R had a GI_{50} of 0.034 µM compared to 0.378 µM in A2780, which equated to a RF of 0.089 (11-fold sensitivity). This was mirrored in 148R clones, which were all shown to have statistically significant sensitivity to AZD4547, except for 148R-N (Figure 4.5). However, just as was seen with other compounds used in cross-resistance profiling, the response to AZD4547 was diverse amongst 148R clones. 148R-M had a GI_{50} of 0.001 µM which was the lowest GI_{50} observed and equated to an RF value of 0.003 (~378-fold sensitivity), 148R-M was therefore considerably more sensitive than A2780-148R (Figure 4.5). Contrary to this, 148R-N had a GI_{50} of 1.113 µM, which whilst just shy of being statistically significant (*p = 0.06,* data not shown), indicated low-level cross-resistance, which 148R-N also displayed to NVP-AEW541 (Figure 4.4 & Figure 4.5). Other 148R clones had a similar GI_{50} to A2780-148R, such as 148R-T and 148R-U, which had GI_{50} values of 0.037 µM (RF = 0.098) and 0.032 µM (RF = 0.085) respectively (Figure 4.5). In summary, these data show that whilst there was considerable variation in response to AZD4547 amongst 148R clones, the majority of were sensitive to AZD4547.
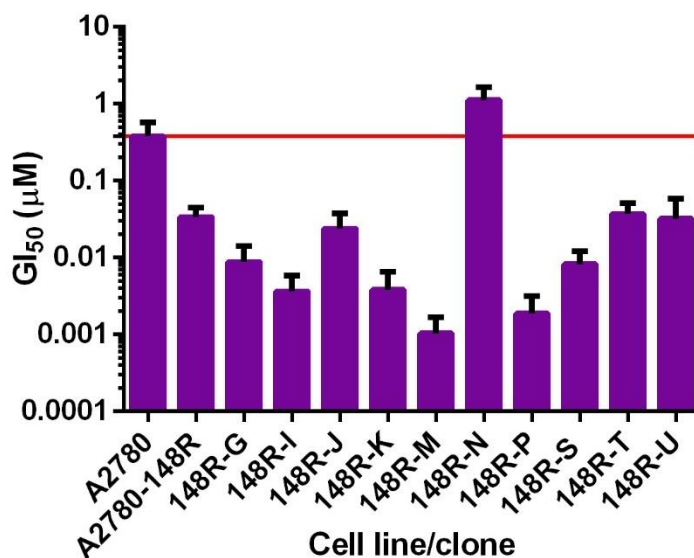
Cell line	GI$_{50}$ (μM)	RF
A2780	0.378 ± 0.196	N/A
A2780-148R	0.034 ± 0.011***	0.089
148R-G	0.009 ± 0.005***	0.024
148R-I	0.004 ± 0.002***	0.011
148R-J	0.024 ± 0.014***	0.063
148R-K	0.004 ± 0.003***	0.011
148R-M	0.001 ± 0.001***	0.003
148R-N	1.113 ± 0.287	2.94
148R-P	0.002 ± 0.001***	0.005
148R-S	0.008 ± 0.004***	0.021
148R-T	0.037 ± 0.014***	0.098
148R-U	0.032 ± 0.026***	0.085

Figure 4.5: Summary of GI$_{50}$ and RF values for AZD4547 in A2780, A2780-148R and 148R clones. Graph and table summarise the GI$_{50}$ and RF values for AZD4547 in A2780, A2780-148R and 148R clones, as determined from a standard 6-day SRB cell viability assay. Graph was generated using GraphPad Prism 6. Bars and table datapoints depict the mean GI$_{50}$ ± SD of all experiments conducted. The red line on the graph y-axis highlights A2780 GI$_{50}$. Statistical significance was calculated using a student's t-test, ***$p \geq$ 0.001*, n ≥ 3 independent experiments.

4.2.2. Analysis of basal signalling in 148R clones

Markers of pathways directly targeted by AT13148 (PAM and ROCK pathways), as well as IGF-1R expression (shown to be upregulated in A2780-148R, Figure 3.10), were investigated at basal level via western blotting in 148R clones. Figure 4.6 shows all 148R clones, as well as A2780-148R, over-expressed IGF-1R when compared to parental A2780 cells, but just as was seen with cross-resistance profiling, there was a high degree of variation in the level of IGF-1R expression amongst 148R clones (Figure 4.6). Some 148R clones, such 148R-J and 148R-T, had much higher expression of IGF-1R than A2780-148R (Figure 4.6). On the other hand, other 148R clones, such as 148R-K, S & U, had a lower expression of IGF-1R versus A2780-148R (Figure 4.6).

Figure 4.6 also shows that there was little difference in AKT S473 and PRAS40 T246 phosphorylation in A2780-148R when compared to A2780, although S473 AKT phosphorylation appeared marginally lower in A2780-148R. This was similar in most 148R clones; the phosphorylation of S473 AKT and T246 PRAS40 was the same or slightly decreased when compared to A2780, however, these markers were increased in some clones (Figure 4.6). 148R-N had a slight increase in the phosphorylation of S473 AKT and a more notable increase in T246 PRAS40 phosphorylation, whereas in 148R-J, G and T, S473 AKT phosphorylation was unaltered/slightly decreased but T246 PRAS40 phosphorylation was increased (Figure 4.6). Further downstream the PAM pathway there were also changes seen within the phosphorylation of S235/236 S6RP, a p70S6K substrate (Figure 4.6). Many clones had decreased S235/236 S6RP phosphorylation, with this being most notable in 148R-K, M and S (Figure 4.6). This appeared to be independent of the changes in AKT and PRAS40 phosphorylation, for example, 148R-N had increased AKT and PRAS40 phosphorylation but decreased S235/236 S6RP phosphorylation (Figure 4.6).

The phosphorylation of T696 MYPT1 was also assessed as a marker of the ROCK pathway. T696 MYPT1 phosphorylation was shown to be relatively unaltered amongst A2780, A2780-148R and 148R clones (Figure 4.6). However, there were a few exceptions to this, with T696 MYPT1 phosphorylation being notably decreased in 148R-G and 148R-P (Figure 4.6). Taken together, these data showed that there was some variation in the

basal signalling in pathways assessed amongst 148R clones, with this being most prominent with IGF-1R expression. Some of these changes, particularly within the PAM pathway, warrant further investigation.
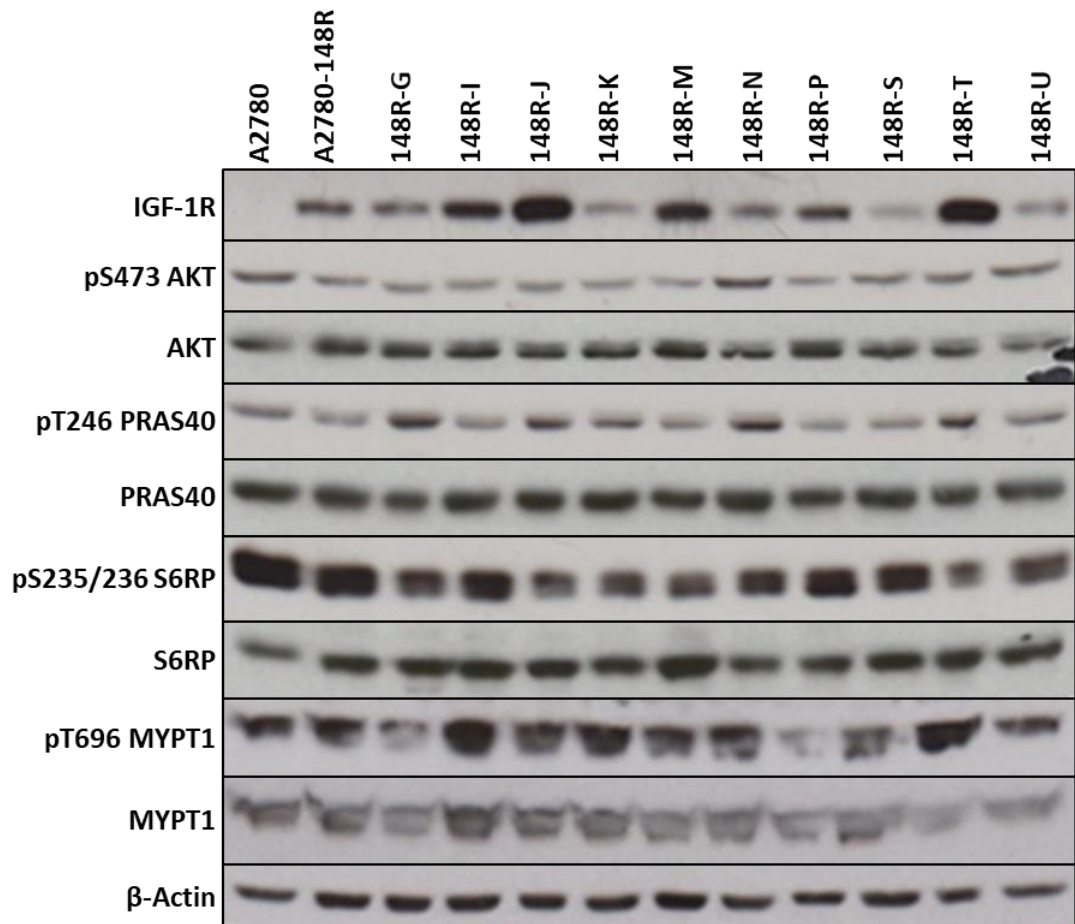
Figure 4.6: Analysis of the basal expression of IGF-1R and markers of the PAM and ROCK pathways in A2780, A2780-148R and 148R clones. Cells were plated at either 0.5 x 10^6 (A2780) or 1 x 10^6 (A2780-148R and 148R clones) cells per 10 cm dish and allowed to grow for 48 hours under standard growth conditions. Cells were then lysed prior to western blot analysis. Western blot membranes were probed with antibodies for phospho-proteins, stripped, and then re-probed with antibodies for total proteins and loading control (β-Actin). Data are representative of three independent experiments.

4.2.3. Selection of 148R clones for further characterisation

The initial characterisation of 148R clones gained insight into the resistance generated against AT13148. In particular, the diverse response amongst the 148R clones to the cross-resistance profiling suggested that there was a degree of heterogeneity within A2780-148R, and therefore the possible existence of several sub-populations with distinct mechanisms of resistance to AT13148. In order to investigate this, three 148R clones: 148R-K, 148R-N and 148R-S, were selected for further, more detailed, characterisation. The rationale for this is highlighted in Table 4.1. Briefly, these clones were selected as they all had robust resistance to AT13148 but represented the range of resistance to AT13148 seen amongst clones in Figure 4.2 (RF value of the three clones was between ~3 and ~9). It was important to have this range represented amongst the selected 148R clones, as different levels of resistance to AT13148 may require distinct mechanisms. Additionally, 148R-K and 148R-S were selected as they were sensitive to AZD4547, with 148R-S also sensitive to NVP-AEW541. In contrast, 148R-N was selected as it appeared to be the most unique clone, displaying cross-resistance to NVP-AEW541 and AZD4547 and displayed markers that indicated altered signalling within the PAM pathway (Figure 4.6, e.g. increased PRAS40 phosphorylation).

Table 4.1: Summary of cross-resistance profiling in 148R clones. Table gives an overview of cross-resistance profiling (Figure 4.2-Figure 4.5), the results of which were used to justify the selection of 148R clones for further characterisation. ✓ and ✘ respectively indicate a positive or negative result for the attribute outlined (e.g. AT13148 resistance). An increasing number of ticks indicates greater resistance/sensitivity. Results that were not statistically significant are marked with a ^. The threshold for resistance/cross-resistance was RF ≥ 2.00 and sensitivity RF ≤ 0.50. Clones that were selected for further characterisation are highlighted in blue.

148R clone	AT13148 resistance	GSK269962 cross-resistance	NVP-AEW541 sensitivity	AZD4547 sensitivity
148R-G	✓✓^	✓^	✘	✓
148R-I	✘	✓	✓	✓
148R-J	✓✓✓	✓✓✓	✘	✓
148R-K	✓	✓	✘	✓
148R-M	✓✓	✓	✘	✓✓✓
148R-N	✓✓✓	✓✓	✘ (Cross-resistant)	✘ (Cross-resistant^)
148R-P	✓	✓	✓	✓✓
148R-S	✓✓	✓✓	✓	✓
148R-T	✓✓	✓^	✘	✓
148R-U	✓✓^	✓✓^	✘ (Cross-resistant)	✓

4.2.4. Light microscopy of selected 148R clones

As with A2780-148R cells in chapter 3, the morphology of selected 148R clones was evaluated under light microscopy, both untreated and treated with 5.2 µM AT13148 (maintenance dose of AT13148), and compared to parental A2780 cells, as well as one another. Figure 4.7 shows that untreated parental A2780 cells displayed a similar morphology as was previous described in chapter 3 (Figure 3.3), growing as 'pebble-like' clusters; having a rounded/polygonal morphology, consistent with an epithelial phenotype, and not undergoing contact inhibition. In general, the morphology of untreated 148R clones was similar to one another and parental A2780 cells; 148R clones retained an epithelial phenotype and did not appear to undergo contact inhibition, as had been previously described for A2780-148R cells in chapter 3 (Figure 3.3 & Figure 4.7). However, there were some subtle differences in morphology amongst 148R clones. Both 148R-K and 148R-S cells grew as distinct compact colonies, not too dissimilar from the 'pebble-like' colonies of A2780, but 148R-N cells grew less compact, as large interconnected 'branches' of cells, in similar manner to A2780-148R cells as described in chapter 3 (Figure 3.3 & Figure 4.7). In addition, 148R-S cells appeared smaller and had more of a rounded morphology, when compared to 148R-K and 148R-N, which had more of a polygonal morphology and appeared larger, particularly 148R-N (Figure 4.7).

The morphology of parental A2780 cells treated with AT13148 was also consistent with what was previously described in chapter 3; a subset of cells were either undergoing membrane blebbing, indicative of apoptosis, or had developed a 'spindle-like' morphology, becoming long and thin (Figure 3.3 & Figure 4.7). This 'spindle-like' morphology was also seen in all 148R clones, but again only in subset of cells, not the total population. As discussed in section 3.3, this 'spindle-like' morphology likely due to the inhibition of ROCK1 and 2 by AT13148, although the effect of other AT13148 targets cannot be discounted.

Taken together, these data show that 148R-K, N and S, despite some subtle differences, have similar morphologies to one another, consistent with an epithelial phenotype, and morphologically respond to AT13148 in similar manner to parental A2780 cells, developing a 'spindle-like' morphology in a subset of the total population.
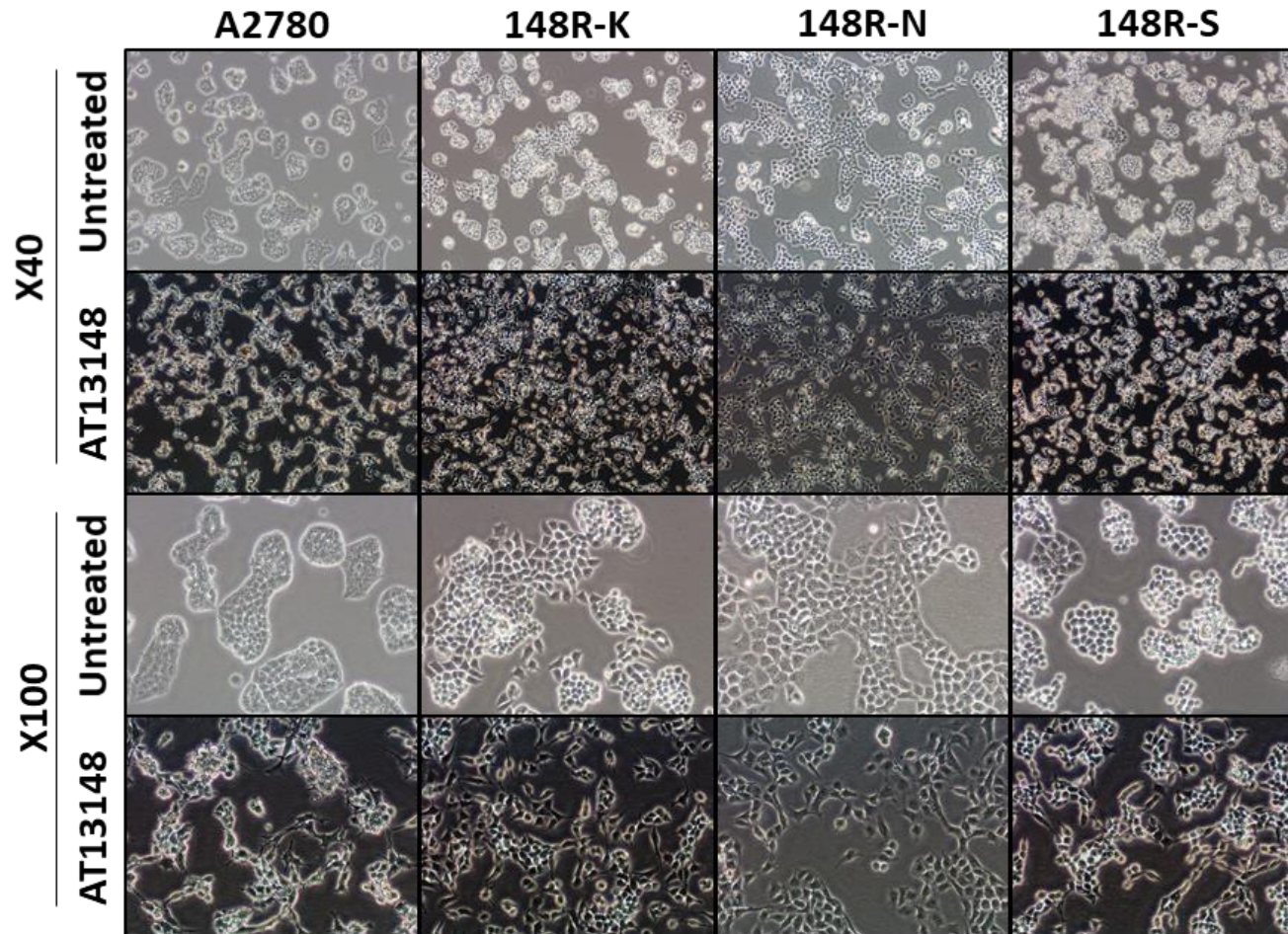
Figure 4.7: Light microscopy images of untreated and AT13148 treated A2780 cells and 148R clones. Cells were split into T25 flasks to allow 2-3 days growth, and either left untreated or treated with 5.2µM AT13148. After 48 hours, when cells were ~70% confluent, cells were observed under a light microscope at x40 or x100 magnification and images taken. Images are representative of two independent experiments.

4.2.5. Growth characterisation of selected 148R clones

As previously mentioned, since growth characterisation assays had not been performed, the seeding densities used for 148R clones (Figure 4.2-Figure 4.5) were determined via trial and error over successive SRB assays. Therefore, prior to the additional characterisation of selected 148R clones, growth characterisation assays were performed to determine the optimal seeding density for 148R clones in a standard 6-day SRB cell viability assay. The optimal seeding density for A2780 and 148R-N was determined to be 800 cells/well and 3200 cells/well respectively (Figure 4.8). This was consistent with the established optimal seeding density for A2780 in chapter 3 and seeding density that had been used for 148R-N in Figure 4.2-Figure 4.5. It was difficult to determine the optimal seeding density for 148R-K and 148R-S as they appeared to be log-phase growth when plated at both 1600 cells/well and 3200 cells/well (Figure 4.8). However, at 3200 cells/well 148R-K cells appeared to be more consistently in log-phase growth, whereas 148R-S abruptly stopped growing at T = 144h (Figure 4.8). This could indicate that the growth of 148R-S cells slowed towards the end of the 96-hour drug treatment window when plated at 3200 cells/well (Figure 4.8). Therefore, the optimal seeding densities selected for 148R-K and 148R-S were 3200 cells/well and 1600 cells/well respectively. 148R-K cells had been plated at 1600 cells/well in Figure 4.2-Figure 4.5.

The doubling times for 148R clones and A2780 cells (when plated at their optimal seeding densities) were also calculated (as shown in shown in section 3.2.1). Whilst there were some differences between the doubling times of A2780, 148R-K and 148R-S (25.9, 32.8 and 30.0 hours respectively), they weren't too dissimilar (Figure 4.9). However, 148R-N had a doubling time of 42.5 hours which was longer than A2780, 148R-K and 148R-S (Figure 4.9). This was also seen when the optimal seeding densities were superimposed on the same graph; A2780, 148R-K and 148R-S were indistinguishable from one another, but 148R-N was more distinctive, albeit not too dissimilar; the curve for 148R-N appeared to be more shallow and the growth for 148R-N plateaued between 144 and 168 hours (Figure 4.9). Taken together, optimal seeding densities for A2780 and 148R clones were established that enabled near-identical growth kinetics over the course of an SRB cell viability assay.
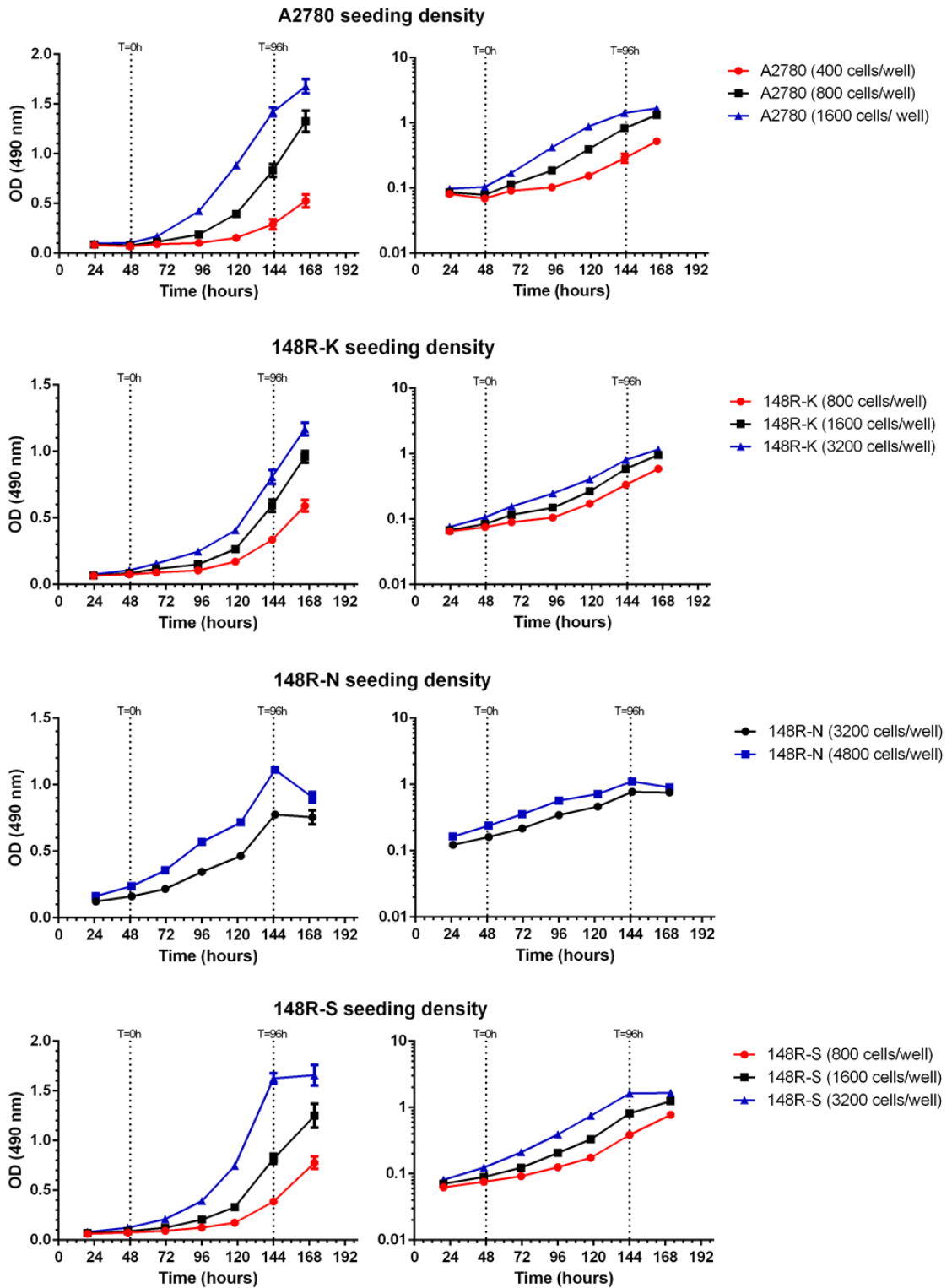
Figure 4.8: Characterisation of the growth of A2780 and 148R clones in a 96-well plate. Cells were plated in 96-well plates at the densities indicated, with 6 replicates per density. A plate was fixed every 24 hours and analysed via SRB assay. Growth curves were generated using GraphPad Prism 6. T = 0h and T = 96h highlights the 96-hour drug treatment window in a standard 6-day SRB cell viability assay. Data points represent the mean ± SD of one representative experiment, n = 3 (A2780), 2 (148R-K and S) or 1 (148R-N) independent experiments.
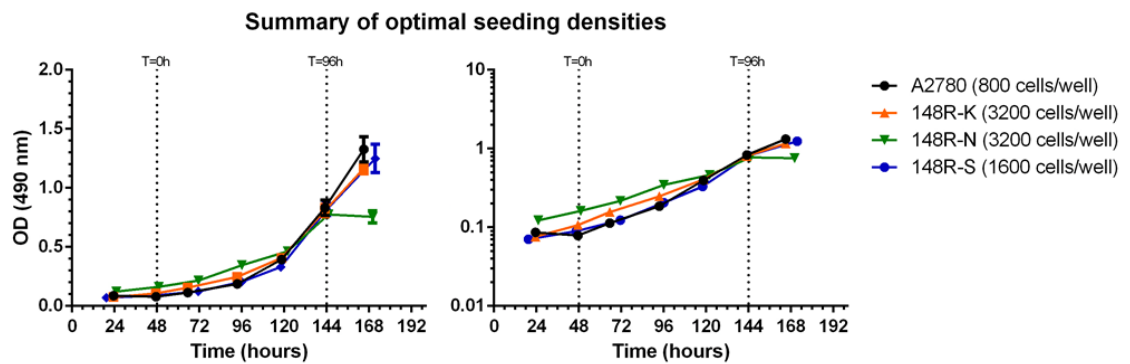
Figure 4.9: Comparison of optimal seeding densities and doubling times in A2780 and 148R clones. Cells were plated as per Figure 4.8. Graphs were generated using GraphPad Prism 6 for the over-lay of optimal seeding densities established in Figure 4.8. Table summarises the doubling times of A2780 and 148R clones over 96-hour drug treatment window when plated at their optimal seeding densities. Data points represent the mean ± SD from one representative experiment. n = 3 (A2780), 2 (148R-K and S) or 1 (148R-N) independent experiments.

4.2.6. Determination of resistance to AT13148 and cross-resistance profiling in selected 148R clones

During the initial cross-resistance profiling, 148R clones were cultured in the absence of AT13148 (Figure 4.2-Figure 4.5). Since selected 148R clones were subsequently cultured in the maintenance dose of AT13148 (5.2 μM) it was necessary to re-validate AT13148 resistance and cross-resistance profiling, as continuous culture in the presence of AT13148 may influence the results originally obtained.

Figure 4.10A shows that selected 148R clones all had statistically significant resistance to AT13148; A2780 had a GI_{50} of 0.16 μM compared to GI_{50} values of 1.65 μM, 1.49 μM and 1.46 μM for 148R-K, N and S respectively. This resulted in an RF of ~9 for 148R-N and 148R-S, and ~10 for 148R-K (Figure 4.10A). For A2780, 148R-N and 148R-S these results were relatively consistent with the previous results obtained in Figure 4.2, but this was not the case for 148R-K. In Figure 4.2 the GI_{50} for 148R-K against AT13148 was 0.76 μM, ~2-fold lower than the GI_{50} obtained in Figure 4.10A, 1.49 μM, equating to RF of ~3. This could be due to inter-assay variation but may indicate that some of the resistance to AT13148 in 148R-K is transient and dependent on chronic exposure to AT13148.

Upon closer inspection of the AT13148 data it appeared that the non-linear regression curve did not fit the data for 148R-N as well as it did for A2780, 148R-K and 148R-S (Figure 4.10A). This appeared to cause an underestimation of the GI_{50} for 148R-N. Analysis of the R^2 values for the non-linear regression curves confirmed this; 148R-N had an R^2 of 0.84 which was lower than what was seen in A2780, 148R-K and 148R-S ($R^2 >$ 0.90, Figure 4.10A). The AT13148 data for 148R-N was therefore re-analysed by joining the datapoints 'dot to dot' and calculating the GI_{50} by using linear regression between the data points before and after 50% viability (Figure 4.10B). Figure 4.10B shows that the re-analysed GI_{50} for 148R-N was 3.25 μM, which was statistically significant when compared to A2780 and gave an RF of ~20, the greatest seen amongst 148R clones. Analysing the data in this manner also highlighted that 148R-N exhibited a distinctive response to AT13148. The inhibition of cell viability occurred in two distinct linear phases; the 1st at concentrations up to 3.3 μM, where viability gradually decreased, and

the 2nd between 3.3 µM and 10.0 µM, where there was sharp decrease in cell viability. Taken together, these data validated resistance to AT13148 in 148R-K, N & S, but again showed that there was diversity in the response to AT13148 amongst 148R clones, particularly 148R-N.

A
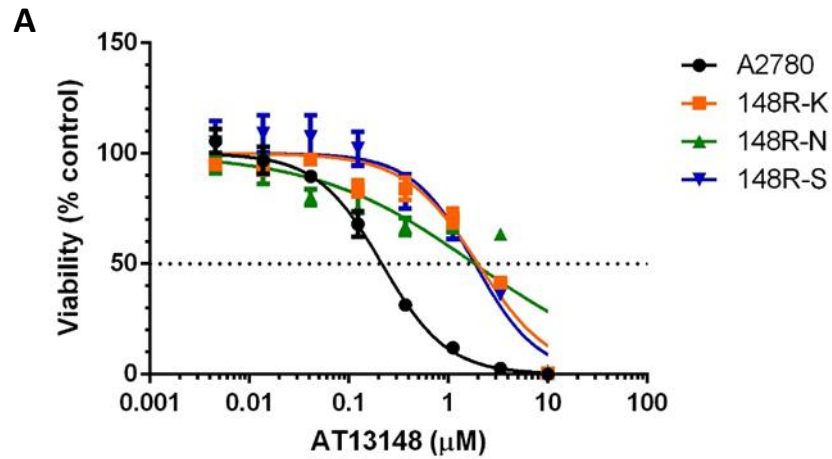
Cell line	GI$_{50}$ (µM)	RF	R^2
A2780	0.16 ± 0.05	N/A	0.97 ± 0.02
148R-K	1.65 ± 0.81***	10.31	0.95 ± 0.03
148R-N	1.49 ± 0.51***	9.31	0.84 ± 0.05
148R-S	1.46 ± 0.53***	9.13	0.92 ± 0.02

B
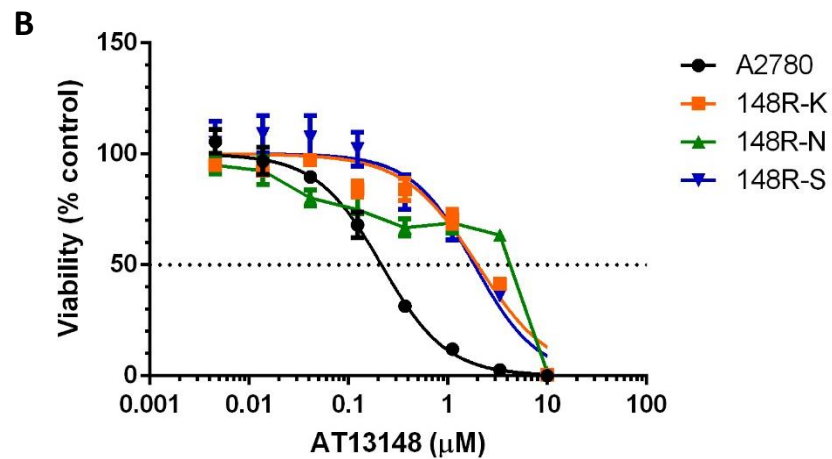
Cell line	GI$_{50}$ (µM)	RF
A2780	0.16 ± 0.05	N/A
148R-K	1.65 ± 0.81***	10.31
148R-N	3.25 ± 0.65***	20.31
148R-S	1.46 ± 0.53***	9.13

Figure 4.10: Dose-response curves and GI$_{50}$ determinations for AT13148 in A2780 and selected 148R clones. Cells were plated in triplicate in a 96-well plate and allowed to grow under standard growth conditions for 48 hours. They were then treated with a serial dilution of AT13148 for 96-hours, prior to being analysed by SRB assay. Dose-response graphs were generated using GraphPad Prism 6. Dotted line marks 50% viability on the y-axis. Data points represent the mean ± SD from one representative experiment. Tables summarise AT13148 GI$_{50}$ and RF, GI$_{50}$ data points depict the mean ± SD of all experiments conducted. **(A)** GI$_{50}$ was calculated with GraphPad Prism 6 using non-linear regression for all cell lines. **(B)** GI$_{50}$ calculated with GraphPad Prism 6 using linear regression for 148R-N and non-linear regression for all other cell lines. Statistical significance was calculated using a student's t-test, *** $p \leq 0.001$. n = 8 independent experiments.

As was seen previously (Figure 4.3) the selected 148R clones were again shown to have a high degree of cross-resistance to the ROCK inhibitor GSK269962 which was statistically significant (Figure 4.11). A2780 had a GI_{50} of 0.028 μM against GSK269962 whereas 148R-K, N and S had GI_{50} values of 3.032 μM (RF = 108.29), 2.180 μM (RF = 77.86) and 3.385 μM (RF = 117.32) respectively (Figure 4.11). The GI_{50} for 148R-K against GSK269962 was ~3-fold higher than was seen during initial cross-resistance profiling (Figure 4.3), which was interesting considering the parallel increase in AT13148 GI_{50} for 148R-K shown in Figure 4.10. This provides further evidence of the intimate link between the level of AT13148 resistance and cross-resistance to GSK269962.

Figure 4.11 also shows that none of the selected 148R clones had sensitivity to the IGF-1R inhibitor NVP-AEW541. The GI_{50} for 148R-K and 148R-S against NVP-AEW541 was 1.34 μM and 1.35 μM respectively, only marginally lower than the GI_{50} of A2780: 1.41 μM (Figure 4.11). This gave RF values for 148R-K and 148R-S of just under 1, 0.95 & 0.96 respectively (Figure 4.11). It should be noted that 148R-S was previously shown to be sensitive to NVP-AEW541, but only to a minimal extent (Figure 4.4), therefore, the lack of sensitivity in Figure 4.11 does not represent a significant shift and is likely due to inter-assay variation. In contrast, 148R-N had low-level cross-resistance to NVP-AEW541 (GI_{50}: 2.98 μM, RF = 2.12), which was statistically significant, consistent with the previous result shown in Figure 4.4 (Figure 4.11).

In addition, Figure 4.11 shows that there was large degree of sensitivity to the FGFR inhibitor AZD4547 in 148R-K and 148R-S; 148R-K and 148R-S had GI_{50} values of 0.011 μM and 0.008 μM respectively (Figure 4.11). This corresponded to ~15-fold sensitivity for 148R-K (RF = 0.06) and ~21-fold sensitivity for 148R-K (RF = 0.05), when compared to A2780 which had a GI_{50} of 0.170 μM, and was shown to be statistically significant (Figure 4.11). It should be noted that that the sensitivity displayed against AZD4547, by 148R-K and 148R-S, was slightly lower than was previously seen in Figure 4.5, but nonetheless substantial. Conversely, 148R-N had statistically significant cross-resistance against AZD4547; 148R-N had a GI_{50} of 0.969 μM which corresponded to an RF of 5.70 (Figure 4.11). Taken together, these data show that the selected 148R clones were all cross-resistant to GSK269962, that 148R-K and 148R-S were highly sensitive to AZD4547, and that 148R-N was cross-resistant to NVP-AEW541 and AZD4547.
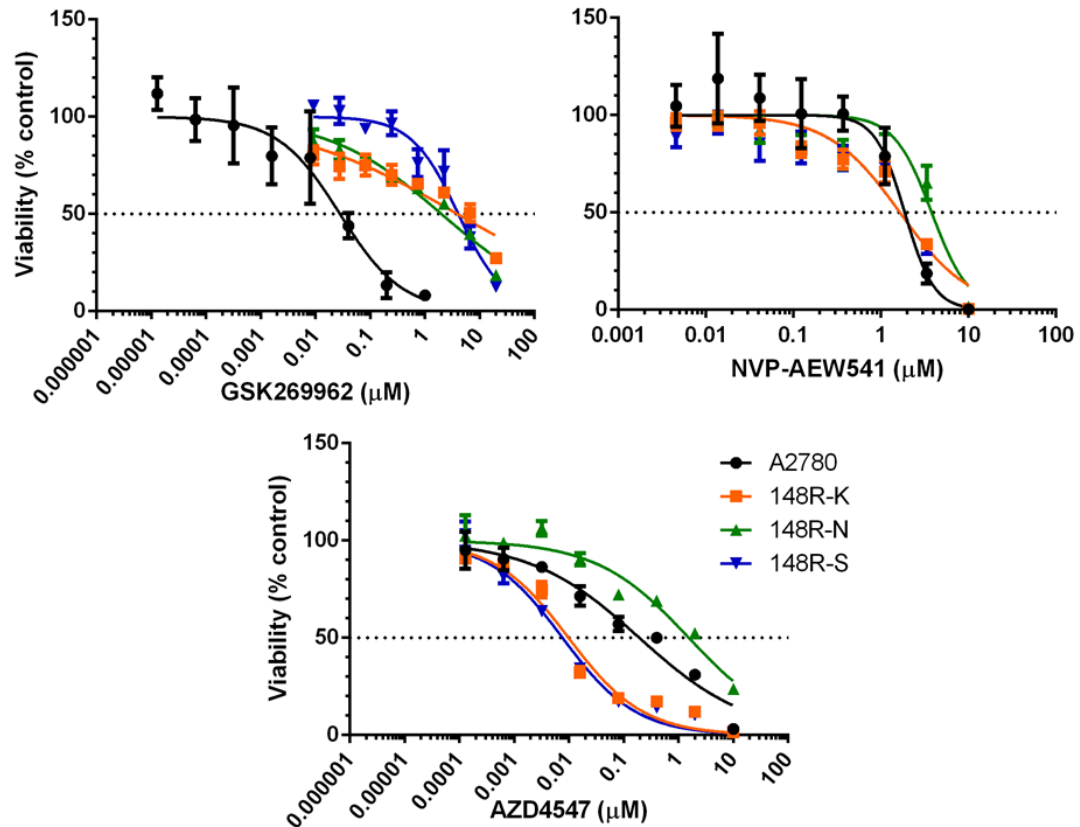
	GSK269962 (ROCK)		NVP-AEW541 (IGF-1R)		AZD4547 (FGFR)	
Cell line	**GI_{50} (µM)**	**RF**	**GI_{50} (µM)**	**RF**	**GI_{50} (µM)**	**RF**
A2780	0.028 ± 0.010	N/A	1.41 ± 0.67	N/A	0.170 ± 0.104	N/A
148R-K	3.032 ± 1.959*	108.29	1.34 ± 0.40	0.95	0.011 ± 0.012*	0.06
148R-N	2.180 ± 0.931**	77.86	2.98 ± 1.17***	2.12	0.969 ± 0.408**	5.70
148R-S	3.285 ± 0.750**	117.32	1.35 ± 0.65	0.96	0.008 ± 0.002*	0.05

Figure 4.11: Dose-response curves and GI_{50} determinations for GSK269962, NVP-AEW541 and AZD4547 in A2780 and selected 148R clones. Cells were plated in triplicate in a 96-well plate and allowed to grow under standard growth conditions for 48 hours. They were then treated with a serial dilution of GSK269962, NVP-AEW541 or AZD4547 for 96-hours, prior to being analysed by SRB assay. Dose-response graphs and non-linear regression curve fits were generated using GraphPad Prism 6. Dotted line marks 50% viability on the y-axis. Data points represent the mean ± SD from one representative experiment. Table summarises GI_{50} and RF, GI_{50} data points depict the mean ± SD of all experiments conducted. Statistical significance was calculated using a student's t-test, * $p ≤ 0.05$, ** $p ≤ 0.01$, n = 5 independent experiments.

4.2.7. Analysis of basal signalling in selected 148R clones

The analysis of basal signalling was also repeated in selected 148R clones to ensure that this had not been altered by continuous culture in AT13148. As was seen previously (Figure 4.6), selected 148R clones were all shown to have a strong over-expression of IGF-1R when compared to A2780, which was most notable in 148R-S which had the highest expression of IGF-1R (Figure 4.12A). Since this was not seen previously; IGF-1R expression was equal amongst 148R-K, N and S in Figure 4.6; this perhaps suggests that there was an induction of IGF-1R expression in 148R-S upon continuous AT13148 treatment. However, a more thorough investigation would be required to ascertain this.

The activation of the PAM pathway was also investigated by western blotting for AKT and two AKT substrates (GSK3β and PRAS40), as well S6RP to assess downstream activation of the PAM pathway. Figure 4.12A shows that there was an increase in the phosphorylation of S473 AKT and S9 GSK3β in 148R-N, when compared to A2780, but no difference in the phosphorylation of T246 PRAS40. This differs from Figure 4.6, where T246 PRAS40 phosphorylation was shown to be increased in 148R-N. In contrast, the phosphorylation of S9 GSK3β was unchanged in 148R-K and 148R-S, as was the phosphorylation of T246 PRAS40 (Figure 4.12A). The phosphorylation of S473 AKT also appeared to be slightly increased in 148R-S, inconsistent with Figure 4.6 and the lack of increase in AKT substrate phosphorylation in Figure 4.12A. However, the total expression of AKT was slightly increased in all 148R clones, suggesting that the increase in AKT phosphorylation within 148R-S might be due to over-loading. The total protein expression of PRAS40 and GSK3β was consistent amongst A2780 and the selected 148R clones (Figure 4.12A). Interestingly, as was seen in Figure 4.6, the phosphorylation of S325/236 S6RP was decreased in all 148R clones, especially in 148R-K and 148R-N, with total S6RP expression unchanged (Figure 4.12A).

The selected 148R clones were also western blotted for MYPT1 as a readout of the activity of the ROCK pathway. The phosphorylation of T696 MYPT1 and MYPT1 total expression were unaltered across A2780 and all selected 148R clones (Figure 4.12B). In addition, the expression of FGFR2 was also assessed to investigate the sensitivity to FGFR inhibition amongst 148R clones. The expression of FGFR2 was shown to be

identical to A2780 in 148R-K and 148R-S, however it was much lower in 148R-N (Figure 4.12B). This was interesting as 148R-N was the only 148R clone not to display cross-resistance to the FGFR inhibitor AZD4547 (Figure 4.5 & Figure 4.11).
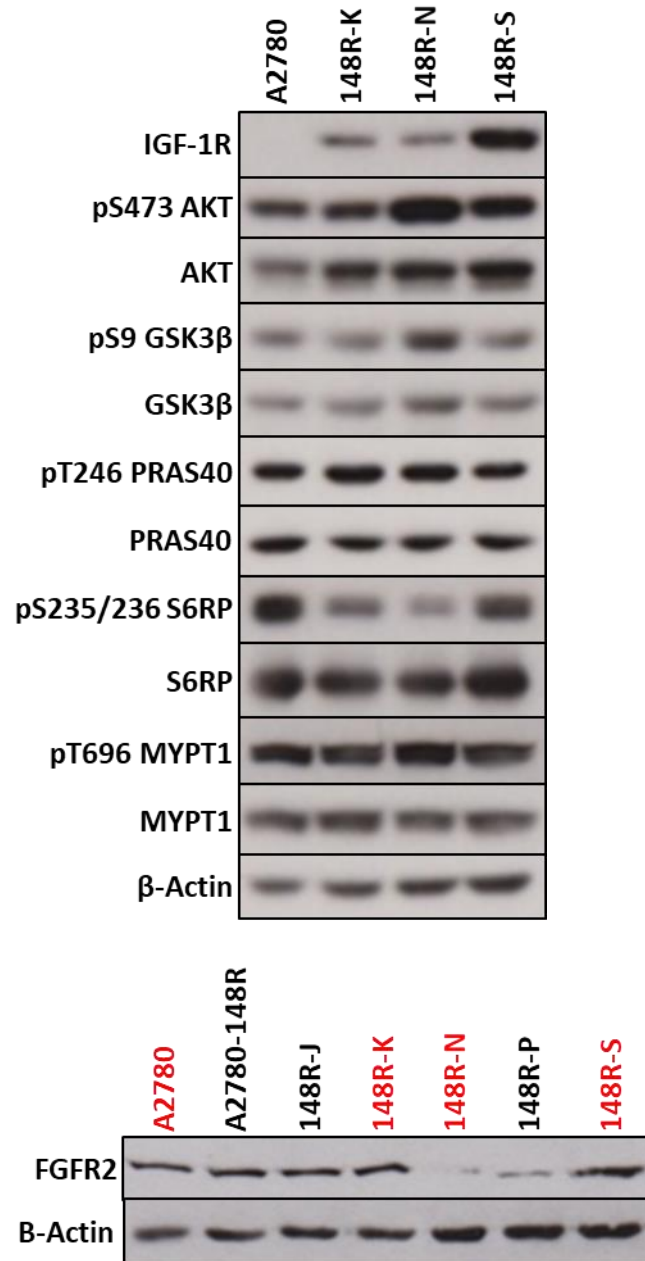
Figure 4.12: Analysis of the basal expression of IGF-1R, FGFR2 and markers of the PAM and ROCK pathways in selected 148R clones. (A, B) Cells were plated at either 0.5 x 10^6 (A2780) or 1 x 10^6 (A2780-148R and 148R clones) cells per 10 cm dish and allowed to grow for 48 hours under standard growth conditions. Cells were then lysed prior to western blot analysis. Western blot membranes were probed with antibodies for phospho-proteins, stripped, and then re-probed with antibodies for total proteins and loading control (β-Actin). A2780 and selected 148R clones are highlighted in red in **(B)**. Data are representative of five independent experiments.

4.2.8. Cross-resistance of 148R clones to AKT and p70S6K inhibition

As shown previously in Figure 4.3 & Figure 4.11, one of the defining features of 148R clones (and A2780-148R) was their strong cross-resistance to the ROCK inhibitor GSK269962. Since ROCK1 and 2 are both targets of AT13148, it was considered that 148R clones may also possess cross-resistance to inhibition of other AT13148 targets. To this end, SRB cell viability assays were performed on 148R clones using MK2206, an allosteric AKT inhibitor, and PF4708671, a p70S6K inhibitor (Hirai *et al.*, 2010; Pearce *et al.*, 2010b).

Remarkably, as shown in Figure 4.13, all 148R clones were shown to have statistically significant cross-resistance to MK2206; A2780 had a GI_{50} of 0.08 µM against MK2206 compared to 0.35 µM, 2.17 µM, 0.50 µM in 148R-K, N and S respectively (Figure 4.13). This equated to an RF of 4.38 and 6.25 in 148R-K and 148R-S, indicating a moderate level of cross-resistance, and an RF of 27.13 in 148R-N, indicating a strong degree of cross-resistance to MK2206 (Figure 4.13). There was also some cross-resistance to PF4708671; A2780 had a GI_{50} of 8.78 µM compared to 25.81 µM, 15.37 µM and 20.82 µM in 148R-K, N and S respectively (Figure 4.13). This was statistically significant (in all 148R clones) and equated to an RF of ~2-3 in 148R clones, demonstrating low-level cross-resistance (Figure 4.13). Taken together, these data showed that 148R clones had cross-resistance to AKT and p70S6K inhibition, key targets of AT13148.
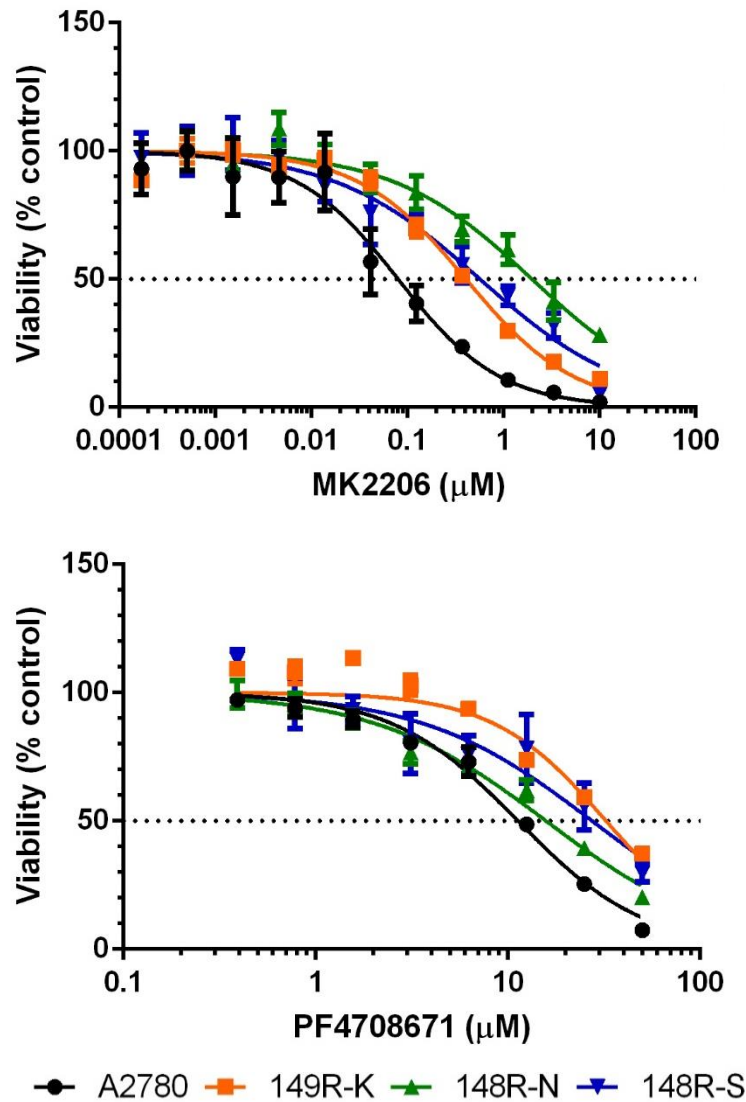
Cell line	MK2206 (AKT)		PF4708671 (p70S6K)	
	GI_{50} (μM)	RF	GI_{50} (μM)	RF
A2780	0.08 ± 0.04	N/A	8.78 ± 3.04	N/A
148R-K	0.35 ± 0.11**	4.38	25.81 ± 7.00**	2.94
148R-N	2.17 ± 0.85*	27.13	15.37 ± 0.65*	1.75
148R-S	0.50 ± 0.19*	6.25	20.82 ± 8.09*	2.37

Figure 4.13: Dose-response curves and GI_{50} determinations for MK2206 and PF4708671 in A2780 and 148R clones. Cells were plated in triplicate in a 96-well plate and allowed to grow under standard growth conditions for 48 hours. They were then treated with a serial dilution of MK2206 or PF4708671 for 96-hours, prior to being analysed by SRB assay. Dose-response graphs and non-linear regression curve fits were generated using GraphPad Prism 6. Dotted line marks 50% viability on the y-axis. Data points represent the mean ± SD from one representative experiment. Table summarises GI_{50} and RF, GI_{50} data points depict the mean ± SD of all experiments conducted. Statistical significance was calculated using a student's t-test, * $p \leq 0.05$, ** $p \leq 0.01$, n = 4 independent experiments.

4.2.9. Response of signalling pathways to AT13148 treatment in 148R clones

4.2.9.1. Markers of PAM signalling

The previously described cross-resistance to selective inhibitors of AKT and p70S6K, two targets of AT13148, may indicate that the mechanism of resistance to AT13148 is proximal to the PAM pathway. To investigate this A2780 and 148R clones were treated with AT13148 for 4 hours and then analysed by western blot for markers of PAM pathway signalling. Figure 4.14 shows that T246 PRAS40 phosphorylation, a marker of AKT inhibition, was partially refractory to AT13148 in all 148R clones; 5 µM of AT13148 was able to abolish T246 PRAS40 phosphorylation in A2780, but this was not the case in 148R clones. In 148R-K and 148R-S, 5 µM of AT13148 did cause a slight decrease in T246 PRAS40 phosphorylation, with 10 µM causing a further reduction without completely abolishing the phosphorylation of T246 PRAS40 (Figure 4.14). This was similar in 148R-N, but T246 PRAS40 phosphorylation was maintained to a greater extent than in 148R-K and 148R-S (Figure 4.14). The total protein expression of PRAS40 was consistent across all cell lines and was unaffected by AT13148 treatment (Figure 4.14).

As with PRAS40 phosphorylation, the phosphorylation of S235/236 S6RP was also partially refractory to AT13148 (Figure 4.14). In A2780, S235/236 S6RP phosphorylation was strongly inhibited with 0.5 µM AT13148 and completely abolished at ≥ 1 µM (Figure 4.14). In contrast, there was only a small decrease in S235/236 S6RP phosphorylation with 0.5 µM AT13148 in 148R clones, and ≥ 5 µM was required to completely abolish the phosphorylation of S235/236 S6RP (Figure 4.14). Despite some changes in 148R-N, in response to AT13148, total S6RP expression was mostly unaffected by AT13148 treatment and was consistent across all cell lines (Figure 4.14). Taken together, these data suggest that PAM pathway was partially refractory to AT13148 inhibition in 148R clones, this could play a role in AT13148 resistance and warrants further investigation.
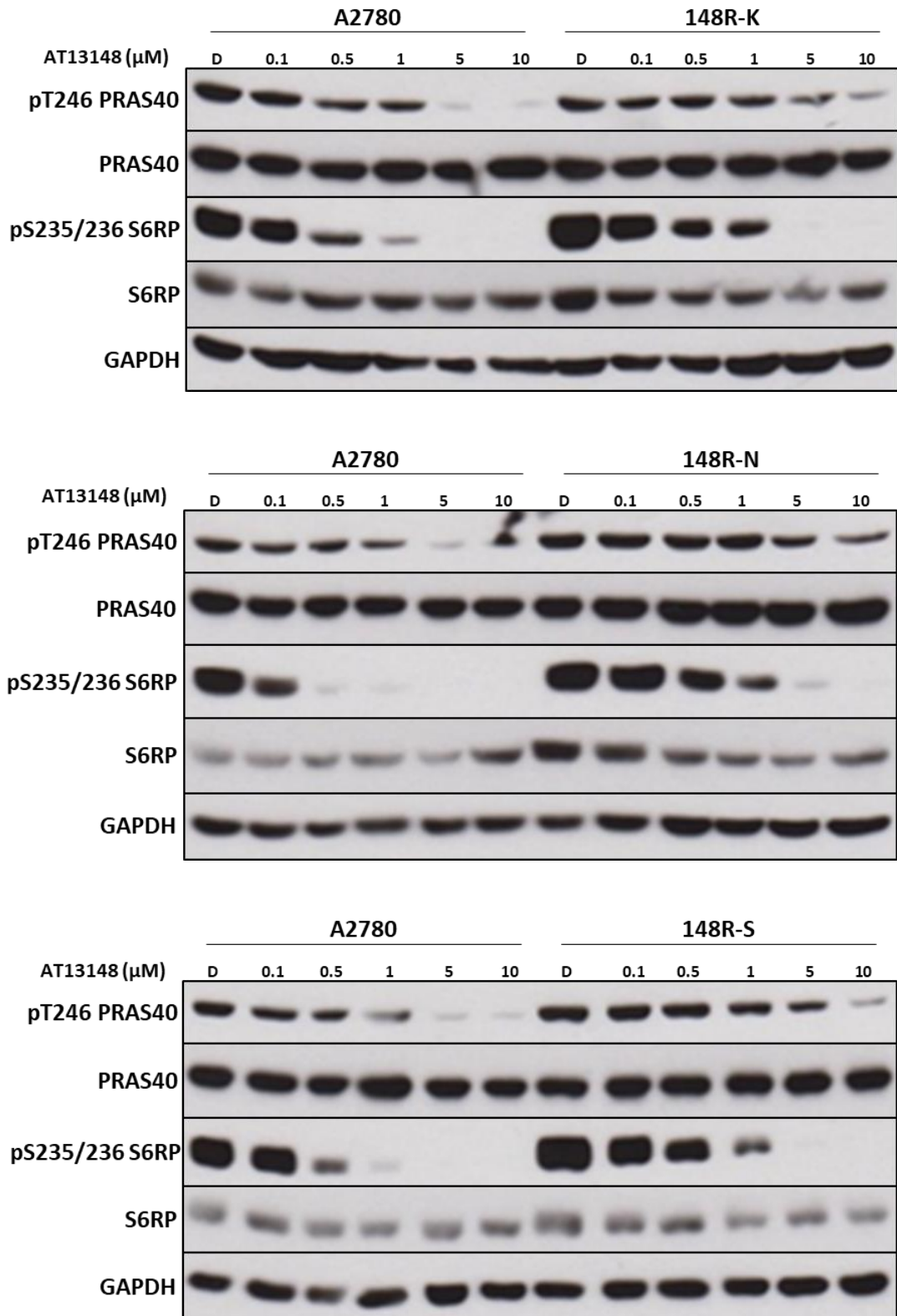
Figure 4.14: Analysis of the response of the PAM pathway to AT13148 in 148R clones. Cells were plated at either 0.5 x 10^6 (A2780) or 1 x 10^6 (148R clones) cells per 10 cm dish and allowed to grow for 48 hours under standard growth conditions. Cells were then treated with AT13148, as shown, or D: DMSO vehicle control for 4 hours, prior to being lysed for western blot analysis. Western blot membranes were probed with antibodies for phospho-proteins, stripped, and then re-probed with antibodies for total proteins or loading control (GAPDH). Data are representative of three (PRAS40) or four (S6RP) independent experiments.

4.2.9.2. Markers of ROCK signalling

Since 148R clones all had a strong level of cross-resistance to ROCK inhibition, A2780 cells and 148R clones were also treated with AT13148 to investigate if AT13148 resistance was proximal to the ROCK pathway. The phosphorylation of T696 MYPT1, a substrate of ROCK1 and 2, was used as marker of the inhibition of the ROCK pathway by AT13148. Figure 4.15 shows that in both A2780 and 148R clones 1 μM of AT13148 caused a sharp decrease in the phosphorylation of T696 MYPT1. In 148R-S there was also a sharp decrease in MYPT1 T696 phosphorylation at 0.1 μM AT13148, but at 0.5 μM AT13148 MYPT1 T696 phosphorylation was similar to the DMSO vehicle control for 148R-S (Figure 4.15). An unusual response was also seen in A2780 and 148R-K where there was a slight rebound in T696 MYPT1 phosphorylation with 5-10 μM AT13148 (Figure 4.15). However, this was very slight and only seen with a long film exposure, and therefore perhaps caused by subtle differences in loading (Figure 4.15). The expression of total MYPT1 was unaffected by AT13148 in A2780 and 148R-K, but in 148R-N and 148R-S, when used at 1-10 μM, AT13148 did cause a decrease in the total expression of MYPT1, particularly in 148R-S (Figure 4.15). It should be noted that this was not seen in other biological replicates and was thus most likely caused by an experimental artefact. In summary, there were some differences in the response of the ROCK pathway to AT13148 in A2780 and 148R clones, but in the context of AT13148 resistance, these did not appear sufficient to contribute towards resistance. These differences in response, amongst A2780 and 148R clones, likely reflects the promiscuous nature of MYPT1 phosphorylation (as discussed in section 3.3).

Figure 4.15: Analysis of the response of the ROCK pathway to AT13148 in A2780 and 148R clones. Cells were plated at either 0.5 x 10^6 (A2780) or 1 x 10^6 (A2780-148R) cells per 10 cm dish and allowed to grow for 48 hours under standard growth conditions. Cells were then treated with AT13148, as shown, or D: DMSO vehicle control for 4 hours prior to being lysed for western blot analysis. Western blot membranes were probed with antibodies for phospho-proteins, stripped, and then re-probed with antibodies for total proteins or loading control (β-Actin). (S): short exposure to hyperfilm, (L): long exposure to hyperfilm. Data are representative three independent experiments.

4.2.10. Response of the PAM pathway to MK2206 in A2780 and 148R clones

The response of the PAM pathway to MK2206 was also examined, as 148R clones, particularly 148R-N, had displayed cross-resistance to MK2206. In addition, since the PAM pathway was partially refractory to AT13148, the response to MK2206 may enable the contribution of AKT towards this to be dissected. Figure 4.16 shows that MK2206 potently inhibited the phosphorylation of S473 AKT across A2780 and 148R clones in a similar manner; 0.01 µM caused a sharp decrease in S473 AKT phosphorylation and ≥ 0.1 µM MK2206 abolished phosphorylation. However, there were some differences in the response of the AKT substrates GSK3β and PRAS40 to MK2206 amongst A2780 and 148R clones. In A2780 and 148R-S the phosphorylation of S9 GSK3β and T246 PRAS40 was substantially reduced with 1 µM MK2206, the maximum concentration used, with PRAS40 T246 phosphorylation also exhibiting this response in 148R-N (Figure 4.16). But in contrast, in 148R-N S9 GSK3β phosphorylation was partially refractory; whilst 1 µM of MK2206 caused a decrease in GSK3β S9 phosphorylation, this was to a much lesser extent than in A2780 and 148R-S (Figure 4.16)

A similar phenomenon was also seen with S235/236 S6RP phosphorylation, whereby 0.1 µM MK2206 caused a sharp decrease in S6RP phosphorylation in A2780 and 148R-S but did not do so in 148R-N (Figure 4.16). However, in 148R-N, 1 µM MK2206 did cause substantial decrease in S236/236 S6RP phosphorylation, indiscernible from A2780 and 148R-S, thus indicating that S235/236 S6RP phosphorylation was only partially refractory to MK2206 in 148R-N (Figure 4.16). Since AKT was equally inhibited by MK2206 in A2780 and 148R clones, as shown by a comparable decrease in AKT phosphorylation, the maintenance in the phosphorylation of substrates downstream of AKT in 148R-N would seem to occur in an AKT-independent manner. Taken together, these data suggest that some of the PAM pathway is partially refractory to AKT inhibition in 148R-N, and that this seems to independent of AKT activation.
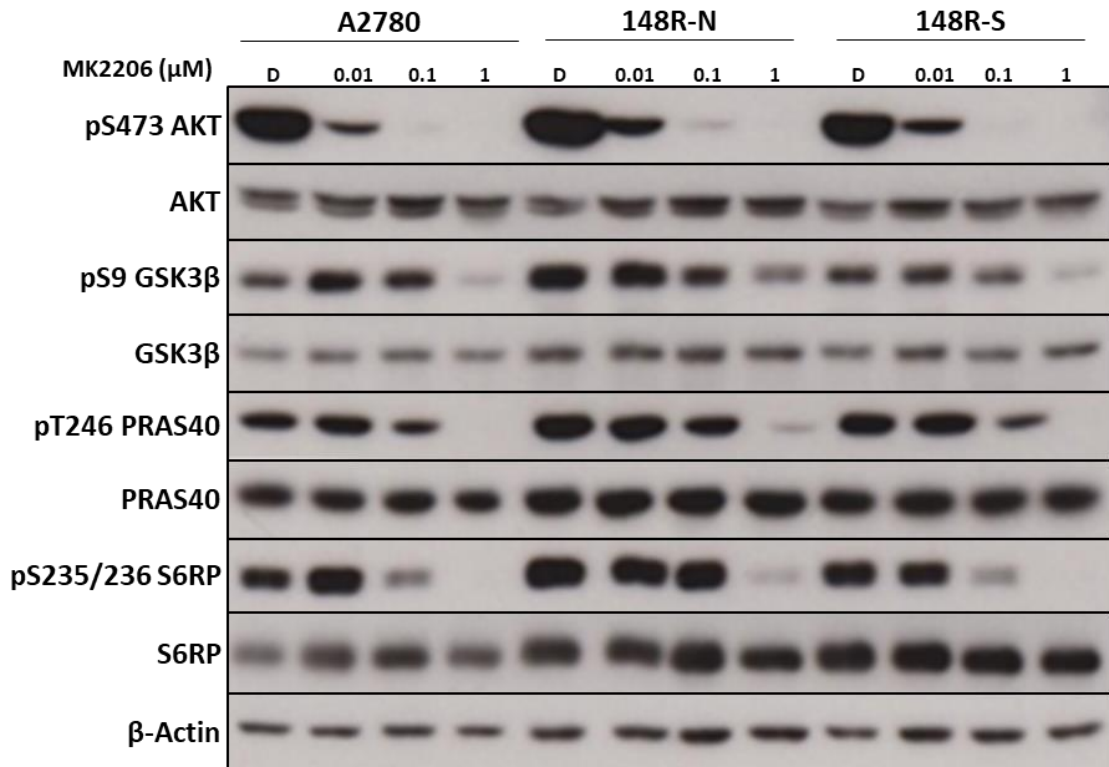
Figure 4.16: Analysis of the response of PAM pathway to MK2206 in A2780 and 148R clones. Cells were plated at either 5 x 10^5 (A2780) or 7.5 x 10^5 (148R clones) cells per 7 cm dish and allowed to grow for 48 hours under standard growth conditions. Cells were then treated with MK2206, as shown, or D: DMSO vehicle control for 4 hours prior to being lysed for western blot analysis. Western blot membranes were probed with antibodies for phospho-proteins, stripped, and then re-probed with antibodies for total proteins or loading control (β-Actin) Data are representative of two (GSK3β) or three (AKT, PRAS40 and S6RP) independent experiments.

4.2.11. Analysis of markers of the MAPK pathway in A2780 and 148R clones

The work presented thus far in this chapter has shown that the PAM pathway was less responsive to AT13148 in 148R clones. This could be caused by changes to AKT and p70S6K, e.g. mutation or increased expression, but alternatively could be caused by changes in another pathway which interacts with the PAM pathway. One such pathway is the MAPK pathway which is known to interact with the PAM pathway on several levels, and was shown in chapter 3 to be altered in A2780-148R (Mendoza *et al.*, 2011., Figure 3.11). Therefore, markers of the MAPK pathway were analysed in A2780 and 148R clones by western blotting.

Figure 4.17 shows that there was a striking increase in the phosphorylation of Thr202/Tyr204 ERK 1/2 in all 148R clones when compared to A2780. This was highest in 148R-S followed by 148R-K and then 148R-N (Figure 4.17). Contrary to what one might expect, there was a decrease in the phosphorylation of S217/221 MEK 1/2 in all 148R clones (Figure 4.17), with this being greatest in 148R-N. This paradoxical increase in ERK 1/2 phosphorylation coupled with a decrease in MEK 1/2 phosphorylation was also seen in A2780-148R in chapter 3 (Figure 3.11), but the increase/decrease was considerably more marked in 148R clones. As discussed in section 3.3, this dichotomy, between ERK 1/2 and MEK 1/2 phosphorylation, could be due to an increase in negative feedback caused by increased phosphorylation of ERK 1/2.

The phosphorylation of two ERK 1/2 substrates, ETS Like-1 protein (Elk-1) and p90 ribosomal S6 kinase (RSK), was also examined to see whether they exhibited a parallel increase in their phosphorylation, in line with increased ERK 1/2 phosphorylation. There were three bands detected for S383 Elk-1 phosphorylation, which was not anticipated as S383 Elk-1 was supposed to be detected as singular band (Figure 4.17). However, the band with lowest molecular weight matched the single band detected for total Elk-1 expression and corresponded to the molecular weight predicted by the antibody manufacturer (62 kDa) for Elk-1, so was therefore determined to be the band representing S383 Elk-1 phosphorylation. Taking this into account, there was a strong increase in the phosphorylation of S383 Elk-1 phosphorylation in 148R-K and 148R-S when compared to A2780, but a decrease in 148R-N (Figure 4.17). In contrast, the

phosphorylation of T359 RSK was slightly lower in all 148R clones, perhaps suggesting that S383 Elk-1 phosphorylation may be a better readout of ERK activity, at least in 148R-K and 148R-S (Figure 4.17). Taken together, these data suggest that the MAPK pathway was altered in 148R clones but not uniformly. This warrants further investigation into how it may contribute towards AT13148 resistance, and as to whether 148R clones have an increased dependency on the MAPK pathway for growth and survival, which could be exploited therapeutically.
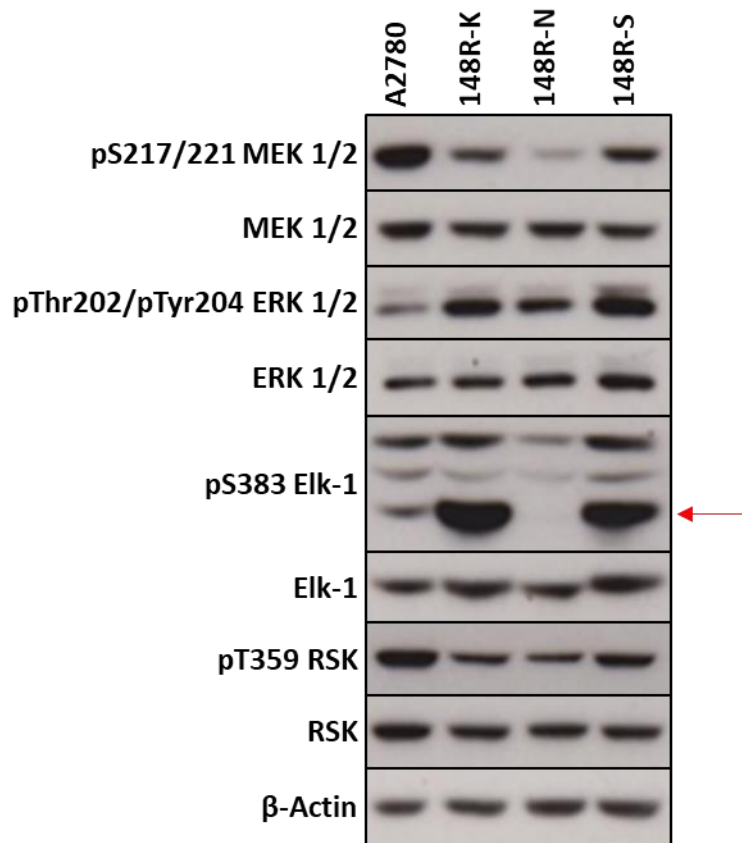
Figure 4.17: Analysis of the basal expression of markers of the MAPK pathway in A2780 and 148R clones. Cells were plated at either 0.5 x 10^6 (A2780) or 1 x 10^6 (148R clones) cells per 10 cm dish and allowed to grow for 48 hours under standard growth conditions. Cells were then lysed prior to western blot analysis. Western blot membranes were probed with antibodies for phospho-proteins, stripped, and then re-probed with antibodies for total proteins and loading control (β-Actin). Red arrow highlights band corresponding to pS383 Elk-1. Data are representative of five independent experiments.

4.3. Discussion

4.3.1. Clone screening and selection

The primary aim of this chapter was to derive isogenic sub-clones from A2780-148R and characterise them in order to identify putative drivers of resistance to AT13148. As has been described in this chapter, 148R clones initially went through two phases of screening, both of which were based upon SRB cell viability assays determining the response to AT13148, GSK269962, NVP-AEW541 and AZD4547, as well as western blot analysis of the basal expression of markers of the PAM and ROCK pathways. The first phase (Figure 4.2-Figure 4.6) was performed on all isolated 148R clones and the second phase (Figure 4.7-Figure 4.12) on three 148R clones; 148R-K, N & S, selected based on the results from phase one. Since phase two was conducted with 148R clones cultured in the presence of AT13148, with optimal seeding densities determined via growth assays, it is likely to be a more accurate representation of 148R clones. However, both were able gain insight into resistance against AT13148.

Prior to getting into a more detailed discussion over the results of the screening of 148R clones it is worth mentioning that the over-arching observation that one can take from this screening is the sheer variability amongst 148R clones. This was most notable in SRB cell viability assays, for example, the RF value for AT13148 in 148R clones ranged from 1.86 to 20.31 (Figure 4.2 & Figure 4.10). A careful interpretation is required in terms of what this means for AT13148 resistance in A2780-148R. This variability could be interpreted as showing that A2780-148R has a high degree of heterogeneity, with several unique sub-populations likely to have distinct mechanisms of resistance to AT13148. However, an equally likely explanation is that this variation is an effect of isolation itself being a stimulus for the production of new phenotypes (Heppner, 1984). Indeed, it has been shown, due to the inherent genetic instability of many cancers, that isolated cancer cells can quickly evolve into a genetically heterogenous population, distinct from the cell lines from which they were derived (Ben-David *et al.*, 2018).

Nonetheless, screening provided evidence that resistance against AT13148 in 148R clones was, for the most part, stable. As mentioned, during the 1st phase of screening,

which took place over a 2-month period, 148R clones were not cultured in the presence of AT13148. Despite this, all but one 148R clone (148R-I) was shown to have > 2-fold resistance to AT13148, thus indicating that resistance was stable (Figure 4.2). This was further validated by the second phase of screening, which showed that routine sub-culture in the presence of AT13148 did not substantially increase resistance to AT13148 (Figure 4.10). 148R-K was an exception to this; there was a ~3-fold increase in AT13148 resistance in phase two of screening. This could of course be caused by inter-assay variation but might also be indicative of transient resistance to AT13148. Whilst most resistance phenotypes tend be stable, the acquisition of transient resistant phenotypes is not uncommon. For example, Stottrup and colleagues (Stottrup *et al.*, 2016) generated resistance against the AKT inhibitor MK2206 in breast cancer cell lines and demonstrated that resistant cells could be partially re-sensitized to MK2206 upon drug withdrawal over a three week period. A similar approach could be employed to ascertain if 148R-K exhibited transient resistance; 148R-K cells could be released from AT13148 for various time points and compared to 148R-K continuously cultured in the presence of AT13148.

Screening 148R clones for their response to AT13148 not only revealed differences in GI_{50} and RF values, but also distinct dose-response curves (Figure 4.10). A2780, 148R-K and 148R-S had typical dose-response curves, that were sigmoidal adhering to the threshold model; whereby, at lower doses, drugs elicit no biological effect until a threshold is met (target inhibition), inhibition then proceeds in linear fashion until target saturation (Reynolds, 2010). The dose-response curve for 148R-N did not adhere to this model; AT13148 appeared to inhibit the viability of 148R-N in two distinct linear phases; at low concentrations there was an incremental decrease in viability, a shallow gradient, followed by a sharp decrease at higher concentrations. This could possibly be due to the broad inhibition elicited by AT13148; the inhibition of high potency targets (e.g. ROCK1 & 2) at low concentrations of AT13148 could cause a small incremental decrease in 148R-N viability, and the additional inhibition of lower potency targets (e.g. AKT) at higher concentrations, could cause the sharp decrease in viability (highlighted in Figure 4.18). However, there are other possible explanations for the distinctive dose-response curve of 148R-N. Fallahi-Sichani and colleagues (Fallahi-Sichani *et al.*, 2013) showed that

PAM pathway inhibitors, such as the mTOR inhibitor PP242, which had dose-response curves with a low hill-slope (as does 148R-N), correlated with a high-level of cell-cell variability of the PAM pathway response to inhibition, demonstrated by immunofluorescence staining of the mTORC1 substrate 4EBP1 and cell cycle marker retinoblastoma protein (Rb). They postulated that this was due to stochastic fluctuations (e.g. in drug target or negative feedback regulation) rather than the presence of distinct genetic sub-populations (Fallahi-Sichani *et al.*, 2013). Since the response of 148R-N to AT13148, up to ~ 3 µM, exhibits a shallow dose-response curve, cell to cell variation (non-genetic) in response to AT13148 could be a possible explanation. Furthermore, AT13148 differentially eliciting cytostatic and cytotoxic effects in 148R-N at different AT13148 concentrations, and 148R-N exhibiting unique growth kinetics (Figure 4.8 & Figure 4.9), could also explain why 148R-N had a distinctive dose-response curve to AT13148. Whatever the exact mechanism, it can be said with certainty, that 148R-N responds to AT13148 in a distinctive manner, which could suggest that 148R-N has a distinct mechanism of resistance to AT13148.
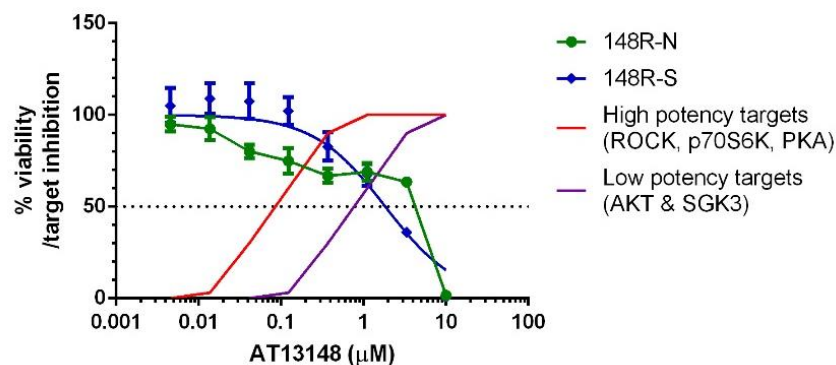
Figure 4.18: Potential influence of AT13148 target inhibition on response of 148R-N to AT13148. Graph shows the response of 148R-N and 148R-S to AT13148 (taken from Figure 4.10B) and the hypothetical inhibition of AT13148 targets at different concentrations of AT13148.

As has been mentioned, the screening of 148R clones revealed a substantial degree of variation. This can especially be seen in response to the ROCK inhibitor GSK269962, where all 148R clones demonstrated cross-resistance, but the extent of this varied considerably (RF 11.42 – 168.77, Figure 4.3). Interestingly, it was shown that there was significant correlation between AT13148 resistance and GSK269962 cross-resistance (Figure 4.3). This would suggest that in order to become resistant to AT13148, cells must find a way of overcoming the inhibition of ROCK1 & 2 by AT13148, the extent of which

determines the magnitude of resistance to AT13148. Of course, it is possible that there is not a direct causal link between AT13148 resistance and GSK269962 cross-resistance, but the strong level of correlation between the two, coupled with the potent inhibition of ROCK 1 and 2 by AT13148, would seem to make a causal link likely.

Another interesting finding of the initial screening was the loss of sensitivity to the IGF-1R inhibitor NVP-AEW541 in 148R clones (Figure 4.4 & Figure 4.11). This was independent of AT13148 exposure; as the second phase of screening on selected 148R clones, which were maintained in AT13148, did not re-establish NVP-AEW541 sensitivity. A2780-148R cells were also shown to have lost their sensitivity to NVP-AEW541, with sensitivity decreasing over the period of time that 148R clones were isolated and expanded (Figure 4.4C). It is therefore likely that the loss of sensitivity in 148R clones was also due to a loss of sensitivity over time, rather than as an artefact of the isolation process.

Remarkably, despite the loss of NVP-AEW541 sensitivity, 148R clones and A2780-148R cells were still shown to over-express IGF-1R, albeit to varying extents (Figure 4.6 & Figure 4.12). Furthermore, unpublished data from the Garrett lab has shown that an IGF-1R expressing sub-population can be selected from AT13148 sensitive parental A2780 cells, when cultured in the presence of 5.2 μM AT13148 (maintenance dose of AT13148; data not shown). This might suggest that during the generation of resistance to AT13148 in parental A2780 cells, an IGF-1R expressing sub-population of A2780 was initially selected for that conferred a dependency on IGF-1R signalling and a survival advantage in the presence of AT13148. However, over time, with dose-escalation and prolonged AT13148 exposure, additional changes occurred/were selected for driving AT13148 resistance to the level seen in A2780-148R and 148R clones, reducing the dependency on IGF-1R signalling for survival. Evidence for this can be seen as despite the loss of NVP-AEW541 sensitivity, and thus IGF-1R dependency, AT13148 resistance was still retained in A2780-148R and 148R clones.

The loss of NVP-AEW541 sensitivity, combined with the previous work conducted investigating IGF-1R as a driver of resistance (Akan, 2015), would seem to exclude IGF-1R over-expression from either driving resistance or being a therapeutic target in

AT13148 resistance. However, further work should be conducted to ascertain the importance of IGF-1R over-expression and dependency as an early driver of AT13148 resistance. If this is validated, then combining AT13148 with an IGF-1R inhibitor could be a therapeutic strategy to prevent the acquisition of AT13148 resistance or prolong the response to AT13148.

In contrast, sensitivity to the FGFR inhibitor AZD4547 was retained in most 148R clones as well as in A2780-148R (Figure 4.5 & Figure 4.11). Of the 148R clones that were selected for further analysis, 148R-K and 148R-S both showed ~20-fold sensitivity (Figure 4.11). The exception to this was 148R-N which was cross-resistant to AZD4547, as well as NVP-AEW541, again, highlighting that 148R-N appears to be distinct from other 148R clones. It was interesting to see that 148R-N also had decreased expression of FGFR2, which may explain why it was cross-resistant, but the expression of FGFR2 was unchanged in 148R-K and 148R-S (Figure 4.12). This is problematic, as the inhibition of FGFR could be a potential therapeutic strategy in AT13148 resistant patients, but this would be difficult without identifying a biomarker of sensitivity. As discussed in section 3.3, other isoforms of FGFR (1,3 & 4) exist, of which FGFR 1 & 3 are also targeted by AZD4547 (in addition to FGFR2), and have been shown to contribute towards resistance to cancer therapies (Yadav *et al.*, 2012; Daly *et al.*, 2017). It would be prudent to investigate the expression and phosphorylation of these FGFRs to try and identify a biomarker of FGFR sensitivity. Sensitivity to FGFR inhibition should also be validated by the use of additional FGFR inhibitors such as BGJ398 and JNJ-42756493, both which have progressed to clinical trials (Desai and Adjei, 2016).

In addition to SRB cell viability assays, 148R clones were also screened by performing western blots investigating the basal expression of markers of the PAM and ROCK pathways, two key AT13148 targets. Again, these assays revealed that 148R-N appeared to be distinct from other 148R clones; 148R-N exhibited increased phosphorylation of AKT substrates (PRAS40 and GSK3β) as well as AKT itself, which was not seen in 148R-K or 148R-S (Figure 4.6 & Figure 4.12). However, it should be noted that there was some discrepancy in the phosphorylation of PRAS40 in 148R-N; PRAS40 phosphorylation was shown to be increased in Figure 4.6 but was unchanged in Figure 4.12. Nonetheless, since AT13148 inhibits AKT1 & 3, changes to AKT and AKT substrate

phosphorylation/expression has the capacity to contribute towards resistance to AT13148, this has been observed in other AKT inhibitors. For example, Stottrup and colleagues (Stottrup *et al.*, 2016) demonstrated that increased expression of AKT3 can drive resistance to the allosteric AKT inhibitor MK2206 in resistant breast cancer cell lines.

It should also be noted that in 148R-K and 148R-N there was decreased phosphorylation of S6RP at a basal level. However, this was not seen in any of the subsequent dose-response western blots (e.g. Figure 4.14), where S6RP phosphorylation was shown to be unchanged at a basal level, so would appear to be caused by variation, either stochastic or experimental, not AT13148 resistance. Nonetheless, the lack of increase in S6RP phosphorylation suggested that the apparent increase in AKT activation in 148R-N does not transmit to the downstream components of the PAM pathway, proximal to mTORC1 and p70S6K.

4.3.2. The role of PAM and ROCK signalling in AT13148 resistance

To investigate the potential consequences of altered AKT signalling, SRB assays were performed using MK2206, a potent and selective allosteric inhibitor of all three AKT isoforms (Hirai *et al.*, 2010; Figure 4.13). 148R-N was shown to be remarkably cross-resistant to MK2206, with an RF value of ~27, but rather unexpectedly, due to lack alterations in the PAM pathway at the basal level, 148R-K and 148R-S also displayed cross-resistance, albeit to a lesser extent (RF ~4-6). Western blotting of PAM pathway markers in response to MK2206 revealed a potential mechanism for cross-resistance in 148R-N; AKT substrate phosphorylation was partially refractory to MK2206, however, this was only seen with GSK3β and not PRAS40 (Figure 4.16). This was not seen in 148R-S.

Since MK2206 is an allosteric inhibitor of AKT, the phosphorylation of AKT was used as a direct marker of inhibition of AKT by MK2206. AKT was inhibited by MK2206 to a near-identical extent across A2780, 148R-N and 148R-S, which suggests, in 148R-N, that the maintenance of GSK3β phosphorylation in response to MK2206 was independent of AKT. In addition, S6RP phosphorylation was also shown to be partially refractory to MK2206 in 148R-N. Considering PRAS40 phosphorylation was not maintained in 148R-

N, and that PRAS40 is an upstream regulator of mTORC1, therefore PAM pathway substrates downstream of mTORC1, such as S6RP, the maintenance of S6RP might be due to changes proximal to mTORC1 and p70S6K. Since the PAM pathway was equally responsive to MK2206 in A2780 and 148R-S, it would seem likely that MK2206 cross-resistance is caused by changes outside the PAM pathway in 148R-S

With regards to 148R-N, despite the maintenance of GSK3β phosphorylation appearing to be independent of AKT, it may still be dependent upon PI3K. Indeed, there is increasing evidence to suggest that AKT is not the only effector of PI3K, and that some tumours are PI3K dependent but AKT independent. Gagliardi and colleagues (Gagliardi *et al.*, 2012) demonstrated that the knockdown of PDK1 caused a loss of malignant phenotype in breast cancer cells harbouring *PIK3CA* mutations, which could not be recovered by the expression of constitutively active AKT. In a similar study, Vasudevan and colleagues (Vasudevan *et al.*, 2009) identified that cancer cell lines that were driven by activating *PIK3CA* mutations, but AKT independent, were dependent upon SGK3.

As discussed in section 1.5, SGK3 is one of three isoforms of SGK (SGK1, 2 & 3) which, like AKT, are members of the AGC family of protein kinases and share significant homology with one another and AKT (Bruhn *et al.*, 2010). All isoforms of SGK have been shown to act as AKT independent effectors of PI3K; they are activated in a PI3K/PDK1 dependent manner, with some evidence that they also depend upon mTORC2 for their activation (Bruhn *et al.*, 2010, 2013). Furthermore, SGK isoforms have overlapping substrate specificity with AKT (Bruhn *et al.*, 2013). Shared substrates between AKT and SGK include GSK3β, FOXO3a, TSC2 and BAD, with SGK isoforms shown to either phosphorylate the same residue as AKT (e.g. S9 GSK3β) or a different residue (e.g. S315 FoXO3a) (Brunet *et al.*, 2001; Bruhn *et al.*, 2010).

Therefore, in 148R-N an increase in SGK expression or activation could explain the maintenance of GSK3β phosphorylation, that was seen in response to MK2206, which may also occur in response to other AKT inhibitors, such as AT13148 (Figure 4.19). Alternatively, alterations in upstream regulators of SGK activation, such as PI3K, PTEN, PDK1 and RTK's could enable the by-pass of AKT via SGK (Figure 4.19). This perhaps might be more likely a mechanism in 148R-N, since the phosphorylation of AKT was increased at a basal level, indicating that there may be changes upstream of AKT and

SGK. However, it should be considered that AT13148 can inhibit SGK3, so SGK1 and 2 might be more likely involved in AT13148 resistance. Interestingly, it has been shown that elevated SGK1 expression can predict resistance to AKT inhibition in breast cancer cell lines, thus highlighting the potential of SGK to overcome AKT inhibition (Sommer *et al.*, 2013).

It is also worth noting that there are several additional kinases, not regulated by PI3K and PDK1, that can also phosphorylate GSK3β, including RSK, ERK and PKA (Mendoza *et al.*, 2011; Beurel *et al.*, 2015). These should also be considered as contributing to the maintenance of GSK3β phosphorylation in response to AKT inhibition. A more comprehensive investigation of the response of AKT substrates to MK2206 would gain some mechanistic insight; if the phosphorylation of several shared AKT and SGK substrates is maintained in response to MK2206 it would make it likely that this is SGK dependent. However, caution would be required when interpreting these results, as some of the aforementioned kinases can also phosphorylate AKT/SGK substrates; e.g. ERK and RSK can phosphorylate TSC2 (Mendoza *et al.*, 2011). Analysis of the phosphorylation of a specific SGK substrate, such as N-Myc downstream regulated (NDRG) 1 and 2, would provide more conclusive evidence of the contribution of SGK isoforms; e.g. increased NDRG phosphorylation would suggest an SGK dependent mechanism (Murray *et al.*, 2004).
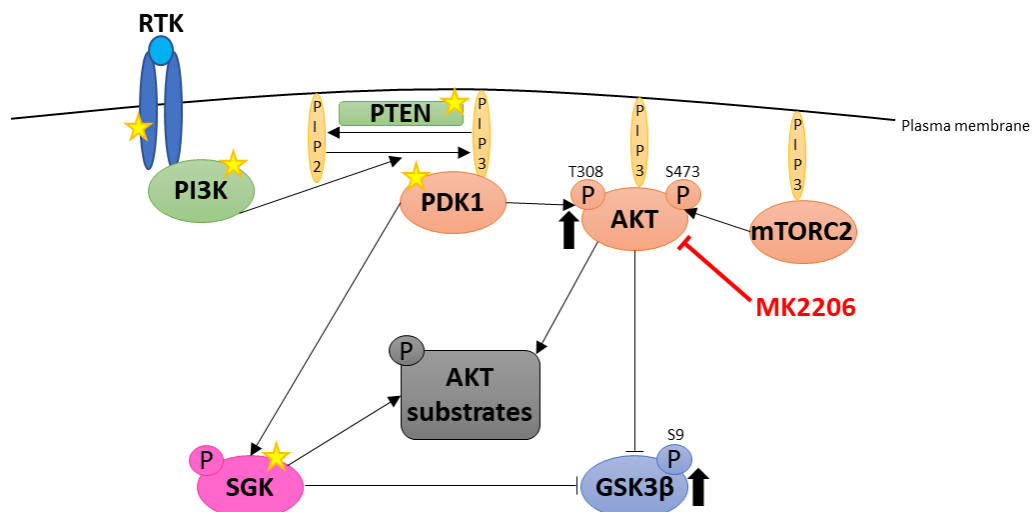
Figure 4.19: Potential by-pass of AKT inhibition via SGK in 148R-N. SGK and AKT share the same upstream activation (PI3K/PDK1 dependent) and have overlapping substrate specificities. Increased activation or expression of SGK might enable the maintenance of GSK3β phosphorylation in the presence of AKT inhibition. This could also enable the maintenance of other shared AKT/SGK substrates. Alternatively, hyperactivation of upstream regulators of AKT and SGK (highlighted with yellow stars, e.g. PDK1), may enable the by-pass of AKT inhibition via SGK.

Investigating the response of the PAM pathway to AT13148 also provided insight into AT13148 resistance (Figure 4.14). Remarkably, the phosphorylation of the AKT substrate PRAS40 and the p70S6K substrate S6RP were both partially refractory to AT13148 in 148R-K, N & S. This suggests that the re-activation of substrates downstream of the AT13148 targets AKT and p70S6K could be a potential mechanism of AT13148 resistance in 148R clones. Interestingly, as previously mentioned PRAS40 phosphorylation was not refractory to MK2206 in 148R-N or 148R-S, nor was S6RP phosphorylation in 148R-S. This would therefore suggest that the maintenance of PRAS40 phosphorylation in response to AT13148 was independent of AKT in 148R-N and 148R-S, and that in 148R-S, the maintenance of S6RP phosphorylation in response to AT13148 was also independent of AKT. In 148R-N, since S6RP phosphorylation was maintained in response to both MK2206 and AT13148, the mechanism outlined in Figure 4.19 could be contributing to both. In hindsight, it would have been prudent to also assess the phosphorylation of GSK3β in response to AT13148, to determine if the mechanism highlighted in Figure 4.19, which appears specific to 148R-N, also exists in response to AT13148. The maintenance of S6RP phosphorylation, may also explain why there was low-level cross-resistance in all 148R clones to the p70S6K inhibitor PF4708671 (Figure 4.13).

In contrast to the response of the PAM pathway, the ROCK pathway responded in a similar manner in A2780 and 148R clones in response to AT13148 (Figure 4.15). This was ascertained by using the phosphorylation of the ROCK substrate T696 MYPT1 as a marker of ROCK inhibition. However, as discussed in section 3.3 there are limitations in using T696 MYPT1 phosphorylation as a marker of ROCK inhibition; it can be phosphorylated by other kinases, which causes an incomplete response to ROCK inhibition. Additionally, the decrease of T696 MYPT phosphorylation in response to AT13148 did not proceed in a linear fashion in A2780 or 148R clones, the extent and magnitude of which varied across biological replicates (data not shown). This further questions the validity of using T696 MYPT1 phosphorylation, alone, as a marker of ROCK pathway inhibition in response to AT13148. Therefore, whilst it appears that the ROCK pathway is equally responsive to AT13148 in A2780, A2780-148R and 148R clones, this should be interpreted with caution. In light of the aforementioned intimate link between

AT13148 resistance and ROCK cross-resistance, which was highlighted in Figure 4.3, it will be important to determine the mechanism in which A2780-148R and 148R clones have overcome ROCK inhibition, as this is likely to contribute towards AT13148 resistance. To this end, it would be worthwhile to use additional substrates of ROCK and other markers of the ROCK pathway to comprehensively assess the response of the ROCK pathway to AT13148.

4.3.3. Alterations in the MAPK pathway in 148R clones

One of the most striking results of chapter 4 was the increase in the phosphorylation of ERK 1/2 at a basal level that was seen in 148R clones, most notably in 148R-S (Figure 4.17). Whilst this was observed within A2780-148R in chapter 3, the extent of the increase was far more dramatic in 148R clones. As discussed in section 3.3, the magnitude of the increase in ERK 1/2 phosphorylation in A2780-148R did appear to be quite variable, possibly suggesting the existence of sub-populations with high ERK 1/2 phosphorylation within A2780-148R, that were selected for over time and under different culture/experimental conditions. The identification of 148R clones that have an increased level of phosphorylated ERK 1/2 gives additional credence to this. Since ERK 1/2 is a major regulator of growth, proliferation and survival, its increased activation alone has the capacity to contribute to AT13148 resistance. In addition, the MAPK pathway can interact with the PAM pathway at multiple levels, so increased ERK 1/2 phosphorylation could be contributing to the maintenance of the PAM pathway in response to AT13148 (Figure 4.14), as discussed in section 4.3.2 (Mendoza, Er and Blenis, 2011).

Paradoxically, the phosphorylation of MEK 1/2 was decreased in all 148R clones. Again, in chapter 3, A2780-148R was also shown to have a decrease in the phosphorylation of MEK 1/2, but to a much lesser extent. Interestingly, the decrease in the phosphorylation of MEK 1/2 was inversely related to the phosphorylation of ERK 1/2, with the exception to this being 148R-N, which had the lowest phosphorylation of both ERK 1/2 and MEK 1/2 amongst 148R clones. This inverse relationship between ERK 1/2 and MEK 1/2 phosphorylation might be explained by the extensive negative feedback regulation of the MAPK pathway, the vast majority of which emanates from ERK 1/2. For example, ERK 1/2 can phosphorylate MEK 1/2, BRAF and CRAF negatively regulating their activity

(Eblen *et al.*, 2004; Dougherty *et al.*, 2005; Ritt *et al.*, 2010). This likely explains how an increase in ERK 1/2 could co-exist with decreased MEK 1/2 phosphorylation; as ERK 1/2 phosphorylation increased, so would ERK 1/2 mediated negative feedback, which in turn would decrease MEK 1/2 phosphorylation. However, negative feedback via ERK 1/2 ultimately functions to decrease the phosphorylation of ERK 1/2 itself; this has obviously been disrupted in 148R clones. Therefore, a mechanism must exist within 148R clones that enables a sustained increase in the phosphorylation of ERK 1/2 in the absence of increased MEK 1/2 activation, which warrants further investigation

In addition, the increased activation of ERK 1/2 in 148R clones was not reflected in RSK, an ERK 1/2 substrate, which was shown to have decreased phosphorylation in all 148R clones (Figure 4.17). However, the phosphorylation and activation of many ERK 1/2 substrates is under tight regulatory control, which may explain why RSK phosphorylation was decreased in all 148R clones. For example, upon full activation RSK undergoes autophosphorylation at S732 in its D-domain, an ERK 1/2 binding site. The effect of this differs depending on which RSK isoform this takes place, of which there are four (RSK1-4). In RSK1 & 2 this causes ERK 1/2 to dissociate from RSK, which enables the engagement of a wider range of RSK substrates, but at the cost of a rapid RSK inactivation (Roux *et al.*, 2003; Kidger and Cook, 2018). But in RSK3, ERK 1/2 does not dissociate which enables a more sustained activation of RSK3 (Roux *et al.*, 2003). Therefore, depending on the prevalence of RSK isoforms, RSK may not be a good biomarker of sustained ERK 1/2 activation.

In contrast, the phosphorylation of Elk-1, a nuclear substrate of ERK 1/2, was increased in both 148R-K and 148R-S (Figure 4.17). Elk-1 is a transcription factor, a member of the ternary complex factor (TCF) sub-family of ETS-domain transcription factors (Yoon and Seger, 2006). Phosphorylation of Elk-1, by ERK 1/2, causes its activation which enables the rapid transcription of immediate early genes (IEG's) such as *c-fos* (Yoon and Seger, 2006). c-fos and c-Jun (another IEG) form the activator protein 1 (AP-1) transcriptional complex, which in turn promotes the transcription of late response genes promoting proliferation and cell survival (Yoon and Seger, 2006; Mendoza *et al.*, 2011). Interestingly, c-fos is an unstable protein and requires phosphorylation by ERK 1/2 and RSK to prevent its degradation (Yoon and Seger, 2006; Anjum and Blenis, 2008). It would

therefore be interesting target to look at in 148R clones to investigate if sustained ERK 1/2 activation, in the absence of sustained RSK activation, can lead to a stable increase in the expression downstream transcriptional regulators (Figure 4.20). This might be required for increased ERK 1/2 activation to be able to contribute towards AT13148 resistance.
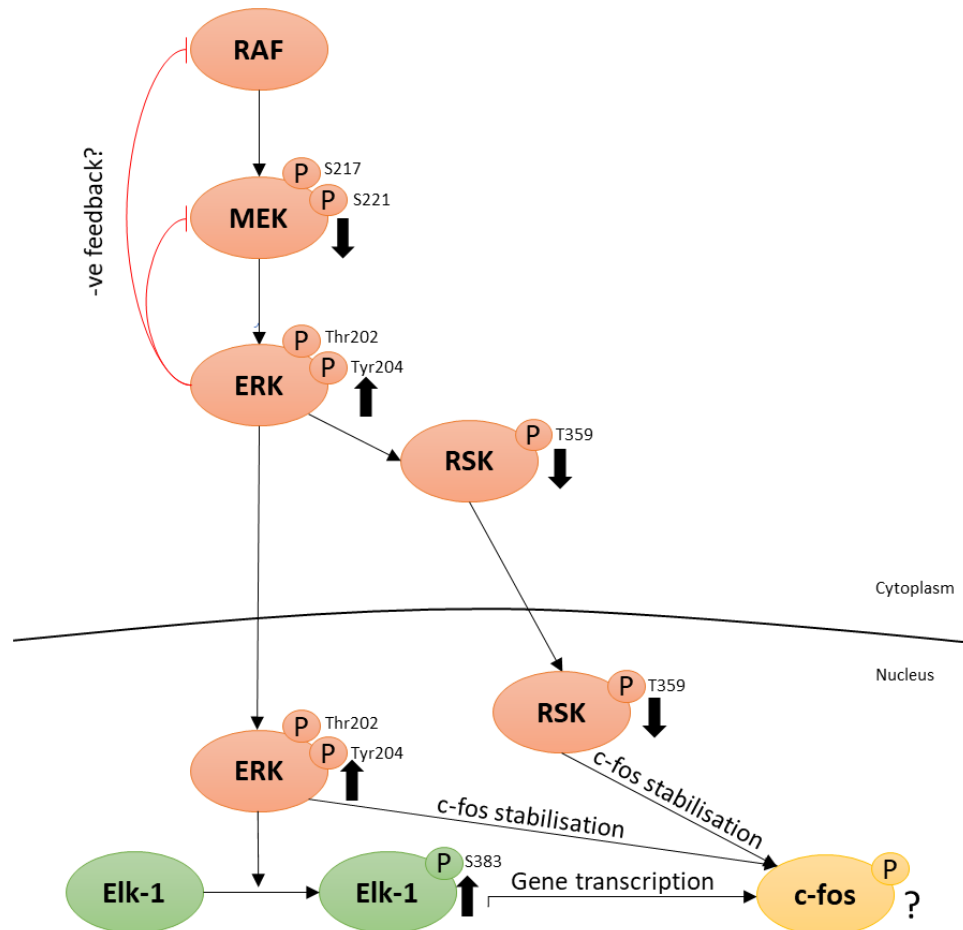
Figure 4.20: Status of the MAPK pathway in 148R-K and 148R-S. In 148R-K and 148R-S there is an increase in the phosphorylation of ERK 1/2 but a decrease in MEK 1/2 phosphorylation, possibly via ERK 1/2 mediated negative feedback. Of the two ERK 1/2 substrates analysed, Elk-1 phosphorylation was increased but RSK phosphorylation was decreased. Increased Elk-1 phosphorylation is likely to lead to an increase in the expression of its transcriptional targets, such as c-fos, which drives cell cycle progression and proliferation. RSK, which translocates to the nucleus upon activation, and ERK both phosphorylate c-fos to prevent its degradation. The lack of RSK activation could limit the expression of c-fos, therefore proliferation and cell survival and perhaps the ability of ERK 1/2 to contribute to AT13148 resistance.

Contrary to 148R-K and 148R-S, there was a substantial decrease in Elk-1 phosphorylation in 148R-N. This means there is no evidence that increased ERK 1/2 activation causes a sustained activation of ERK 1/2 substrates in 148R-N. However, 160 substrates of ERK 1/2 have been identified, the phosphorylation of which are dependent on the abundance of scaffold proteins and other regulatory mechanisms (Yoon and

Seger, 2006). It's quite possible that a subset of these are regulated by increased ERK 1/2 phosphorylation in 148R-N, but as of yet have not been identified.

In summary, in this chapter isogenic 148R clones have been derived from A2780-148R cells, of which three; 148R-K, N & S, were selected for further characterisation. Of these three, 148R-N appeared the most distinct lacking sensitivity to the FGFR inhibitor AZD4547 and having changes within the PAM pathway proximal to AKT. Interestingly, in all three 148R clones, the PAM pathway was shown partially refractory to AT13148. Since AT13148 targets the PAM pathway, via AKT and p70S6K inhibition, the reactivation of the PAM pathway in response to AT13148 could be contributing to AT13148 resistance. In addition, 148R-K, N and S were shown to have increased phosphorylation of ERK 1/2, which has the potential to act as a driver of AT13148 resistance. Subsequent chapters will focus on investigating the contribution of PAM pathway re-activation and increased ERK 1/2 phosphorylation to AT13148 resistance in 148R clones.

Chapter 5

**Investigating ERK 1/2 as a driver
of AT13148 resistance**

5. Investigating ERK 1/2 as a driver of AT13148 resistance

5.1. Introduction

One of the key findings of previous chapters has been the identification of increased ERK 1/2 phosphorylation in both A2780-148R and 148R clones. It was reasoned, that since ERK 1/2 is a major regulator of cell growth, proliferation and survival, that increased phosphorylation of ERK 1/2 had the potential to act as a driver of resistance to AT13148. Indeed, ERK 1/2 has frequently been associated with resistance to numerous cancer therapies, either directly through alterations to ERK 1/2, or indirectly through changes in upstream components of the MAPK pathway. For example, Ercan and colleagues (Ercan *et al.*, 2012) generated resistance in an *EGFR* (T790M) mutant NSCLC cell line against WZ4002, a 3rd generation EGFR inhibitor with activity against T790M mutant EGFR, and found that the *MAPK1* gene, which encodes ERK2, was amplified, rendering ERK 1/2 phosphorylation refractory to WZ4002. Subsequently, inhibition of ERK and MEK were shown to overcome resistance, restoring sensitivity to WZ4002. In addition, the MAPK pathway is frequently mutated to overcome BRAF (V600E) inhibition in melanoma (as discussed in section 1.6.2.1), for example via activating mutations in *NRAS* and *MEK1* (Nazarian *et al.*, 2010; Wagle *et al.*, 2011).

However, the aforementioned examples of MAPK pathway driven resistance are against therapies which directly target the MAPK pathway, and in which resistance is generated via mechanisms that reactivate the MAPK pathway. Since AT13148 is not known to directly inhibit the MAPK pathway, increased activation of ERK 1/2 is unlikely to generate resistance to AT13148 in this manner. One way in which increased ERK 1/2 activation might drive AT13148 resistance is by facilitating the by-pass of AT13148 targets, such as the PAM pathway, which AT13148 targets via its inhibition of AKT and p70S6K. Increased ERK 1/2 activation might enable this as the MAPK and PAM pathways are both major growth factor pathways, and as such display some redundancy, converging on many of the same functional outputs, such as cell cycle progression and survival. For example, both ERK 1/2 and AKT regulate the expression of cyclin D1, albeit via different mechanisms, which promotes cell cycle progression. ERK 1/2 increases the transcription of cyclin D1 via the transcription of c-fos (shown in Figure 4.20), which in turn promotes

cyclin D1 expression; AKT promotes cyclin D1 stability by phosphorylating GSK3β, which inhibits its activity, preventing GSK3β from phosphorylating cyclin D1 and promoting its degradation (Chang *et al.*, 2003; Torii *et al.*, 2006). Furthermore, in regards to pro-survival signalling, the MAPK and PAM pathway are both known to negatively regulate many of the same pro-apoptotic proteins including BAD, BIM and FOXO3a, thus promoting cell survival (Chang *et al.*, 2003; Qi *et al.*, 2006; O'Reilly *et al.*, 2009).

As well the MAPK pathway converging upon the same functional outputs of the PAM pathway, the MAPK pathway is also known to cross-activate the PAM pathway at several levels (Mendoza *et al.*, 2011). For example, ERK 1/2 and RSK, an ERK 1/2 substrate, are known to phosphorylate TSC2 in a similar manner to AKT, inhibiting its GAP function and promoting mTORC1 activity (Mendoza *et al.*, 2011). In addition, ERK 1/2 and RSK can also phosphorylate RAPTOR (regulatory associated protein of mTOR), a subunit of mTORC1, which promotes the phosphorylation of 4E-BP1 by mTORC1 (Mendoza *et al.*, 2011). It is therefore possible that increased ERK 1/2 phosphorylation could also promote AT13148 resistance by cross activating the PAM pathway, maintaining its activation in the presence of AT13148.

As one might expect, due to the intimate link between the PAM and MAPK pathways, both pathways have been shown to compensate for one another in therapy resistance. Villanueva and colleagues (Villanueva *et al.*, 2010) generated resistance to BRAF inhibition, in *BRAF* V600E mutant melanoma cells, and identified that persistent IGF-1R signalling induced PI3K/AKT activation. This cooperated with RAF isoform switching to drive resistance to BRAF inhibition, in part, by maintaining the expression of myeloid cell leukaemia 1 (Mcl-1), a pro-survival factor jointly regulated by the PAM and MAPK pathway (Villanueva *et al.*, 2010). Furthermore, increased IGF-1R expression and AKT phosphorylation were found in post-relapse patient samples, in the absence of MAPK pathway mutations, highlighting the clinical relevance of PAM pathway activation in BRAF inhibitor resistance (Villanueva *et al.*, 2010). The inverse (MAPK pathway compensation for PAM pathway inhibition) has also been observed in HER2 over-expressing breast cancer cells, albeit in an intrinsic resistance setting, where PI3K inhibition has been shown to induce the phosphorylation of ERK 1/2, attenuating the response to PI3K inhibition, despite robust inhibition of the PAM pathway (Serra *et al.*,

2011). Subsequently, co-inhibition of PI3K and MEK was found to cause a much greater reduction in cell proliferation and increased apoptosis, when compared to single agent alone (Serra *et al.*, 2011).

For the reasons outlined, the aim of this chapter was to investigate the ability of increased ERK 1/2 phosphorylation in 148R clones to act as a driver of AT13148 resistance. Initially, the response of 148R clones to single agent MEK and ERK inhibition was assessed, to ascertain if there was any sensitivity or cross-resistance and to gain insight into the regulation of the MAPK pathway in 148R clones. Subsequently, ERK 1/2 was validated as a driver of AT13148 resistance in 148R clones by performing combination SRB cell viability assays with AT13148 and ERK inhibitors.

5.2. Results

5.2.1. Response of A2780 and 148R clones to MEK and ERK inhibitors

Having detected altered MAPK signalling in all three 148R clones, as shown in Figure 4.17, the response to MEK and ERK inhibitors (inhibitors of the MAPK pathway) was studied in A2780 and 148R-K, N & S. Figure 5.1A shows the response and GI_{50} determinations for A2780 and 148R clones against the allosteric MEK inhibitors PD0325901 and selumetinib (AZD6244; Yeh *et al.*, 2007; Barrett *et al.*, 2008; Wu and Park, 2015). A2780 had a GI_{50} of 0.027 µM against PD0325901 and a GI_{50} of 0.68 µM against selumetinib (Figure 5.1A). Strikingly, there was a statistically significant increase in the GI_{50} for PD0325901 in both 148R-K and 148R-S, which had GI_{50} values of 0.139 µM and 0.072 µM respectively (Figure 5.1A). This equated to an RF of 5.15 for 148R-K and 2.67 for 148R-S, indicating cross-resistance to PD0325901 (Figure 5.1A). This was also the case for selumetinib; 148R-K had a GI_{50} of 3.51 µM, representing an RF of 5.16, and 148R-S had a GI_{50} of 1.25 µM, an RF of 1.84 (Figure 5.1A). However, cross-resistance against selumetinib was only statistically significant in 148R-K (Figure 5.1A). In contrast, 148R-N had low-level sensitivity to PD0325901 and selumetinib (Figure 5.1A). The GI_{50} for 148R-N was 0.015 µM against PD0325901 and 0.19 µM against selumetinib, this equated to an RF of 0.56 (1.8-fold sensitivity) and 0.28 (3.6-fold sensitivity) respectively (Figure 5.1A). However, this sensitivity was not shown to be statistically significant.

Unlike the response to MEK inhibitors, 148R clones and parental A2780 cells did not show any substantial differences (cross-resistance or sensitivity) in response to the ATP-competitive ERK inhibitors GDC-0994 and SCH772984 (Morris *et al.*, 2013; Blake *et al.*, 2016; Kidger *et al.*, 2018) (Figure 5.1B). Against GDC-0994, A2780 had a GI_{50} of 0.93 µM compared to 0.79 µM for 148R-K, 0.87 µM for 148R-N and 1.18 µM for 148R-S, which equated to RF values of 0.85, 0.94 and 1.27 respectively (Figure 5.1B). This was similar for SCH772984; A2780 had a GI_{50} of 0.071 µM compared to 0.064 µM for 148R-K, 0.062 µM for 148R-N, and 0.048 µM for 148R-S, which represented RF values of 0.90, 0.87 and 0.68 respectively (Figure 5.1B). Taken together, these data show that 148R-K and 148R-

S, particularly 148R-K, are cross-resistant to MEK inhibition, but that 148R clones respond in similar manner as parental A2780 cells to ERK inhibition.

A

	PD0325901 (MEK)		Selumetinib (MEK)	
Cell line	**GI$_{50}$ (µM)**	**RF**	**GI$_{50}$ (µM)**	**RF**
A2780	0.027 ± 0.014	N/A	0.68 ± 0.42	N/A
148R-K	0.139 ± 0.091**	5.15	3.51 ± 1.60*	5.16
148R-N	0.015 ± 0.009	0.56	0.19 ± 0.08	0.28
148R-S	0.072 ± 0.030**	2.67	1.25 ± 0.52	1.84

B

	GDC-0994 (ERK)		SCH772984 (ERK)	
Cell line	**GI$_{50}$ (µM)**	**RF**	**GI$_{50}$ (µM)**	**RF**
A2780	0.93 ± 0.39	N/A	0.071 ± 0.023	N/A
148R-K	0.79 ± 0.13	0.85	0.064 ± 0.012	0.90
148R-N	0.87 ± 0.28	0.94	0.062 ± 0.035	0.87
148R-S	1.18 ± 0.35	1.27	0.048 ± 0.008	0.68
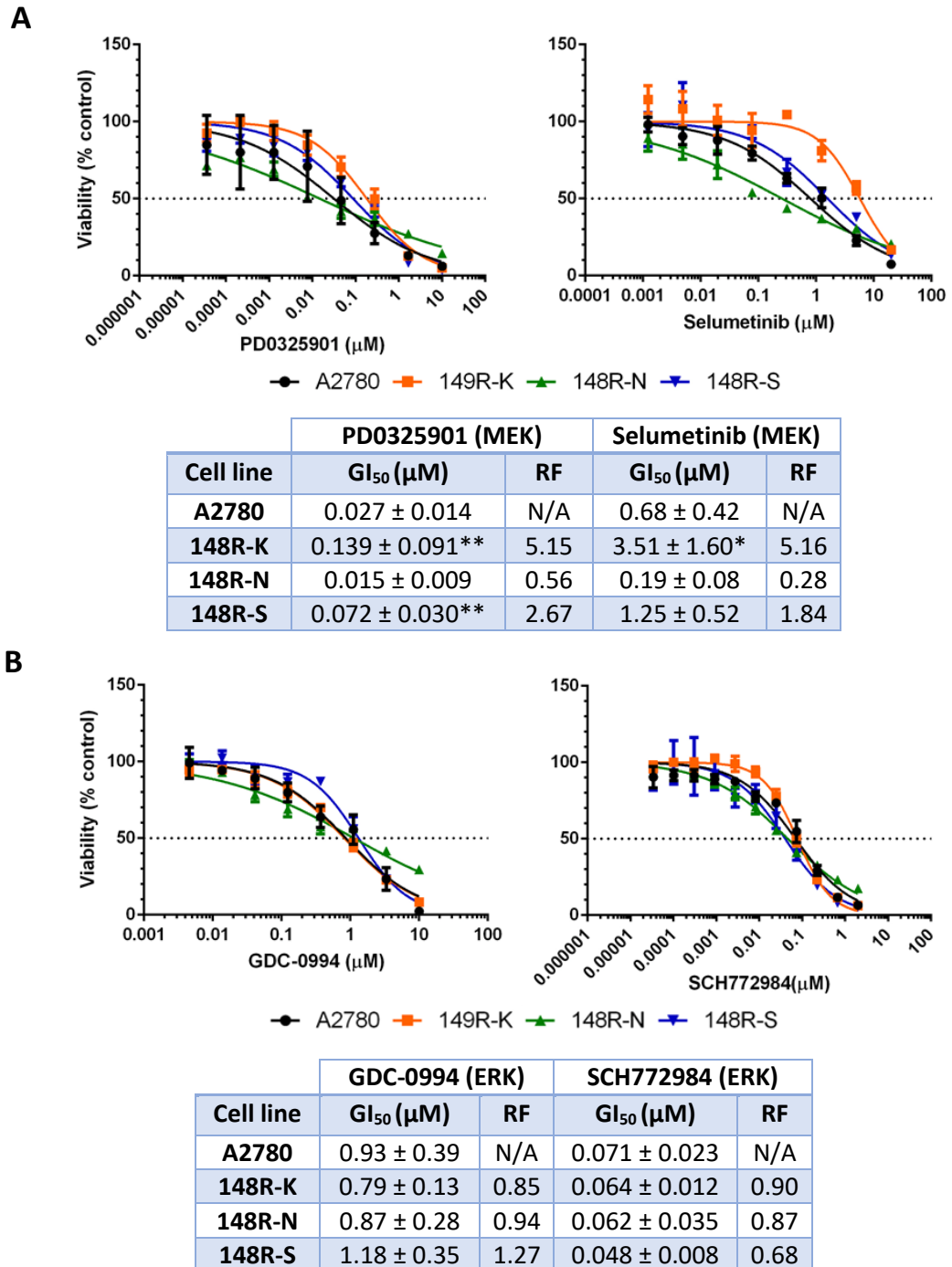
Figure 5.1: Dose-response curves and GI$_{50}$ determinations for MEK and ERK inhibitors in A2780 and 148R clones. Cells were plated in triplicate in a 96-well plate and allowed to grow under standard growth conditions for 48 hours. They were then treated with a serial dilution of **(A)** PD0325901 or selumetinib, or **(B)** GDC-0994 or SCH772984 for 96-hours, prior to being analysed by SRB assay. Dose-response graphs and non-linear regression curve fits were generated using GraphPad Prism 6. Dotted lines mark 50% viability on the y-axis. Data points represent the mean ± SD from one representative experiment. Tables summarise GI$_{50}$ and RF values, GI$_{50}$ data points depict the mean ± SD of all experiments conducted. Statistical significance was calculated using a student's t-test, n = 3 (SCH772984), 5 (GDC-0994 & selumetinib) or 9 (PD0325901) independent experiments.

5.2.2. Response of MAPK pathway to MEK inhibition in A2780 and 148R clones

To further investigate cross-resistance to MEK inhibition, the phosphorylation of ERK 1/2 was analysed in parental A2780 cells and 148R clones after treatment with the MEK inhibitor PD0325901. The phosphorylation of Thr202/Tyr204 ERK 1/2 was potently inhibited in parental A2780 cells at 5-10 nM of PD0325901 (Figure 5.2). In contrast, 5-10 nM PD0325901 only caused a slight decrease in Thr202/Tyr204 ERK 1/2 phosphorylation in 148R clones, much less so than what was seen in A2780 (Figure 5.2). However, 50-100 nM PD0325901 did cause an additional decrease in Thr202/Tyr204 ERK 1/2 phosphorylation in all 148R clones, particularly in 148R-N but to a lesser extent in 148R-K and 148R-S. (Figure 5.2). Total ERK 1/2 expression was mostly the same between cell lines and in response to PD0325901, but appeared to be slightly lower in 148R-N and 148R-S, when compared to parental A2780 cells (Figure 5.2). Taken together, these data suggest that ERK 1/2 phosphorylation was partially refractory to the MEK inhibitor PD0325901 in 148R clones; this could explain why some 148R clones are cross-resistant to MEK inhibition.
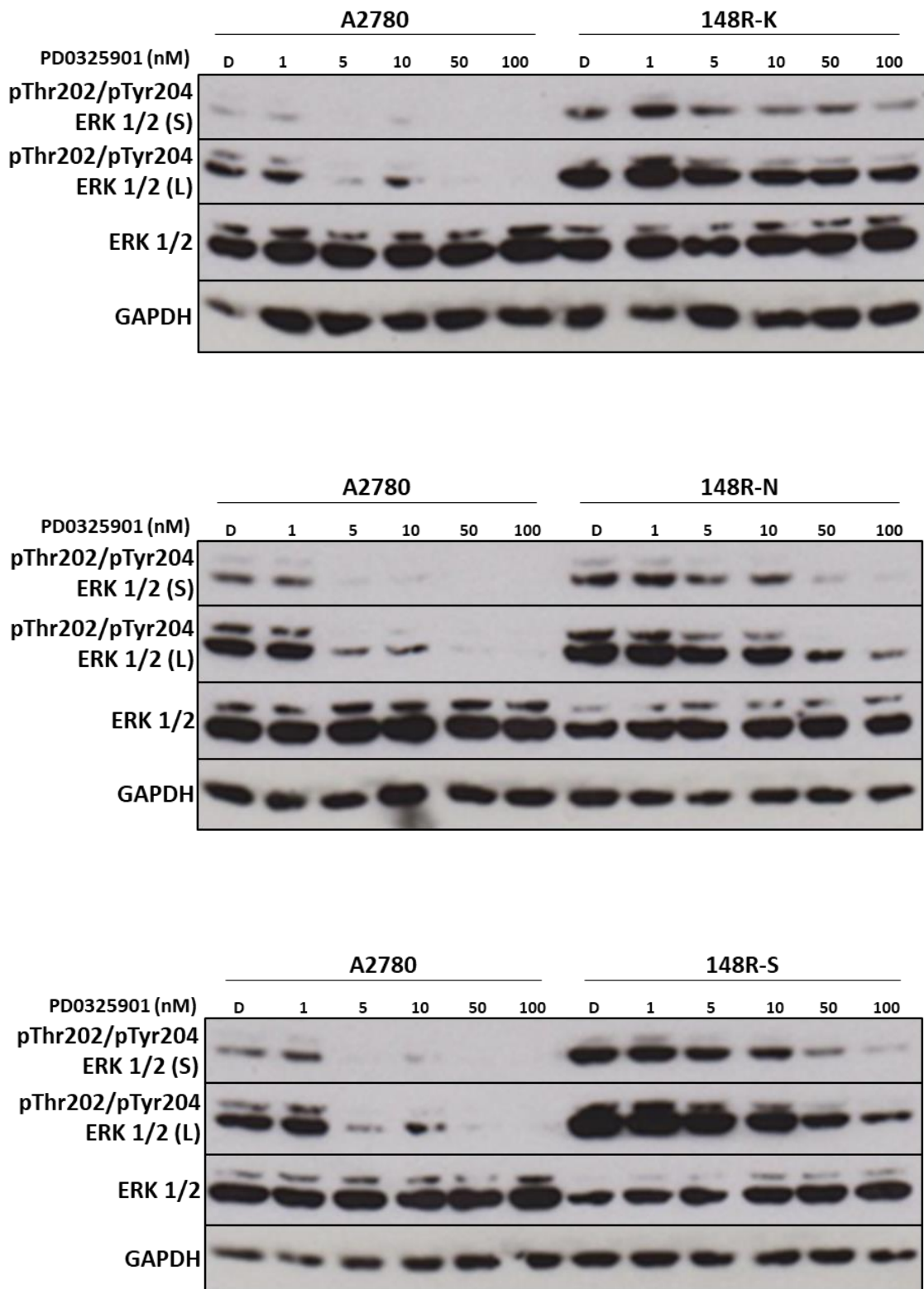
Figure 5.2: Response of the MAPK pathway to PD0325901 in A2780 and 148R clones. Cells were plated at either 5×10^5 (A2780) or 7.5×10^5 (148R clones) cells per 7 cm dish and allowed to grow for 48 hours under standard growth conditions. Cells were then treated with PD0325901, as shown, or D: DMSO vehicle control for 4 hours prior to being lysed for western blot analysis. Western blot membranes were probed with antibodies for phospho-proteins, stripped, and then re-probed with antibodies for total proteins or loading control (GAPDH). (S): short exposure to hyperfilm, (L): long exposure to hyperfilm. Data are representative of four experiments.

5.2.3. Response of MAPK pathway to ERK inhibition in A2780 and 148R clones

The response of the MAPK pathway to ERK inhibition was also examined in order to investigate why the response of 148R clones to ERK inhibition did not mirror that of MEK inhibition (cross-resistance or sensitivity, Figure 5.1). Figure 5.3 shows the response of A2780 and 148R clones to the ERK inhibitor GDC-0994, using phosphorylation of Elk-1, an ERK 1/2 substrate, as a biomarker of ERK inhibition. In parental A2780 cells, 0.1-0.2 µM of GDC-0994 was required to cause a significant reduction in the phosphorylation of S383 Elk-1, and despite a much lower basal phosphorylation of S383 Elk-1, 148R-N responded in a similar manner (Figure 5.3). In contrast, S383 Elk-1 phosphorylation was maintained in 148R-K and 148R-S; whilst S383 Elk-1 phosphorylation still decreased at 0.1-0.2 µM GDC-0994 in 148R-K and 148R-S, this was to a much lesser extent than in A2780 and 148R-N, with Elk-1 phosphorylation still detectable at 1 µM, most notably in 148R-K (Figure 5.3). This was especially interesting considering 148R-K and 148R-S had not been shown to be cross-resistant to ERK inhibition (Figure 5.1). The expression of total Elk-1 was mostly consistent across A2780 and 148R clones and unaffected by GDC-0994 (Figure 5.1).

The response of MEK 1/2 phosphorylation to GDC-0994 was also studied to investigate if the decrease in MEK 1/2 phosphorylation in 148R clones, shown in Figure 4.17, was caused by an increase in negative feedback from ERK 1/2; i.e. If the decrease in MEK 1/2 phosphorylation was caused by ERK 1/2 negative feedback, then one would expect inhibition of ERK to relieve this and cause an increase in MEK 1/2 phosphorylation. Figure 5.3 shows that this response was exhibited in both A2780 and 148R clones, but the magnitude and dynamics of the response differed. In parental A2780 cells, there was a strong increase in S217/221 MEK 1/2 phosphorylation at 0.05 µM GDC-0994, followed by incremental increases between 0.1 µM and 1 µM (Figure 5.3). This response was mirrored in 148R-N, but the magnitude of the response was much lower (Figure 5.3). 148R-K and 148R-S had a different response; 0.01 µM and 0.05 µM GDC-0994 only caused a subtle increase in S217/221 MEK 1/2 phosphorylation, but there was a more notable increase at 0.1 µM followed by successive strong increases at 0.2 µM and 1 µM (Figure 5.3). The total expression of MEK 1/2 was unaffected by GDC-0994 in all cell lines, but did appear to be slightly lower in 148R-S, compared to parental A2780 cells (Figure

5.3). Taken together, these data provided evidence that ERK 1/2 mediated negative feedback was responsible for decreased MEK 1/2 phosphorylation, particularly in 148R-K and 148R-S.
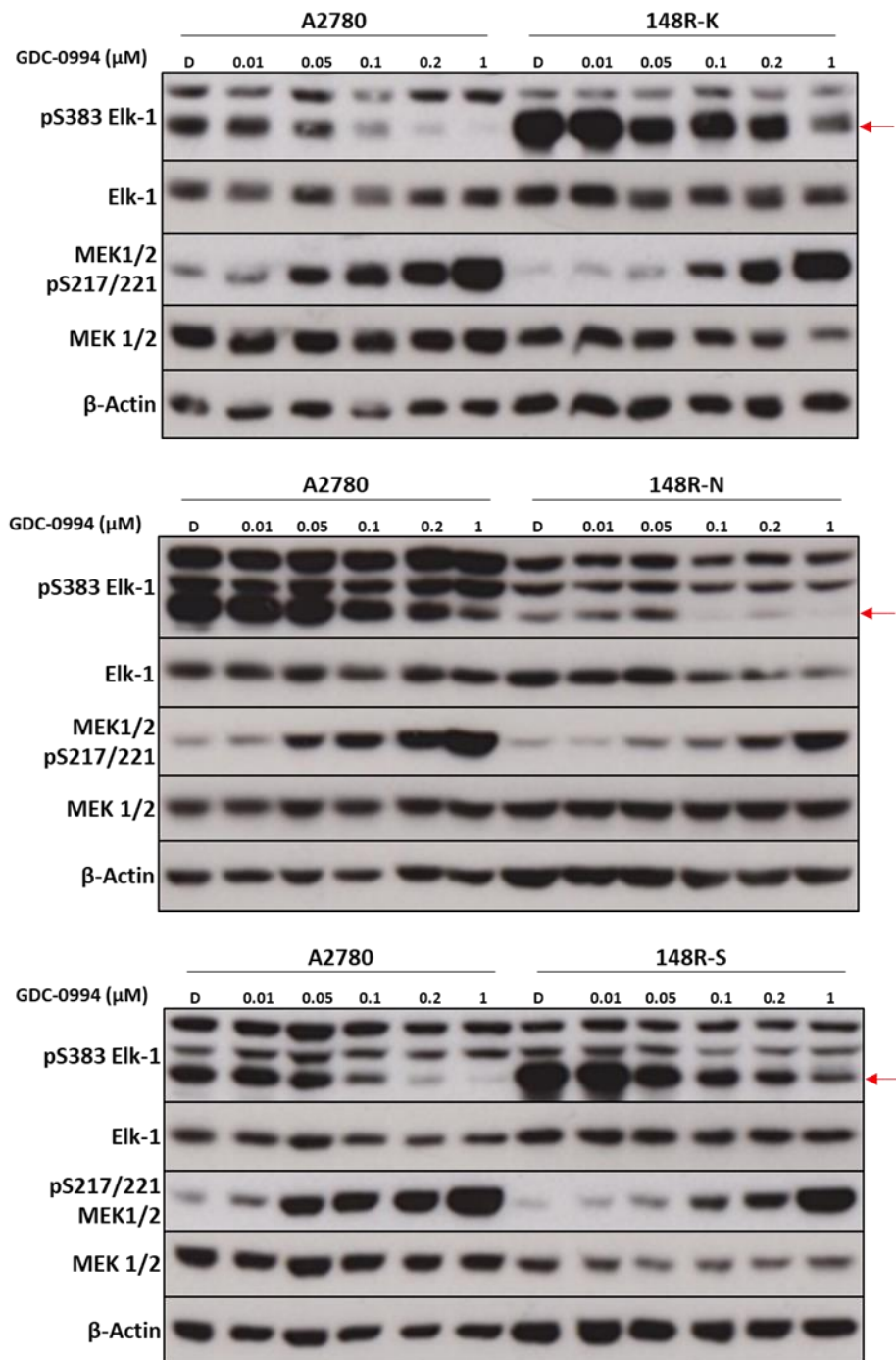
Figure 5.3: Response of the MAPK pathway to GDC-0994 in A2780 and 148R clones. Cells were plated at either 5×10^5 (A2780) or 7.5×10^5 (148R clones) cells per 7 cm dish and allowed to grow for 48 hours under standard growth conditions. Cells were then treated with GDC-0994, as shown, or D: DMSO vehicle control for 4 hours prior to being lysed for western blot analysis. Western blot membranes were probed with antibodies for phospho-proteins, stripped, and then re-probed with antibodies for total proteins or loading control (β-Actin). Red arrow highlights band corresponding to pS383 Elk-1. Data are representative of three experiments.

5.2.4. Response of the MAPK pathway to AT13148 in A2780 and 148R clones

The data thus far presented in this chapter does not suggest increased ERK 1/2 phosphorylation causes an increased dependency on the MAPK pathway for cell growth and survival in 148R clones, as shown by the lack of sensitivity to ERK inhibition (Figure 5.1) However, increased phosphorylation of ERK 1/2 may still contribute towards AT13148 resistance; 148R clones might only become dependent upon the MAPK pathway when in the presence of AT13148. This could be through additional changes induced in the MAPK pathway by AT13148, as was demonstrated in Figure 3.13, whereby AT13148 increased ERK 1/2 phosphorylation when used at 5 & 10 µM in A2780-148R cells. To investigate this, 148R clones were treated with AT13148 and western blot analysis performed for detection of Thr202/Tyr204 ERK 1/2 phosphorylation as a biomarker of MAPK pathway activation.

In A2780, higher concentrations of AT13148 (5 and 10 µM) caused a striking increase in the phosphorylation of Thr202/Tyr204 ERK 1/2, but the phosphorylation was mostly unchanged at lower concentrations, except for a notable decrease below the DMSO vehicle control at 1 µM AT13148 (Figure 5.4). The response in 148R clones was remarkable; increasing the concentration of AT13148 mostly led to successive increases in Thr202/Tyr204 ERK 1/2 phosphorylation, with phosphorylation peaking at 10 µM AT13148, the highest concentration used, in all 148R clones (Figure 5.4). However, there were some exceptions; 1 µM of AT13148 in 148R-K and 5 µM in 148R-N did not cause an increase in Thr202/Tyr204 ERK 1/2 phosphorylation above that of the previous concentrations, 0.5 µM and 1 µM respectively, but phosphorylation was still greater than their respective DMSO vehicle controls (Figure 5.4). The total expression of ERK 1/2 did not appear to be greatly affected by AT13148, but was lower in 148R clones, compared to A2780, particularly in 148R-K and 148R-S (Figure 5.4).

Taken together, AT13148 increased the phosphorylation of ERK 1/2 in 148R clones, which when combined with elevated basal phosphorylation of ERK 1/2 in 148R clones, enabled ERK 1/2 phosphorylation to be vastly greater across all concentrations of AT13148 in 148R clones, when compared to parental A2780 cells. This warrants further investigation as to whether this might contribute to AT13148 resistance in 148R clones.
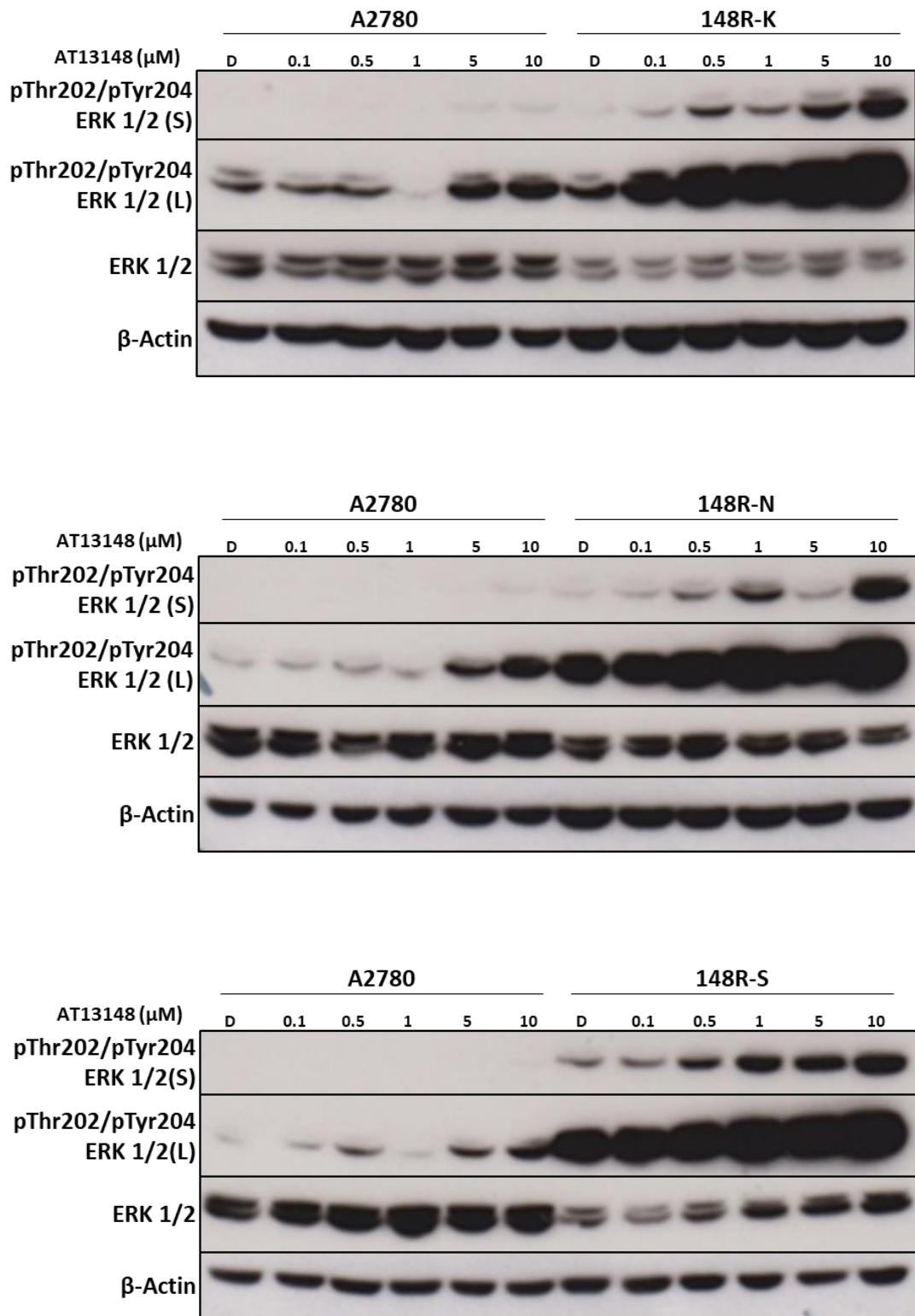
Figure 5.4: Response of the MAPK pathway to AT13148 in A2780 and 148R clones. Cells were plated at either 5 x 10^5 (A2780) or 7.5 x 10^5 (148R clones) cells per 7 cm dish and allowed to grow for 48 hours under standard growth conditions. Cells were then treated with AT13148, as shown, or D: DMSO vehicle control for 4 hours prior to being lysed for western blot analysis. Western blot membranes were probed with antibodies for phospho-proteins, stripped, and then re-probed with antibodies for total proteins or loading control (β-Actin). (S): short exposure to hyperfilm, (L): long exposure to hyperfilm. Data are representative of four experiments.

5.2.5. Response of A2780 and 148R clones to the combination of AT13148 and GDC-0994

5.2.5.1. GI_{50} determinations and Bliss independence synergy scores

To investigate the potential contribution of ERK 1/2 towards AT13148 resistance, single doses of the ERK inhibitor GDC-0994 were combined with a standard titration of AT13148 in a 6-day SRB cell viability assay. If ERK 1/2 was contributing towards AT13148 resistance, one would expect that ERK inhibition would re-sensitize 148R clones to AT13148. GDC-0994 was used at concentrations that corresponded to the GI_{05}, GI_{10}, GI_{20} values for each respective cell line. These values were calculated from the data presented in Figure 5.1 and are highlighted in Table 5.1, most of which were shown to cause ERK inhibition in Figure 5.3. In addition, low concentrations of GDC-0994 (GI_{05} – GI_{20}) were used to mitigate any off-target effects caused by GDC-0994, so that one could be confident that any effect of combination was due to ERK inhibition alone.

Table 5.1: Summary table of GI_{05}, GI_{10} and GI_{20} values for GDC-0094 in A2780 and 148R clones. Table summarises the concentrations of GDC-0994 used in combination with AT13148. GI values were calculated using CalcuSyn software using data presented in Figure 5.1. Data points represent the mean ± SD, n = 5 independent experiments.

	A2780	148R-K	148R-N	148R-S
GDC-0994 GI_{05} (µM)	0.054 ± 0.054	0.023 ± 0.015	0.007 ± 0.006	0.054 ± 0.026
GDC-0994 GI_{10} (µM)	0.083 ± 0.055	0.052 ± 0.032	0.014 ± 0.007	0.118 ± 0.057
GDC-0994 GI_{20} (µM)	0.228 ± 0.131	0.149 ± 0.062	0.035 ± 0.003	0.341 ± 0.175

Figure 5.5 shows the response of A2780 and 148R clones to the combination of AT13148 and GDC-0994. In both 148R-K and 148R-S, GDC-0094 caused a striking shift left in their dose-response curves to AT13148 indicating that there was a degree of re-sensitisation to AT13148 (Figure 5.5B, D). This was reflected in the GI_{50} determinations for AT13148, particularly when in combination with GI_{20} GDC-0994; the GI_{50} against AT13148 alone was 1.396 µM for 148R-K and 1.408 µM for 148R-S, but when combined with GI_{20} GDC-0994, GI_{50} values for 148R-K and 148R-S were 0.210 µM and 0.198 µM respectively (Figure 5.5E, F). This represented a 6.65-fold decrease for 148R-K and 7.11-fold decrease for 148R-S, when compared to respective AT13148 alone GI_{50} values, which were both statistically significant, remarkably lowering the GI_{50} against AT3148 to that of A2780

(A2780, AT13148 alone: 0.171 µM; Figure 5.5E, F). The GI_{05} and GI_{10} GDC-0994 combinations also caused a ~2-3-fold shift in AT13148 GI_{50}, of which there was statistical significance for GI_{05} and GI_{10} GDC-0994 in 148R-S and GI_{10} GDC-0994 in 148R-K (Figure 5.5E, F). It should be noted that whilst combination with GDC-0994 did shift the GI_{50} against AT13148 in 148R-K and 148R-S, the effect of combination became more attenuated at higher concentrations of AT13148 (> 1 µM; Figure 5.5).

In stark contrast to 148R-K and 148R-S, GDC-0994 did not appear to cause re-sensitisation to AT13148 in 148R-N (Figure 5.5C). The combination of AT13148 with GI_{20} GDC-0994 did cause a slight decrease in the GI_{50} against AT13148 in 148R-N (AT13148 alone: 3.664 µM vs GI_{20} GDC-0994: 2.197 µM), that was statistically significant, but this only represented a 1.67-fold decrease and was still substantially greater than the GI_{50} of A2780 (A2780, AT13148 alone: 0.171 µM, Figure 5.5E, F). The GI_{05} and GI_{10} GDC-0994 combinations had even less of an effect on the GI_{50} of 148R-N against AT13148, only causing a 1.07 and 1.10-fold decrease respectively (Figure 5.5E, F).

Interestingly, A2780 was also sensitized to AT13148 by combination with GDC-0994, with the greatest effect seen by combination with GI_{20} GDC-0994 (Figure 5.5A). In A2780, the GI_{50} against AT13148 in combination with GI_{20} GDC-0994 was 0.033 µM, which was 5.18-fold lower than the GI_{50} of AT13148 alone: 0.171 µM, and statistically significant (Figure 5.5E, F). The combination of AT13148 with GI_{05} and GI_{10} GDC-0994 also caused a ~2-3-fold decrease in the GI_{50} against AT13148, which was also shown to be statistically significant (Figure 5.5E, F). Taken together, these data show that A2780, 148R-K and 148R-S can be sensitised to AT13148 by combination with low concentrations of GDC-0994, further implicating ERK 1/2 as contributing towards AT13148 resistance, both intrinsic and acquired.

The level of synergistic growth inhibition, for the combinations of AT13148 with GDC-0994, was also calculated using the Bliss independence model. Synergy can be defined as when the combination of two drugs has an effect greater than the expected additive effect of the two drugs (i.e. the combined effect is greater than the sum of its individual components). The inverse of this is antagonism in which the combination of two drugs has an effect less than the expected additive effect of the two drugs (i.e. the combined effect is less than the sum of its individual components). However, when determining

synergy/antagonism, one must be able to statistically define the expected combined effect of two drugs (the additive effect). There are numerous methods to predict the combined effect of two drugs, but for the purposes of this study the Bliss independence model was used. Foucquier and Guedi (Foucquier and Guedj, 2015) state that "the *Bliss Independence* model is based on the principle that drug effects are outcomes of probabilistic processes and assumes that drugs act independently in such a manner that neither of them interferes with the other (different sites of action), but each contributes to a common result". The expected additive effect of the combination of two drugs can be calculated as follows when using the Bliss independence model: $E_T = E_A \times E_B$**,** where E_T*:* combined effect*, and* E_A and E_B: individual effects of drugs A and B, with each effect (E) expressed as fractional activity relative to control between 0 (100% inhibition) and 1 (0% inhibition). By subtracting the actual effect of a combination from the predicted additive effect it can be ascertained if the combination was synergistic > 0, additive = 0 or antagonistic < 0, with the calculated value representing the excess above or below Bliss. For example, if two drugs each caused a 50% inhibition in cell viability, the predicted additive response for combination would be 25%, as $0.5 \times 0.5 = 0.25$. If the actual effect of combination was 10% then it would be 0.15 (15%) in excess above bliss, as $0.25 - 0.10 = 0.15$, and therefore indicative of synergy.

The tables in Figure 5.6 show the excess above Bliss for the combination of GDC-0994 (GI_{05}, GI_{10}, GI_{20}) with the serially diluted range of AT13148 concentrations. In 148R-K and 148R-S, in line with the shift in dose-response described in Figure 5.5, there was a degree of synergy with combinations of AT13148 and GDC-0994 (Figure 5.6). This was strongest when 0.123 - 1.111 µM AT13148 was combined with GI_{20} GDC-0994; at these combinations the combined effect was 0.09-0.13 in excess of Bliss in 148R-K and 0.11 - 0.14 in excess of Bliss in 148R-S, indicating synergy. There was also synergy when AT13148 was combined with GI_{05} and GI_{10} GDC-0994, but to a lesser extent (0 - 0.10 in excess of Bliss, Figure 5.6). Synergy was also seen in A2780 but was strongest when 0.041 - 0.370 µM AT13148 was combined with GI_{10} GDC-0994; at these combinations the combined effect was 0.12 - 0.15 in excess of Bliss (Figure 5.6). These concentrations of AT13148 also had synergy with GI_{05} GDC-0994 (0.04 – 0.10 in excess of Bliss) and GI_{20} GDC-0994 (0.07 – 0.12 in excess of Bliss, Figure 5.6). In contrast, 148R-N did not show

any synergy, with most combinations of AT13148 and GDC-0994 displaying an additive or weakly antagonistic effect. Taken together, these data suggest that AT13148 and GDC-0994 interact in a synergistic manner when combined in A2780, 148R-K and 148R-S, adding further credence to the role of ERK 1/2 in AT13148 resistance.
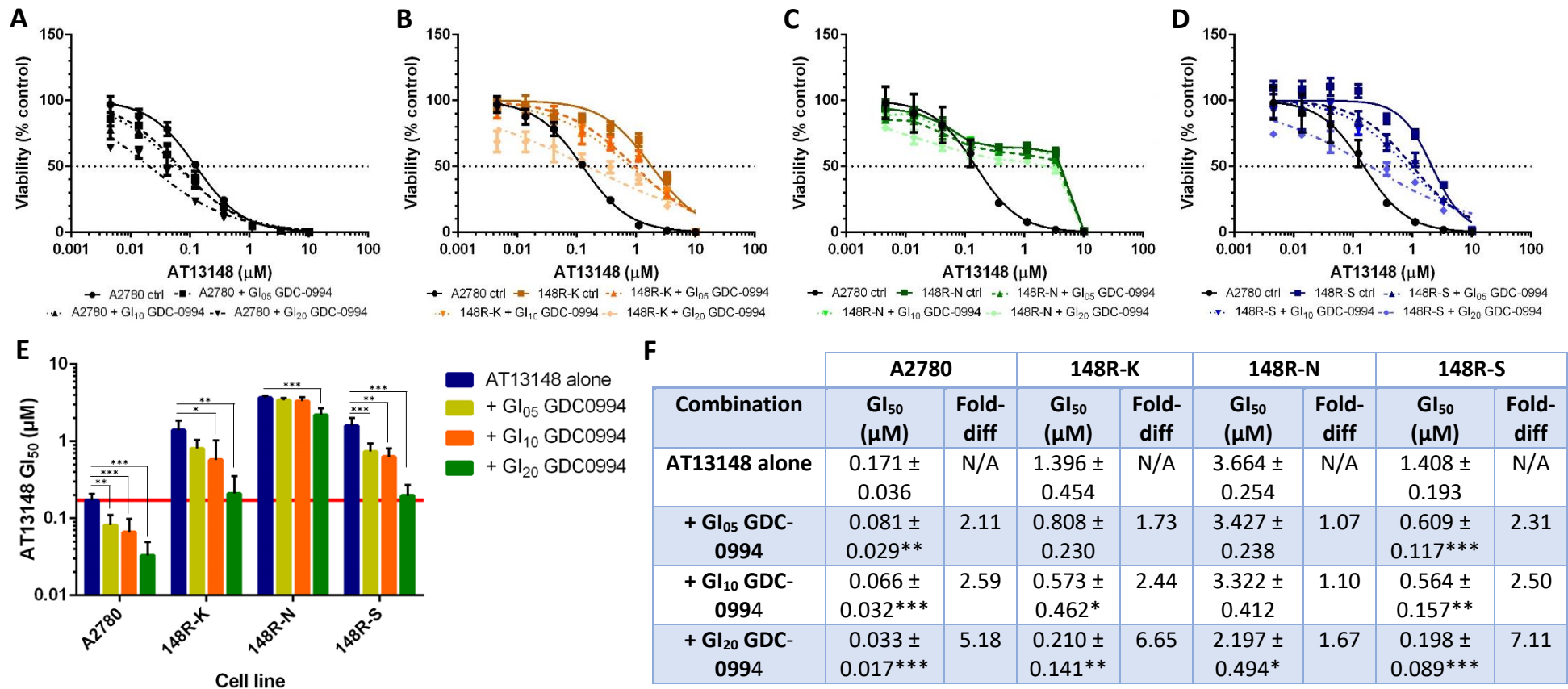
Figure 5.5: Dose-response curves and GI₅₀ determinations for AT13148 and GDC-0994 combination in A2780 and 148R clones. Cells were plated in triplicate in a 96-well plate and allowed to grow under standard growth conditions for 48 hours. They were then treated with a serial dilution of AT13148 alone, or in combination with GDC-0994, as shown, for 96-hours prior to being analysed by SRB assay. (A-D) Dose-response graphs and non-linear regression curve fits were generated using GraphPad Prism 6 (148R-N as described in Fig Figure 4.10). Dotted lines mark 50% viability on the y-axis. Data points represent the mean ± SD from one representative experiment. **(E & F)** GI₅₀ summary graph and table, bars and data points represent the mean ± SD of all experiments conducted, red line highlights A2780 GI₅₀ against AT13148 alone. Statistical significance and fold-diff (difference) compare AT13148 alone to respective GDC-0994 combinations within each cell line. Statistical significance was calculated using a student's t-test, n ≥ 3 independent experiments.

		A2780							
		AT13148 (µM)							
		10.000	3.333	1.111	0.370	0.123	0.041	0.014	0.005
GDC0994	GI05	0.00	0.00	0.01	0.04	0.10	0.09	0.03	0.03
	GI10	0.00	0.00	0.01	0.12	0.13	0.15	0.10	0.04
	GI20	0.00	0.00	0.01	0.07	0.12	0.11	0.04	0.00

		148R-K							
		AT13148 (µM)							
		10.000	3.333	1.111	0.370	0.123	0.041	0.014	0.005
GDC0994	GI05	0.00	0.04	0.05	0.03	0.03	-0.06	-0.03	-0.02
	GI10	0.00	0.05	0.10	0.08	0.09	0.01	0.01	0.01
	GI20	0.00	0.06	0.12	0.09	0.13	0.01	0.03	0.04

		148R-N							
		AT13148 (µM)							
		10.000	3.333	1.111	0.370	0.123	0.041	0.014	0.005
GDC0994	GI05	0.00	0.01	0.00	0.00	0.01	0.00	0.00	0.03
	GI10	0.00	0.01	-0.03	-0.03	-0.01	0.00	-0.04	-0.01
	GI20	-0.01	0.01	-0.02	-0.01	0.01	-0.01	-0.01	-0.02

		148R-S							
		AT13148 (µM)							
		10.000	3.333	1.111	0.370	0.123	0.041	0.014	0.005
GDC0994	GI05	0.00	0.01	0.02	0.04	0.08	0.04	0.00	-0.02
	GI10	-0.01	0.05	0.07	0.06	0.07	-0.03	-0.06	-0.02
	GI20	-0.01	0.06	0.11	0.11	0.14	0.07	0.00	-0.04

Key (excess above bliss):

≥ 0.00	0.10	0.20	0.30	0.40	0.50

Figure 5.6: Determination of synergy with the combination of AT13148 and GDC-0994 in A2780 and 148R clones. Tables summarise the synergy of AT13148 and GDC-0994 in A2780 and 148R clones for the assays conducted in Figure 5.5**.** Synergy was calculated using the Bliss independence model, where values > 0, highlighted in red, show an effect greater than the combined fractional inhibition of single agents, indicating synergy. Data points in tables represent the mean Bliss independence score for designated combinations, n ≥ 3 independent experiments

5.2.5.2. Analysis of AT13148 and GDC-0994 biomarkers

To validate the target inhibition of AT13148 and GDC-0994 at the concentrations used in Figure 5.5 & Figure 5.6, as well as investigate the mechanism(s) in which GDC-0994 sensitises cells to AT13148, a combination western blot was performed. Parental A2780 cells and 148R clones were treated with AT13148, at either 0.2 µM or 1 µM, GDC-0994, at GI_{20} concentrations for each respective cell line, or combinations of AT13148 and GDC-0994, for four hours, prior to western blotting for biomarkers of AT13148 (phosphorylation of S6RP) and GDC-0994 (phosphorylation of Elk-1). The GI_{20} concentrations of GDC-0994 were used as these caused the greatest sensitisation to AT13148 and synergy in Figure 5.5 & Figure 5.6.

Figure 5.7 shows that GDC-0994 alone was able to cause a reduction in the phosphorylation of S383 Elk-1 phosphorylation in A2780, 148R-K and 148R-S, indicating the inhibition or ERK 1/2. However, GDC-0994 did not decrease S383 Elk-1 phosphorylation in 148R-N, but it should be noted that some biological replicates did show a slight reduction in S383 Elk-1 phosphorylation (data not shown). Perhaps this variability suggests that the inhibition of ERK 1/2 is on the limit of detection at the GI_{20} concentration of GDC-0994 in 148R-N.

Interestingly, in 148R-S 1 µM of AT13148 alone was able to cause a slight increase in S383 Elk-1 phosphorylation, but this was overcome when AT13148 was combined with GDC-0994; S383 Elk-1 phosphorylation was decreased to the level seen with GDC-0994 alone (Figure 5.7). This increase, in S383 Elk-1 phosphorylation in response to 1 µM AT13148, was also seen in 148R-N, however, whilst the combination of AT13148 and GDC-0994 also decreased S383 Elk-1 phosphorylation, as in 148R-S, in 148R-N S383 Elk-1 phosphorylation was decreased below the level seen in with GDC-0994 alone (Figure 5.7). In contrast, AT13148 alone did not increase S383 Elk-1 phosphorylation in 148R-K, with S383 Elk-1 phosphorylation still retained below the level seen in the DMSO control when AT13148, both at 0.2 µM and 1 µM, was combined with GDC-0994, but it should be noted that S383 Elk-1 phosphorylation was elevated above the level seen with GDC-0994 alone when 1 µM AT13148 was combined with GDC-0994 in 148R-K (Figure 5.7). The phosphorylation of S383 Elk-1 was mostly unaffected by AT13148 in parental A2780

cells, with the level of S383 Elk-1 phosphorylation identical to the decrease caused by GDC-0994 alone, when used in combination (Figure 5.7). The total expression of Elk-1 was similar across all cell lines and conditions used (Figure 5.7).

In both A2780 and 148R clones the phosphorylation of S235/236 S6RP was unaffected by GDC-0994 alone, and AT13148 was able to decrease S235/236 S6RP phosphorylation in a manner consistent with Figure 4.14; S235/236 S6RP phosphorylation was potently inhibited in A2780 but was partially refractory in 148R clones (Figure 5.7). However, remarkably, the combination of AT13148 and GDC-0994 potentiated the decrease in S6RP phosphorylation caused by AT13148 alone (Figure 5.7). This was seen in all 148R clones where the combination of 1 µM of AT13148 with GDC-0994 caused a greater decrease in S235/236 S6RP phosphorylation than 1 µM AT13148 alone (Figure 5.7). In parental A2780 cells a similar affect was also observed with 0.2 µM AT13148 and 1 µM AT13148 when used in combination with GDC-0994, although this was clearer with a longer hyperfilm exposure (data not shown; Figure 5.7). Total S6RP expression was similar across A2780 and 148R clones and was not greatly affected by the conditions used (Figure 5.7)

Taken together, these data show that the combination of GDC-0994 with AT13148 was able to potentiate the decrease in S6RP phosphorylation caused by AT13148 in A2780 and 148R clones. This could, in part, explain why GDC-0994 sensitised cells to AT13148 and suggests that the refractory response of S6RP phosphorylation in 148R clones, shown in Figure 4.14, is dependent on ERK 1/2 activation, again, implicating ERK 1/2 in AT13148 resistance.
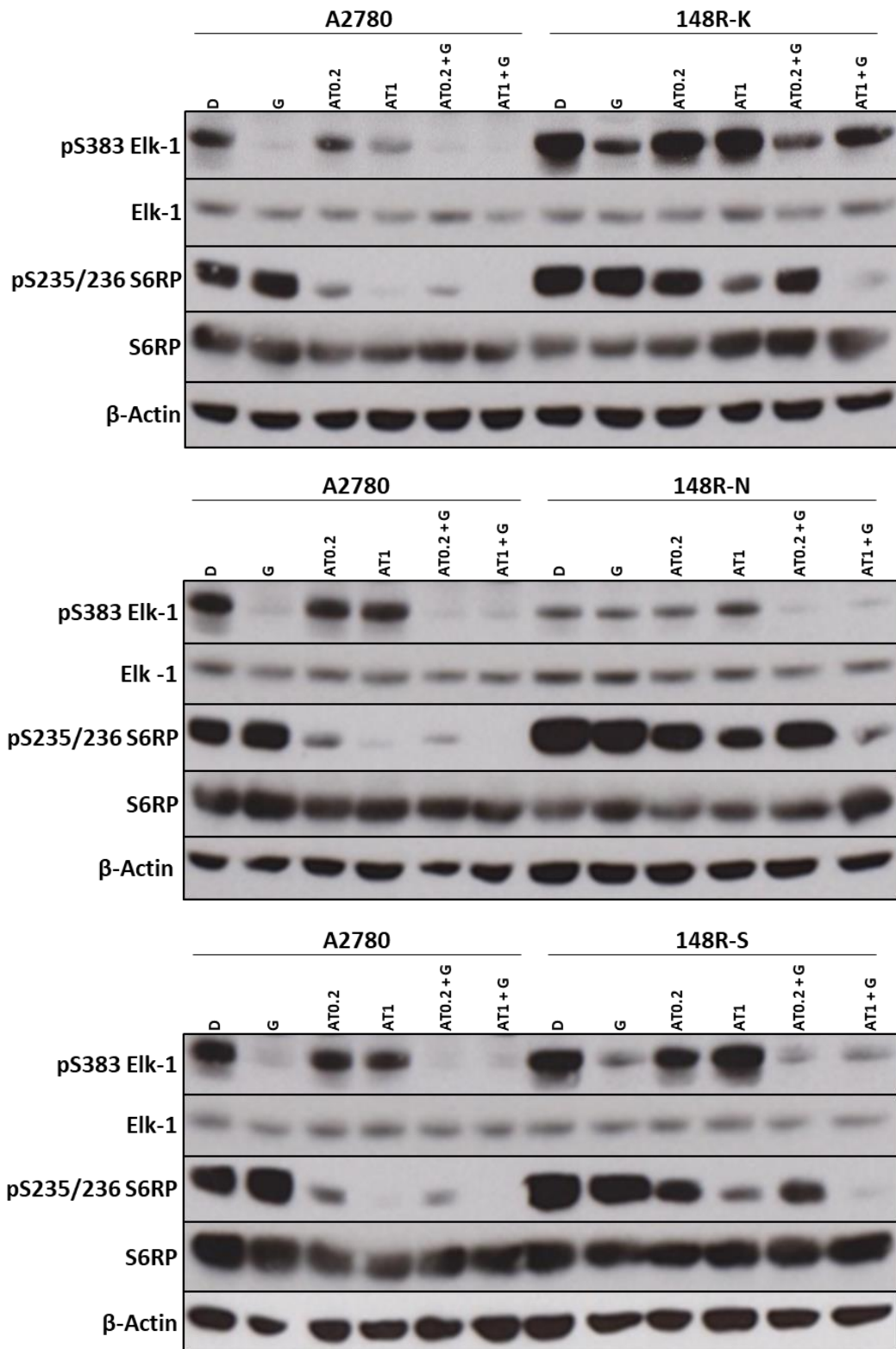
Figure 5.7: AT13148 and GDC-0994 biomarker response to AT13148 and GDC-0994 combination in A2780 and 148R clones. Cells were plated at either 5 x 10^5 (A2780) or 7.5 x 10^5 (148R clones) cells per 7 cm dish and allowed to grow for 48 hours under standard growth conditions. Cells were then treated with AT13148 at 0.2 μM (AT0.2) or 1 μM (AT1); GDC-0994 at its GI$_{20}$ concentration (G), as shown in Table 5.1; a combination of AT13148 and GDC-0994; or DMSO vehicle control (D), for 4 hours prior to being lysed for western blot analysis. Western blot membranes were probed with antibodies for phospho-proteins, stripped, and then re-probed with antibodies for total proteins or loading control (β-Actin). Data are representative of three experiments.

5.2.6. Response of A2780 and 148R clones to the combination of AT13148 and SCH772984

To further validate the contribution of ERK 1/2 towards AT13148 resistance, additional combination assays were performed using SCH772984, an ERK inhibitor with a different mechanism of action to GDC-0994; SCH772984 has a dual-mechanism of action decreasing the phosphorylation of ERK 1/2, as well as ERK 1/2 substrates (Morris *et al.*, 2013; Blake *et al.*, 2016; Kidger *et al.*, 2018). Just as with GDC-0994, low concentrations of SCH772984 were used (1 nM, 5 nM and 10 nM), so as to mitigate any off-targets effects. The effect of these concentrations on cell viability, when used as single agents, is highlighted in Table 5.2. In addition, the assays were focused on 148R-S and A2780, since GDC-0994 was shown to cause the greatest sensitisation to AT13148 in 148R-S (Figure 5.5).

Table 5.2: Effect of SCH772984 on cell viability in A2780 and 148R-S when used as a single agent. Table summarises the effect of SCH772984 on cell viability when used as a single agent at the concentrations used in combination assays with AT13148. Each SCH772984 concentration was plated in triplicate in parallel with combination assays (Figure 5.8) and cell viability was determined in a standard 6-day SRB cell viability assay. Data points represent the mean ± SD, n ≥ 2 independent experiments.

	Cell viability (%)	
SCH772984 (nM)	**A2780**	**148R-S**
5	93.1 ± 1.7	94.5 ± 8.7
10	98.4 ± 0.4	104.0 ± 2.0
20	85.2 ± 6.5	77.9 ± 0.8

As expected, Figure 5.8B shows that 148R-S was sensitised to AT13148 by combination with SCH772984. This was most dramatic when AT13148 was combined with 20 nM SCH772984 in 148R-S; the AT13148 GI_{50} for this combination was 0.202 µM which was 15.66-fold lower than the GI_{50} of AT13148 alone in 148R-S: 3.163 µM, and statisitcally significant (Figure 5.8C, D). In addition, this combination lowered the GI_{50} against AT13148 below that of A2780 (A2780, AT13148 alone: 0.389 µM), indicating 148R-S had been re-sensitised to AT13148 (Figure 5.8C, D). Combination of AT13148 with 1 nM and 5 nM SCH772984 also sensitsed 148R-S cells to AT13148 by ~2-fold, but this was only statistically significant with the combination of 1 nM SCH772984 (Figure 5.8C, D). Whilst this was not as substantial as the sensitisation caused by 20 nM SCH772984, it was nonetheless remarkable, considering that these concentrations of SCH772984 had little

to no effect on cell viability when used as single agents (Table 5.2). Furthermore, parental A2780 cells were also sensitised to AT13148 by SCH772984, albeit to a much lesser extent when compared to 148R-S cells (Figure 5.8A). Only combination with 20 nM SCH772984 was able to cause a statistically signficant sensitation to AT13148; in A2780 the GI_{50} for AT13148 in combination with 20 nM SCH772984 was 0.117 μM which was 3.32-fold less than AT13148 alone: 0.389 μM (Figure 5.8C, D). Combination with 5nM and 10nM SCH772984 caused a < 2-fold sensitisation to AT13148, neither of which were statistically significant (Figure 5.8C, D)

The sensitiation caused by SCH772984 to AT13148 was also reflected when calculating the level of synergy of the combinations of AT13148 and SCH772984. Figure 5.8E shows that all concentrations of SCH772984 displayed synergy across a wide range of AT13148 concentrations in 148R-S. The peak of this was when 10 nM or 20 nM of SCH772984 was combined with 0.041 – 1.111 μM AT13148; these combinations were between 0.17 and 0.25 in excess of Bliss, thus indicating synergy (Figure 5.8E). In contrast, whilst there was synergy in A2780 it was lower and confined to much narrower set of concentrations. Synergy appeared to be at it highest, in A2780, when concentrations of SCH772984 were combined with 0.370 μM and 0.123 μM AT13148, a peak of 0.19 in excess of Bliss was observed when 20 nM SCH772984 was combined with 0.123 μM AT13148 (Figure 5.8E). Outside of this narrow range, combinations displayed a mostly additive or weakly synergistic response in parental A2780 cells (Figure 5.8E).

Taken together, these data show that SCH772984 was able to senisitise A2780 and 148R-S cells to AT13148, and that combination of SCH772984 and AT13148 displayed synergy. Interestingly, the level of sensitisation and synergy by SCH772984 appeared far greater in 148R-S than A2780, and in 148R-S greater than that seen when GDC-0994 was combined with AT13148 (Figure 5.5 & Figure 5.6). These data add further evidence of the contribution of ERK 1/2 to AT13148 resistance and the possibility of co-targetting ERK 1/2 to overcome AT13148 resistance in the clinic.

A

B

C

D

Combination	A2780		148R-S	
	GI$_{50}$ (µM)	Fold-diff	GI$_{50}$ (µM)	Fold-diff
AT13148 alone	0.389 ± 0.110	N/A	3.163 ± 0.573	N/A
+ 5nM SCH772984	0.233 ± 0.110	1.67	1.534 ± 0.185*	2.06
+ 10nM SCH772984	0.246 ± 0.034	1.58	1.447 ± 0.539	2.19
+ 20nM SCH772984	0.117 ± 0.062*	3.32	0.202 ± 0.013**	15.66
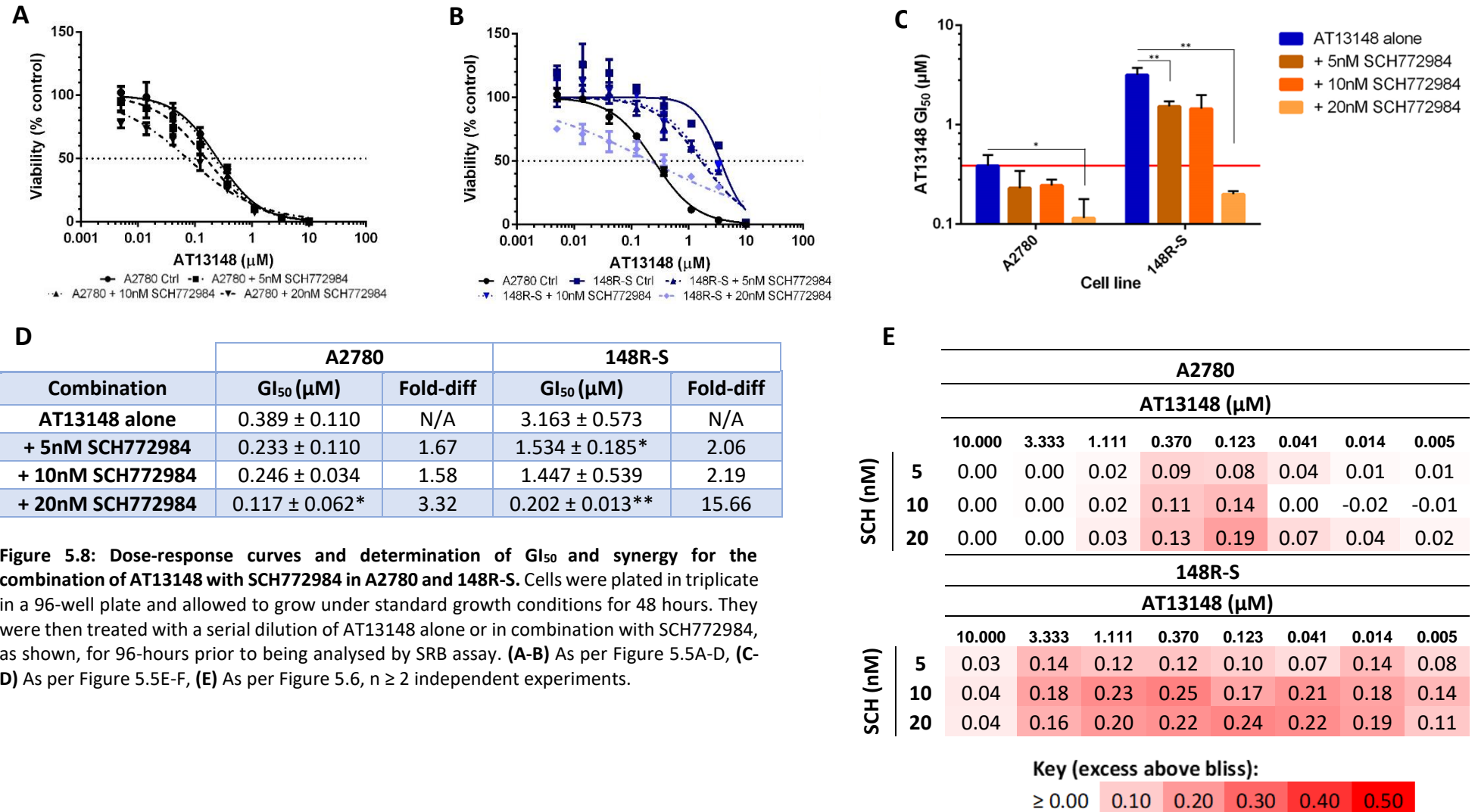
Figure 5.8: Dose-response curves and determination of GI$_{50}$ and synergy for the combination of AT13148 with SCH772984 in A2780 and 148R-S. Cells were plated in triplicate in a 96-well plate and allowed to grow under standard growth conditions for 48 hours. They were then treated with a serial dilution of AT13148 alone or in combination with SCH772984, as shown, for 96-hours prior to being analysed by SRB assay. **(A-B)** As per Figure 5.5A-D, **(C-D)** As per Figure 5.5E-F, **(E)** As per Figure 5.6, n ≥ 2 independent experiments.

E

A2780

AT13148 (µM)

SCH (nM)	10.000	3.333	1.111	0.370	0.123	0.041	0.014	0.005
5	0.00	0.00	0.02	0.09	0.08	0.04	0.01	0.01
10	0.00	0.00	0.02	0.11	0.14	0.00	-0.02	-0.01
20	0.00	0.00	0.03	0.13	0.19	0.07	0.04	0.02

148R-S

AT13148 (µM)

SCH (nM)	10.000	3.333	1.111	0.370	0.123	0.041	0.014	0.005
5	0.03	0.14	0.12	0.12	0.10	0.07	0.14	0.08
10	0.04	0.18	0.23	0.25	0.17	0.21	0.18	0.14
20	0.04	0.16	0.20	0.22	0.24	0.22	0.19	0.11

Key (excess above bliss):

≥ 0.00 0.10 0.20 0.30 0.40 0.50

5.2.7. Response of A2780 and 148R clones to the combination AT13148 and PD0325901

Combination assays were also performed with the MEK inhibitor PD0325901 to investigate if inhibition of MEK could also sensitise cells to AT13148. As with GDC-0994 and SCH772984, low concentrations of PD0325901 were used to alleviate any off-target effects. Most of the PD0325901 concentrations used had been previously shown to inhibit MEK 1/2 in A2780 and 148R-S in Figure 5.2. The effect on cell viability when the PD0325901 concentrations, used in combination, were used as single agents is shown in Table 5.3.

Table 5.3: Effect of PD0325901 on cell viability in A2780 and 148R-S when used as a single agent. Table summarises the effect of PD0325901 on cell viability when used as a single agent at the concentrations used in combination assays with AT13148. Each PD0325901 concentration was plated in triplicate in parallel with combination assays (Figure 5.9) and cell viability was determined in a standard 96-hour SRB cell viability assay. Data points represent the mean ± SD, n ≥ 2 independent experiments.

	Cell viability (%)	
PD0325901 (nM)	A2780	148R-S
1	94.7 ± 1.6	95.0 ± 1.2
5	81.1 ± 19.0	76.9 ± 0.2
10	66.9 ± 14.4	70.2 ± 2.2

Figure 5.9B-D shows that all concentrations of PD0325901 were able to cause a statistically significant sensitisation to AT13148 in 148R-S cells. This was most dramatic when AT13148 was used in combination with 5 nM and 10 nM of PD0325901 (Figure 5.9B-D). Both these concentrations of PD0325901 were able to lower the GI_{50} against AT13148 in 148R-S below that of A2780 (A2780, AT13148 alone GI_{50}: 0.389 µM); 5 nM PD0325901 in combination with AT13148 had a GI_{50} of 0.313 µM and 10 nM PD0325901 a GI_{50} 0.112 µM (Figure 5.9B-D). These GI_{50} values were respectively 10.11 and 28.24-fold lower than the GI_{50} for AT13148 alone in 148R-S: 3.163 µM (Figure 5.9B-D). 1 nM PD0325901 caused a more modest, but statistically significant, 2.51-fold decrease in the GI_{50} of 148R-S against AT13148, which was nonetheless impressive considering the minimal effect on cell viability when 1nM PD0325901 was used as a single agent (Figure 5.9B-D & Table 5.3). A2780 was also sensitised to AT13148 by PD0325901, which whilst to a lesser extent than 148R-S was still considerable, particularly with 5 nM and 10 nM

of PD0325901 (Figure 5.9A). In A2780, combination with 5 nM PD0325901 lowered the GI_{50} against AT13148 by 5.40-fold to 0.072 µM and combination with 10 nM lowered the GI_{50} by 11.79-fold to 0.033 µM, both of which were statistically significant, when compared to AT13148 alone (Figure 5.9C, D). Combination of 1 nM PD0325901 with AT13148 only caused a 1.77-fold decrease in AT13148 GI_{50} in A2780 and was not shown to be statistically significant (Figure 5.9C, D).

To further investigate the sensitisation caused by PD0325901 to AT13148, synergy between the two drugs in combination was determined. In 148R-S, as was seen with SCH772984, there was synergy to all PD0325901 concentrations across a wide range of AT13148 concentrations (Figure 5.9E). Whilst synergy was seen across a broad range of concentrations, the level of synergy was at its greatest when PD0325901 was combined with 0.123 – 1.111 µM AT13148 (Figure 5.9E). The excess above bliss at these concentrations was $0.11 - 0.20$ with 1 nM PD0325901; $0.19 - 0.21$ with 5 nM PD0325901 and $0.22 - 0.25$ with 10nM PD0325901 (Figure 5.9E). This broad range synergy between PD0325901 and AT13148 was also observed in A2780, however the peak in synergy occurred between 0.041 µM and 0.370 µM AT13148 (Figure 5.9E). At these concentrations the excess above Bliss was $0.10 - 0.20$ with 1 nM PD0325901; $0.21 - 0.30$ with 5 nM PD0325901 and $0.19 - 0.26$ with 10 nM PD0325901 (Figure 5.9E).

Taken together, these data show that AT13148 and PD0325901 interact in a synergistic manner in 148R-S and A2780, and that PD0325901 can sensitise 148R-S and A2780 to AT13148. Therefore, in addition to ERK inhibitors, the combination of AT13148 with MEK inhibitors could be a viable therapeutic strategy to overcome AT13148 resistance in the clinic.

D

Combination	A2780		148R-S	
	GI$_{50}$ (μM)	Fold-diff	GI$_{50}$ (μM)	Fold-diff
AT13148 alone	0.389 ± 0.110	N/A	3.163 ± 0.573	N/A
+ 1nM PD0325901	0.220 ± 0.105	1.77	1.258 ± 0.262**	2.51
+ 5nM PD0325901	0.072 ± 0.072*	5.40	0.313 ± 0.136***	10.11
+ 10nM PD0325901	0.033 ± 0.031**	11.79	0.112 ± 0.027**	28.24
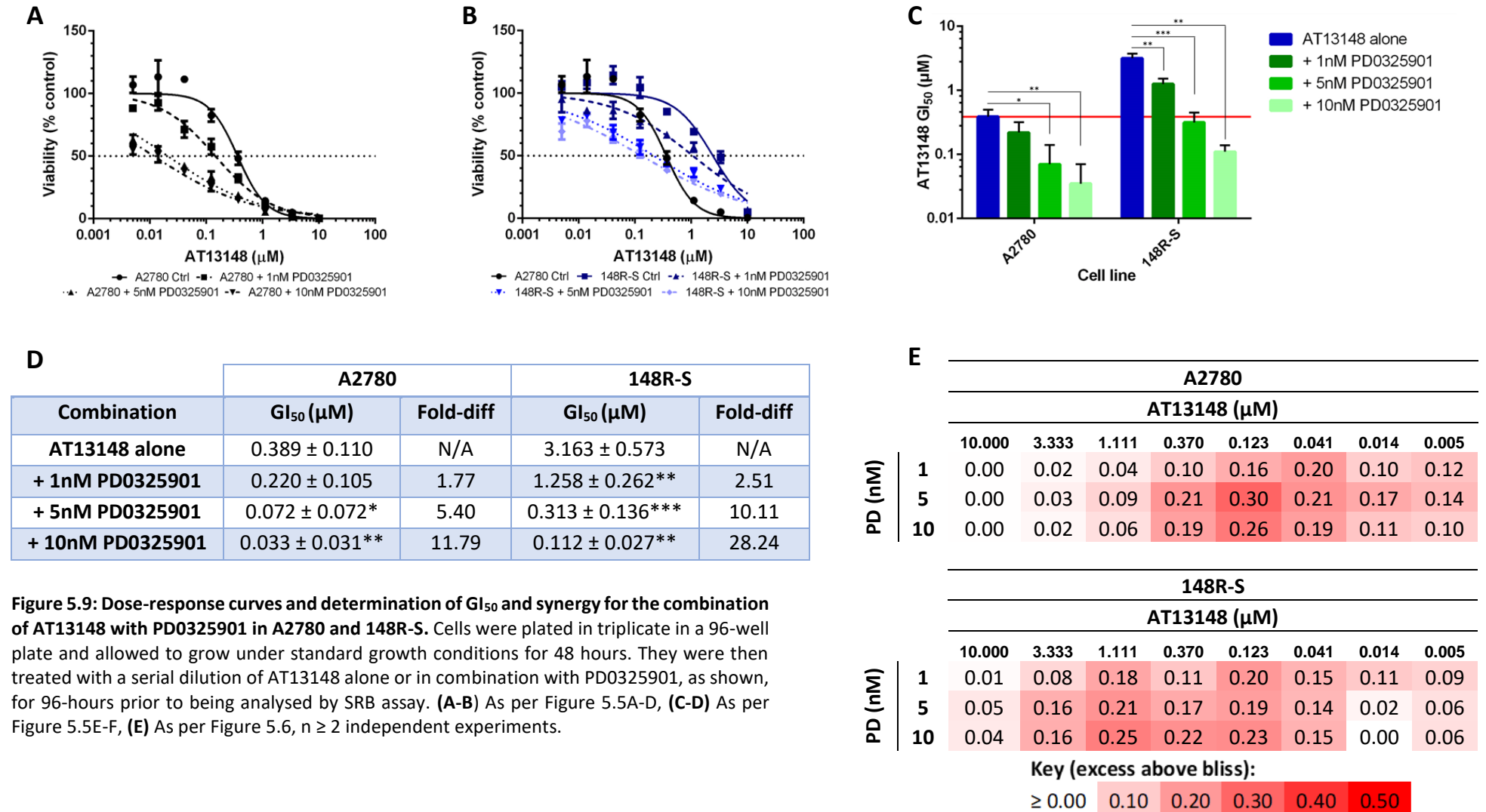
Figure 5.9: Dose-response curves and determination of GI$_{50}$ and synergy for the combination of AT13148 with PD0325901 in A2780 and 148R-S. Cells were plated in triplicate in a 96-well plate and allowed to grow under standard growth conditions for 48 hours. They were then treated with a serial dilution of AT13148 alone or in combination with PD0325901, as shown, for 96-hours prior to being analysed by SRB assay. **(A-B)** As per Figure 5.5A-D, **(C-D)** As per Figure 5.5E-F, **(E)** As per Figure 5.6, n ≥ 2 independent experiments.

E

A2780

AT13148 (μM)

PD (nM)	10.000	3.333	1.111	0.370	0.123	0.041	0.014	0.005
1	0.00	0.02	0.04	0.10	0.16	0.20	0.10	0.12
5	0.00	0.03	0.09	0.21	0.30	0.21	0.17	0.14
10	0.00	0.02	0.06	0.19	0.26	0.19	0.11	0.10

148R-S

AT13148 (μM)

PD (nM)	10.000	3.333	1.111	0.370	0.123	0.041	0.014	0.005
1	0.01	0.08	0.18	0.11	0.20	0.15	0.11	0.09
5	0.05	0.16	0.21	0.17	0.19	0.14	0.02	0.06
10	0.04	0.16	0.25	0.22	0.23	0.15	0.00	0.06

Key (excess above bliss):

≥ 0.00	0.10	0.20	0.30	0.40	0.50

5.3. Discussion

The aim of this chapter was to investigate the contribution of ERK 1/2 to AT13148 resistance. Initially, the response of 148R clones to ERK and MEK inhibition was assessed, as it was thought that increased ERK 1/2 phosphorylation, seen in 148R clones, might correspond with an increased dependency on the MAPK pathway for survival, therefore sensitivity to MAPK pathway inhibitors. It has been shown that an increased MAPK transcriptional signature, which one might expect with increased ERK 1/2 phosphorylation in 148R clones, correlates with increased sensitivity to MAPK pathway inhibition (Wagle *et al.*, 2018). However, despite increased phosphorylation of ERK 1/2, 148R clones did not appear to have an increased dependency on the MAPK pathway for their survival; 148R clones did not display any substantial sensitivity to ERK or MEK inhibition (Figure 5.1A, B). Indeed, 148R-K and 148R-S displayed some cross-resistance to MEK inhibition (Figure 5.1A). Furthermore, it was revealed that ERK 1/2 phosphorylation was refractory to the MEK inhibitor PD0325901 in 148R-K and 148R-S, providing a mechanistic explanation for MEK cross-resistance (Figure 5.2). In 148R-N, which did not display cross-resistance to MEK inhibition, ERK 1/2 phosphorylation was also refractory to PD0325901, albeit to a lesser extent than in 148R-K and 148R-S (Figure 5.2). This perhaps indicates that there is a threshold of ERK 1/2 phosphorylation maintenance, which is required in order to achieve discernible MEK inhibitor cross-resistance in 148R clones (Figure 5.2).

In addition, the maintenance of ERK 1/2 phosphorylation in response to MEK inhibition, provides further evidence that ERK 1/2 phosphorylation has become less dependent upon MEK 1/2 activation. From this we can begin to speculate what might be causing an increase in ERK 1/2 phosphorylation. In general, when there is an increase in the phosphorylation of a protein this can either be caused by an increase in the expression/activation of its kinase, or the loss of expression/activation of its phosphatase. Since MEK 1/2 is the only known kinase responsible for ERK 1/2 phosphorylation and has been shown to have decreased phosphorylation in 148R clones, it would seem likely that the loss of expression/function of an ERK 1/2 phosphatase is responsible for increased ERK 1/2 phosphorylation. One possible

candidate is dual-specificity MAPK phosphatases (MKP's or DUSP's), a subfamily of protein kinases that can de-phosphorylate both the threonine (Thr202) and tyrosine (Tyr204) residues found in the T-X-Y motif of ERK 1/2 (Kidger and Keyse, 2016, mechanism highlighted in Figure 5.10). The expression of DUSP proteins warrants investigation.
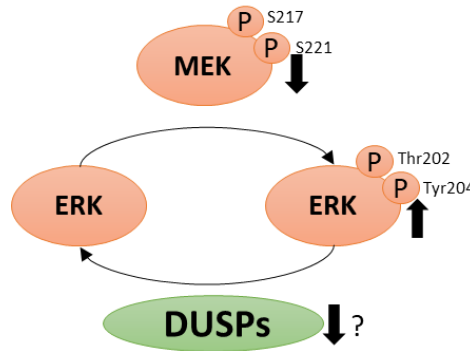
Figure 5.10: Potential mechanism of increased ERK 1/2 phosphorylation in 148R clones. The level of ERK 1/2 phosphorylation is dependent upon the equilibrium between MEK 1/2 activity and the activity of negative regulators such as DUSPs. The loss of expression/function of DUSPs might enable an increase in ERK 1/2 phosphorylation sufficient enough to cause a sustained increase in ERK 1/2 phosphorylation, despite a decrease in MEK 1/2 phosphorylation.

One of the most interesting findings in previous chapters has been the seemingly paradoxical relationship between ERK 1/2 and MEK 1/2 phosphorylation in both A2780-148R and 148R clones; increased ERK 1/2 phosphorylation co-exists with decreased MEK 1/2 phosphorylation (Figure 3.12 & Figure 4.17). A possible explanation for this, that has been proffered in previous chapters, is that MEK 1/2 phosphorylation was decreased due to ERK 1/2 mediated negative feedback. Indeed, the data presented in this chapter has provided evidence of this; the ERK inhibitor GDC-0994 was able to cause a dose-dependent increase in MEK 1/2 phosphorylation in all 148R clones, as well parental A2780 cells (Figure 5.3). This would suggest that the MAPK pathway is under powerful negative feedback control in both A2780 and 148R clones. Therefore, an increase in ERK 1/2 phosphorylation in 148R clones would increase ERK 1/2 mediated negative feedback, reducing the activation of upstream components of the MAPK pathway, such as MEK 1/2 (Figure 5.11A). In contrast, the inhibition of ERK 1/2 in 148R clones relieves negative feedback mediated by increased ERK 1/2 phosphorylation, thus causing an increase in MEK 1/2 phosphorylation (Figure 5.11B).
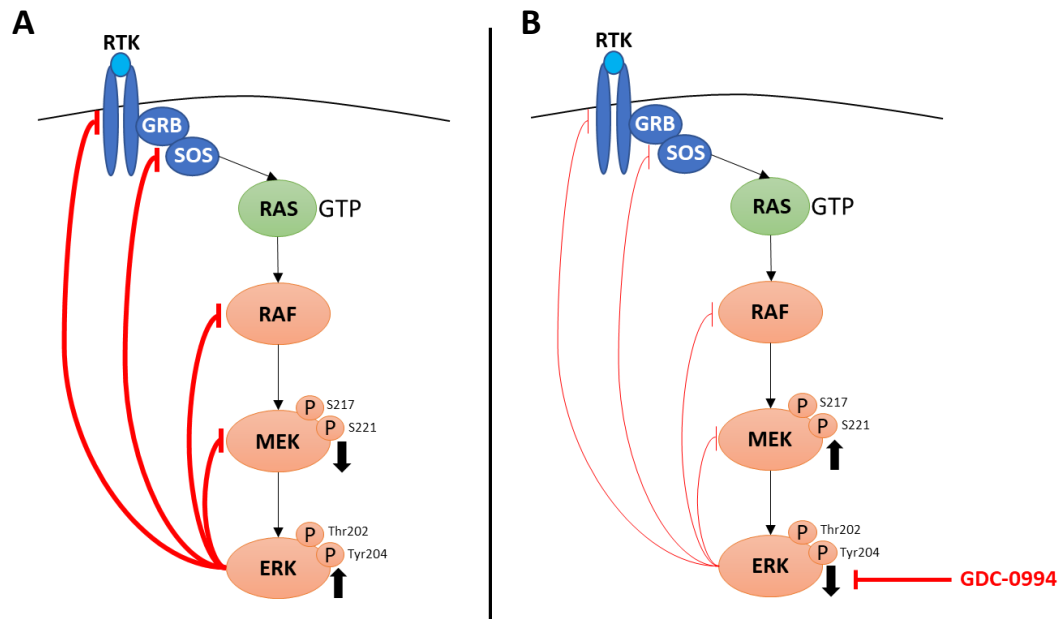
Figure 5.11: ERK 1/2 mediated negative feedback in 148R clones. (A) 148R clones have increased activation of ERK 1/2, which in turn causes an increase in ERK 1/2 mediated negative feedback, decreasing MEK 1/2 phosphorylation. **(B)** When ERK 1/2 is inhibited in 148R clones, by GDC-0994, ERK 1/2 mediated negative feedback is attenuated causing an increase in MEK 1/2 phosphorylation.

Since there is direct evidence that MEK 1/2 phosphorylation was decreased due to ERK 1/2 mediated negative feedback, it is worth considering the mechanisms in which this may occur. For example, Eblen and colleagues (Eblen *et al.*, 2004) demonstrated that ERK2 can directly phosphorylate MEK1 at T292, which whilst not directly effecting MEK 1 activity, prevents the phosphorylation of MEK 1 at S298 by p21 activated kinase (PAK), which is required for required for adhesion-induced MEK1 activation by RAF. However, it not clear whether this ERK-mediated negative feedback applies in other circumstances in which MEK activation is not adhesion-induced, e.g. growth factor stimulation. In addition, BRAF and CRAF are both phosphorylated by ERK 1/2 at multiple sites, which in turn inhibits binding to activate RAS, decreasing the activation of BRAF and CRAF (Dougherty *et al.*, 2005; Ritt *et al.*, 2010). Furthermore, ERK 1/2 can impart inhibitory phosphorylations on several MAPK pathway regulators upstream from RAF and MEK including several RTKs, such as EGFR and FGFR1; the RAS guanine exchange factor (GEF) son of sevenless 1 (SOS1); and adaptor proteins such as FGF receptor substrate 2 (FRS2) (Lake *et al.*, 2016). It should also be noted that ERK 1/2 can mediate negative feedback via the transcriptional induction of several negative feedback regulators, such as sprouty (SPRY) proteins, which can negatively regulate the MAPK pathway at several levels, for example by interacting with CRAF and BRAF and the adaptor proteins growth factor

receptor bound protein 2 (GRB2) and FRS2 (Mason *et al.*, 2006; Lake *et al.*, 2016). In 148R clones, increased ERK 1/2 phosphorylation may induce a decrease in MEK 1/2 phosphorylation by the interaction of several of the aforementioned mechanisms, or one may predominate.

Whilst the use of MAPK pathway inhibitors did help gain some mechanistic insight into the regulation of the MAPK pathway within 148R clones, the lack of sensitivity to inhibitors of the MAPK pathway did create some difficulties in linking increased ERK 1/2 phosphorylation to AT13148 resistance. As discussed, it was initially thought that increased ERK 1/2 phosphorylation may cause increased dependency upon the MAPK pathway for growth and survival, potentially enabling the by-pass of AT13148 targets. The lack of sensitivity to ERK inhibition seemed to suggest that this was not the case. It was also considered that increased ERK 1/2 phosphorylation might drive resistance by maintaining the phosphorylation and activation of constituents of the PAM pathway (e.g. S6RP and PRAS40) in response to AT13148, as was shown in Figure 4.14. This was considered because ERK 1/2 is known to cross-talk with the PAM pathway at multiple levels both directly and indirectly (Mendoza *et al.*, 2011). But if this was the case, one would have expected to have also seen the maintenance of PRAS40 and S6RP phosphorylation in response to AKT inhibition by MK2206 in 148R-S (Figure 4.16). However, 148R clones were also shown to have a dramatic dose-dependent increase in ERK 1/2 phosphorylation in response to AT13148 (Figure 5.4). This was seen to a lesser extent in A2780-148R in chapter 3 in which the potential mechanisms of this response were discussed (Figure 3.13 and section 3.3). This response may in part provide an explanation for the role of ERK 1/2 in AT13148 resistance; the basal increase of ERK 1/2 phosphorylation alone is not sufficient to either by-pass AT13148 targets, or directly compensate for AT13148 inhibition by direct pathway re-activation; but that additional increases in ERK 1/2 phosphorylation caused by AT13148 are, and this drives AT13148 resistance.

To test this hypothesis combination assays were performed with AT13148 and the ERK inhibitor GDC-0994. GDC-0994 was able to re-sensitise 148R-K and 148R-S to AT13148, with the combination shown to be weakly synergistic at several combinations (Figure 5.6 & Figure 5.7). The concentration of GDC-0994 (GI_{20}) that caused the greatest

sensitisation to AT13148 was shown to decrease the phosphorylation of the ERK 1/2 substrate Elk-1 to the same level seen in A2780 in 148R-K, or slightly below in 148R-S (Figure 5.7). This indicated that ERK 1/2 had been sufficiently inhibited, and that ERK 1/2 activation pheno-copied that of A2780. Therefore, the sensitisation to AT13148 caused by GDC-0994 provides evidence that ERK 1/2 is acting as a driver of AT13148 resistance in 148R-K and 148R-S. However, it should be noted that the sensitisation caused by GDC-0994 was incomplete, which could be seen as sensitisation was attenuated it higher concentrations of AT13148. It may be that other changes beyond increased ERK 1/2 phosphorylation also contribute towards AT13148 resistance. Alternatively, this could be caused by the limitations of the experimental set-up, i.e. GDC-0994 may not cause a sustained inhibition of ERK 1/2 over the course of a 6-day SRB assay. Indeed, the phosphorylation of Elk-1 was only assessed over a 4-hour treatment with GDC-0994. Western blot analysis also showed that the combination of AT13148 and GDC-0994 enhanced the loss of S6RP phosphorylation in 148R clones, i.e. combination of GDC-0994 and AT13148 caused a greater decrease in S6RP phosphorylation than AT13148 alone. This, in part, validates the hypothesis suggested earlier that ERK 1/2 contributes to AT13148 resistance by maintaining the phosphorylation of AT13148 targets, as S6RP is a substrate of the AT13148 target p70S6K. Furthermore, in A2780 the combination of AT13148 and GDC-0994 also caused a greater decrease in S6RP phosphorylation than AT13148 alone and sensitised parental A2780 cells to AT13148. This suggests that ERK 1/2 may also contribute to intrinsic AT13148 resistance.

It is worth considering that there are several ways in which ERK 1/2 could contribute towards the maintenance of S6RP phosphorylation in the presence of AT13148. ERK 1/2 can phosphorylate RSK causing its activation, which can in turn directly phosphorylate S6RP at S235/236 (Anjum and Blenis, 2008; Mendoza *et al.*, 2011). Whilst RSK phosphorylation was shown to be decreased at a basal level in Figure 4.17, the increase in ERK 1/2 phosphorylation induced by AT13148 may also cause an increase in RSK phosphorylation, thus maintaining phosphorylation of S6RP in the presence of AT13148 (Figure 5.12). Therefore, the phosphorylation of RSK in response to AT13148 should be investigated. Alternatively, ERK 1/2 can phosphorylate the AKT substrate TSC2 inhibiting its GAP (GTPase activating protein) activity, which increases the abundance of RHEB-GTP

(Ras homolog enriched in brain), an activator of mTORC1 (Mendoza *et al.*, 2011). mTORC1 activates p70S6K (targeted by AT13148) which phosphorylates S6RP, therefore increased ERK 1/2 could lead to an increased activation of p70S6K to the extent in which it was refractory to AT13148 and could maintain S6RP phosphorylation (Figure 5.12). Interestingly, both RSK and p70S6K phosphorylate S6RP at S235/236, but p70S6K can also phosphorylate at S6RP at S240/244 (Mendoza *et al.*, 2011). With this in mind, interrogation of the S240/244 phospho-site may help identify the kinase downstream of ERK 1/2 responsible for the maintenance of S6RP phosphorylation in response to AT13148.
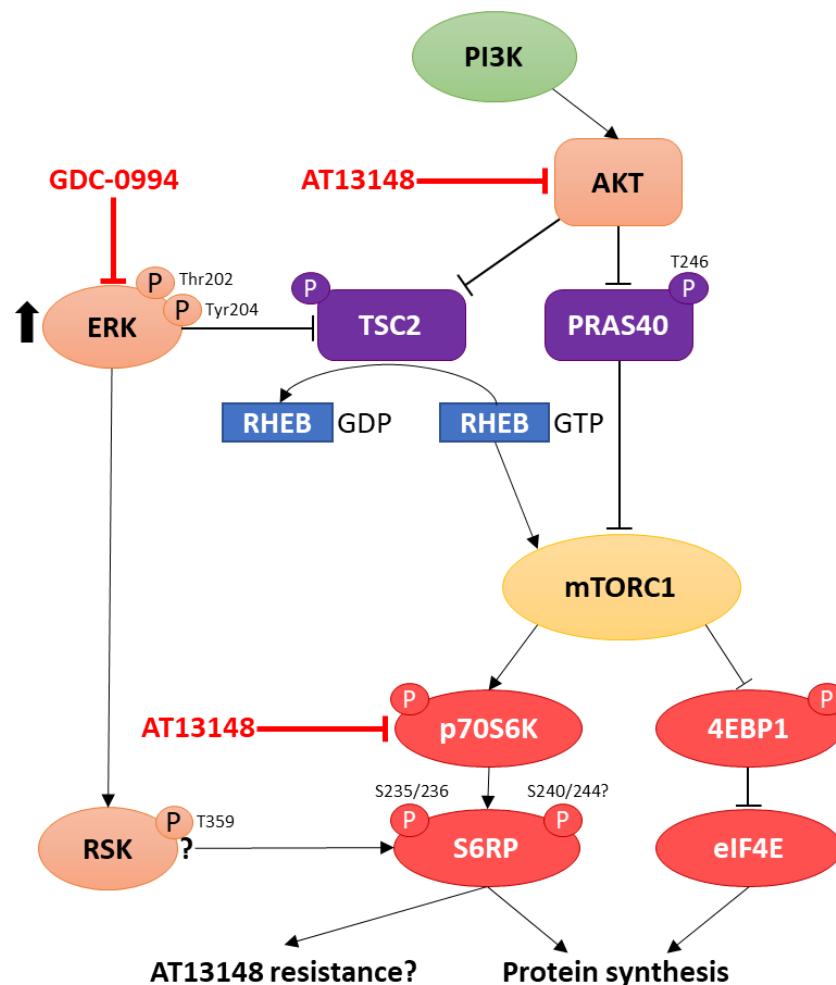
Figure 5.12: Potential mechanisms of ERK 1/2 mediated S6RP phosphorylation and AT13148 resistance in 148R clones. S6RP is refractory to AT13148 in 148R clones but this can be overcome with combined ERK inhibition, which also sensitises 148R clones to AT13148. ERK 1/2 may maintain S6RP phosphorylation via its activation of RSK, which can phosphorylate S6RP at S235/236. Alternatively, ERK 1/2 can impart an inhibitory phosphorylation on TSC2, which in turn, via mTORC1, may increase the activation of p70S6K, overcoming inhibition by AT13148 and maintaining the phosphorylation of S6RP at S235/236 as well as S240/244.

In addition to S6RP, there is extensive crosstalk and convergence between the MAPK and PAM pathways (Mendoza *et al.*, 2011). Therefore, increased ERK 1/2 phosphorylation in 148R-K and 148R-S has the capacity to compensate for the inhibition of the PAM pathway by AT13148 at several levels. For example, both AKT and ERK 1/2 phosphorylate the transcription factor FoXO3a at distinct sites, which either causes its exclusion from the nucleus (AKT mediated phosphorylation) or degradation (ERK 1/2 mediated phosphorylation) (Wang *et al.*, 2017). Both mechanisms act to negatively regulate FoXO3a, preventing its positive regulation of apoptosis and cell cycle arrest (Wang *et al.*, 2017). Thus, inhibition of AKT by AT13148 and subsequent loss of negative regulation of FOXO3a, could be compensated by increased ERK 1/2 activation. Therefore, the effect of the combination of AT13148 and GDC-0994 should be evaluated throughout the PAM pathway, to investigate the ability of ERK 1/2 to compensate for AT13148 mediated inhibition.

In contrast to 148R-K and 148R-S, 148R-N was not sensitised to AT13148 by combination with GDC-0994 (Figure 5.5 & Figure 5.6). This might be caused by the lack of ERK inhibition at the concentrations of GDC-0994 used in 148R-N. This could be seen as the GI_{20} concentration of GDC-0994 was unable to cause a decrease in Elk-1 phosphorylation, an ERK 1/2 substrate, in 148R-N (Figure 5.7). But there are some difficulties in interpreting this data as Elk-1 phosphorylation does not correspond with increased ERK 1/2 phosphorylation in 148R-N and is thus likely to be a poor biomarker of ERK inhibition in 148R-N (Figure 4.17). Indeed, as was seen in 148R-K and 148R-S, in 148R-N the combination of AT13148 and GDC-0994 also enhanced the reduction in S6RP phosphorylation (Figure 5.7). This itself could be a biomarker of ERK inhibition and suggests that ERK 1/2 also has the capacity to maintain the phosphorylation of substrates downstream of AT13148 targets in 148R-N (at least downstream of p70S6K). However, as mentioned, the inhibition of ERK 1/2 is insufficient to sensitise 148R-N to AT13148, despite the effect of the combination on S6RP phosphorylation. It is therefore likely that other mechanisms exist to drive AT13148 resistance in 148R-N in addition to increased ERK 1/2 phosphorylation. The AKT independent mechanism highlighted in Figure 4.19 is a possible candidate.

Whilst ERK 1/2 did not appear to contribute towards AT13148 resistance in 148R-N, the ability of ERK 1/2 to act as a driver of resistance in 148R-S was further validated; 148R-S cells were also sensitised to AT13148 by combination with an additional ERK inhibitor, SCH772984 (Figure 5.8). Together, this meant that two ERK inhibitors, GDC-0994 and SCH772984 had been able to re-sensitise 148R-S to AT13148. Interestingly, SCH772984 preferentially sensitised 148R-S over A2780, and sensitised 148R-S cells to a much greater extent than was seen with GDC-0994, with a greater level of synergy. This was probably due to the different mechanisms of ERK inhibition by GDC-0994 and SCH772984. GDC-0994 acts as a classical type I kinase inhibitor of ERK 1/2, binding to ERK 1/2 in its phosphorylated/active confirmation and functioning in an ATP-competitive manner inhibiting catalytic activity. In contrast, SCH772984 is said to have a 'dual-mechanism' of action; whilst also acting in an ATP-competitive manner inhibiting ERK 1/2 catalytic activity, SCH772984 additionally locks ERK 1/2 in its inactive/unphosphorylated state preventing phosphorylation by MEK 1/2 (Kidger *et al.*, 2018).

Due to the relief of negative feedback inhibition during ERK inhibition, GDC-0994 can induce ERK 1/2 hyperphosphorylation, whilst still retaining its catalytic inhibition (Kidger *et al.*, 2018). Consequently, upon GDC-0994 degradation during the course of a 6-day SRB assay, hyperphosphorylated ERK 1/2 would be primed for re-activation, potentially attenuating its ability to sensitise 148R clones to AT13148 (Kidger *et al.*, 2018). In addition, hyperphosphorylated ERK 1/2, induced by GDC-0994, may accumulate in the nucleus where it can cause cell cycle progression in a kinase independent manner, which may also attenuate the ability of GDC-0994 to sensitise 148R clones to AT13148 (Rodríguez *et al.*, 2010). Since SCH772984 retains ERK 1/2 in its inactive state, inhibition of ERK 1/2 by SCH772984 would neither prime ERK 1/2 for activation nor cause its nuclear accumulation. Therefore, SCH772984 may have increased efficacy as an ERK inhibitor, and thus be better at overcoming ERK 1/2 driven resistance, such as that seen in 148R-S. It would be interesting to investigate if the combination of AT13148 and SCH72984 causes a greater reduction in S6RP phosphorylation than that caused by the combination of GDC-0994 and AT13148. Nonetheless, regardless of mechanism of action, the data presented in this chapter suggests that combination of an ERK inhibitor

with AT13148 could be an effective therapeutic strategy to overcome AT13148 resistance, should it emerge in the clinic.

Interestingly both A2780 and 148R-S were also sensitised to AT13148 by combination with the MEK inhibitor PD0325901 (Figure 5.9). Whilst this was unexpected in 148R-S, due to ERK 1/2 phosphorylation being refractory to MEK inhibition, this is of therapeutic interest, as several MEK inhibitors, such as trametinib and cobimetinib, are currently used clinically (Cheng and Tian, 2017). Since ERK inhibitors have not yet progressed beyond clinical trials, co-targeting MEK 1/2 to overcome AT13148 resistance has more potential as a therapeutic strategy. It would therefore be prudent to investigate if a clinically approved MEK inhibitor could also sensitise 148R clones to AT13148.

In summary, the data in this chapter has implicated ERK 1/2 as a driver of AT13148 resistance in 148R-K and 148R-S. This has been validated using ERK inhibitors, which were shown to act synergistically with AT13148 and sensitise 148R-K and 148R-S to AT13148. However, the exact mechanism of how ERK 1/2 contributes to AT13148 resistance is not fully understood, but ERK 1/2 has been shown to be responsible for the refractory response of S6RP phosphorylation to AT13148 in 148R clones. In contrast, 148R-N lacked sensitisation to AT13148 caused by ERK Inhibition and is likely to have a distinct mechanism of resistance from 148R-K and 148R-S. The mechanism of how ERK 1/2 phosphorylation has been increased in 148R clones would appear to be due to a loss of a negative ERK 1/2 regulator, such as DUSPs, the investigation of which will be focus of the next chapter.

Chapter 6

**Investigation into loss of DUSP6
as a mechanism of AT13148
resistance**

6. Investigation into loss of DUSP6 as a mechanism of AT13148 resistance

6.1. Introduction

The work presented thus far in this thesis implicates increased ERK 1/2 phosphorylation as a driver of acquired resistance to AT13148 in 148R clones (148R-K and 148R-S). This has been validated by combination assays in which inhibition of ERK was shown to re-sensitise 148R-K and 148R-S to AT13148 (Figure 5.5 & Figure 5.8). However, the mechanism(s) by which ERK 1/2 phosphorylation is increased has not been elucidated. As previously discussed, the decrease in MEK 1/2 phosphorylation, suggests that the increase in ERK 1/2 phosphorylation is caused by loss of expression/function of an ERK 1/2 phosphatase. There are several protein phosphatases that are known to de-phosphorylate ERK 1/2 but the most well characterised of these is the dual-specificity MAPK phosphatase (DUSPs or MKP's) sub-family (Keyse, 2000; Lake *et al.*, 2016).

The DUSP sub-family of protein phosphatases is unique among ERK 1/2 phosphatases due to the ability of DUSPs to de-phosphorylate both the threonine (Thr202) and tyrosine (Tyr204) residues of the T-X-Y motif found in the activation loop of ERK 1/2 (Kidger and Keyse, 2016). This motif is also found in the related stress-activated protein kinases, c-Jun amino terminal kinase (JNK) and p38 MAPK, which can also be dephosphorylated by some DUSPs (Kidger and Keyse, 2016). Currently, 10 DUSPs have been identified, which can be categorised into three groups based upon their selectivity and sub-cellular localisation. The 1st group comprises the inducible nuclear DUSPs: DUSP1, DUSP2, DUSP4 and DUSP5; the 2nd, cytoplasmic DUSPs: DUSP6, DUSP7 and DUSP9; and the 3rd contains DUSPs which are specific for stress-activated protein kinases: DUSP8, DUSP10 and DUSP16 (Kidger and Keyse, 2016; Lake *et al.*, 2016). The specificity of nuclear inducible and cytoplasmic DUSPs is varied; some are specific to ERK 1/2 (DUSP5, DUSP6 and DUSP7), whereas others, whilst de-phosphorylating ERK 1/2, can also de-phosphorylate p38 MAPK and JNK (DUSP1, DUSP2, DUSP4 and DUSP9) (Kidger and Keyse, 2016). DUSP6 is a focus of this introduction due to its ERK 1/2

specificity, and association with resistance to several cancer therapies (Kidger and Keyse, 2016).

Figure 6.1 shows the domain structure of DUSP6, similar amongst all DUSPs, consisting of a non-catalytic N-terminal domain and catalytic C-terminal domain, which contains a conserved protein tyrosine phosphatase (PTPase) active site consensus sequence (Kidger and Keyse, 2016). The non-catalytic domain contains a nuclear export sequence (NES), which is responsible for the cytoplasmic localisation of DUSP6, and as such, is also present in other cytoplasmic DUSPs (Dickinson and Keyse, 2006). The non-catalytic domain also contains two regions which have sequence homology with the catalytic domain of cdc25 phosphatases (Dickinson and Keyse, 2006). This is found in all DUSPs and reflects a common evolutionary origin for this domain in the rhodanese family of sulphotransferases (Dickinson and Keyse, 2006). In addition, the non-catalytic domain contains a kinase interaction motif (KIM) which facilitates the binding of DUSP6 to ERK 1/2 (Kidger and Keyse, 2016). Specifically, the KIM contains a D-domain, a domain commonly found on ERK 1/2 binding partners, which binds to the common docking (CD) region of ERK 1/2, a site used by ERK 1/2 to bind its substrates (Yoon and Seger, 2006). This interaction is crucial, since unbound DUSP6 is catalytically inactive but becomes active upon binding ERK 1/2, due an allosteric rearrangement within the active site of its catalytic domain (Kidger and Keyse, 2016). It is this interaction that enables DUSP6 to specifically dephosphorylate ERK 1/2. Interestingly, since DUSP6 can bind both inactive and active ERK 1/2, it has also been shown to act as a cytoplasmic anchor of ERK 1/2 (Karlsson *et al.*, 2004; Kidger and Keyse, 2016).
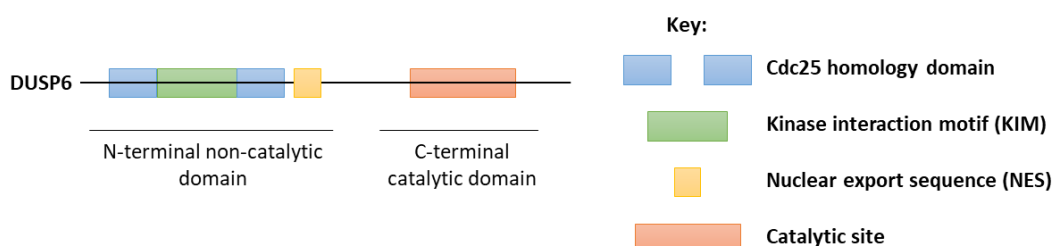
Figure 6.1: Domain structure of DUSP6. Schematic diagram highlighting the domain structure of DUSP6. The C-terminal domain contains a PTPase active site consensus sequence responsible for ERK 1/2 dephosphorylation. The N-terminal non-catalytic domain regulates the cytoplasmic localisation of DUSP6, via NES, and its binding to ERK 1/2, via KIM. Image adapted from Kidger and Keyse, 2016.

The expression of DUSP6 is inducible by ERK 1/2, i.e. activation of ERK 1/2 drives the expression of DUSP6. This is thought to be largely regulated at the transcriptional level by the ERK 1/2 targets ETS-1 and ETS-2 (ETS proto-oncogene 1 & 2), transcription factors of the ETS (E26 transformation specific) family, that are phosphorylated by ERK 1/2 (Yang *et al.*, 1996; Ekerot *et al.*, 2008; Zhang *et al.*, 2010). Upon phosphorylation by ERK 1/2, ETS-1 & 2 bind to transcriptional co-activators, such as CREB binding protein (CBP) or p300, causing an increase in the expression of target genes, such as DUSP6 (Nelson *et al.*, 2010; Tetsu and McCormick, 2017). The ERK 1/2 inducible expression of DUSP6 enables DUSP6 to act as a classical negative feedback regulator of the MAPK pathway (Figure 6.2). In addition, ERK 1/2 has been shown to phosphorylate DUSP6 at two serine sites (S159 and S197) which promotes the proteasomal degradation of DUSP6 (Marchetti *et al.*, 2005). This, in contrast, creates a positive feedback loop between ERK 1/2 and DUSP6; ERK 1/2 activation can decrease DUSP6 expression, which in turn, further increases ERK 1/2 activation (Figure 6.2). This dual regulation of DUSP6 expression by ERK 1/2 enables DUSP6 to finely tune the magnitude and duration of ERK 1/2 activation, although DUSP6 has been predominantly associated as a negative feedback regulator of ERK 1/2 (Kidger and Keyse, 2016).
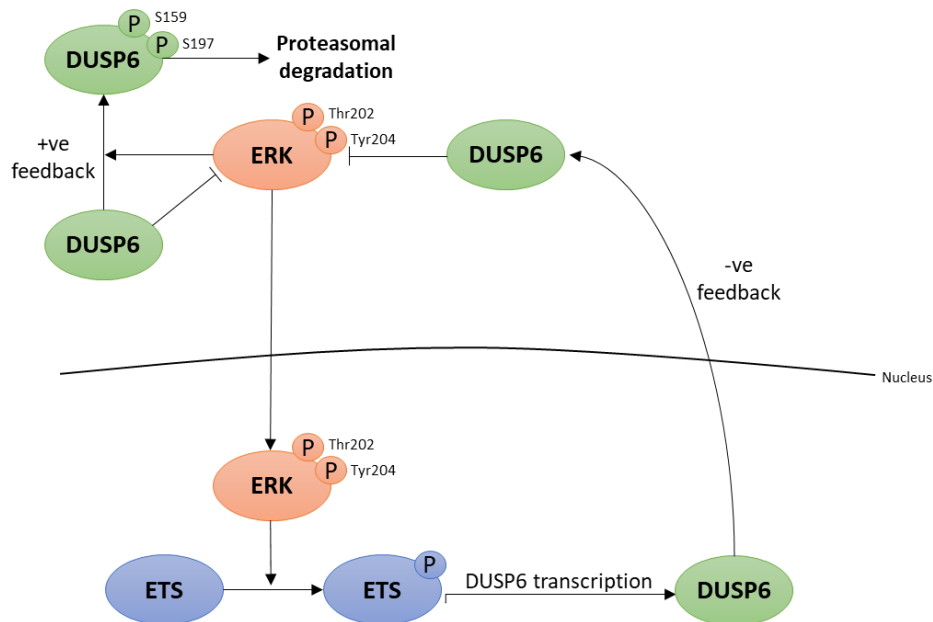
Figure 6.2: ERK 1/2 mediated regulation of DUSP6 expression facilitates positive and negative feedback regulation of ERK 1/2. Upon activation ERK 1/2 can translocate to the nucleus and activate ETS-1 & 2, regulating *DUSP6* transcription. DUSP6 can then translocate to the cytoplasm and dephosphorylate ERK 1/2, thus enabling DUSP6 to act as a classical negative feedback regulator. Alternatively, ERK 1/2 can directly phosphorylate DUSP6, inducing DUSP6 proteasomal degradation, enabling DUSP6 to act as a positive feedback regulator.

As one might expect, due the negative regulation of ERK 1/2 by DUSP6, DUSP6 has often been found to act as a tumour suppressor. Furukawa and colleagues (Furukawa *et al.*, 2003), using immunohistochemistry on patient samples, showed that DUSP6 expression was decreased in advanced/invasive PDAC but increased in primary (in-situ) PDAC tissues, when compared to normal pancreatic tissue. Since the majority of PDAC cells harbour gain-of function *KRAS* mutations, they hypothesised that in primary PDAC tissues the effects of hyperactivated KRAS can be dampened by increased expression of DUSP6 (via ERK 1/2 mediated negative feedback), which in turn decreases ERK 1/2 phosphorylation causing a more attenuated phenotype, thus DUSP6 acts as tumour suppressor (Figure 6.3A). However, in advanced PDAC cells DUSP6 is lost, further increasing ERK 1/2 phosphorylation, enabling a more invasive/aggressive phenotype (Figure 6.3B). Furthermore, they also demonstrated that DUSP6 expression was lost in 7 out of 8 PDAC cell lines tested; the re-expression of DUSP6 in these cell lines led to a decrease in the phosphorylation of ERK 1/2 and induced strong growth suppression and apoptosis, giving further evidence to the role of DUSP6 as a tumour suppressor in PDAC (Furukawa *et al.*, 2003). DUSP6 has also been shown to act in a similar manner (as a tumour suppressor) in *KRAS*-mutant lung cancer, where it has been shown that DUSP6 expression is inversely related to both growth activity and histological grade (Okudela *et al.*, 2009; Kidger and Keyse, 2016).

In contrast, whilst DUSP6 has been shown to act as a tumour suppressor, there is some evidence to suggest that DUSP6 may also function in a pro-oncogenic manner (Kidger and Keyse, 2016). Shojaee and colleagues (Shojaee *et al.*, 2015) showed that the acute activation of oncogenes (BCR-ABL, NRAS[G12D]) induced cell death in the vast majority of human pre-B cells, but that the small fraction of cells that survived, and eventually gave rise to malignant transformation, had high expression of DUSP6 and other negative regulators of the MAPK pathway. Primary samples from patients with pre-B cell acute lymphoblastic leukaemia (ALL) were also shown to have a greater expression of DUSP6 than bone marrow pre-B cells (Shojaee *et al.*, 2015). These data suggested that the high expression of DUSP6 appeared to provide a survival advantage to pre-B cells following oncogenic transformation. Additionally, a potential pro-oncogenic role for DUSP6 has also been identified in melanoma (Wittig-Blaich *et al.*, 2017). Wittig-Blaich and

colleagues (Wittig-Blaich *et al.*, 2017), found that *DUSP6* mRNA expression was consistently elevated in melanoma samples from patients and melanoma cell lines. They hypothesised that high DUSP6 expression may compensate for excessive MAPK pathway activation caused by BRAF V600E in melanoma (Wittig-Blaich *et al.*, 2017). Indeed, it was shown in BRAF V600E melanoma cells, where DUSP6 expression and MAPK activation were high, that DUSP6 KD (knockdown) caused cell death via induction of apoptosis, thus indicating a pro-oncogenic role for DUSP6 (Wittig-Blaich *et al.*, 2017). However, in contrast, in BRAF WT melanoma cells where DUSP6 expression and MAPK pathway activation were lower, it was shown that DUSP6 KD caused either no effect or promoted growth, as would be expected for a tumour suppressor (Wittig-Blaich *et al.*, 2017). This eloquently highlights how DUSP6 can either act in a pro-oncogenic manner or as tumour suppressor in a context dependent fashion.
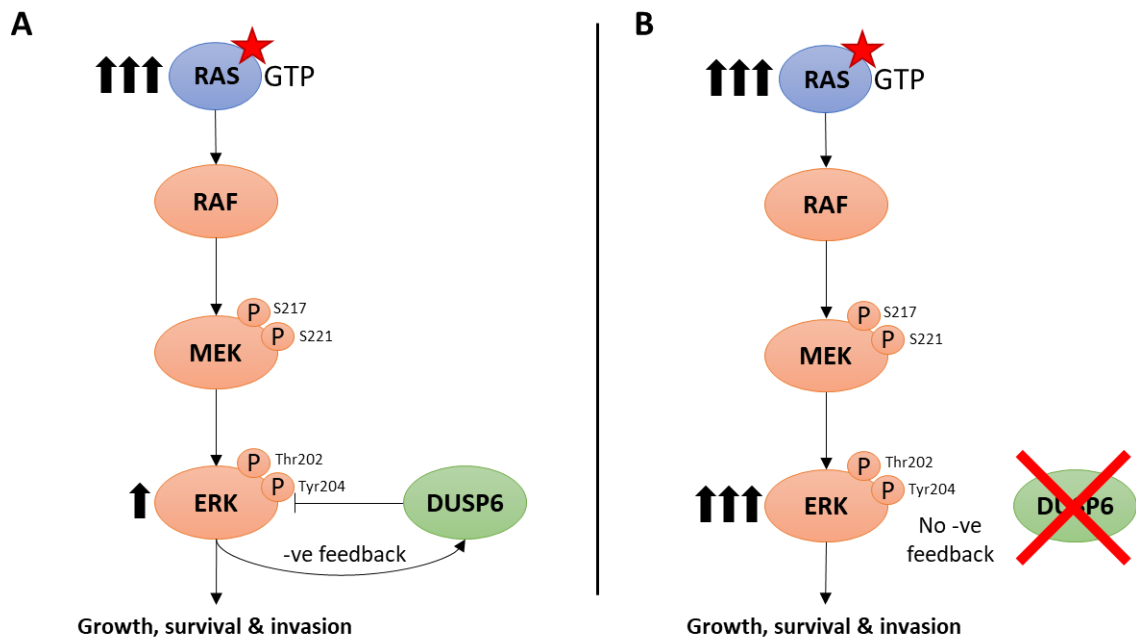
Figure 6.3: DUSP6 acts as tumour suppressor in PDAC. *KRAS* is mutated in the majority PDAC (indicated with red star). **(A)** In primary PDAC tissues this only leads to a slight increase in ERK 1/2 phosphorylation (or no increase at all) due to negative feedback elicited by DUSP6, therefore a less aggressive/invasive phenotype. **(B)** In advanced/invasive PDAC, DUSP6 expression is decreased/lost, which facilitates a greater increase in ERK 1/2 phosphorylation, and therefore a more aggressive/invasive phenotype.

On reflection, the exact role of DUSP6, pro-oncogenic or tumour suppressor, would appear to be determined via the level of ERK 1/2 phosphorylation present within cells. In cells where ERK 1/2 phosphorylation is at low/normal physiological levels (e.g. *BRAF* WT melanoma), DUSP6 acts as a tumour suppressor; the loss of DUSP6 causes an increase in ERK 1/2 phosphorylation to a level in which it can promote oncogenic growth

and survival. However, in cells where ERK 1/2 phosphorylation is high, and already driving oncogenic growth and survival (e.g. *BRAF* V600E melanoma), DUSP6 effectively acts in an oncogenic manner; acting as a buffer to prevent the phosphorylation of ERK 1/2 from reaching a lethal signalling threshold (Unni *et al.*, 2018). In these circumstances, the loss of DUSP6 causes the phosphorylation of ERK 1/2 to go beyond a lethal signalling threshold, thus inducing cell death or senescence (Unni *et al.*, 2018).

Due to the intimate regulation of ERK 1/2 phosphorylation by DUSP6, it is not surprising that DUSP6 has been implicated in resistance to cancer therapies, particularly to tyrosine kinase inhibitor (TKI) therapies (Kidger and Keyse, 2016). In NSCLC, 14% of patients harbour mutations in *EGFR*, however, only 5% of patients achieve tumour reduction > 90% when treated with EGFR TKI's, such as erlotinib (Phuchareon *et al.*, 2015). Phuchareon and colleagues (Phuchareon *et al.*, 2015), investigated the mechanisms of intrinsic EGFR TKI resistance in NSCLC using gefitinib (EGFR TKI) and HCC827, an *EGFR* mutant NSCLC cell line insensitive to EGFR TKI. They identified that whilst gefitinib inhibited ERK 1/2 phosphorylation at 1 hour in HCC827 cells, ERK 1/2 phosphorylation was reactivated after 6-24 hours of gefitinib treatment. They also showed that DUSP6 expression decreased in response to gefitinib treatment and that ectopically expressing DUSP6 in HCC827 cells completely inhibited gefitinib induced ERK 1/2 re-activation. Whilst they didn't investigate if ectopic DUSP6 expression sensitised HCC827 cells to gefitinib, the aforementioned inhibition of gefitinib induced ERK 1/2 re-activation by ectopic DUSP6 expression, suggests that DUSP6 may contribute to intrinsic gefitinib resistance in NSCLC.

The loss of DUSP6 expression has also been implicated in acquired resistance to ALK inhibition in *ALK* fusion-positive (*ALK*[+]) lung adenocarcinoma cells (Hrustanovic *et al.*, 2015). Hrustanovic and collagues (Hrustanovic *et al.*, 2015) generated resistance against the ALK inhibitors crizotinib and ceritinib in the *ALK*[+] cell line H3122. All resistant sub-clones generated were shown to have ERK 1/2 phosphorylation that was refractory to ALK inhibition. Interestingly, two resistant sub-clones were shown to have a marked reduction in the expression of DUSP6, and thus the loss of DUSP6 expression was hypothesised to cause resistance to ALK inhibition. The re-expression of DUSP6 in these sub-clones re-established the inhibition of ERK 1/2 phosphorylation by ALK inhibition,

therefore restoring sensitivity to ALK inhibitors. Conversely, the shRNA (short hairpin RNA) mediated KD of DUSP6 in parental H3122 cells, made ERK 1/2 phosphorylation refractory to ALK inhibition, driving ALK inhibitor resistance. Together, these data showed that loss of DUSP6 expression can drive acquired resistance to ALK inhibition in ALK^+ lung adenocarcinoma cells. This was also validated clinically in patient tumour samples; DUSP6 expression was decreased in post ALK-inhibitor-resistance tumour samples compared to pre-treatment samples. A similar mechanism of resistance has been identified to pazopanib, a TKI that targets several RTK's, in synovial sarcoma (SS) cells (Yokoyama *et al.*, 2017). Yokohama and colleagues (Yokoyama *et al.*, 2017) generated resistance to pazopanib in SS cells and found that ERK 1/2 phosphorylation was refractory to pazopanib in resistant cells. Again, DUSP6 expression was shown to be decreased in resistant cells and DUSP6 KD in parental SS cells was able to recapitulate the resistant phenotype.

In summary, DUSP6 is a critical regulator of ERK 1/2 phosphorylation and loss of expression is associated with therapy resistance. Therefore, the aim of this chapter was to investigate the loss of the expression/function of DUSP6, and other DUSPs, in 148R clones, as a mechanism of increased ERK 1/2 phosphorylation, and thus AT13148 resistance. Initially the expression of several DUSPs was assessed in A2780 and 148R clones using western blotting. The contribution of the altered expression of DUSP6 to AT13148 resistance was subsequently investigated using pharmacological inhibition, siRNA KD and a lentivirus expressing DUSP6.

6.2. Results

6.2.1. Expression of DUSPs in A2780, A2780-148R and 148R clones

The expression of DUSP6 was initially assessed at a basal level in A2780 and 148R clones (K, N & S). Figure 6.4A shows that there was a remarkable loss in the expression of DUSP6 in 148R-K, N & S, when compared to parental A2780 cells. Even with a long hyperfilm exposure (as is shown in Figure 6.4A) only a very faint signal for DUSP6 could be detected in 148R-S, and in 148R-K and 148R-N DUSP6 was undetected (Figure 6.4A). This was in stark contrast to parental A2780 cells, where a strong and robust signal for DUSP6 was detected (Figure 6.4A). Of note, DUSP6 was detected as a doublet, consistent with what has been previously described (Dowd *et al.*, 1998; Zhang *et al.*, 2010). The two bands correspond to two translational products initiating at the first ATG and an internal ATG (Met14)(Dowd *et al.*, 1998; Zhang *et al.*, 2010). The phosphorylation of Thr202/Tyr204 ERK 1/2 was increased in 148R-N, K & S, consistent with what was previously described in chapter 4 (Figure 6.4A & Figure 4.17).

In addition, the expression of DUSP4 and DUSP5 was also assessed, as they both dephosphorylate ERK 1/2 and have been associated with resistance to cancer therapies (Menyhart *et al.*, 2017; Liu *et al.*, 2018). In contrast to DUSP6, DUSP4 and DUSP5 did not show any substantial difference in expression amongst A2780 and 148R clones, but DUSP5 did appear slightly increased in 148R-S, when compared to parental A2780 cells (Figure 6.4A). DUSP5 was also detected as a doublet, again, this was consistent with previous results, and is thought to be caused by ERK 1/2 dependent phosphorylation of DUSP5 causing a gel mobility shift (Kucharska *et al.*, 2009).

Since DUSP6 expression was shown to be downregulated in 148R-K, N and S (clones that were selected for further characterisation in chapter 4), the expression of DUSP6 was also evaluated in A2780-148R. Interestingly, DUSP6 was shown to be downregulated in A2780-148R, but to a much lesser extent than was seen in 148R-K, N, and S (Figure 6.4B). Figure 6.4B also shows the expression of DUSP6 in 148R-J and 148R-P (two clones not selected for further characterisation in chapter 4). Whilst DUSP6 was decreased in 148R-P, to a similar extent as in 148R-K, N & S, DUSP6 expression was unchanged in 148R-J (Figure 6.4A, B).

Taken together, these data show that there was a loss of DUSP6 expression in 148R-K, 148R-N and 148R-S, compared to parental A2780 cells. This warrants further investigation into the contribution of DUSP6 loss to increased ERK 1/2 phosphorylation and thus AT13148 resistance in 148R clones.
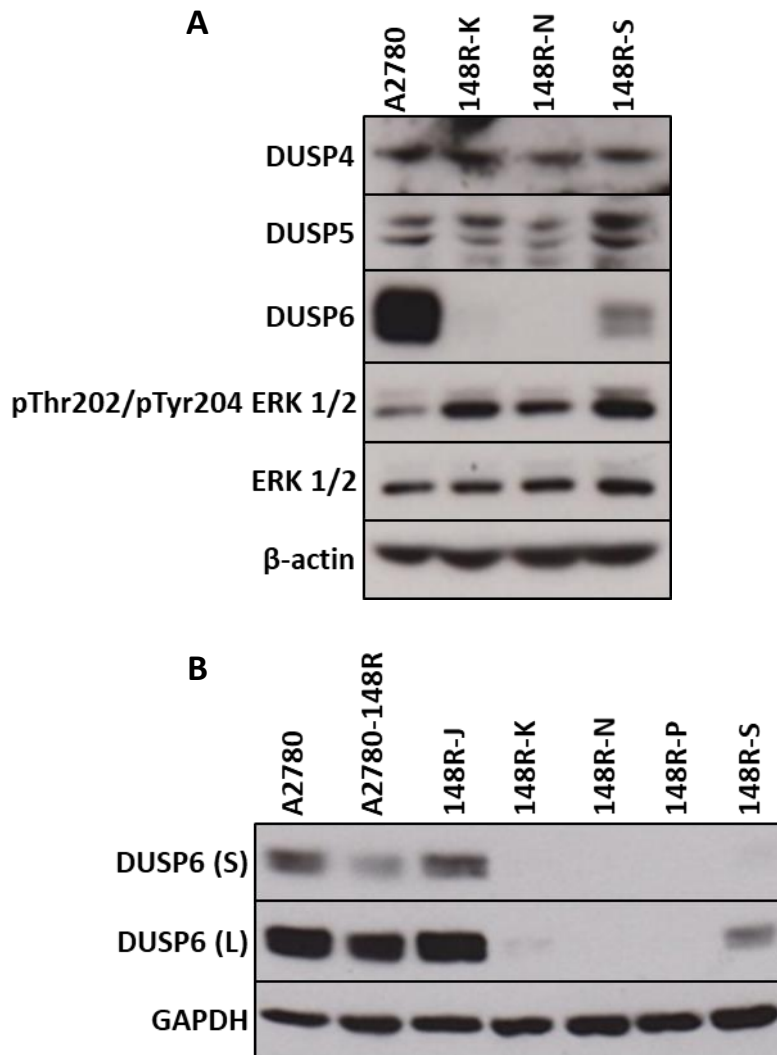
Figure 6.4: Expression of DUSPs in A2780, A2780-148R and 148R clones. (A, B) Cells were plated at either 5 x 10^5 (A2780) or 7.5 x 10^5 (A2780-148R & 148R clones) cells per 7 cm dish and allowed to grow for 48 hours under standard growth conditions. Cells were then lysed prior to western blot analysis. Western blot membranes were probed with antibodies for phospho-proteins, stripped, and then re-probed with antibodies for total proteins and loading control (β-Actin or GAPDH). Data are representative of ≥ 3 independent experiments.

6.2.2. Response of DUSP6 expression to AT13148 in A2780 and 148R clones

The expression of DUSP6 in A2780, 148R-N and 148R-S, was also evaluated in response to AT13148. Figure 6.5 shows that AT13148 did not alter the expression of DUSP6 in parental A2780 cells. The effect of AT13148 on DUSP6 expression in 148R-N could not be determined as DUSP6 was undetected, despite a prolonged hyperfilm exposure (as shown by the over-exposed DUSP6 signal for A2780, Figure 6.5). In 148R-S, there did appear to be some response in the expression of DUSP6 to AT13148; 1 μM was able to cause a slight reduction in the expression of DUSP6, however, DUSP6 expression was unchaged with 0.1 μM and 10 μM AT13148 (Figure 6.5). Taken together, DUSP6 expression did not exhibit a significant response to AT13148 in either A2780 or 148R clones.
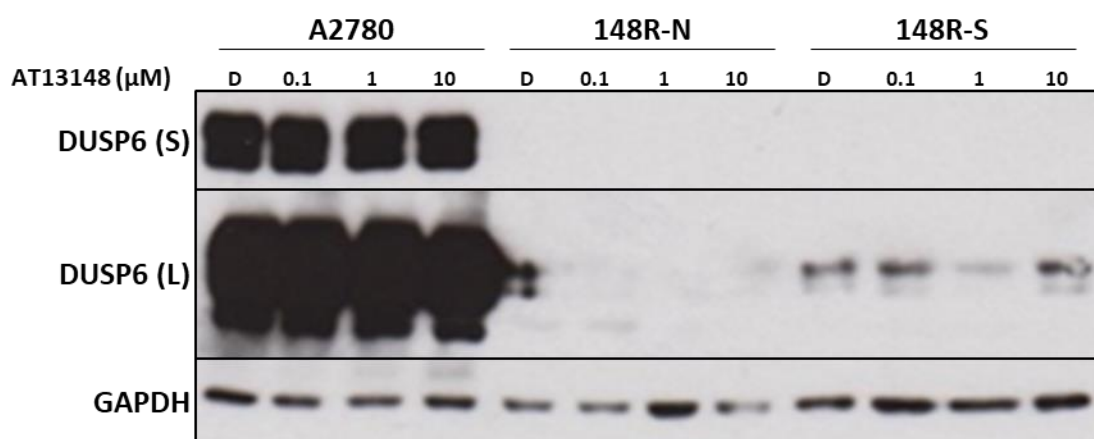
Figure 6.5: Response of DUSP6 expression to AT13148 in A2780 and 148R clones. Cells were plated at either 5×10^5 (A2780) or 7.5×10^5 (148R clones) cells per 7 cm dish and allowed to grow for 48 hours under standard growth conditions. Cells were then treated with AT13148, at the concentrations shown, or D: DMSO vehicle control for 4 hours prior to being lysed for western blot analysis. Western blot membranes were probed with an antibody for DUSP6, stripped, and then re-probed with loading control antibody (GAPDH). (S): short exposure to hyperfilm, (L): long exposure to hyperfilm. Data are representative of two independent experiments

6.2.3. The effect of DUSP6 inhibition on ERK 1/2 phosphorylation and AT13148 resistance

6.2.3.1. Response of ERK 1/2 phosphorylation to BCI in A2780

As previously mentioned, loss of DUSP6 in 148R clones may contribute to the increase seen in ERK 1/2 phosphorylation (Figure 6.4). To investigate this, the effects of BCI (2-benzylidene-3-(cyclohexylamino)-1-indanone hydrochloride), a small molecule allosteric inhibitor of DUSP6, which also has activity against DUSP1, were initially examined on ERK 1/2 phosphorylation in parental A2780 cells (Molina *et al.*, 2009). These cells were treated with 0.01 μM – 1.00 μM of BCI for 4 hours, and western blots conducted to assess ERK 1/2 phosphorylation, compared to a 148R-S untreated sample.

Figure 6.6 shows that BCI caused a dose-dependent increase in the phosphorylation of Thr202/Tyr204 ERK 1/2. However, an exception to this was 0.05 μM BCI which unexpectedly caused a decrease in ERK 1/2 Thr202/Tyr204 phosphorylation (Figure 6.6). Interestingly, at 1 μM BCI the level of Thr202/Tyr204 ERK 1/2 phosphorylation, in parental A2780 cells, was approximately equal to that of the 148R-S untreated control (Figure 6.6). Total ERK 1/2 expression was consistent across all BCI concentrations and the DMSO vehicle control in A2780 but did appear to be lower in the 148R-S untreated control (Figure 6.6). Together, these data show that inhibition of DUSP6 (and DUSP1), by BCI, was able to recapitulate the increase in ERK 1/2 phosphorylation seen in 148R-S and other 148R clones. This provided evidence of a link between DUSP6 loss in 148R clones and increased ERK 1/2 phosphorylation.
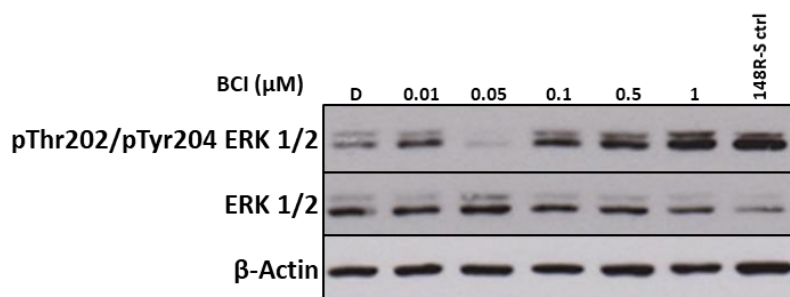
Figure 6.6: The effect of BCI on ERK 1/2 phosphorylation in A2780 cells. Cells were plated at either 5 x 10^5 (A2780) or 7.5 x 10^5 (148R-S) cells per 7 cm dish and allowed to grow for 48 hours under standard growth conditions. Cells were then treated with BCI, at the concentrations shown, or D: DMSO vehicle control for 4 hours prior to being lysed for western blot analysis. 148R-S ctrl was also treated with DMSO vehicle control. Western blot membranes were probed with antibodies for phospho-proteins, stripped, and then re-probed with antibodies for total proteins or loading control (β-Actin). Data are representative of four independent experiments.

6.2.3.2. *Response of A2780 and 148R clones to BCI*

The loss of DUSP6 may have affected how 148R clones responded to BCI. Therefore, the response of A2780 and 148R clones to BCI was assessed over the course of a standard 6-day SRB cell viability assay. Figure 6.7 shows that A2780 had GI_{50} of 0.76 μM against BCI, but that 148R-K and 148R-N had GI_{50} values of 1.14 μM and 1.50 μM, respectively (Figure 6.7). This equated to an RF value of 1.50 for 148R-K and 1.97 for 148R-N, indicating slight cross-resistance to BCI, but this was only statistically significant in 148R-K (Figure 6.7). In contrast, 148R-S had a GI_{50} against BCI of 0.50 μM, which was lower than that of A2780, representing an RF value of 0.66, but this was not statistically significant (Figure 6.7). In summary, these data do not show any substantial difference in response to BCI between 148R clones and the parental A2780 cell line.
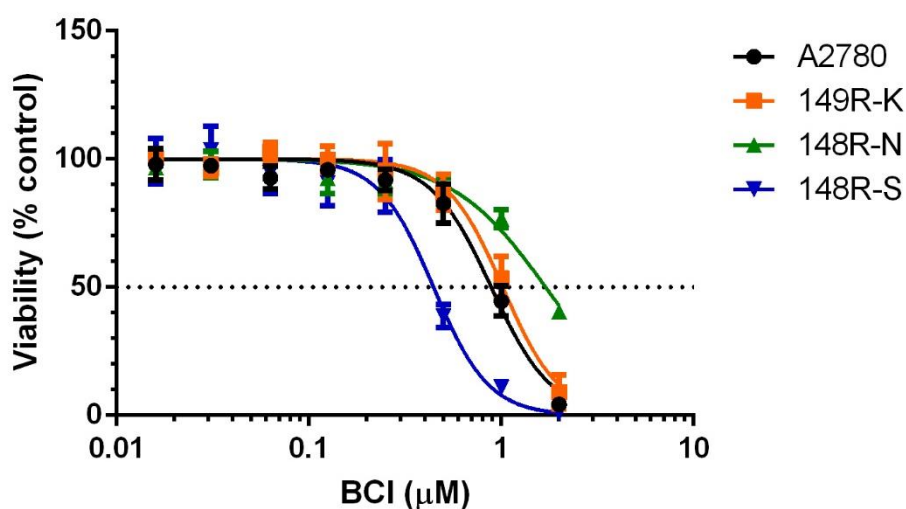
	BCI	
Cell line	**GI_{50} (μM)**	**RF**
A2780	0.76 ± 0.24	N/A
148R-K	1.14 ± 0.12*	1.50
148R-N	1.50 ± 0.41	1.97
148R-S	0.50 ± 0.09	0.66

Figure 6.7: Dose-response curves and GI_{50} determinations for BCI in A2780 and 148R clones. Cells were plated in triplicate in a 96-well plate and allowed to grow under standard growth conditions for 48 hours. Cells were then treated with a serial dilution of BCI for 96-hours, prior to being analysed by SRB assay. Dose-response graphs and non-linear regression curve fits were generated using GraphPad Prism 6. Dotted line marks 50% viability on the y-axis. Data points represent the mean ± SD from one representative experiment. Table summarises GI_{50} and RF values; GI_{50} data points represent the mean ± SD of all experiments conducted. Statistical significance was calculated using a student's t-test, * *p ≤ 0.05*, n ≥ 4 independent experiments.

6.2.3.3. Response of A2780 cells to the combination of AT13148 and BCI

Since BCI was able to cause an increase in ERK 1/2 phosphorylation in A2780, it was thought that BCI could mimic the loss of DUSP6 seen in 148R clones and therefore be used as a tool to validate DUSP6 loss as a mechanism of AT13148 resistance. To this end, A2780 cells were treated with a combination of AT13148 and BCI over the course of a standard 6-day SRB cell viability assay, to investigate if inhibition of DUSP6 by BCI could induce resistance to AT13148. The concentrations of BCI that were used in combination with AT13148 were selected as they had been shown to increase the phosphorylation of ERK 1/2 and have minimal toxicity (Figure 6.6 & Figure 6.7).

Figure 6.7 shows the response of A2780 cells to the combination of AT13148 and BCI. As expected, BCI had a minimal effect on cell viability when used as a single agent at concentrations used in combination with AT13148; respectively, cell viability was 104.7% and 93.8% for 0.01 μM and 0.10 μM BCI (Figure 6.8). However, the combination did not seem to greatly affect the response to AT13148; the GI_{50} against AT13148 alone was 0.20 μM compared to 0.17 μM when used in combination with 0.01 μM BCI and 0.14 μM in combination with 0.10 μM BCI. Contrary to what was anticipated, this represented a 1.18 and 1.43-fold decrease in AT13148 GI_{50}, when AT13148 was combined with 0.01 μM and 0.10 μM BCI respectively (Figure 6.8). This was not shown to be statistically significant (Figure 6.8). Taken together, these data show that the combination of BCI with AT13148 in parental A2780 cells does not recapitulate the resistance to AT13148 seen in 148R clones. Due to the limitations of the use of BCI to mimic DUSP6 loss in A2780 (e.g. co-inhibition of DUSP1), the loss of DUSP6 as a mechanism of AT13148 resistance was further examined using alternative techniques.

Combination	Viability (%)	GI$_{50}$ (µM)	Fold-diff
AT13148 alone	N/A	0.20 ± 0.04	N/A
+ 0.01 µM BCI	104.7 ± 1.1	0.17 ± 0.02	1.18
+ 0.10 µM BCI	93.8 ± 3.3	0.14 ± 0.04	1.43
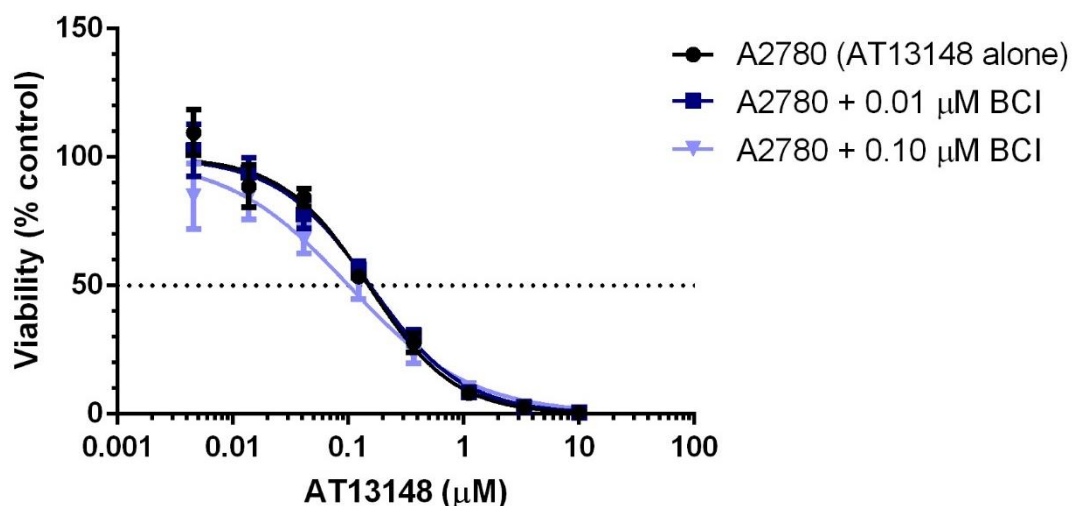
Figure 6.8: Dose-response curve and GI$_{50}$ determinations for the combination of AT13148 and BCI in A2780. Cells were plated in triplicate in a 96-well plate and allowed to grow under standard growth conditions for 48 hours. They were then treated with single agent BCI or a serial dilution of AT13148 alone, or in combination with BCI, for 96-hours, prior to being analysed by SRB assay. Dose-response graph and non-linear regression curve fits were generated using GraphPad Prism 6. Dotted line marks 50% viability on the y-axis. Data points represent the mean ± SD from one representative experiment. Table summarises GI$_{50}$, fold-difference (fold-diff) and % viability for single agent BCI. GI$_{50}$ and viability data points represent the mean ± SD of all experiments conducted. Statistical significance was calculated using a student's t-test, n ≥ 2 independent experiments.

6.2.4. Investigation of DUSP6 loss as a mechanism of resistance using RNA interference

RNA interference has been used previously to successfully validate loss of DUSP6 as a mechanism of resistance to pazopanib and ALK inhibitors in synovial sarcoma and ALK[+] lung adenocarcinoma respectively (Hrustanovic *et al.*, 2015; Yokoyama *et al.*, 2017). Therefore, loss of DUSP6 alone, as a mechanism of resistance to AT13148, was investigated using siRNA mediated KD of DUSP6 expression. To this end, DUSP6 siRNA KD was performed in A2780 parental cells, to see if the phenotype in 148R clones could be recapitulated; increased phosphorylation of ERK 1/2 and resistance to AT13148.

6.2.4.1. Optimisation of siRNA transfection conditions

Initially, siRNA transfection conditions were optimised for the use of Lipofectamine 2000, a cationic lipid-based transfection reagent, to identify those that enabled the greatest transfection efficiency and lowest transfection reagent toxicity. Briefly, A2780 cells were plated at 5,000 – 10,000 cells per well in a 96-well plate and reverse transfected with 0.05 – 0.20% Lipofectamine 2000 combined with non-targeting siRNA (NT) or death control siRNA (a pooled blend of siRNA's that target genes essential for cell survival). A mock transfection control was also used which just contained Lipofectamine 2000 and no siRNA. Mock and NT were used to assess transfection reagent toxicity, and death control siRNA was used to assess transfection efficiency. After reverse transfection, cells were left to grow in standard growth conditions for 4-days and cell viability assessed by SRB assay.

Figure 6.9A shows that death control siRNA reduced cell viability in a Lipofectamine 2000 concentration dependent manner at all cell densities. This indicated that Lipofectamine 2000 was able to successfully transfect siRNA into A2780 cells. The concentration of death control siRNA used (either 5 nM or 25 nM), did not appear to cause a great difference in the reduction of cell viability (Figure 6.9A). However, the mock and NT controls also caused a concentration dependent reduction in cell viability, indicating that there was some transfection reagent toxicity (Figure 6.9A). Both transfection efficiency and transfection reagent toxicity were also affected by cell density; the higher the cell density the more Lipofectamine 2000 needed for transfection efficiency and

transfection reagent toxicity (Figure 6.9A). Taking all these factors into account it was determined that 0.15% Lipofectamine 2000 and plating density of 10,000 cells/well were optimal for siRNA transfection in parental A2780 cells (Figure 6.9A). Under these conditions there was the greatest window between transfection efficiency and transfection reagent toxicity. In addition, growth characterisation assays were performed, which demonstrated that parental A2780 cells were in log-phase over the course of a 4-day SRB cell viability assay when plated at 10,000 cells/well (Figure 6.9B).

A

B
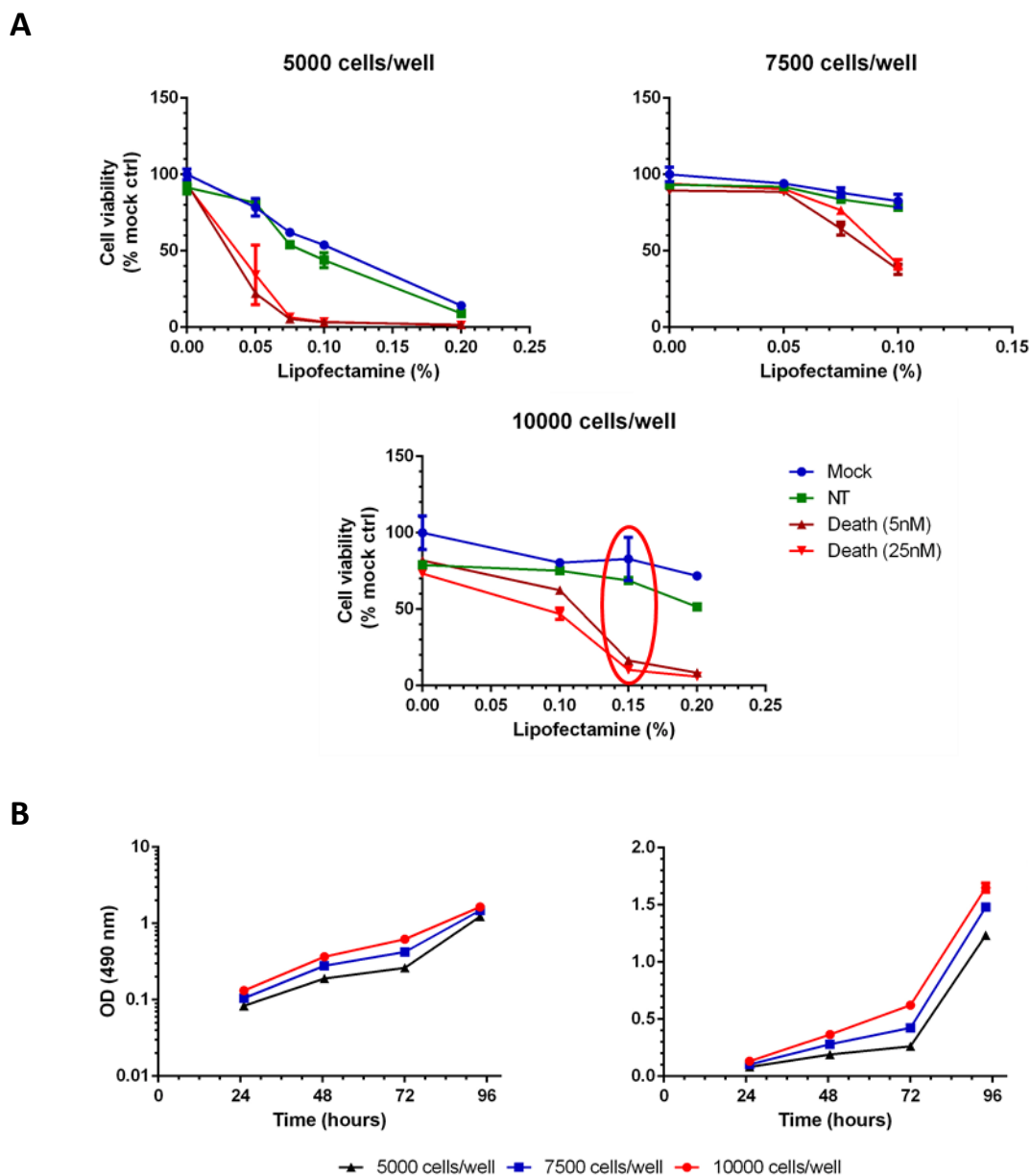
Figure 6.9: Optimisation of Lipofectamine 2000 siRNA transfection in A2780 cells. (A) A2780 cells were reverse transfected in duplicate, at the plating densities shown, with Lipofectamine 2000, at the concentrations indicated, in a total volume of 160 µl/well in a 96-well plate. This was either alone (mock), with 25 nM non-targeting Allstars negative control siRNA (NT) or Allstars cell death control siRNA (Death, 5 nM or 25nM). Cells were then incubated for 24 hours under standard growth conditions, prior to the addition of 40 µl/well of complete DMEM, followed by an additional 72 hours of incubation under standard growth conditions. Cells were then analysed by an SRB assay. Graphs were generated using GraphPad Prism 6, data points on graphs represent the mean ± SD from one representative experiment and are normalised to mock untransfected (0% lipofectamine 2000) control. Data points highlighted in red indicate the optimal transfection conditions identified. n ≥ 2 independent experiments. **(B)** Growth characterisation assays were performed as described in Figure 3.1 & Figure 4.8, over 4-days. n = 1

6.2.4.2. Knockdown of DUSP6 using pooled DUSP6 siRNA

After the optimal siRNA transfection conditions were identified, DUSP6 siRNA KD was performed in parental A2780 cells to investigate if loss of DUSP6 alone could act as mechanism of resistance to AT13148. Initially, this was performed using pooled DUSP6 siRNA, which contained 4 siRNA duplexes targeting DUSP6 mRNA at distinct sites. Since siRNA KD is transient, and therefore lost over time, an adapted 4-day SRB cell viability assay was performed to maximise the time in which DUSP6 expression would be decreased. Briefly, parental A2780 cells were reverse transfected with DUSP6 siRNA (and controls) in a 96-well plate, left to incubate for 24 hours prior to the addition of a serial dilution of AT13148. They were than left to incubate for a further 72 hours prior to analysis via an SRB assay. In parallel to this, A2780 cells were reverse transfected with DUSP6 siRNA (and transfection controls) in 6-well plates, using conditions appropriately scaled from Figure 6.9. These were then lysed for western blot analysis, in order to monitor the expression of DUSP6 and phosphorylation of ERK 1/2 over the time course of a 4-day SRB cell viability assay.

Figure 6.10 shows that all concentrations of pooled DUSP6 siRNA caused a decrease in the expression of DUSP6 across all timepoints, when compared to transfection controls (untransfected, mock and NT), i.e. pooled DUSP6 siRNA caused KD of DUSP6. The level of DUSP6 KD seemed to peak at 24 hours (which corresponds to when AT13148 was added in 4-day SRB cell viability assay), followed a slight decrease at 48 hours (Figure 6.10). Whilst there was still some noticeable DUSP6 KD at 96 hours (which corresponds to the end of a 4-day SRB cell viability assay), this was to a much lesser extent than was seen at 24 and 48 hours (Figure 6.10). The level of DUSP6 KD was not particularly affected by the concentration of pooled DUSP6 siRNA (5, 10 & 25 nM), but 25 nM did cause a greater level of DUSP6 KD at 48 hours and 96 hours (Figure 6.10). Of note, even when DUSP6 KD was at its greatest, at 24 hours with 10 or 25 nM pooled DUSP6 siRNA, the expression of DUSP6 was still above that of the 148R-K control (Figure 6.10). However, this should be interpreted with some caution, as the 148R-K control was obtained from a previous experiment, and thus would have been grown under different conditions.

The level of ERK 1/2 phosphorylation appeared to correlate with the level of DUSP6 KD (Figure 6.10). At 24 hours, where DUSP6 KD was at its greatest, there was a small, but notable increase in Thr202/Tyr204 ERK 1/2 phosphorylation, when compared to transfection controls (Figure 6.10). In addition, at 24 hours, 25 nM pooled DUSP6 siRNA appeared to cause a slightly greater increase in ERK 1/2 phosphorylation, when compared to 5 or 10 nM pooled DUSP6 siRNA (Figure 6.10). This increase in Thr202/Tyr204 ERK 1/2 phosphorylation was not seen at 48 hours and 96 hours, possibly due to the decrease in the level of DUSP6 KD seen at these timepoints (Figure 6.10). It should be noted, that at 96 hours, ERK 1/2 phosphorylation was inconsistent amongst siRNA controls, making it difficult to determine if ERK 1/2 phosphorylation was altered in response to pooled DUSP6 siRNA (Figure 6.10). The total expression of ERK 1/2 was consistent within each timepoint, across all transfection controls and concentrations of pooled DUSP6 siRNA (Figure 6.10).
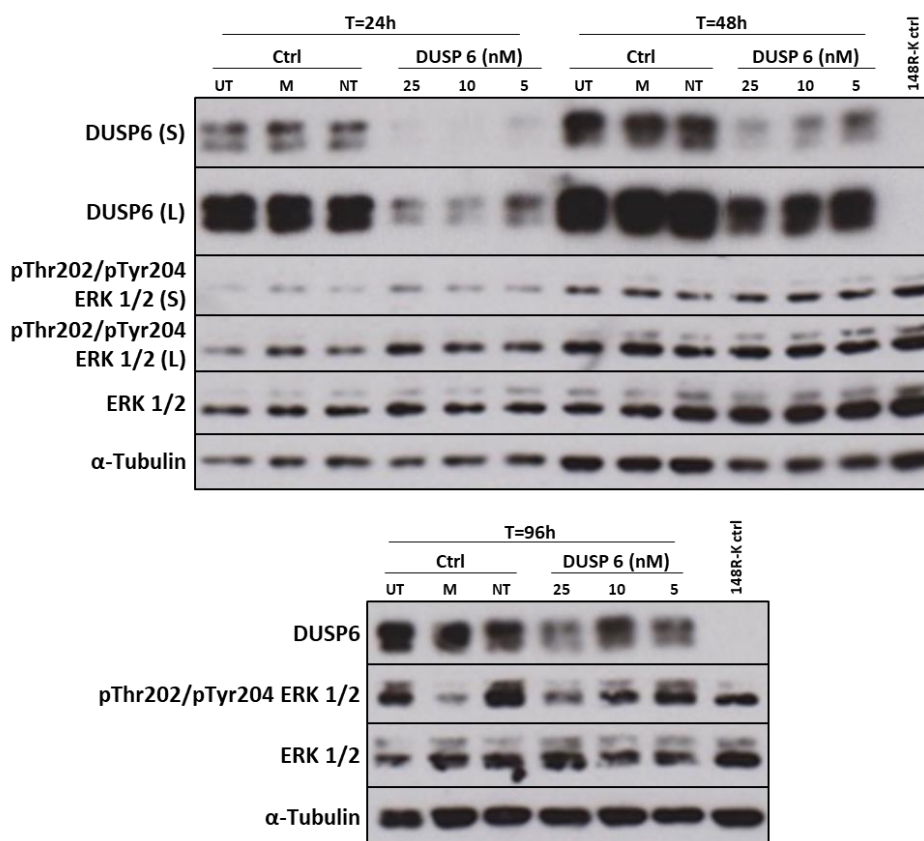
Figure 6.10: Knockdown of DUSP6 in A2780 cells using pooled DUSP6 siRNA. A2780 cells were reverse transfected in 6-well plates, at 1×10^5 cells/well, with 0.15% Lipofectamine 2000 and pooled DUSP6 siRNA, at the concentrations indicated, or 25 nM non-targeting Allstars negative control siRNA (NT). Cells were then incubated under standard growth conditions for 24, 48 or 96 hours prior to lysis and western blot analysis, alongside a 148R-K lysate from a previous experiment, as described in Figure 6.4. UT: un-transfected, M: mock transfected. Data are representative of 2 independent experiments

Figure 6.11 shows the effect of pooled DUSP6 siRNA KD on the sensitivity to AT13148 in parental A2780 cells, over the course of a 4-day SRB cell viability assay. As previously mentioned, this was to determine if loss of DUSP6 expression could act as mechanism of resistance to AT13148. The KD of DUSP6 using pooled DUSP6 siRNA was unable to induce resistance to AT13148 in parental A2780 cells (Figure 6.11A, B, D). The GI_{50} against AT13148 for pooled DUSP6 siRNA KD was 0.28 µM, which was near identical to the GI_{50} for mock transfection and NT siRNA, 0.30 µM and 0.25 µM respectively (Figure 6.11A, B, D). This equated to an RF value of 0.93, which was not statistically significant (Figure 6.11A, B, D). In addition, pooled DUSP6 siRNA did not affect the viability of untreated parental A2780 cells; the viability for parental A2780 cells transfected with pooled DUSP6 siRNA was 102.5% (Figure 6.11C, D).

Taken together, these data (Figure 6.10 & Figure 6.11) show that that KD of DUSP6 using pooled DUSP6 siRNA was unable to recapitulate the phenotype seen in 148R clones: sustained increase in ERK 1/2 phosphorylation and AT13148 resistance. However, the strength and duration of DUSP6 KD caused by pooled DUSP6 siRNA did not match what was seen in 148R clones and may explain why pooled DUSP6 siRNA did not recapitulate the resistance phenotype in parental A2780 cells.
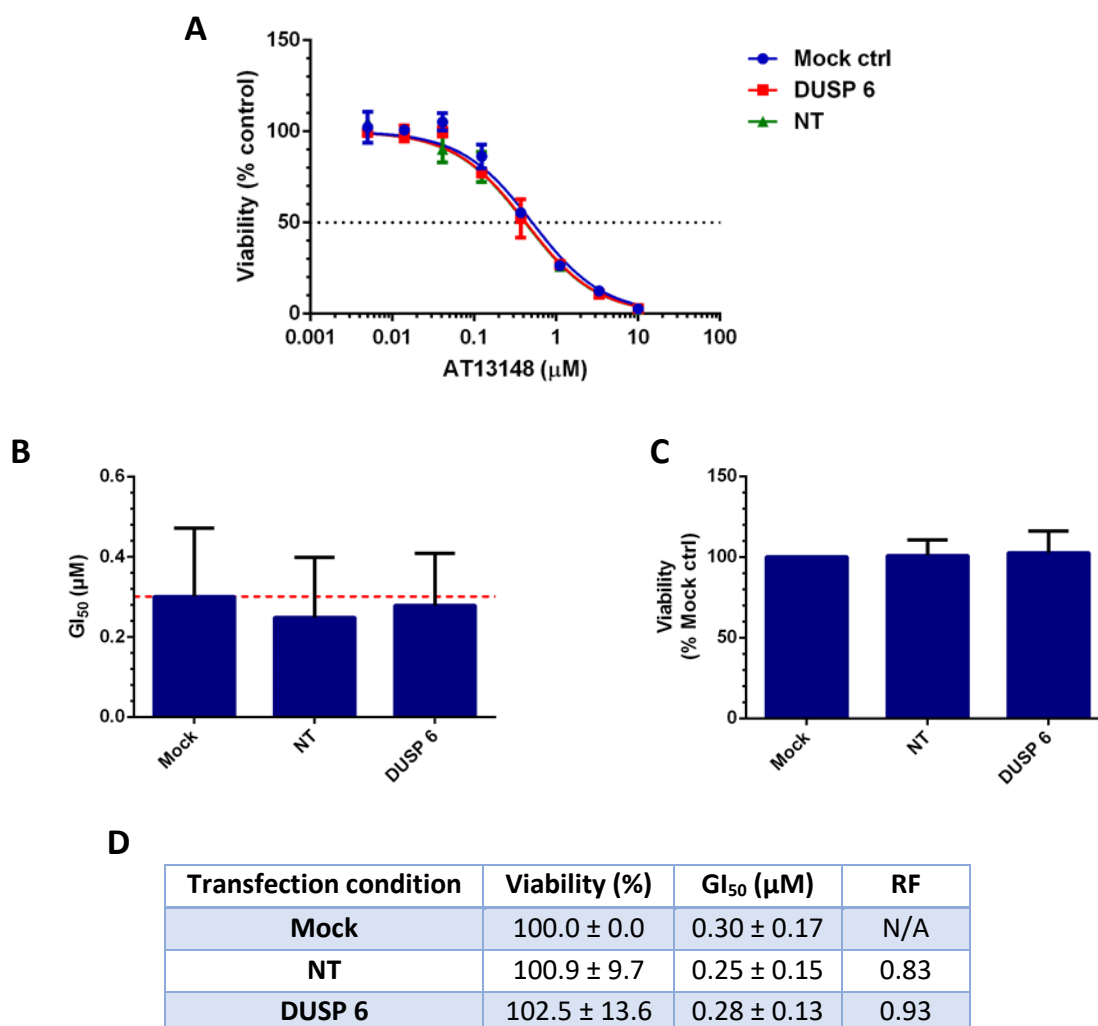
Figure 6.11: Effect of pooled DUSP6 siRNA knockdown on sensitivity to AT13148 in A2780 cells. A2780 cells were reverse transfected in triplicate in 96-well plates, at 10,000 cells/well, with 0.15% Lipofectamine 2000 and 25 nM pooled DUSP6 siRNA, or 25 nM non-targeting Allstars negative control siRNA (NT). Cells were also mock transfected with Lipofectamine 2000 alone. They were then left to incubate under standard growth conditions for 24 hours, prior to the addition of a serial dilution of AT13148 and a further incubation for 72 hours, under standard growth conditions. Cells were then analysed by SRB assay. Data was normalised to untreated control for each respective transfection condition unless otherwise stated **(A)** Dose-response graph was generated as previously described in Figure 6.7, data points represent the mean ± SD from one representative experiment **(B-D)** Graphs and table summarise GI_{50}, RF (relative to mock transfected) and cell viability (normalised to mock untreated control) of untreated AT13148 controls for each respective transfection condition. Data points and bars represent the mean ± SD of all experiments conducted. Dotted red line on GI_{50} graph highlights the mock GI_{50}. Statistical significance, relative to mock transfected, was calculated using a student's t-test, n = 3 independent experiments.

6.2.4.3. Knockdown of DUSP6 using individual DUSP6 siRNAs

One of the limitations of using siRNA to KD gene expression, is that siRNA's may cross-react with non-targeted mRNAs, even those with limited sequence similarity, decreasing the expression of non-targeted genes, thus producing off-target effects (Jackson *et al.*, 2003). The use of pooled DUSP6 siRNA (Figure 6.10 & Figure 6.11), a combination of siRNAs that target different sequences within DUSP6 mRNA, may amplify the number of off-target effects, making it difficult to interpret any phenotypes observed (or lack thereof). In addition, pooled DUSP6 siRNA may contain siRNAs with limited efficacy in the KD of DUSP6, which may compete and interfere with higher efficacy siRNAs within the pool. Therefore, the individual DUSP6 siRNAs, which comprised the pool used in Figure 6.10 & Figure 6.11, were used to KD DUSP6 expression in parental A2780 cells.

Figure 6.12 shows the expression of DUSP6 in response to KD by DUSP6 siRNAs (D6-01, D6-03, D6-04 & D6-05) in parental A2780 cells, 24 hours post siRNA transfection. All of the DUSP6 siRNAs were able to decrease DUSP6 expression, but the extent of this varied quite drastically (Figure 6.12). The decrease in DUSP6 expression caused by D6-05, when compared to mock and NT controls, was marginal, but other DUSP6 siRNAs caused a much more notable decrease (Figure 6.12). In particular, D6-03 caused the strongest decrease in DUSP6 expression; the expression of DUSP6 was only just detectable with a long hyperfilm exposure (Figure 6.12). In parallel to this, D6-03 caused the greatest increase in Thr202/Tyr204 ERK 1/2 phosphorylation (Figure 6.12). Other DUSP6 siRNAs also caused an increase in Thr202/Tyr204 ERK 1/2 phosphorylation, but to a lesser extent (Figure 6.12). Interestingly, despite near identical KD of DUSP6 caused by D6-01 and D6-04, D6-01 caused a greater increase in Thr202/Tyr204 ERK 1/2 phosphorylation than D6-04 (Figure 6.12). Furthermore, D6-05 was still able to increase Thr202/Tyr204 ERK 1/2 phosphorylation, despite only causing a marginal decrease in DUSP6 expression (Figure 6.12). There also appeared to be a slight increase in total ERK 1/2 expression in D6-01, D6-03 and D6-04, but this did not appear to account for the aforementioned increase in ERK 1/2 phosphorylation (Figure 6.12).

Taken together these data show that individual DUSP6 siRNAs are an effective strategy for the KD of DUSP6 expression in parental A2780 cells. The variability in DUSP6 KD by

individual DUSP6 siRNAs suggests that they may have improved efficacy over pooled DUSP6 siRNA, thus should be used for further validation.
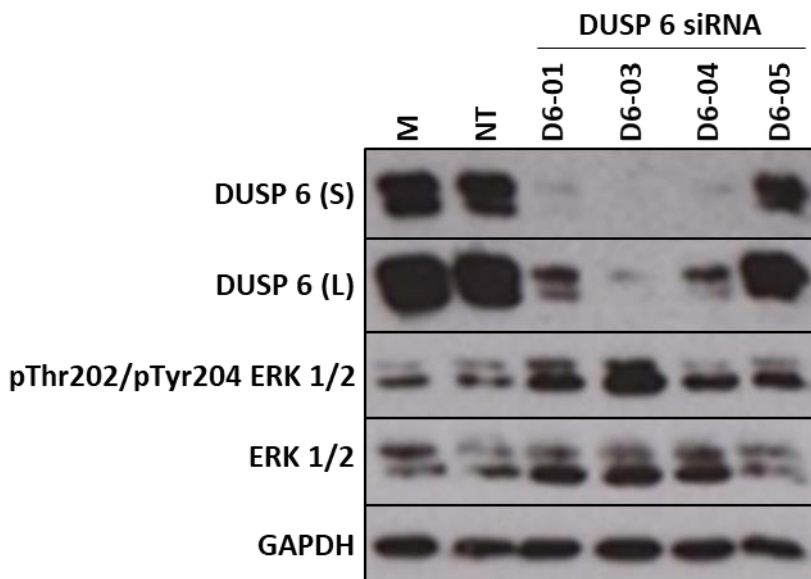
Figure 6.12: Knockdown of DUSP6 in A2780 cells using individual DUSP6 siRNAs. A2780 cells were reverse transfected in 6-well plates, at 1 x 10^5 cells/well, with 0.15% Lipofectamine 2000 and 10 nM of DUSP6 siRNA's (D6-01, D6-03, D6-04 or D6- 05) or 10 nM non-targeting Allstars negative control siRNA (NT). Cells were then incubated under standard growth conditions for 24 hours prior to lysis and western blot analysis, as described in Figure 6.4. M: mock transfected. Data are representative of 2 independent experiments

To this end, based upon their KD of DUSP6 expression and increase in ERK 1/2 phosphorylation, D6-01 and D6-03 were selected for use in additional experiments, to determine if loss of DUSP6 alone in parental A2780 cells could act as mechanism of resistance to AT13148. Based on the experience with pooled DUSP6 siRNA, i.e. limited duration of DUSP6 KD, it was decided to perform a 2-day SRB cell viability assay. Cells were reverse transfected and incubated for 4 hours prior to the addition of AT13148, followed by a further 48 hours incubation and analysis via an SRB assay. As before, western blot analysis was performed in parallel with SRB cell viability assays, across the 2-day time course. However, to ensure a more accurate depiction DUSP6 expression during an SRB cell viability assay, cells were plated in a 24-well plate for both SRB cell viability assays and western blot analysis.

Figure 6.13 shows the expression of DUSP6 in parental A2780 cells over a 2-day time course, following transfection of individual DUSP6 siRNA's (D6-01 and D6-03). Control lysates for A2780 and 148R-S from a previous experiment were also analysed, so as to assess if siRNA KD of DUSP6, in parental A2780 cells, was able to recapitulate the loss of

DUSP6 seen in 148R-S (Figure 6.4). Remarkably, D6-01 and D6-03 were able to decrease the expression of DUSP6 4 hours post-transfection, when compared to mock and NT controls, which was also seen at 28 hours but to a greater extent. A decrease in DUSP6 expression was also caused by D6-01 and D6-03 at 52 hours post-transfection, when compared to mock and NT controls, but this appeared to be to a lesser extent than was seen at 28 hours (Figure 6.13). However, it was difficult to accurately compare the level of DUSP6 KD at 28 hours and 52 hours, since the expression of DUSP6 in mock and NT controls had also increased between these timepoints (Figure 6.13). Nonetheless, whilst D6-01 and D6-03 decreased the expression of DUSP6 in A2780 cells across all timepoints, this was not to the same extent as was seen in the 148R-S control (Figure 6.13).

Interestingly, despite the incomplete KD of DUSP6, D6-01 and D6-03 caused an increase in Thr202/Tyr204 ERK 1/2 phosphorylation at both 4 and 28 hours, compared to mock and NT controls (Figure 6.13). The increase in Thr202/Tyr204 ERK 1/2 phosphorylation appeared to be similar to the increase seen in the 148R-S control (when compared to the A2780 control), particularly at 28 hours (Figure 6.13). However, this increase in Thr202/Tyr204 ERK 1/2 phosphorylation was lost at 52 hours (Figure 6.13). The total expression of ERK 1/2 was consistent across all timepoints and the A2780 control but was lower in the 148R-S control (Figure 6.13).
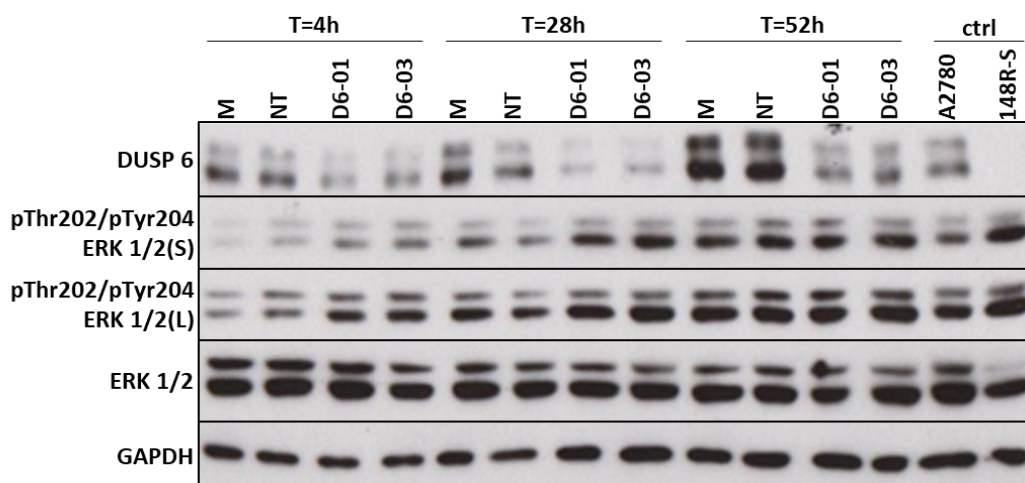
Figure 6.13: Knockdown of DUSP6 over a 2-day time course in A2780 cells using individual DUSP6 siRNAs. A2780 cells were reverse transfected in 24-well plates, at 2.5×10^4 cells/well, with 0.15% Lipofectamine 2000 and 10 nM of DUSP6 siRNA (D6-01 or D6-03) or 10 nM non-targeting Allstars negative control siRNA (NT). Cells were then incubated under standard growth conditions for 4, 24 or 52 hours prior to lysis and western blot analysis, alongside an A2780 and 148R-S lysate from a previous experiment, as described in Figure 6.4. M: mock transfected. Data are representative of 4 independent experiments.

As mentioned, the effect of DUSP6 KD, using individual siRNA's (D6-01 & D6-03), on the response of parental A2780 cells to AT13148 was also assessed in parallel with the 2-day western blot time course. Due to being performed in a 24-well plate format the number of AT13148 concentrations used was reduced from 8, the number of concentrations in standard SRB cell viability assay, to 5. Figure 6.14A shows that the viability of A2780 cells transfected with D6-03 was greater than mock and NT controls at every concentration of AT13148 tested, except 10 µM (Figure 6.14A). However, this difference was small and only statistically significant at 0.5 µM AT13148, where the % viability of D6-03 was 62.5% ± 5.4, compared to 54.1% ± 4.3 in the mock control (Figure 6.14A, E). The viability of A2780 cells transfected with D6-01 was mostly indistinguishable from the mock and NT controls, across all AT13148 concentrations (Figure 6.14A).

Despite the limited number of AT13148 concentrations used, the GI_{50} against AT13148 was still able to be accurately determined. Transfection of A2780 parental cells with D6-03 also increased the GI_{50} against AT13148; D6-03 GI_{50} was 1.15 µM compared to 0.74 µM in the mock control, a statistically significant difference, which equated to an RF value of 1.55, relative to the mock control (Figure 6.14B, C, E). The GI_{50} for A2780 cells transfected with D6-01 was 0.95 µM, which was also above that of the mock control, but the GI_{50} for A2780 cells transfected with NT siRNA was very similar, 0.89 µM, thus indicating that the increase in GI_{50} caused by D6-01 was likely due to a generic effect of siRNA transfection (Figure 6.14B, C, E). Interestingly, untreated parental A2780 cells transfected with D6-01 and D6-03 had decreased viability compared to mock control, a 12.5% and 9.0% decrease respectively, which was statistically significant in D6-01 (Figure 6.14D, E). However, the viability of parental A2780 cells transfected with NT was also reduced by a similar amount (7.4%) and shown to be statistically significant, which again suggests a generic effect caused by siRNA transfection (Figure 6.14D, E).

Taken together, these data (Figure 6.13 & Figure 6.14) show that knockdown of DUSP6 using individual DUSP6 siRNAs was unable to cause a sustained increase in ERK 1/2 phosphorylation or sufficiently increase viability or GI_{50} against AT13148. However, just as with pooled DUSP6 siRNA, the KD of DUSP6 by D6-01 and D6-03 siRNA did not match the loss of expression seen in 148R clones. This could explain the inability to recapitulate

the resistance phenotype. Therefore, the loss of DUSP6 alone, as mechanism of AT13148 resistance, warrants further investigation using alternative techniques.

E

Transfection conditions	Viability (%)	GI$_{50}$ (μM)	RF
Mock	100.0 ± 0.0	0.74 ± 0.23	N/A
NT	92.6 ± 1.3*	0.89 ± 0.20	1.20
D6-01	87.5 ± 2.0*	0.95 ± 0.13	1.28
D6-03	91.0 ± 10.6	1.15 ± 0.30*	1.55
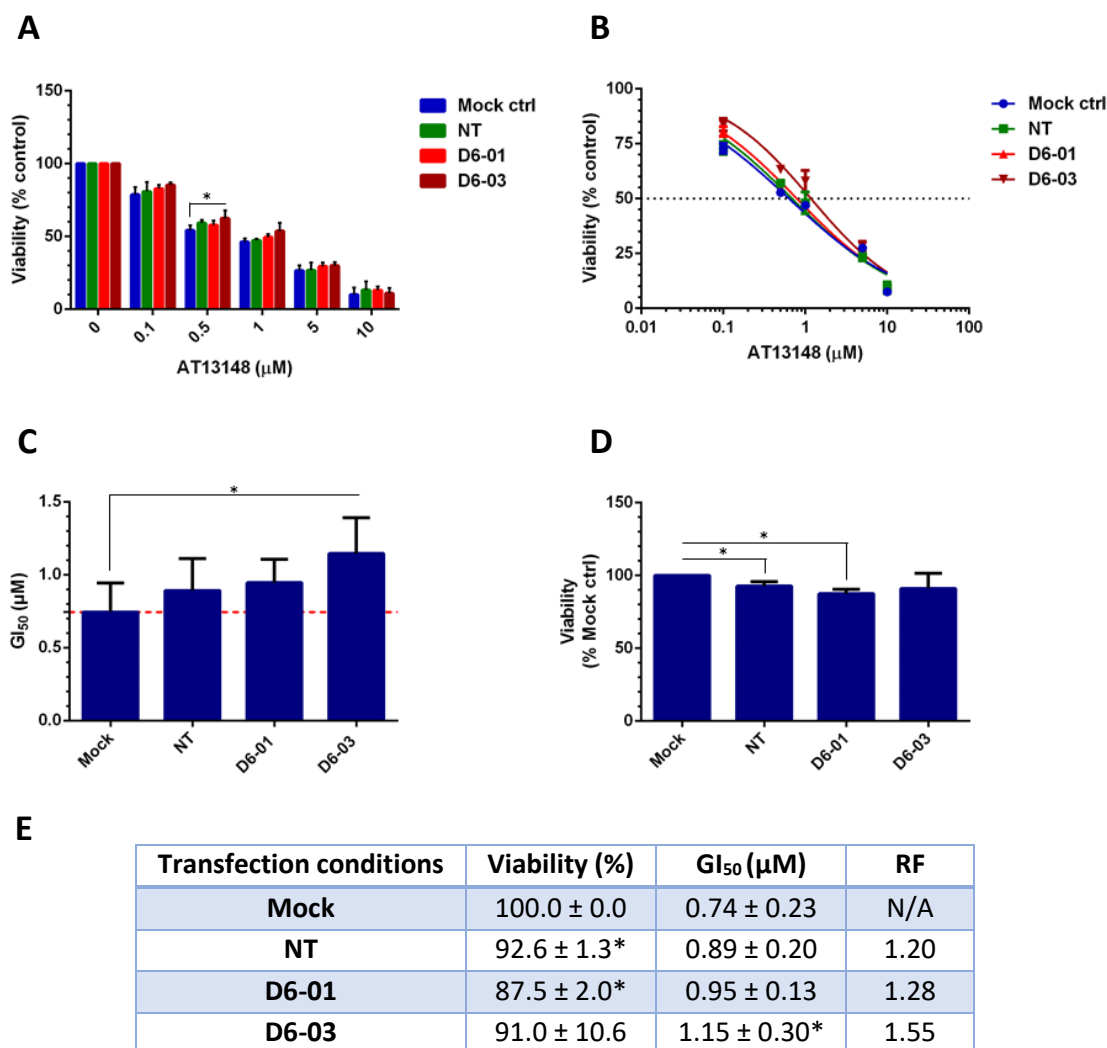
Figure 6.14: Effect of individual DUSP6 siRNA knockdown on sensitivity to AT13148 in A2780 cells. A2780 cells were reverse transfected in duplicate in 24-well plates, at 2.5×10^4 cells/well, with 0.15% Lipofectamine 2000 and 10 nM DUSP6 siRNA (D6-01 or D6-03), or 10 nM non-targeting Allstars negative control siRNA (NT). Cells were also mock transfected with 0.15% Lipofectamine 2000 alone. Cells were then left to incubate under standard growth conditions for 4 hours, prior to the addition of AT13148, at the concentrations shown, followed by a further incubation for 48 hours under standard growth conditions. Cells were then analysed by SRB assay. Data was normalised to untreated control for each respective transfection condition, unless otherwise stated. **(A)** Graph summarises the effect of AT13148 on cell viability, data points represent the mean ± SD from all experiments conducted. **(B)** Dose-response graph was generated as previously described in Figure 6.7; data points represent the mean ± SD from one representative experiment. **(C-E)** Graphs and table summarise GI$_{50}$, RF (relative to mock transfected) and cell viability (normalised to mock untreated control) of untreated AT13148 controls for each respective transfection condition. Data points and bars represent the mean ± SD of all experiments conducted. Dotted red line on GI$_{50}$ graph highlights the mock GI$_{50}$. Statistical significance, relative to mock transfected, was calculated using a student's t-test, *$p \geq 0.05$, n ≥ 3 independent experiments.

6.2.5. Ectopic re-expression of DUSP6 in 148R-S cells using a lentiviral strategy

6.2.5.1. Un-purified DUSP6 expressing lentivirus

In addition to DUSP6 siRNA KD in parental A2780 cells an alternative strategy was employed, whereby DUSP6 was ectopically re-expressed in 148R-S cells to see if this could re-sensitise 148R-S to AT13148. 148R-S cells were selected as they had the highest phosphorylation of ERK 1/2 and exhibited the greatest sensitivity to the combination of AT13148 with an ERK inhibitor (Figure 6.4 & Figure 5.5). In contrast to siRNA KD experiments, which attempted to answer whether loss of DUSP6 alone was sufficient for resistance, the ectopic re-expression of DUSP6 attempted to answer if loss of DUSP6 expression was necessary for AT13148 resistance. To this end, 148R-S cells were infected with a lentivirus expressing Myc and FLAG-tagged DUSP6 (henceforth referred to as DUSP6 lentivirus) and subsequently analysed to see if this could abolish the resistance phenotype: increased ERK 1/2 phosphorylation and AT13148 resistance. The presence of a Myc and FLAG tag enabled ectopic DUSP6 to be distinguished from endogenous DUSP6 via a gel mobility shift (i.e. higher molecular weight). It should also be noted that ectopic re-expression was only transient, as DUSP6 lentivirus did not contain a selectable marker for expression in mammalian cells

Initially, un-purified DUSP6 lentivirus was used; lentivirus obtained directly from the media of HEK293T cells that had been co-transfected with lentiviral plasmids. 148R-S cells were infected with un-purified DUSP6 lentivirus at 1-500 µl/ml, to identify conditions that optimally re-established DUSP6 expression. Figure 6.15 shows the expression of DUSP6 48 hours post-infection with DUSP6 lentivirus. DUSP6 was only re-expressed in 148R-S cells when DUSP6 lentivirus was used at 500 µl/ml, the maximum concentration used (Figure 6.15). However, whilst the level of ectopically expressed DUSP6 was stronger than endogenous DUSP6 in 148R-S cells infected with 500 µl/ml DUSP6 lentivirus, it was still dramatically below the expression of DUSP6 in parental A2780 cells. These data show that un-purified DUSP6 lentivirus was able to induce ectopic expression of DUSP6 in 148R-S cells but was unable to re-express DUSP6 at the level seen in parental A2780 cells.
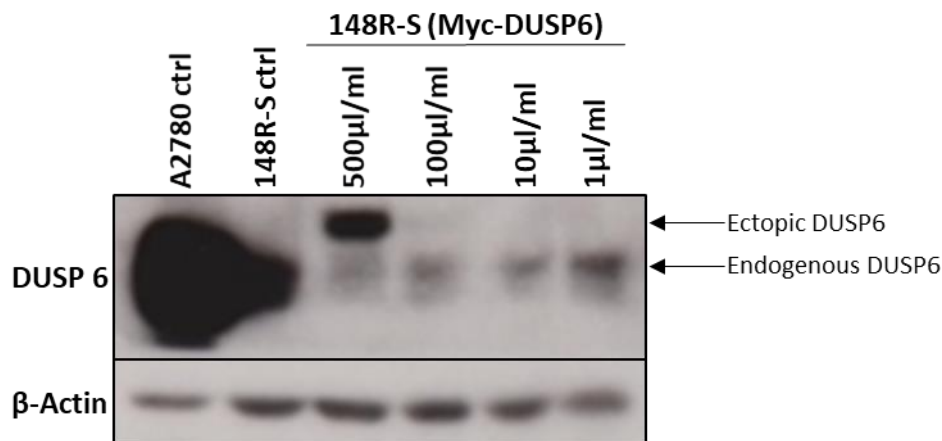
Figure 6.15: Ectopic re-expression of DUSP6 in 148R-S cells using un-purified lentivirus. Cells were plated in 6-well plates at 5 x 10^5 cells/well and left to incubate overnight under standard growth conditions. Subsequently, media was replenished with complete DMEM containing 5 µg/ml polybrene and a lentivirus expressing Myc and FLAG-tagged DUSP6 at the concentrations shown. A2780 and 148R-S control cells (ctrl) were not infected with lentivirus. Cells were then incubated for 24 hours under standard growth conditions, prior to media, containing lentivirus, being replaced with complete DMEM and a further incubation for 24 hours under standard growth conditions. Cells were subsequently lysed for western blot analysis, as described in Figure 6.4. n = 1 experiment.

Despite being unable to re-express DUSP6 in 148R-S cells at the level seen in A2780 parental cells, un-purified DUSP6 lentivirus was used in 148R-S cells to investigate if re-expression of DUSP6 could decrease ERK 1/2 phosphorylation and re-sensitise 148R-S to AT13148. Since the ectopic expression of DUSP6 using DUSP6 lentivirus was transient, a 4-day SRB assay was used in a 96-well plate format (as previously described in section 6.2.4.2). In parallel to this, cells were plated in 6-well plates, to evaluate the expression of DUSP6 and ERK 1/2 phosphorylation over the time-course of a 4-day SRB cell viability assay. In addition, to maximise the expression of DUSP6, un-purified DUSP6 lentivirus was used undiluted, as well as at 500 µl/ml, and with 10 µg/ml polybrene, as well as 5 µg/ml polybrene which was used in Figure 6.15. Polybrene (Hexadimethrine Bromide) is a cationic polymer which reduces the charge repulsion between cell membranes and lentivirus, facilitating greater lentiviral adsorption; increasing polybrene concentration may improve lentiviral transduction efficiency (Davis *et al.*, 2004).

Figure 6.16 shows the expression of DUSP6 in 148R-S over a time-course following infection with un-purified DUSP6 lentivirus. The 48-hour and 120-hour post-infection timepoints respectively correspond to the addition of AT13148 during a 4-day SRB cell viability assay and its end. At both timepoints, using un-purified DUSP6 lentivirus

undiluted improved the ectopic expression of DUSP6, when compared to 500 µl/ml, but the concentration of polybrene (5 or 10 µg/ml) seemed to have a limited effect on the ectopic expression of DUSP6 (Figure 6.16). Unfortunately, despite improved ectopic DUSP6 expression, DUSP6 expression in 148R-S cells was still much lower than the level seen in parental A2780 cells (Figure 6.16). Moreover, ectopic DUSP6 expression decreased at 120 hours post-infection, when compared to 48 hours post-infection, under all lentiviral conditions used (Figure 6.15). Thus, further compounding the ability of un-purified DUSP6 lentivirus to sufficiently re-express DUSP6 (Figure 6.16).

Interestingly, at 48 hours post-infection, undiluted un-purified DUSP6 lentivirus caused a decrease in the phosphorylation of Thr202/Tyr204 ERK 1/2 in 148R-S cells, when compared to 148R-S control. This decrease lowered Thr202/Tyr204 ERK 1/2 phosphorylation to approximately the same level as in parental A2780 cells (Figure 6.16). However, the decrease in ERK 1/2 phosphorylation coincided with a decrease in total ERK 1/2 expression, which may therefore, in part, explain the decrease in ERK 1/2 phosphorylation (Figure 6.16). Furthermore, Thr202/Tyr204 ERK 1/2 phosphorylation was not decreased at 120 hours post-infection, under all lentiviral conditions used (Figure 6.16). Total ERK 1/2 expression appeared to be mostly consistent within each timepoint, apart from the aforementioned decrease (Figure 6.16).

In summary, these data showed that using un-purified DUSP6 lentivirus undiluted can increase the ectopic expression of DUSP6 in 148R-S cells. However, the expression does not match that of parental A2780 cells, is not durable across the time-course of 4-day SRB cell viability assay and does not cause a sustained decrease in ERK 1/2 phosphorylation.
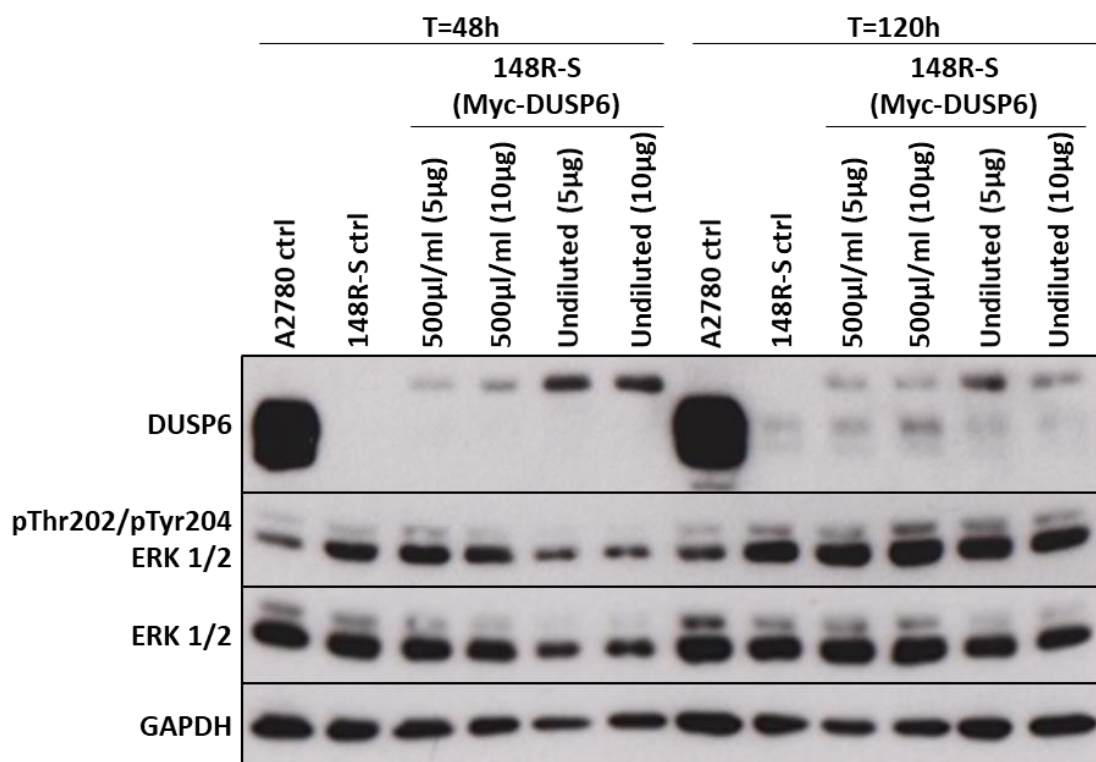
Figure 6.16: Time-course of DUSP6 re-expression in 148R-S cells using an un-purified lentivirus. Cells were plated in 6-well plates at 5 x 10^5 cells/well and left to incubate overnight under standard growth conditions. Subsequently, media was replenished with complete DMEM containing 5 or 10 µg/ml polybrene (indicated by 5 µg or 10 µg) and un-purified lentivirus expressing Myc and FLAG-tagged DUSP6, at the concentrations shown. A2780 and 148R-S control cells (ctrl) were not treated with lentivirus. Cells were then incubated for 24 hours under standard growth conditions, prior to being split into a new 6-well dish at either 5 x 10^5 cells/well (48 hours post-infection timepoint) or 1 x 10^5 cells/well (120-hours infection timepoint). Cells were than incubated for an additional 24 or 96-hours, according to timepoint, under standard growth conditions, prior to lysis and western blot analysis, as described in Figure 6.4. Data are representative of 2 (controls and 500 µl/ml with 5µg/ml polybrene) or 1 (all other conditions) independent experiment.

Whilst the ectopic expression of DUSP6 in 148R-S cells was insufficient, even when un-purified DUSP6 lentivirus was used undiluted, SRB celll viability assays were still conducted, as ectopic expression of DUSP6 was above the level of endogenous DUSP6 expression in 148R-S cells, so therefore might be able to cause some sensitisaion to AT13148 (Figure 6.15 & Figure 6.16). However, Figure 6.17 shows that ectopic expression of DUSP6, via un-purified DUSP6 lentivirus, was unable to re-sensitise 148R-S cells to AT13148. In a 4-day SRB cell viability assay with AT13148, A2780 (A2780 ctrl) was shown to have a GI_{50} of 0.27 µM compared to 2.49 µM in un-infected 148R-S control cells (148R-S ctrl), a statistically significant difference equating to an RF value of 9.22, consistent with previous results (Figure 6.17, previous result Figure 4.10). Unexpectedly, there was a small increase in the GI_{50} against AT13148 in 148R-S cells infected with un-

purified DUSP6 lentivirus at 500 µl/ml, when compared to 148R-S control cells; the GI_{50} was 3.00 µM with 5 µg/ml polybrene and 3.12 µM with 10 µg/ml polybrene, equating to RF values of 11.11 and 11.56 respectively (Figure 6.17). But these were not shown to be statistically significant when compared to AT13148 GI_{50} values for A2780 and 148R-S control cells (Figure 6.17). However, whilst not statistically significant, there was a decrease in the GI_{50} against AT13148 in 148R-S cells infected with undiluted un-purified DUSP6 lentivirus; the GI_{50} was 1.94 µM with 5 µg/ml polybrene and 2.23 µM with 10 µg/ml polybrene, equating to an RF value of 7.19 and 8.26 respectively (Figure 6.17). Whilst this was a small decrease in AT13148 GI_{50}, undiluted un-purified DUSP6 lentivirus was unable to completely re-establish DUSP6 expression (as shown in Figure 6.16). Therefore, this may suggest that further increasing the level of DUSP6 re-expression in 148R-S cells might cause a greater re-sensitisation to AT13148.
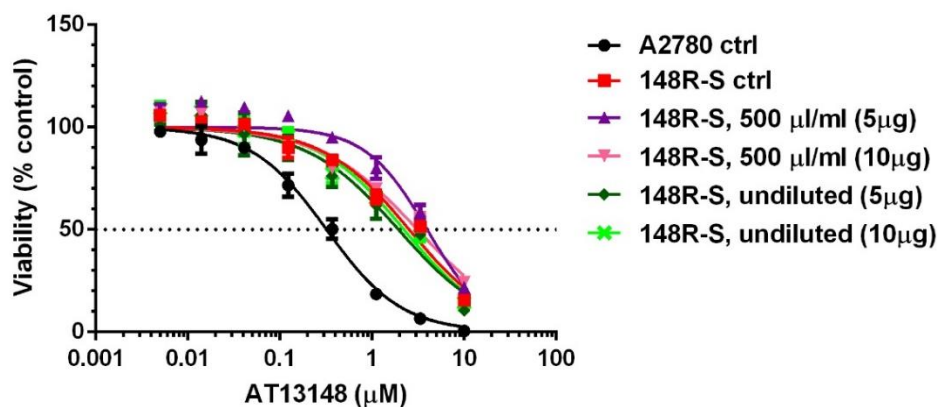
Cell line/condition	GI_{50} (µM)	RF
A2780 ctrl	0.27 ± 0.05*	N/A
148R-S ctrl	2.49 ± 0.81^	9.22
148R-S, 500 µl/ml (5 µg)	3.00 ± 0.97	11.11
148R-S, 500 µl/ml (10 µg)	3.12	11.56
148R-S, undiluted (5µg)	1.94	7.19
148R-S, undiluted (10µg)	2.23	8.26

Figure 6.17: Effect of ectopic DUSP6 re-expression in 148R-S cells, using un-purified DUSP6 lentivirus, on response to AT13148. Cells were plated in 6-well plates at 5 x 10^5 cells/well and left to incubate overnight under standard growth conditions. Subsequently, media was replenished with complete DMEM containing 5 or 10 µg/ml polybrene (indicated by 5 µg or 10 µg) and lentivirus expressing Myc and FLAG-tagged DUSP6, at the concentrations shown. A2780 and 148R-S control cells (ctrl) were not infected with lentivirus. Cells were then incubated for 24 hours under standard growth conditions, prior to being split into a 96-well plate at 1 x 10^4 cells/well, followed by an additional 24 hours incubation under standard growth conditions. AT13148 was then added at the concentrations indicated and cells incubated for 72 hours under standard growth conditions, followed by SRB assay analysis. Graph and table were generated as described previously in Figure 6.7. Statistical significance, relative to A2780 (^) or 148R-S (*) ctrl, was calculated using a student's t-test, ^ or * $p \leq 0.05$, n = 4 (control cells), 2 (500 µl/ml with 5µg/ml polybrene) or 1 (all other conditions) independent experiment(s).

6.2.5.2. Purified DUSP6 expressing lentivirus

In the work presented thus far, DUSP6 was re-expressed using un-purified/un-concentrated DUSP6 lentivirus. As has been mentioned, even when used undiluted, un-purified DUSP6 lentivirus could not sufficiently re-express DUSP6 in 148R-S cells and this may explain why re-expression of DUSP6 did not re-sensitise 148R-S cells to AT13148 (Figure 6.17). To overcome this, DUSP6 lentivirus was purified using PEG 6000 precipitation, to increase the concentration of DUSP6 lentivirus, thus the ectopic expression of DUSP6 in 148R-S cells. Following this, the assays conducted in Figure 6.16 & Figure 6.17 were repeated using purified/concentrated DUSP6 lentivirus.

Figure 6.18 shows the expression of DUSP6 in 148R-S over a time-course, parallel to a 4-day SRB cell viability assay, following infection with purified DUSP6 lentivirus. At 48-hours post-infection, when purified DUSP6 lentivirus was used at 50 and 100 µl/ml the ectopic expression of DUSP6 in 148R-S cells at least equalled the level of DUSP6 expression in parental A2780 cells (Figure 6.18). In fact, when purified DUSP6 lentivirus was used at 100 µl/ml, where ectopic expression of DUSP6 was at its greatest, ectopic expression of DUSP6 in 148R-S was slightly above the level of DUSP6 expression seen in parental A2780 cells (Figure 6.18). Just as was seen previously (Figure 6.16), the ectopic expression of DUSP6 decreased at 120-hours post-infection, when compared to 48-hours, with both 50 and 100 µl/ml of purified DUSP6 lentivirus (Figure 6.18). Unfortunately, this meant that the ectopic expression of DUSP6 in 148R-S cells was below the level of DUSP6 expression in parental A2780 cells at this timepoint. However, the ectopic expression was still strong at 120-hours, particularly with 100 µl/ml purified DUSP6 lentivirus, where ectopic DUSP6 expression was only slightly lower than DUSP6 expression in parental A2780 cells (Figure 6.18).

Interestingly, at 48-hours, when purified DUSP6 lentivirus was used at 50 and 100 µl/ml, the ectopic expression of DUSP6 caused a dramatic reduction in Thr202/Tyr204 ERK 1/2 phosphorylation in 148R-S cells. At these concentrations, Thr202/Tyr204 ERK 1/2 phosphorylation was approximately the same level as was seen in parental A2780 cells (Figure 6.18). Thr202/Tyr204 ERK 1/2 phosphorylation was also decreased by ectopic DUSP6 expression at 120-hours, with both 50 and 100 µl/ml purified DUSP6 lentivirus,

however, this was to a much lesser extent, with ERK 1/2 phosphorylation being above the level seen in parental A2780 cells at this timepoint (Figure 6.18). It should be noted, that in the repeat of this assay (data not shown), ectopic DUSP6 expression did not cause a decrease in Thr202/Tyr204 ERK 1/2 phosphorylation at 120-hours, indicating a degree of inter-assay variation. The phosphorylation of the ERK 1/2 substrate Elk-1, at S383, was also assessed and corresponded to ERK 1/2 phosphorylation; decreased at 48-hours but this was lost at 120-hours (Figure 6.18). Total expression of ERK 1/2 and Elk-1 was consistent within each timepoint (Figure 6.18)

In addition, the phosphorylation of MEK 1/2 was also evaluated to ascertain if ectopic expression of DUSP6, and subsequent decrease in ERK 1/2 phosphorylation, might restore the phosphorylation of MEK 1/2 in 148R-S. MEK 1/2 phosphorylation was previously shown to be decreased in 148R clones, due to negative feedback mediated by increased ERK 1/2 phosphorylation (Figure 4.17 & Figure 5.3). Figure 6.18 shows that S217/221 MEK 1/2 phosphorylation increased in 148R-S cells in response to ectopic expression DUSP6, in both timepoints. This, in part, seemed to be dependent upon the level of DUSP6 expression; within each timepoint as the level of ectopic DUSP6 expression increased so did S217/221 MEK 1/2 phosphorylation. Therefore, in both timepoints S217/221 MEK 1/2 phosphorylation peaked with 100 μl/ml purified DUSP6 lentivirus, where ectopic DUSP6 expression was at its greatest (Figure 6.18). Furthermore, this increase in S217/221 MEK 1/2 phosphorylation seemed strongest at 120 hours (Figure 6.18). This may, in part, explain why the decrease in ERK 1/2 phosphorylation was not sustained at 120 hours. However, even at its peak, S217/221 MEK 1/2 phosphorylation was still below the level seen in parental A2780 cells (Figure 6.18). Total expression of MEK 1/2 was consistent within each time point (Figure 6.18)

Taken together, these data show that purified DUSP6 lentivirus can restore DUSP6 expression to the same level seen in A2780 parental cells. However, this expression was lost over time, therefore purified DUSP6 lentivirus was unable to maintain DUSP6 expression during the time-course of a 4-day SRB assay. Additionally, ectopic expression of DUSP6, via purified DUSP6 lentivirus, was shown to abolish the MAPK pathway alterations seen in 148R-S: increased ERK 1/2 and Elk-1 phosphorylation, and decreased MEK 1/2 phosphorylation; particularly at 48 hours.
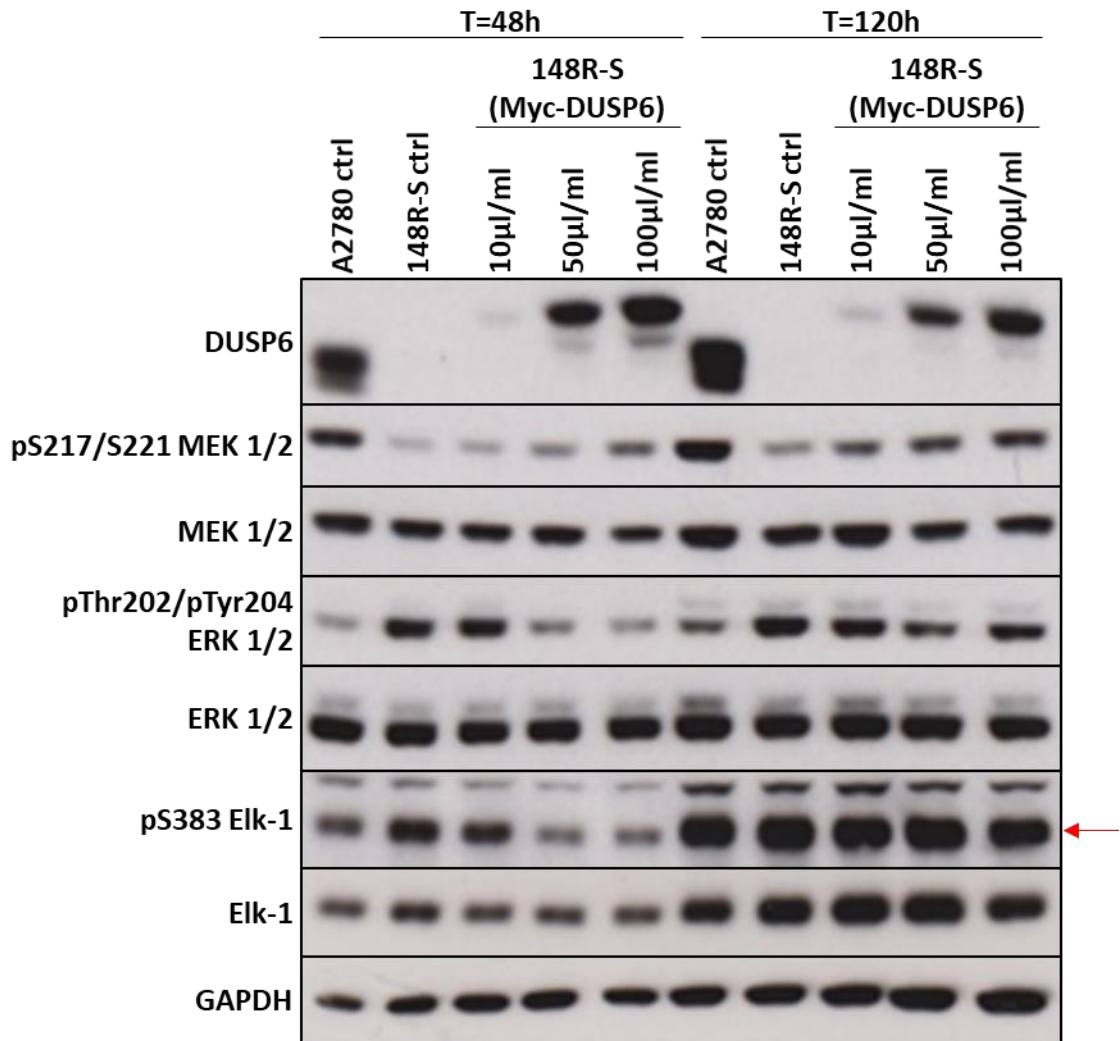
Figure 6.18: Time-course of ectopic DUSP6 re-expression in 148R-S cells using purified lentivirus. Cells were plated in 6-well plates at 5 x 10^5 cells/well and left to incubate overnight under standard growth conditions. Subsequently, media was replenished with complete DMEM containing 10 µg/ml polybrene and a purified lentivirus expressing Myc and FLAG-tagged DUSP6, at the concentrations shown. A2780 and 148R-S control cells (ctrl) were not infected with lentivirus. Cells were then incubated for 24 hours under standard growth conditions, prior to being split into a new 6-well dish at either 5 x 10^5 cells/well (48 hours post-infection timepoint) or 1 x 10^5 cells/well (120-hours infection timepoint). Cells were than incubated for an additional 24 or 96 hours, according to timepoint, under standard growth conditions, prior to lysis and western blot analysis, as described in Figure 6.4. Red arrow highlights band corresponding to pS383 Elk-1. Data are representative of 2 independent experiment.

Whilst purified DUSP6 lentivirus did not optimally re-express DUSP6, it was an improvement upon what was achieved with un-purified DUSP6 lentivirus and was able to appropriately alter the MAPK pathway (e.g. decreased ERK 1/2 phosphorylation), albeit only temporarily (Figure 6.18). Therefore, purified DUSP6 lentivirus was used in an SRB cell viability assay to evaluate if DUSP6 re-expression could re-sensitise 148R-S cells to AT13148. Figure 6.19 shows the response of 148R-S cells ectopically expressing DUSP6, via purified DUSP6 lentivirus, to AT13148 over the course of a 4-day SRB cell

viability assay. Interestingly, the GI_{50} of 148R-S cells ectopically expressing DUSP6 against AT13148 was lower than 148R-S control cells (uninfected); the GI_{50} for 148R-S cells infected with 50 and 100 µl/ml purified DUSP6 lentivirus was 1.44 µM and 1.83 µM respectively, compared to 2.49 µM in 148R-S control cells (Figure 6.19). However, these differences only represented a < 2-fold difference and were not shown to be statistically significant, compared to 148R-S control cells. In addition, the GI_{50} of 148R-S cells ectopically expressing DUSP6 was still substantially greater than the GI_{50} of A2780 cells for AT13148: 0.27 µM (Figure 6.19). Therefore, 148R-S cells ectopically expressing DUSP6 still had RF values of 5.33 and 6.77, for 50 and 100 µl/ml purified DUSP6 lentivirus respectively, only slightly below the RF value for 148R-S control cells: 9.22 (Figure 6.19). It should also be noted that the GI_{50} against AT13148 for 148R-S control cells and 148R-S cells infected with 50 µl/ml purified DUSP6 lentivirus was shown to be statistically significant, when compared to parental A2780 cells (Figure 6.19).

In summary, these data show that ectopic expression of DUSP6, via purified DUSP6 lentivirus, does not re-sensitise 148R-S cells to AT13148. However, this might be explained by the loss of ectopic DUSP6 expression over the time course a 4-day SRB cell viability assay, as shown in Figure 6.18.
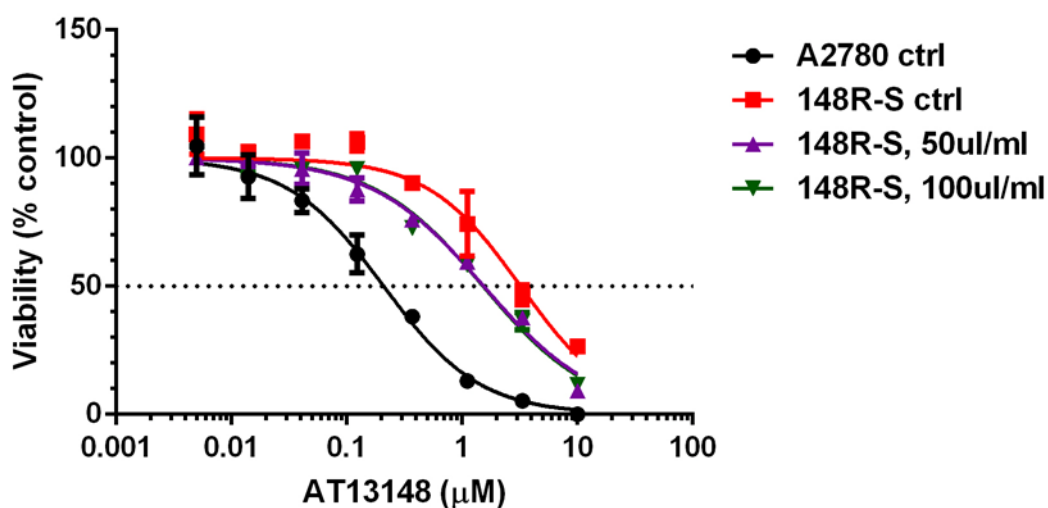
Cell line/condition	GI$_{50}$ (µM)	RF
A2780 ctrl	0.27 ± 0.05*	N/A
148R-S ctrl	2.49 ± 0.81^	9.22
148R-S, 50 µl/ml, purified	1.44 ± 0.11^	5.33
148R-S, 100 µl/ml, purified	1.83 ± 0.30	6.77

Figure 6.19: Effect of ectopic DUSP6 re-expression in 148R-S cells, using a purified DUSP6 lentivirus, on response to AT13148. Cells were plated in 6-well plates at 5 x 10^5 cells/well and left to incubate overnight under standard growth conditions. Subsequently media was replenished with fresh complete DMEM containing 10 µg/ml polybrene and a purified lentivirus expressing Myc and FLAG-tagged DUSP6, at the concentrations shown. A2780 and 148R-S control cells (ctrl) were not infected with lentivirus. Cells were then incubated for 24 hours under standard growth conditions, prior to being split into a 96-well plate at 1 x 10^4 cells/well, followed by an additional 24 hours incubation under standard growth conditions. Subsequently AT13148 was added at the concentrations indicated and cells were incubated for 72 hours under standard growth conditions, followed by SRB assay analysis. Graph and table were generated as described previously in Figure 6.7. Statistical significance, relative to A2780 (^) or 148R-S (*) ctrl, was calculated using a student's t-test, ^ or * $p ≤ 0.05$, n = 2 (50 & 100 µl/ml lentivirus) or 4 (controls cells) independent experiments.

6.2.5.3. Summary of the response of 148R-S cells ectopically re-expressing DUSP6 to AT13148

The response of 148R-S cells ectopically re-expressing DUSP6 across all DUSP6 lentiviral conditions used is summarised in Figure 6.20. In summary, there did seem to be a trend; as conditions became more optimal for strong and durable ectopic expression of DUSP6 (e.g. via lentivirus purification/concentration) the GI_{50} against AT13148 decreased (Figure 6.20). However, none of the conditions used, to ectopically express DUSP6, were able to significantly re-sensitise 148R-S cells to AT13148 (Figure 6.20). As was mentioned, even with purified DUSP6 lentivirus the ectopic expression of DUSP6 was not durable over the course of a 4-day SRB cell viability assay. In addition, Figure 6.20 highlights that due to time constraints only 1-2 independent experiments were conducted for each lentiviral condition. Therefore, the ability of DUSP6 re-expression to abolish the resistance phenotype in 148R-S cells warrants a more thorough investigation.
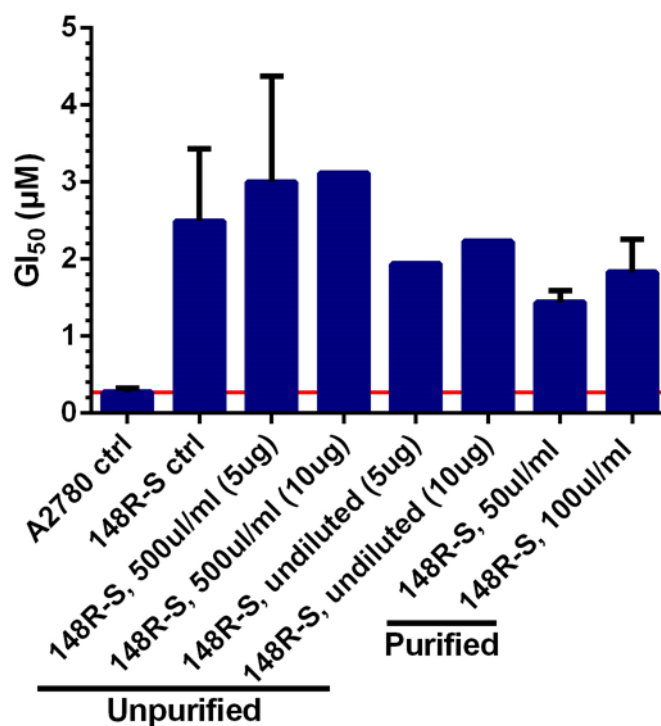
Cell line/condition	GI$_{50}$ (µM)	RF	n
A2780 ctrl	0.27 ± 0.05*	N/A	4
148R-S ctrl	2.49 ± 0.81^	9.22	4
148R-S, 500 µl/ml (5 µg)	3.00 ± 0.97	11.11	2
148R-S, 500 µl/ml (10 µg)	3.12	11.56	1
148R-S, undiluted (5µg)	1.94	7.19	1
148R-S, undiluted (10µg)	2.23	8.26	1
148R-S, 50 µl/ml, purified	1.44 ± 0.11^	5.33	2
148R-S, 100 µl/ml, purified	1.83 ± 0.30	6.77	2

Figure 6.20: Summary of AT13148 GI$_{50}$ and RF in 148R-S cells ectopically expressing DUSP6 via lentivirus. Graph and table summarise the data shown in Figure 6.17 & Figure 6.19. Data points and bars represent the mean ± SD of all experiments conducted. Red line highlights the GI$_{50}$ of A2780 control. Unless otherwise stated (5 µg or 10 µg), 10 µg/ml polybrene was used. Statistical significance, relative to A2780 (^) or 148R-S (*) ctrl, was calculated using a student's t-test, ^ or * $p \leq 0.05$, number of independent experiments conducted are shown in table.

6.2.6. Response of MAPK pathway to FGFR inhibition in A2780 and 148R clones

Whilst the experiments presented in this chapter have not definitively excluded loss of DUSP6 alone as a mechanism of resistance to AT13148, it seems likely that other factors may also contribute. Specifically, other factors may be required for a sustained increase in ERK 1/2 phosphorylation, a driver of AT13148 resistance. Evidence for this can be seen as KD of DUSP6 in parental A2780 cells and ectopic DUSP6 expression in 148R-S cells only caused a temporary respective increase or decrease in ERK 1/2 phosphorylation (Figure 6.13 & Figure 6.18). One possible candidate for regulation of increased ERK 1/2 phosphorylation is FGFR signalling, as FGFR's are known to regulate MAPK pathway activation, therefore ERK 1/2 phosphorylation, and most 148R clones had been shown to be sensitive to FGFR inhibition (Desai and Adjei, 2016., Figure 4.5 & Figure 4.9).

To investigate this A2780, 148R-N and 148R-S cells, were treated with the FGFR inhibitor AZD4547, and western blotted for markers of the MAPK pathway. 148R-N and 148R-S were selected as they were respectively shown to be cross-resistant or sensitive to AZD4547 (Figure 4.11). The phosphorylation of Thr202/Tyr204 ERK 1/2 and S217/221 MEK 1/2 appeared to be refractory to AZD4547 in A2780 and 148R-N (Figure 6.21). It should be noted that there was a slight decrease in ERK 1/2 and MEK 1/2 phosphorylation with 0.1 µM AZD4547 in parental A2780 cells, but this did not occur with 0.01 µM or 1 µM AZD4547 (Figure 6.21). In contrast, the MAPK pathway exhibited a strong response to AZD4547 in 148R-S cells; at 0.01 µM there was a slight increase in ERK 1/2 phosphorylation, whilst MEK 1/2 phosphorylation was unchanged, followed by consecutive decreases in both ERK 1/2 and MEK 1/2 phosphorylation at 0.1 µM and 1 µM AZD4547 (Figure 6.21). The decrease in ERK 1/2 phosphorylation appeared to be much more marked than the decrease in MEK 1/2 phosphorylation (Figure 6.21). The total expression of ERK 1/2 and MEK 1/2 was mostly consistent across all cell lines and AZD4547 concentrations

Since FGFR can also regulate the activation of the PAM pathway the phosphorylation of AKT was also evaluated (Desai and Adjei, 2016). Phosphorylation of S473 AKT was shown to be refractory to AZD4547 in both A2780 and 148R-N (Figure 6.21). However, AZD4547 was able to decrease S473 AKT phosphorylation in 148R-S, albeit to a small extent and

only at 1 µM, the maximum AZD4547 concentration used (Figure 6.21). The total expression of AKT appeared to be consistent across all cell lines and concentrations of AZD4547 (Figure 6.21).

Taken together, these data show the MAPK pathway is responsive to FGFR inhibition in 148R-S cells but is not in 148R-N or parental A2780 cells. This may explain why 148R-S is sensitive to FGFR inhibition by AZD4547, and suggests that FGFR signalling may also contribute to the increased phosphorylation of ERK 1/2 seen in 148R-S. Therefore, FGFR signalling and its contribution to increased ERK 1/2 phosphorylation, thus AT13148 resistance, warrants further investigation.
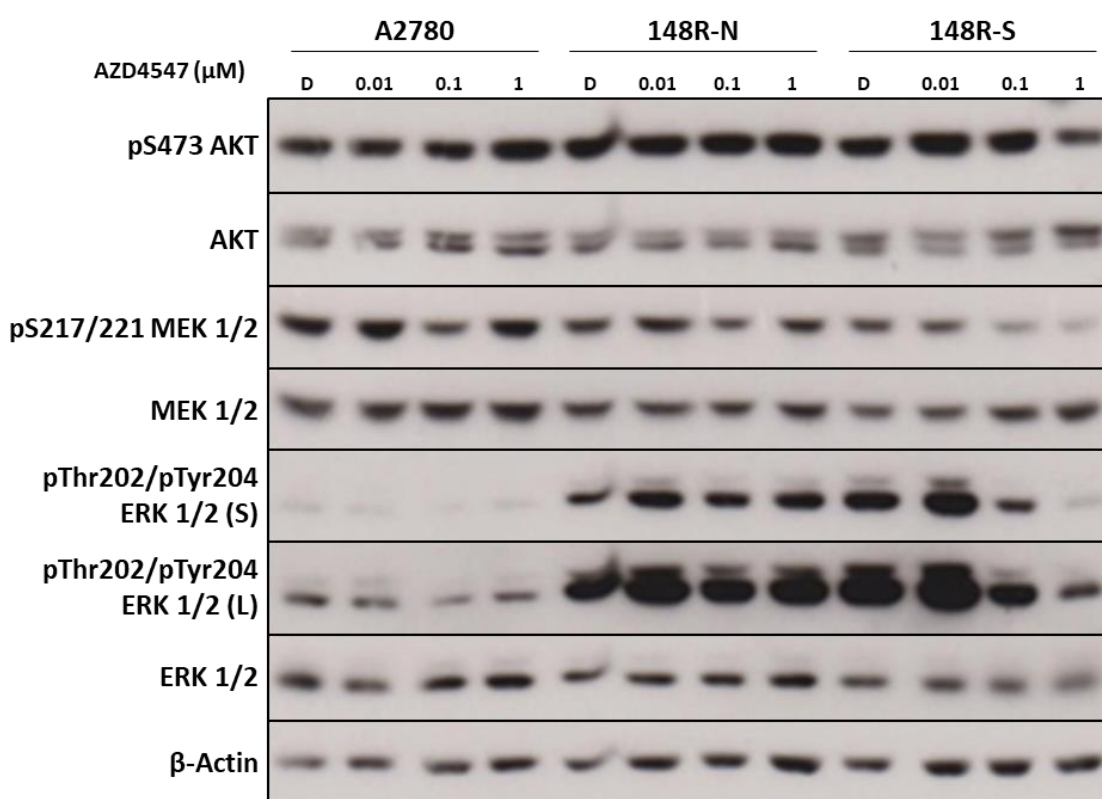
Figure 6.21: Response of AKT phosphorylation and MAPK pathway to AZD4547 in A2780 and 148R clones. Cells were plated at either 5 x 10^5 (A2780) or 7.5 x 10^5 (148R clones) cells per 7 cm dish and allowed to grow for 48 hours under standard growth conditions. Cells were then treated with AZD4547, as shown, or D: DMSO vehicle control, for 9 hours prior to being lysed for western blot analysis. Western blot membranes were probed with antibodies for phospho-proteins, stripped, and then re-probed with antibodies for total proteins and loading control (β-Actin). (S): short exposure to hyperfilm, (L): long exposure to hyperfilm. Data are representative of 3 independent experiments.

6.3. Discussion

6.3.1. Potential mechanisms of DUSP6 loss

The aim of this chapter was to investigate the contribution of DUSP6, and other DUSPs, to increased ERK 1/2 phosphorylation and AT13148 resistance. In order to do this a candidate approach was used, in which the expression of selected DUSPs, that could dephosphorylate ERK 1/2 and had been associated with resistance to cancer therapies, were assessed using western blot analysis. This was a successful approach as it was shown that 148R-K, N & S all had a drastic decrease in the expression of DUSP6 (Figure 6.4A). In contrast, DUSP4 and DUSP5 did not show any substantial differences amongst parental A2780 cells and 148R clones. The expression of DUSP6 was also investigated in 148R-J and 148R-P, two 148R clones that were discontinued from further investigation in chapter 4, where it was shown that DUSP6 was also lost in 148R-P but not in 148R-J (Figure 6.4B). This may suggest that A2780-148R contained sub-populations with differential expression of DUSP6 (high vs low). Indeed, further evidence of this was seen as A2780-148R was only shown to have a slight reduction in DUSP6 expression, much less so than was seen in 148R-K, N, P & S (Figure 6.4B).

Interestingly, amongst 148R clones where DUSP6 expression was decreased, there was variation in the expression of DUSP6; DUSP6 expression was greatest in 148R-S, followed by 148R-K, and 148R-N, where DUSP6 expression was never detected (data not shown). This could indicate that 148R clones have lost DUSP6 expression via distinct mechanisms. Whilst not investigated here, it is worth considering the mechanisms in which DUSP6 expression could have been lost and how this could be investigated in future.

One way to interrogate regulation of DUSP6 expression would be by performing reverse transcriptase quantitative polymerase chain reaction (RT-Q-PCR) assays, to assess the expression of *DUSP6* at the mRNA level. If *DUSP6* mRNA was unchanged between parental A2780 cells and 148R clones, this would suggest that the loss of DUSP6 expression was post-transcriptional. As was discussed in section 6.1, DUSP6 is known to undergo proteasomal degradation, if this process was to become enhanced then DUSP6 expression would be decreased at the protein level but not at the mRNA level (Marchetti

et al., 2005). 148R clones could be treated with a proteasome inhibitor, such as bortezomib, to see if this restored DUSP6 expression, or alternatively, treated with a protein translation inhibitor, such as tetracycline, to see if DUSP6 protein had a decreased half-life in 148R clones compared to parental A2780 cells.

If *DUSP6* mRNA was decreased in 148R clones, this would suggest that the loss of DUSP6 expression occurred at the genetic, epigenetic or transcriptional level, which could be further investigated. At the transcriptional level this could be caused by the loss of expression/function of a DUSP6 transcriptional activator. As well as being transcriptionally regulated by ETS-1 and ETS-2, DUSP6 can also be transcriptionally regulated by p53 (Ekerot *et al.*, 2008; Piya *et al.*, 2012). In addition, the *DUSP6* promoter region has also been shown to contain putative binding sites for a number of transcription factors including NF-kB and FoxO transcription factors (Ekerot *et al.*, 2008). Global gene expression could be analysed (e.g. via microarray analysis), to assess if 148R clones have a gene signature indicative of a deficiency in the aforementioned transcription factors. At the epigenetic level, DUSP6 expression could be lost via hypermethylation of the *DUSP6* promoter, which has been previously characterised in advanced PDAC (Xu *et al.*, 2005). 148R clones could be treated with a DNA methyl transferase inhibitor, such as 5-azacytidine, to see if this restored DUSP6 expression, which would indicate hypermethylation of the *DUSP6* promoter as a mechanism of DUSP6 loss. Finally, at the genetic level copy number variations in the *DUSP6* gene or mutations that cause a truncated DUSP6 protein, could cause a decrease in the expression of DUSP6. This could be investigated by Sanger DNA sequencing of the DUSP6 gene and FISH (fluorescence *in situ* hybridisation) assays.

6.3.2. Inhibition of DUSP6 via BCI

Whatever the mechanism of the loss of DUSP6 expression in 148R clones, its contribution to increased ERK phosphorylation and therefore AT13148 resistance, was worthy of extensive investigation. Initially, DUSP6 was manipulated in parental A2780 cells, to investigate if the loss of DUSP6 alone could recapitulate the AT13148 resistance phenotype, i.e. is DUSP6 loss alone sufficient to drive AT13148 resistance. Parental A2780 cells were treated with the dual DUSP1 and DUSP6 inhibitor BCI, to mimic the

loss of DUSP6 in 148R clones (Molina *et al.*, 2009). BCI was able to increase ERK 1/2 phosphorylation in a dose-dependent manner, thus highlighting the intimate link between DUSP6 and ERK 1/2 phosphorylation in parental A2780 cells (Figure 6.6). There was an exception to this; low concentrations of BCI (0.05 µM) paradoxically caused a decrease in ERK 1/2 phosphorylation. Unni and colleagues (Unni *et al.*, 2018), saw a similar phenomenon in the lung adenocarcinoma cell line A549, whereby a decrease in ERK 1/2 phosphorylation was seen with lower concentrations of BCI, but higher concentrations increased ERK 1/2 phosphorylation. This could perhaps be explained by the interplay between the increase in ERK 1/2 phosphorylation and subsequent increase in ERK 1/2 mediated negative feedback that would occur in response to DUSP6 inhibition by BCI.

Despite BCI increasing ERK 1/2 phosphorylation in parental A2780 cells, the combination of BCI with AT13148 did not generate resistance against AT13148 (Figure 6.8). However, this was not unexpected as there were a number of limitations in using BCI to mimic DUSP6 loss in parental A2780 cells; the most obvious being that BCI can also inhibit DUSP1 (Molina *et al.*, 2009; Korotchenko *et al.*, 2014). DUSP1 is exclusively localised in the nucleus and can also de-phosphorylate JNK and p38 MAPK, as well as ERK 1/2 (Kidger and Keyse, 2016). It's therefore likely that the phosphorylation of JNK and p38 MAPK was increased in parental A2780 cells treated with BCI. Indeed, Shojaee and colleagues (Shojaee *et al.*, 2015) showed that both JNK and p38 MAPK phosphorylation, as well as ERK 1/2 phosphorylation, increased in response to BCI in human pre-B ALL cells. In general, JNK and p38 MAPK are phosphorylated/activated in response to environmental stresses, and induce apoptosis upon activation (Morrison, 2012). Therefore, any survival advantage against AT13148, conferred by increased ERK 1/2 phosphorylation in BCI treated A2780 cells, might be offset by an increase in the phosphorylation of JNK and p38 MAPK.

It should also be taken into consideration that BCI has been shown to cause whole organism toxicity in a Zebrafish model, when used at concentrations approximately the same as the BCI IC_{50}, as determined by biochemical assays, for DUSP1 and DUSP6 (Korotchenko *et al.*, 2014). Since toxicity has not been observed in *DUSP1* and *DUSP6* knock-out mice, it seems likely that whole organism toxicity is caused by off-target

effects of BCI (Wu *et al.*, 2006; Maillet *et al.*, 2008). Furthermore, shojaee and colleagues (Shojaee *et al.*, 2015) demonstrated that that BCI caused a global reduction in cellular phospho-tyrosine in human pre-B ALL cells, giving further evidence of the off-target effects of BCI. Indeed, 0.10 µM BCI, when used as a single agent, did cause a slight reduction in the viability of parental A2780 cells (Figure 6.8). Therefore, any survival advantage gained from increased ERK 1/2 phosphorylation, might be overcome by BCI associated off-target effects.

6.3.3. Knockdown of DUSP6 using siRNA

The ability of DUSP6 loss alone to recapitulate the resistance phenotype in parental A2780 cells was also investigated using siRNA mediated KD of DUSP6. Initially, pooled siRNA was used to KD DUSP6, in a 4-day SRB cell viability assay, but this did not confer resistance against AT13148 (Figure 6.11). However, when using pooled DUSP6 siRNA, DUSP6 KD did not last over the course of a 4-day SRB cell viability assay (Figure 6.10). Furthermore, even when DUSP6 KD was at its peak, pooled DUSP6 siRNA failed to reduce DUSP6 expression to the level seen in 148R clones. Therefore, a 2-day SRB cell viability assay was performed, to compensate for the limited duration of DUSP6 KD. Additionally, individual DUSP6 siRNAs were used, to improve DUSP6 KD efficiency, and minimize off-targets effects (as discussed in section 6.2.4.3). Despite the KD of DUSP6 being more effectively maintained over the course of a 2-day SRB assay (Figure 6.13), DUSP6 KD via individual siRNAs did not generate resistance against AT13148 either (Figure 6.14). However, as with pooled DUSP6 siRNA, individual DUSP6 siRNAs were unable to decrease DUSP6 expression to the level seen in 148R clones, even when DUSP6 KD was at its peak. Consequently, the inability of DUSP6 KD, using both pooled and individual siRNA, to generate AT13148 resistance in parental A2780 cells, might be explained by experimental limitations: i.e. the inability of siRNA KD to cause a sufficient and sustained decrease in DUSP6 expression. It is worth considering the reasons for these experimental limitations, so that they might be overcome in future.

One such reason is that the conditions for siRNA transfection were not optimal. The conditions selected for siRNA KD were identified via a series of siRNA optimisation assay, however, under these conditions there was still some residual cell viability (~10%) in

cells transfected with death control siRNA, indicating incomplete siRNA transfection efficiency (Figure 6.9). This may, in part, explain why DUSP6 KD was insufficient in strength and duration. Since Lipofectamine 2000 was the only transfection reagent assessed in siRNA optimisation assays, a broader range of siRNA transfection reagents should also be evaluated to identify the most optimal siRNA transfection conditions, thus improving the KD of DUSP6 in parental A2780 cells.

It should also be considered that DUSP6 has several attributes which make its expression difficult to manipulate using siRNA. The half-life of both DUSP6 mRNA and protein is incredibly short at ~30 minutes and ~60 minutes respectively (Marchetti *et al.*, 2005; Blüthgen *et al.*, 2009). Larsson and colleagues (Larsson *et al.*, 2010) have shown that mRNA's with short half-life's, thus a high rate of turnover, are inherently resistant to KD with siRNA. Under these circumstances, mRNA that is degraded by siRNA can quickly be replaced. This therefore may explain why is was difficult to cause a strong and durable KD of DUSP6 using siRNA. In addition, the ERK 1/2 inducible expression of DUSP6 may make it difficult to KD with siRNA (Unni *et al.*, 2018). This is because as the expression of DUSP6 is decreased by siRNA there is an increase in ERK 1/2 activation, this in turn induces the transcription of *DUSP6* mRNA, which can overcome the effects of DUSP6 siRNA, causing a re-bound in DUSP6 expression.

As has been discussed, the experimental limitations of siRNA KD may explain why resistance against AT13148 was not generated in parental A2780 cells by DUSP6 siRNA KD. However, there was some evidence to suggest that this may be because the loss of DUSP6 alone was not sufficient to drive resistance to AT13148 in parental A2780 cells. This can be seen as DUSP6 KD, using either individual or pooled siRNA, despite not decreasing DUSP6 expression to the level seen in 148R clones, was able cause an increase in ERK 1/2 phosphorylation in parental A2780 cells, up to 24-28 hours post-transfection, similar to the level seen in 148R clones (Figure 6.10 & Figure 6.13). But this increase was lost at ≥ 48 hours post-transfection, which may, in part, be due to the aforementioned loss of DUSP6 KD over time. This was certainly the case 96-hours post transfection with pooled DUSP6 siRNA, where there was substantial loss of in the level of DUSP6 KD (Figure 6.10). However, there was not much difference, if any, between the level of DUSP6 KD at 24/28 hours and 48/52 hours post-transfection, and yet, ERK

1/2 phosphorylation was only increased at 24/28 hours post-transfection (highlighted in Figure 6.22). Furthermore, individual DUSP6 siRNA was able to cause an increase in ERK 1/2 phosphorylation at 4 hours post transfection, despite the level of DUSP6 KD being less than it was at 52 hours, where phosphorylation of ERK 1/2 was unchanged (highlighted in Figure 6.22). What this might suggest is that KD of DUSP6 alone did not induce resistance to AT13148 as it only caused a temporary increase in the phosphorylation of ERK 1/2, rather than the sustained increase required for AT13148 resistance. The inefficiencies in DUSP6 siRNA KD cannot entirely explain this, it's possible that other factors are required for a sustained increase in ERK 1/2 phosphorylation to drive resistance against AT13148.
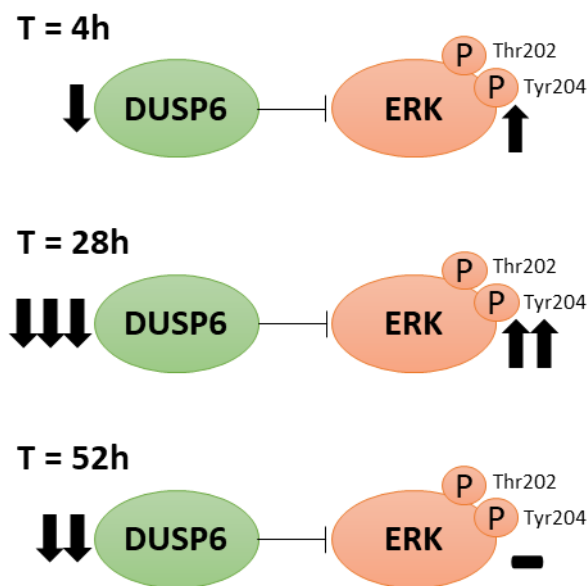
Figure 6.22: Discrepancy between the level of siRNA mediated DUSP6 KD and ERK 1/2 phosphorylation. Diagram is a graphical representation of DUSP6 expression and ERK 1/2 phosphorylation over a time-course, in response to KD of DUSP6 using individual siRNA's, as shown in Figure 6.13. Times shown indicate hours post-transfection. Phosphorylation of ERK 1/2 at 52 hours post-transfection was unchanged despite the level of DUSP6 KD being greater than what was seen at 4 hours post-transfection, where ERK 1/2 phosphorylation was increased. It's possible that other factors, other than loss of DUSP6, are required to cause sustained increase in ERK 1/2 phosphorylation, driving resistance against AT13148

Since ERK 1/2 is under tight regulatory control, the initial increase in ERK 1/2 phosphorylation in response to DUSP6 KD may lead to a compensatory increase in other negative feedback regulators of ERK 1/2, preventing a sustained increase in ERK 1/2 phosphorylation. This may be mediated by other DUSP proteins, as many of them are also inducible by ERK 1/2 activation, such as DUSP5 and DUSP7 (Kidger and Keyse, 2016., highlighted in Figure 6.23). Indeed, it has been observed that siRNA KD of DUSP proteins can cause compensatory increases in other DUSPs. Buffet and colleagues (Buffet *et al.*,

2017) showed that there was an increase in DUSP6 expression in response to the siRNA mediated KD of DUSP5 in the human thyroid cancer cell line 8505c. Additionally, Caunt and colleagues (Caunt *et al.*, 2008) demonstrated in Hela cells stimulated with PDBu, phorbol 12,12-dibutyrate, that siRNA KD of DUSP1 and DUSP2 caused a respective compensatory increase in *DUSP2* and *DUSP1* mRNA. Alternatively, upon DUSP6 KD ERK 1/2 mediated feedback could act upstream of the MAPK pathway, e.g. via ERK 1/2 mediated inhibitory phosphorylation of MEK 1/2, BRAF & CRAF, to overcome the initial increase in ERK 1/2 phosphorylation caused by DUSP6 KD (Eblen *et al.*, 2004; Dougherty *et al.*, 2005; Ritt *et al.*, 2010., highlighted in Figure 6.23). Disruption of these negative feedback loops, in addition to loss of DUSP6, may also be required to cause a sustained increase in ERK 1/2 phosphorylation, to drive resistance against AT13148. This could be investigated by analysing MEK 1/2 phosphorylation and the expression of inducible DUSPs in response to DUSP6 siRNA KD in parental A2780 cells. Furthermore, DUSP6 expression should be manipulated in A2780 cells using alternative techniques, such as CRISPR (clustered regularly interspaced short palindromic repeats)-mediated knock-out or shRNA, to cause a sufficient and durable decrease in DUSP6 expression, so that it can be definitively shown that DUSP6 loss alone is not sufficient to drive AT13148 resistance.
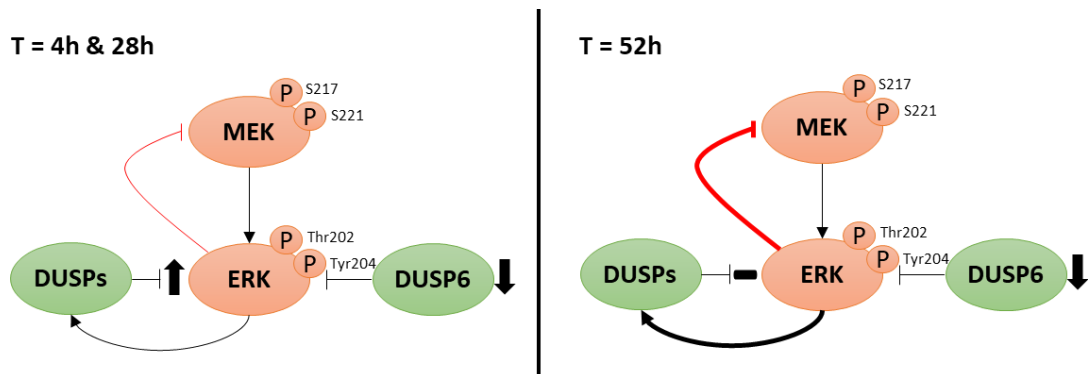
Figure 6.23: Potential increase in ERK 1/2 mediated negative feedback in response to individual DUSP6 siRNA KD. In A2780 cells, at 4 and 28-hours post-transfection DUSP6 KD causes an increase in ERK 1/2 phosphorylation, but this is lost at 52 hours post-transfection (shown in Figure 6.13). As shown in Figure 6.22, this cannot entirely be explained by the difference in the level of DUSP6 KD across these timepoints. It may be explained by ERK 1/2 mediated negative feedback; at 4 and 28-hours negative feedback is low and cannot not overcome the increase in ERK 1/2 phosphorylation caused by DUSP6 KD, but at 52 hours negative feedback has increased and overcome the initial increase in ERK 1/2 phosphorylation caused by DUSP6 KD. ERK 1/2 mediated negative feedback may work on two levels; increased expression of inducible DUSPs (e.g. DUSP5) or increased inhibitory phosphorylation of upstream components of the MAPK pathway (e.g. MEK 1/2).

6.3.4. Lentiviral mediated ectopic re-expression of DUSP6

To investigate if loss of DUSP6 was necessary, if not sufficient, for AT13148 resistance, DUSP6 was transiently re-expressed using a DUSP6 lentivirus in 148R-S cells, to assess if this could re-sensitise cells to AT13148. For the purposes of this discussion, results obtained using purified DUSP6 lentivirus will be focused on, as this caused the strongest and most durable re-expression of DUSP6. Whilst purified DUSP6 lentivirus did cause a decrease in the GI_{50} of 148R-S cells against AT13148, this was a < 2-fold decrease, and still represented an RF of > 5 (Figure 6.17). It should be noted, that the DUSP6 lentiviral experiments should be interpreted with some caution, as a limited number of independent experiments were performed. Additional biological replicates may have enabled greater statistical significance to be demonstrated, but it's likely that that magnitude of the effect would still be marginal.

However, as with DUSP6 siRNA KD, the ectopic re-expression in 148R-S cells was not sustained over the course of a 4-day SRB cell viability assay; at 48 hours post infection, ectopic DUSP6 expression matched the expression of DUSP6 in parental A2780 cells, but was decreased, compared to A2780 cells, at 120 hours post-infection (Figure 6.18). This could explain why the re-expression of DUSP6 did not re-sensitise 148R-S cells to AT13148. It is worth noting that it was always going to be difficult to transiently re-express DUSP6 at a sufficient level, due to its short half-life (Marchetti *et al.*, 2005). For this reason, a lentivirus was used rather than a standard mammalian expression vector (e.g. pcDNA3); lentiviral DNA integrates into the host genome, whereas a standard mammalian expression vector does not. Therefore, with a standard mammalian expression vector transgene DNA is not passed on to daughter cells, thus the expression of a protein with short half-life, such as DUSP6, would be rapidly lost. In contrast, since lentiviral DNA is passed on to daughter cells, assuming a high infection efficiency, the expression of a transgene, even one with short half-life, should be much more durable. However, even under optimised conditions, lentiviral infection efficiency is never 100%, and transient expression is lost over time, as was seen with ectopic expression of DUSP6 in 148R-S cells. This could be overcome by using a mammalian expression vector (viral or plasmid), which contains selectable marker for expression in mammalian cells, such as neomycin resistance, to generate 148R-S cells which stably re-express DUSP6.

Furthermore, DUSP6 should be under the control of an inducible promoter (e.g. Tet-on system), so that the expression of DUSP6 can be finely controlled.

Additional evidence as to why ectopic re-expression of DUSP6 did not re-sensitise 148R-S cells to AT13148, can be seen by looking at ERK 1/2 phosphorylation; re-expression of DUSP6 did not cause a sustained decrease in ERK 1/2 phosphorylation (Figure 6.18). At 48 hours post infection DUSP6 re-expression decreased the phosphorylation of ERK 1/2 to the level seen in parental A2780 cells, but at 120 hours post infection, whilst the phosphorylation of ERK 1/2 was still below that of 148R-S control cells, it was above the level seen in parental A2780 cells. A similar pattern was also seen in the phosphorylation of the ERK 1/2 substrate Elk-1 (Figure 6.18). This may be explained by the decrease in DUSP6 expression over this time period, i.e. the re-expression of DUSP6 was not sufficiently maintained to cause a sustained decrease in ERK 1/2 phosphorylation. But in parallel to this, there was an increase in MEK 1/2 phosphorylation, which peaked at 120 hours post-infection. What this might suggest is that in response to DUSP6 re-expression there was an initial decrease in ERK 1/2 phosphorylation, however, over-time there was an increase in MEK 1/2 phosphorylation, likely due to relief of ERK 1/2 mediated negative feedback, which prevented DUSP6 re-expression from causing a sustained decrease in ERK 1/2 phosphorylation, thus 148R-S cells were not re-sensitised to AT13148. Interestingly, a similar phenomenon has been observed by McCormick and colleagues (Phuchareon *et al.*, 2015), whereby ectopic expression of DUSP6 caused an increase in the phosphorylation of MEK 1/2 in HCC827 cells.

6.3.5. Contribution of FGFR signalling to AT13148 resistance

In many ways the results obtained from DUSP6 siRNA KD in parental A2780 cells and ectopic DUSP6 expression in 148R-S cells were similar; neither were able to generate the hypothesised phenotype: respectively, to re-capitulate or abolish AT13148 resistance. In addition, both suffered experimental limitations (e.g. duration of DUSP6 KD or re-expression), which may in part explain why the appropriate alteration to ERK 1/2 phosphorylation was not sustained over the course of an SRB cell viability assay, thus the hypothesised phenotype not generated. However, as discussed, there was also evidence suggesting that experimental limitations alone did not explain the inability to

cause a sustained increase or decrease in ERK 1/2 phosphorylation. Therefore, whilst the role of DUSP6 in AT13148 resistance cannot be dismissed, it was deemed likely that other factors contributed to ERK 1/2 phosphorylation and AT13148 resistance.

With this in mind, and due to the sensitivity to FGFR inhibition exhibited by most 148R clones (Figure 4.5 & Figure 4.11), the contribution of FGFR signalling to MAPK signalling was investigated, by assessing the MAPK pathway response to AZD4547, an FGFR inhibitor. Remarkably, there was a strong decrease in MEK 1/2 and ERK 1/2 phosphorylation in 148R-S, but not in A2780 and 148R-N (Figure 6.21). Interestingly, it also appeared that FGFR signalling preferentially activated the MAPK pathway over the PAM pathway within 148R-S cells, as AZD4547 only had a minimal effect upon AKT phosphorylation. This is consistent with what has been previously reported, as it has been shown that hyperactivation of FGFR signalling and FGFR inhibitor sensitivity are associated with a MAPK pathway gene signature (Nakanishi, Akiyama, *et al.*, 2015; Nakanishi, Mizuno, *et al.*, 2015).

It would therefore seem that the MAPK pathway has an increased dependency on FGFR signalling in 148R-S cells. This likely explains why 148R-S cells were much more sensitive to FGFR inhibition than A2780 and 148R-N cells (Figure 4.11). It may also explain why DUSP6 siRNA KD in parental A2780 cells did not generate AT13148 resistance; perhaps an increase in FGFR signalling is also required for a sustained increase in ERK 1/2 phosphorylation. It is well established that DUSP6 is an important negative feedback regulator of FGFR signalling. For example, DUSP6 knock-out mice exhibit phenotypes consistent with hyperactive FGFR signalling, and the DUSP6 inhibitor BCI was discovered as part of a screen to identify compounds that could hyperactivate FGFR signalling (Li *et al.*, 2007; Molina *et al.*, 2009). Therefore, a sustained increase in ERK 1/2 phosphorylation may not be mediated by increased FGFR signalling alone due DUSP6 mediated negative feedback, and as discussed, loss of DUSP6 alone might be unable to cause a sustained increase due to increased ERK 1/2 mediated negative feedback upstream the MAPK pathway (Figure 6.24A, B). However, together, whilst there would still be ERK 1/2 mediated negative feedback (exemplified by the decrease in MEK 1/2 phosphorylation in 148R-S; Figure 4.17), in the absence of DUSP6, this might be

sufficient to cause a sustained increase in ERK 1/2 phosphorylation, driving AT13148 resistance (Figure 6.24C).
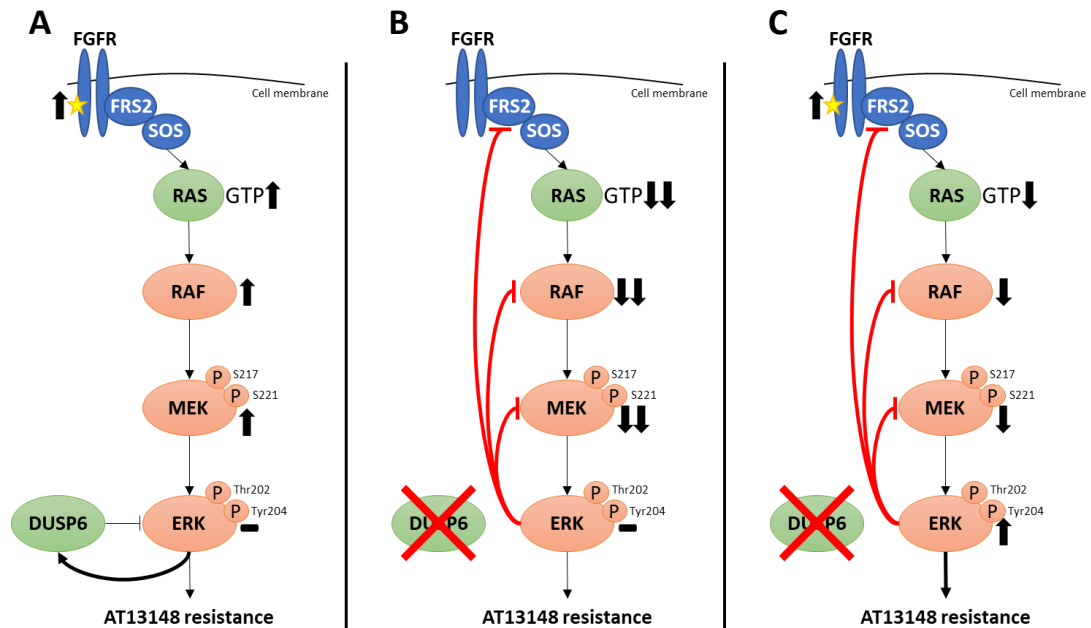
Figure 6.24: Potential cooperation of FGFR signalling and DUSP6 loss to generate AT13148 resistance. Diagram highlights how increased FGFR signalling (e.g. via mutation or increased expression of FGFR's) and DUSP6 loss might cooperate to increase ERK 1/2 phosphorylation and drive AT13148 resistance. **(A)** Increased FGFR signalling alone might increase activation of upstream components of the MAPK pathway but not ERK 1/2 due to negative feedback regulation by DUSP6. **(B)** Any initial increase in ERK 1/2 phosphorylation caused by loss of DUSP6 alone, may be overcome by ERK 1/2 mediated negative feedback on upstream components of the MAPK pathway. **(C)** Together, increased FGFR signalling and DUSP6 loss might cooperate to cause a sustained increase in ERK 1/2 phosphorylation, driving AT13148 resistance. In this scenario, ERK 1/2 mediated negative feedback would still exist, but be sufficiently overcome.

For the reasons outlined above, the contribution of FGFR signalling to AT13148 resistance, either alone or in combination with DUSP6 loss, warrants further investigation. Combination SRB cell viability assays should be conducted in 148R-S cells, in which low concentrations of AZD4547 are combined with a standard titration of AT13148. If AZD4547 sensitised 148R-S cells to AT13148 this would suggest that FGFR is driving resistance. Interestingly, preliminary combination assays, as described, have been performed, and have shown some re-sensitisation to AT13148 caused by AZD4547 (data not shown). If the resistance mechanism shown in Figure 6.24C is correct, and DUSP6 re-expression is also required for sensitisation, it may be necessary to ectopically express DUSP6 during these combination assays to fully re-sensitise 148R-S cells to AT13148. Furthermore, FGFR signalling could be activated in parental A2780 cells to assess if this alone, or in combination with DUSP6 siRNA KD, could generate resistance

against AT13148. Since the exact mechanism by which 148R-S cells have acquired an increased dependency on FGFR is unknown (e.g. increased FGFR expression), this could be undertaken by using an FGF ligand, such as FGF2. This approach was used by Yadav and colleagues (Yadav *et al.*, 2012), with great success, to validate hyperactive FGFR signalling as a resistance mechanism to vemurafenib in *BRAF* V600E mutant melanoma.

In summary, the data in this chapter showed there was a dramatic decrease in the expression of DUSP6 in 148R-K, N & S. The loss of DUSP6 expression was subsequently hypothesised as a mechanism of increased ERK 1/2 phosphorylation, thus AT13148 resistance. This was investigated by siRNA KD of DUSP6 in parental A2780 cells and transient ectopic expression of DUSP6 in 148R-S cells, of which neither were able to respectively re-capitulate or abolish the resistance phenotype. These results may, in part, be explained by experimental limitations of these techniques, but it is likely that other factors may be required for AT13148 resistance. To this end, 148R-S cells were found to have an increased dependency on FGFR signalling for MAPK pathway activation. Therefore, the contribution of FGFR signalling to AT13148 resistance, alone or in combination with DUSP6 loss, warrants further investigation.

Chapter 7

General discussion

7. General discussion

7.1. Introduction

The AGC family of protein kinases regulate growth, proliferation, survival and migration, and as such, AGC kinases are often deregulated in cancer, driving oncogenesis. Due to their role in oncogenesis there are a number of agents that are currently in clinical development targeting AGC kinases, the majority of which are AKT inhibitors (Prêtre and Wicki, 2018). AT13148 was discovered as part of a drug discovery programme between the ICR and Astex Pharmaceuticals, to identify potent and selective AKT inhibitors (Yap *et al.*, 2012). However, whilst inhibiting AKT1 and AKT3, AT13148 was also shown to inhibit other AGC kinases: PKA, ROCK1, ROCK2, p70S6K, SGK3 and RSK1, of which PKA, p70S6K and ROCK1/2, were inhibited more potently than AKT (Yap *et al.*, 2012). Most inhibitors targeting kinases within the AGC family (e.g. AKT inhibitors), that are currently in clinical development, show a much greater degree of selectivity, versus AT13148, but have been shown to have limited efficacy when used as a monotherapy (Prêtre and Wicki, 2018). It was hoped that by targeting several AGC kinases, both within and outside the PAM pathway, AT13148 might have an improved efficacy, when compared to more selective AKT inhibitors and other inhibitors of AGC kinases. For example, as discussed in section 1.5, by inhibiting several kinases of the PAM pathway (AKT, p70S6K and SGK3), AT13148 may provide a more robust inhibition of the pathway, thus have a greater efficacy in treating PAM pathway dysregulated cancers. For these reasons, AT13148 progressed to clinical development; AT13148 has recently completed a phase 1 clinical trial, the results of which are yet to be published (*clinicaltrials.gov – identifier: NCT01585701*). However, acquired drug resistance is a major obstacle in the success of many targeted cancer therapies, and likely to occur to AT13148, despite the predicted improved efficacy afforded by targeting several AGC kinases simultaneously.

Pre-clinical studies of acquired drug resistance are effective at identifying drivers and mechanisms of resistance, often with clinical relevance, providing a means of accurately studying acquired resistance whilst a drug is in clinical development (Garraway and Jänne, 2012). In doing so, these studies can help identify therapeutic strategies to overcome acquired resistance, and facilitate the stratification of patients based on

predicted drug sensitivity (Garraway and Jänne, 2012). Currently, there are no publications that report the identification of acquired mechanisms of resistance to AT13148. Therefore, the primary aim of this thesis was to identify and validate acquired mechanisms of resistance to AT13148 using pre-clinical cell line models. The work presented in this thesis identified ERK 1/2 as a driver of AT13148 resistance and several therapeutic strategies to potentially overcome AT13148 resistance. These findings may assist in the future clinical development of AT13148 and potentially improve the efficacy of AT13148 treatment, should AT13148 progress to new drug approval.

This chapter discusses the main findings of this thesis, their implications to the future clinical development of AT13148, and how future work might best be conducted to further our understanding of AT13148 resistance, to improve the efficacy of AT13148 in the clinic.

7.2. Summary of main findings and future work

7.2.1. Increased ERK 1/2 phosphorylation as a driver of AT13148 resistance

In chapter 3, it was first shown in A2780-148R cells that there was increased phosphorylation of ERK 1/2 in parallel with a decrease in the phosphorylation of MEK 1/2. However, the magnitude of the increase in ERK 1/2 phosphorylation did vary across experiments; in basal western blot experiments there was only a slight increase, but in dose-response western blots, in untreated A2780-148R cells, there was a much more substantial increase in ERK 1/2 phosphorylation (Figure 3.11, Figure 3.13 & Figure 3.15). This suggested that there might be distinct sub-populations cells of within the A2780-148R population, with differing levels of ERK 1/2 phosphorylation, that were selected for over-time/under different experimental conditions.

Indeed, in chapter 4, several isogenic sub-clones: 148R-K, N & S, derived from A2780-148R cells, exhibited a marked increase in ERK 1/2 phosphorylation, much more so than was seen in A2780-148R, and with a greater degree of consistency across experiments (Figure 4.17). This increase in ERK 1/2 phosphorylation in 148R clones was greatest in 148R-S, followed by 148R-K, then 148R-N (Figure 4.17). As with A2780-148R, increased ERK 1/2 phosphorylation was seen in parallel with a decrease in MEK 1/2 phosphorylation in 148R clones, but again, this was to a much greater extent than was

seen in A2780-148R (Figure 4.17). Moreover, in 148R-K and 148R-S, increased ERK 1/2 phosphorylation corresponded with an increase in the phosphorylation of Elk-1, an ERK 1/2 substrate, which therefore could be used as a biomarker of ERK 1/2 activation in 148R-K and 148R-S (Figure 4.17).

In addition to ERK 1/2 phosphorylation being increased at a basal level, ERK 1/2 phosphorylation also exhibited a response to AT13148 in A2780-148R and 148R clones, as well as in parental A2780 cells (Figure 3.13 & Figure 5.4). Whilst there were some inconsistencies between datasets, in A2780 cells ERK 1/2 phosphorylation was increased at higher concentrations of AT13148 but was either decreased or unchanged at lower concentrations; whereas in A2780-148R and 148R clones, the phosphorylation of ERK 1/2 tended to progressively increase with increasing concentrations of AT13148 (Figure 3.13 & Figure 5.4). This response was much more notable in 148R clones, particularly 148R-S. Since AT13148 is not known to directly target the MAPK pathway, it is currently unknown how AT13148 may elicit this response. However, as highlighted in Figure 3.17A & B, targets of AT13148 are known to regulate the MAPK pathway, the inhibition of which could be responsible for the response of ERK 1/2 phosphorylation to AT13148. A greater understanding of how AT13148 regulates ERK 1/2 phosphorylation could aid the clinical development of AT13148 and should therefore be further investigated in future work. For example, PKA and AKT impart an inhibitory phosphorylation on CRAF at S259, of which there are commercial antibodies available for detection by western blot analysis (Zimmermann and Moelling, 1999; Pursiheimo *et al.*, 2002; Dumaz *et al.*, 2006). It would be interesting to see if there was a reduction in S259 CRAF phosphorylation in response to AT13148; if this was the case, it would suggest that the inhibition of PKA and/or AKT by AT13148, and subsequent decrease in inhibitory phosphorylation of CRAF, is responsible for the AT13148 mediated increase in ERK 1/2 phosphorylation (Figure 7.1A & B).
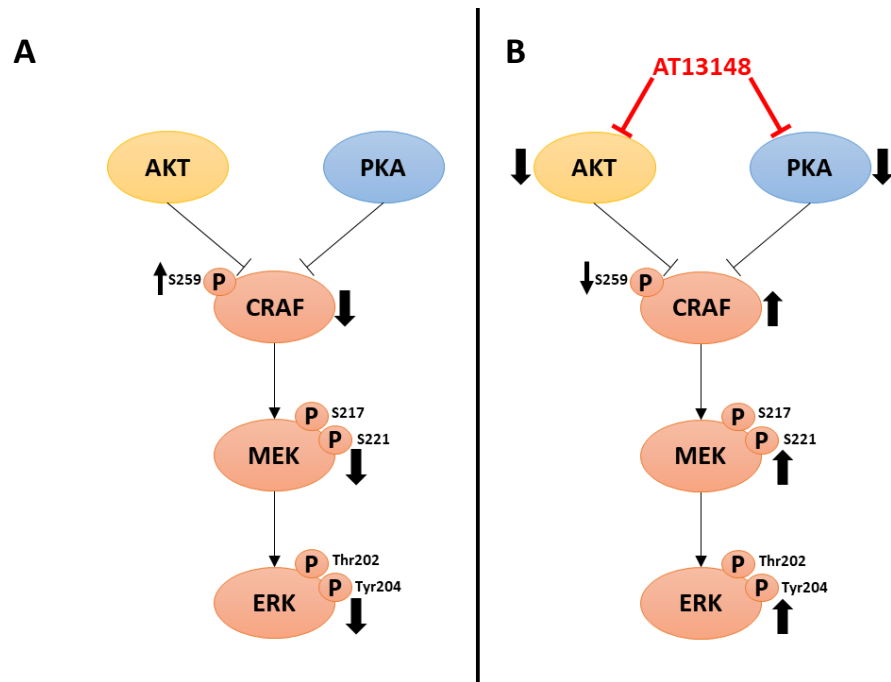
Figure 7.1: Relief of CRAF inhibition as a mechanism of increased ERK 1/2 phosphorylation in response to AT13148. (A) In untreated cells, AKT and PKA can phosphorylate CRAF at S259, inhibiting CRAF activation and activation of downstream components of the MAPK pathway. **(B)** The inhibition of AKT and PKA by AT13148 might cause a decrease in S259 CRAF phosphorylation, increasing the activation of CRAF and downstream components of the MAPK pathway, such as ERK 1/2.

Nonetheless, the consequence of increased basal ERK 1/2 phosphorylation, combined with the aforementioned ERK 1/2 response to AT13148, was that ERK 1/2 phosphorylation was much greater in A2780-148R and 148R clones, across all concentrations of AT13148 used. It was therefore reasoned that ERK 1/2 might act as a driver of resistance to AT13148. Indeed, in chapter 5, the combination of AT13148 with the ERK inhibitor GDC-0994 demonstrated synergistic growth inhibition in 148R-K and 148R-S cells, re-sensitising 148R-K and 148R-S to AT13148 (Figure 5.5 & Figure 5.6). In both 148R-K and 148R-S, the greatest re-sensitisation was seen when AT13148 was combined with respective GI_{20} concentrations of GDC-0994, where the combination lowered the GI_{50} against AT13148 ~7-fold, to approximately the same GI_{50} value shown by A2780 to AT13148 (Figure 5.5). Western blot analysis showed that respective GI_{20} concentrations of GDC-0994 decreased Elk-1 phosphorylation in 148R-K and 148R-S, to approximately the same level as parental A2780 cells, if not slightly below (Figure 5.7). Therefore, the re-sensitisation and synergy caused by the combination of AT13148 and GDC-0994, provided evidence that increased activation of ERK 1/2 was acting as a driver of AT13148 resistance in 148R-K and 148R-S. This was further validated in 148R-S, as an

additional ERK inhibitor, SCH772984, also demonstrated synergy with AT13148 and re-sensitised 148R-S cells (Figure 5.8). Interestingly, parental A2780 cells were also sensitised to AT13148 by the synergistic combination with GDC-0994 or SCH772984, suggesting that the response of ERK 1/2 phosphorylation in A2780 cells (in response to AT13148), may cause a level of intrinsic resistance to AT13148 (Figure 5.5, Figure 5.6 & Figure 5.8).

It should be noted that the sensitisation to AT13148 caused by ERK inhibition was attenuated at higher concentrations of AT13148 in A2780, 148R-K and 148R-S (Figure 5.5, Figure 5.6 & Figure 5.8). This could be due to the experimental set-up; ERK inhibitors may be unable to sufficiently inhibit ERK 1/2 over the 96-hour drug treatment during a standard SRB cell viability assay, which in turn attenuated sensitisation to AT13148 at higher concentrations. Western blot analysis only assessed the inhibition of ERK 1/2 by GDC-0994 at 4 hours, therefore combination assays should be repeated to assess ERK inhibition at additional time points to ensure ERK inhibition is durable (Figure 5.7). Alternatively, if inhibition of ERK was shown to be sustained, it's possible that other drivers of AT13148 resistance may co-exist with ERK 1/2, the inhibition of which may also be required to fully re-sensitise cells to AT13148.

Combinations assays also provided evidence of how ERK 1/2 may contribute to AT13148 resistance. In 148R clones, the combination of AT13148 and GDC-0994 was able to cause a greater decrease in S6RP phosphorylation than that seen with AT13148 alone (Figure 5.7). In chapter 4, S6RP phosphorylation was shown to be refractory to inhibition by AT13148 in 148R clones (Figure 4.14). Therefore, ERK 1/2 might act as driver of AT13148 resistance, at least in part, by maintaining phosphorylation of S6RP. To be more precise, in 148R clones, it would seem that ERK 1/2 can compensate for the AT13148 mediated inhibition of p70S6K, by maintaining the phosphorylation of S6RP. The potential mechanisms of how ERK 1/2 might facilitate the maintenance of S6RP phosphorylation were discussed in section 5.3 and highlighted in Figure 5.12.

The maintenance of S6RP phosphorylation alone might make a significant contribution to AT13148 resistance, due to regulation of protein synthesis driven through S6RP, a process that cancer cells are often dependent upon for their growth and survival (Grzmil and Hemmings, 2012). However, it should also be considered that PRAS40

phosphorylation was also maintained in response to AT13148 in 148R clones, and that ERK 1/2, either directly or via its substrate RSK, can phosphorylate several substrates of the AT13148 targets AKT and p70S6K, many of which are highlighted in Figure 7.2 (Figure 4.14; Mendoza, Er and Blenis, 2011). Consequently, in 148R-K and 148R-S, ERK 1/2 could potentially drive AT13148 resistance by maintaining the phosphorylation of several substrates of AKT and p70S6K, including S6RP, rendering the PAM pathway refractory to AT13148, driving growth and survival. Therefore, in future, western blot analysis should be conducted to evaluate if the phosphorylation of other AKT and p70S6K substrates is also maintained in response to AT13148, and if so, whether ERK inhibition can overcome this. Alternatively, global gene expression could be analysed (e.g. by using gene microarray analysis or RNA sequencing) in A2780 and 148R clones, both untreated and treated with AT13148, to investigate if a PAM pathway gene signature could be maintained in the presence of AT13148 (Heinonen *et al.*, 2008; Zhang *et al.*, 2017)
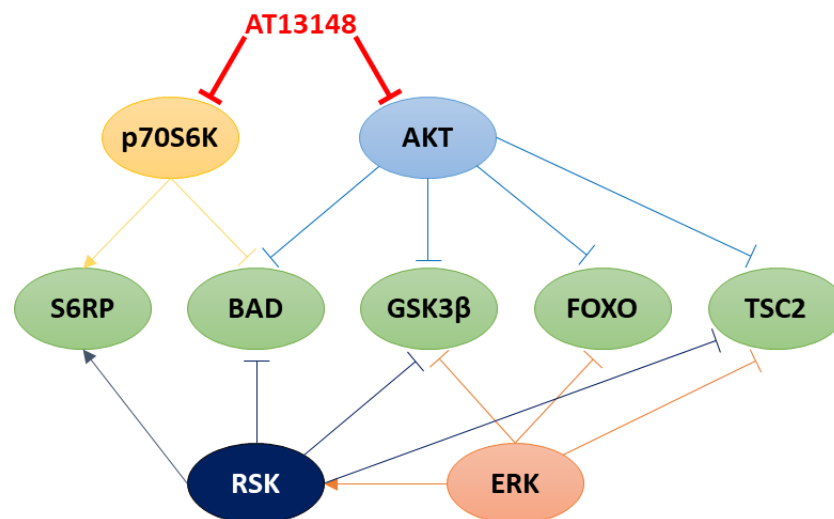
Figure 7.2: Model to show how ERK 1/2 may compensate for the inhibition of AKT and p70S6K by AT13148. Diagram highlights how ERK 1/2, either directly or via RSK, might compensate for the inhibition of AKT and p70S6K by AT13148. ERK 1/2 and RSK share many of the same substrates as AKT and p70S6K, therefore increased activation of ERK 1/2, either at a basal level or in response to AT13148, could enable the phosphorylation of AKT and p70S6K substrates to be maintained in response to AT13148. This has been shown with the p70S6K substrate S6RP, as combining AT13148 with an ERK inhibitor was able to overcome refractory S6RP phosphorylation in response to AT13148 in 148R clones (Figure 5.7).

Interestingly, 148R-K and 148R-S were also shown to have low-level cross-resistance to the allosteric AKT inhibitor MK2206, exhibiting RF values of ~4 and ~6 respectively (Figure 4.13). However, in contrast to AT13148, in 148R-S cells (148R-K was not assessed) western blot analysis did not reveal any maintenance in the phosphorylation of components of the PAM pathway (S6RP, PRAS40 & GSK3β) in response to the MK2206

(Figure 4.16). If the basal increase in ERK 1/2 phosphorylation alone was responsible for the maintenance of S6RP phosphorylation in response to AT13148, and potentially other PAM pathway components, then one would have also expected to see this response to MK2206.

This suggests that the maintenance of S6RP phosphorylation, and possibly other PAM pathway components, could be unique to AT13148 and not seen with other inhibitors of the PAM pathway, such as MK2206. This might be due to the further induction of ERK 1/2 phosphorylation mediated by AT13148 in 148R clones (Figure 5.4). However, since AKT can cross-inhibit the MAPK pathway, future studies should investigate if MK2206 can also increase ERK 1/2 phosphorylation (Zimmermann and Moelling, 1999; Guan *et al.*, 2000). If MK2206 was shown not to increase ERK 1/2 phosphorylation, it would suggest that the maintenance of S6RP phosphorylation in response to AT13148 was dependent upon the induction of ERK 1/2 phosphorylation. In addition, combination SRB cell viability assays should be performed with MK2206 and ERK inhibitors, to assess the contribution of ERK 1/2 to MK2206 cross-resistance. Despite, the lack of PAM pathway maintenance, ERK 1/2 could still contribute to MK2206 via an alternative mechanism, such as enabling a functional by-pass of the PAM pathway (e.g. maintenance of cell cycle progression), which could also be relevant to AT13148 resistance.

In summary, increased basal ERK 1/2 phosphorylation appeared to act as a driver of acquired AT13148 resistance in 148R-K and 148R-S, although other unidentified drivers may also exist. ERK 1/2 phosphorylation was also further enhanced upon AT13148 exposure, which is likely to be important for AT13148 resistance. ERK 1/2 may act as driver of AT13148 resistance by maintaining the phosphorylation of S6RP, and potentially other components of the PAM pathway, in the presence of AT13148.

7.2.2. Cross-resistance to ROCK inhibition

Another major finding presented in this thesis was cross-resistance to ROCK inhibition. This was initially observed in chapter 3, where A2780-148R cells were shown to be cross-resistant to the ROCK inhibitors GSK429286A and GSK269962 (Figure 3.5). The cross-resistance to these ROCK inhibitors, exhibited by A2780-148R, was quite substantial, particularly against GSK269962, which had the greatest potency against ROCK1 and 2,

where A2780-148R was shown to have an RF value of 86.00 (Figure 3.5; Lotz-Jenne *et al.*, 2016). Cross-resistance to GSK269962 was also seen in 148R clones, which had RF values between 11.42 and 168.77 (Figure 4.3). Furthermore, across A2780, A2780-148R and 148R clones, the GI_{50} values for GSK269962 showed strong positive correlation with AT13148 GI_{50} values (Figure 4.3). Due to the potent inhibition of ROCK1 & 2 by AT13148, this suggests that for AT13148 resistance to develop the inhibition of ROCK1 & 2 must be overcome.

The exact mechanism(s) by which ROCK1 & 2 inhibition has been overcome, has not been elucidated. In both A2780-148R and 148R clones, the ROCK pathway seemed to be equally inhibited in response to AT13148, when compared to parental A2780 cells, as indicated by a decrease in the phosphorylation of the ROCK substrate MYPT1 (Figure 3.12 & Figure 4.15). This data alone would suggest that the ROCK pathway has been by-passed in A2780-148R and 148R clones; i.e. A2780-148R and 148R clones have activated another signalling pathway, to drive growth and survival in the presence of ROCK inhibition. However, as discussed in section 3.3, there are issues with using the phosphorylation of MYPT1, alone, as a readout of ROCK pathway inhibition, mostly concerning the phosphorylation of MYPT1 by alternative kinases, such as MRCK (Wilkinson *et al.*, 2005). Consequently, the response of MYPT1 phosphorylation to AT13148 may be misleading; not giving an accurate reflection of the response of the ROCK pathway to AT13148. Other ROCK substrates are also phosphorylated by alternative kinases and so would present a similar issue when used as a biomarker of ROCK inhibition (Kümper *et al.*, 2016). Therefore, the response of a range of ROCK pathway substrates; such as MLC, LIMK and cofilin, to AT13148, should be investigated in future, in order to more accurately determine the response of the ROCK pathway to AT13148, to determine how ROCK inhibition has been overcome in AT13148 resistance.

Since ERK 1/2 was the only driver of AT13148 resistance identified in the work presented in this thesis, it should be considered that ERK 1/2 may also contribute to cross-resistance to ROCK inhibition. Indeed, this may be in part how ERK 1/2 contributes to AT13148 resistance. Interestingly, ERK 1/2 is known to phosphorylate and activate myosin light chain kinase (MLCK), which in turn can phosphorylate the ROCK substrate MLC2 (Klemke *et al.*, 1997). Therefore, increased ERK 1/2 phosphorylation could

contribute to ROCK cross-resistance, and AT13148 resistance, by activating MLCK, rendering MLC2 phosphorylation refractory to ROCK inhibition (Figure 7.3). Maintenance of phosphorylated MLC2 might be important for ROCK cross-resistance/AT13148 resistance, as MLC2 positively regulates actin-myosin contractility, which is required for cell cycle progression by providing the contractile strength for cytokinesis (Matsumura, 2005). However, phosphorylation and activation of MLCK by ERK 1/2 is currently poorly understood (Tanimura and Takeda, 2017)
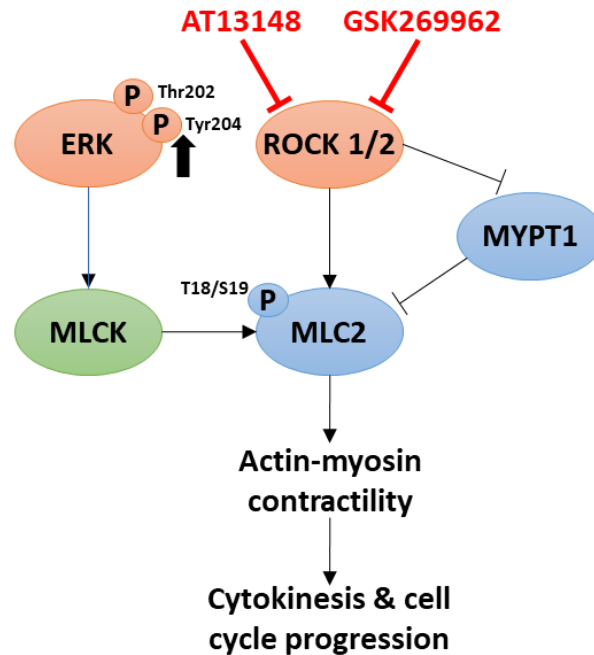
Figure 7.3: Potential contribution of ERK 1/2 to ROCK cross-resistance. Diagram shows that ERK 1/2 can activate MLCK, which in turn can phosphorylate the ROCK substrate MLC2. Therefore, increased ERK 1/2 phosphorylation, in 148R clones, might render MLC2 phosphorylation refractory to ROCK inhibition, thus facilitate actin-myosin contractility and cell cycle progression in the presence of a ROCK inhibitor.

Cell viability assays, in which GSK269962 is combined with an ERK inhibitor, would enable the contribution of ERK 1/2 activity to ROCK cross-resistance to be determined. If ERK inhibition was able to re-sensitise 148R clones to GSK269962 it would suggest that increased ERK 1/2 phosphorylation was responsible for ROCK cross-resistance. Furthermore, it would suggest that ERK 1/2 acts as a driver of AT13148 resistance, in 148R clones, by overcoming ROCK inhibition by AT13148. This should be an immediate focus of any future work, as a lack of understanding of the mechanism of ROCK cross-resistance, and its relevance to AT13148 resistance, is a limitation in the work presented in this thesis. Moreover, since AT13148 could potentially be used in the clinic as a ROCK

inhibitor (e.g. in pancreatic cancer), understanding ROCK cross-resistance may have clinical relevance (Rath *et al.*, 2018).

7.2.3. Loss of DUSP6 as a mechanism of AT13148 resistance

Due to the identification of increased ERK 1/2 phosphorylation as a driver of acquired AT13148 resistance, the focus of chapter 6 was to investigate the mechanism by which ERK 1/2 phosphorylation had been upregulated. For the following reasons a candidate approach was undertaken, focusing on the DUSP sub-family of ERK 1/2 phosphatases: 1) in 148R clones, increased ERK 1/2 phosphorylation existed in parallel with a reduction in phosphorylation of MEK 1/2; 2) the phosphorylation of ERK 1/2 was refractory to MEK inhibition in 148R clones (Figure 4.17 & Figure 5.2). Therefore, since MEK 1/2 is the only known kinase responsible for ERK 1/2 phosphorylation, it was deemed likely that the loss of an ERK 1/2 phosphatase, of which the DUSP sub-family is the most well characterised, was responsible for the increase in ERK 1/2 phosphorylation observed in 148R clones.

Indeed, this proved to be a successful approach, as it was shown that there was a drastic loss of DUSP6 expression in 148R-K, N & S (Figure 6.4). Subsequently, DUSP6 siRNA KD was performed in parental A2780 cells, to see if this caused a sustained increase in ERK 1/2 phosphorylation and AT13148 resistance. Conversely, a DUSP6 lentivirus was used to ectopically re-express DUSP6 in 148R-S cells, to see if this restored ERK 1/2 phosphorylation to the level seen in parental A2780 cells and re-sensitised 148R-S to AT13148. Neither of these experiments achieved their desired outcome; DUSP6 siRNA KD did not induce AT13148 resistance in parental A2780 cells, nor did ectopic re-expression of DUSP6 sensitise 148R-S cells to AT13148 (Figure 6.14 & Figure 6.20). Furthermore, both experiments only caused a temporary respective increase or decrease in ERK 1/2 phosphorylation, which was lost at later timepoints (Figure 6.10, Figure 6.13 & Figure 6.18). This may be due to both experiments failing to cause a sustained manipulation to DUSP6 expression, as was discussed in sections 6.3.3 & 6.3.4 (Figure 6.10, Figure 6.13 & Figure 6.18). Therefore, in order to definitively exclude loss of DUSP6 alone as a mechanism of AT13148 resistance, these experiments should be repeated using alternative techniques, to cause a more sustained decrease or increase

in DUSP6 expression. CRISPR could be used to cause a stable knockout of DUSP6 in parental A2780 cells and DUSP6 could be stably re-expressed in 148R-S cells, by using an expression vector containing a selectable marker for expression in mammalian cells.

However, despite the limitations of these experiments, there was evidence to suggest that the loss of DUSP6 alone might not be sufficient for AT13148 resistance, which was discussed at length in sections 6.3.3 & 6.3.4. It would appear that other factors, in addition to DUSP6 loss, are required to cause a sustained increase in ERK 1/2 phosphorylation, thus generating AT13148 resistance. This is likely due to the powerful negative feedback control of the MAPK pathway in parental A2780 cells and 148R clones. Evidence for this can be seen as the inhibition of ERK, by GDC-0994, was able to cause a substantial increase in MEK 1/2 phosphorylation, in both A2780 and 148R clones (Figure 5.3). This might explain why DUSP6 KD, in parental A2780 cells, only caused a temporary increase in ERK 1/2 phosphorylation, as this could be overcome by increased ERK 1/2 mediated negative feedback, and why DUSP6 re-expression, in 148R-S cells, only caused a temporary decrease in ERK 1/2 phosphorylation, as this could be overcome by a relief in ERK 1/2 mediated negative feedback. Direct evidence of this can be seen as ectopic expression of DUSP6 in 148R-S cells caused an increase in MEK 1/2 phosphorylation, which was likely the reason why increased ERK 1/2 phosphorylation was not sustained (Figure 6.18).

7.2.4. FGFR signalling and AT13148 resistance

It was reasoned that FGFR signalling could potentially play a role in causing a sustained increase in ERK 1/2 phosphorylation, thus AT13148 resistance, due to the sensitivity to AZD4547, an FGFR inhibitor, that had been observed in A2780-148R and most 148R clones (Figure 3.6, Figure 4.5 & Figure 4.11). Furthermore, it was shown that AZD4547 was able to cause a decrease in MEK 1/2 and ERK 1/2 phosphorylation in 148R-S cells, but not in parental A2780 cells or 148R-N, which was cross-resistant to AZ4547 (Figure 6.21). This suggested that in 148R-S cells ERK 1/2 phosphorylation was dependent on FGFR signalling. Taking this into account, a new putative mechanism of AT13148 resistance was established, in which increased FGFR signalling, yet to be defined, and loss of DUSP6 combine to cause a sustained increase in ERK 1/2 phosphorylation, driving

AT13148 resistance in 148R clones, such as 148R-S. As highlighted in Figure 6.24, these two changes could cooperate to cause a sustained increase in ERK 1/2 phosphorylation, by compensating for the increase in ERK 1/2 mediated negative feedback that would be caused by either change alone. The investigation of this putative mechanism of resistance should be focused upon in future work, which was discussed in section 6.3.5. For example, by performing cell viability combination assays, with AT13148 and AZD4547, on 148R-S cells that ectopically re-express DUSP6.

7.2.5. Alternative mechanism of AT13148 resistance in 148R-N cells

Throughout this thesis 148R-N cells appeared to have a distinctive phenotype, when compared to other 148R clones. For example, 148R-N had the greatest level of resistance to AT13148 with an RF value of 20.31, ~2-fold greater than 148R-K and 148R-S (Figure 4.10). Not only did 148R-N have the greatest resistance, but also responded to AT13148 in a distinctive manner, so much so that the GI_{50} of AT13148 could not be determined accurately by non-linear regression, as was discussed in section 4.3.1 (Figure 4.10). In addition, unlike other 148R clones, 148R-N lacked any sensitivity to the FGFR inhibitor AZD4547, in fact, 148R-N displayed cross-resistance to AZD4547 (Figures 4.5 & 4.11). Most importantly, in contrast to 148R-K and 148R-S, 148R-N was not re-sensitised to AT13148 by the ERK inhibitor GDC-0994, despite 148R-N also exhibiting increased ERK 1/2 phosphorylation (Figure 4.17 & Figure 5.5). Together, this suggests that there is an alternative driver/mechanism of resistance to AT13148 in 148R-N.

An alternative driver of AT13148 resistance is yet to elucidated for 148R-N, but there is evidence to suggest that it may be proximal to AKT. 148R-N exhibited increased phosphorylation of AKT and GSK3β, an AKT substrate, as well as ~27-fold cross-resistance to the AKT inhibitor MK2206, versus parental A2780 cells, much greater than the level of MK2206 cross-resistance seen in 148R-K and 148R-S (Figure 4.12 & Figure 4.13). Furthermore, the phosphorylation of GSK3β was partially refractory to MK2206 in 148R-N (Figure 4.16). However, AKT phosphorylation was equally inhibited by MK2206, when compared to parental A2780 cells, which suggested that GSK3β phosphorylation was maintained independently of AKT (Figure 4.16). This might be via the increased activation or expression of SGK, since as discussed in section 4.3.2, AKT and SGK have

overlapping substrate specificities, including GSK3β (Bruhn *et al.*, 2010, 2013; Figure 7.4). Therefore, an increased activation/expression of SGK could enable AKT inhibition to be overcome, driving MK2206 cross-resistance, and possibly contributing to AT13148 resistance in 148R-N cells (Figure 7.4). It should be noted that there are three isoforms of SGK, of which SGK3 is known to be inhibited by AT13148, thus inhibition of AKT is more likely be by-passed by increased activation/expression of SGK1 and SGK2. The mechanisms by which SGK activation may be increased are highlighted in Figure 4.19 & Figure 7.4 and include increased activation of upstream regulators such as PI3K.
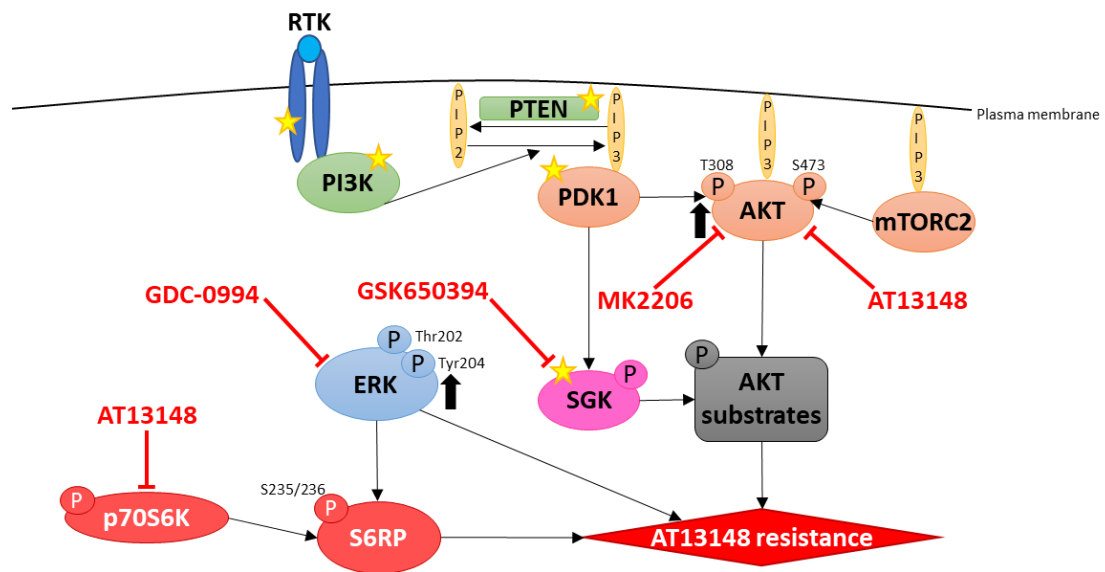
Figure 7.4: Summary of the potential mechanisms of AT13148 resistance in 148R-N. Diagram depicts how SGK could contribute to AT13148 resistance by enabling the by-pass of AKT inhibition. This could be caused by increased expression or activation of SGK (marked with a star), or alterations in the upstream regulators of SGK activation (also marked with a star). This may act alone, or combination with increased ERK 1/2 phosphorylation, to drive AT13148 resistance in 148R-N cells. The contribution of SGK to AT13148 resistance could evaluated by using the SGK inhibitor GSK650394 in combination with AT13148.

Aside from western blotting for additional AKT and SGK substrates, as discussed in section 4.3.2, the role of SGK in AT13148 resistance could be investigated by performing combination assays with AT13148 and an SGK inhibitor. If SGK inhibition was able to sensitise 148R-N cells to AT13148, it would suggest that SGK is contributing to AT13148 resistance. Currently, there are no selective SGK inhibitors in clinical development, however a tool compound, GSK650394, is available, which inhibits SGK1 and SGK2, displaying a ~30-fold selectivity over AKT (Sherk *et al.*, 2008). In addition, the role of ERK 1/2 in AT13148 resistance in 148R-N cells should not be entirely discounted, as despite the lack of sensitisation to AT13148 caused by ERK inhibition, the combination of

AT13148 and GDC-0994 was shown to potentiate the decrease in S6RP phosphorylation in 148R-N, as seen in 148R-K and 148R-S (Figure 5.7). Therefore, if ERK 1/2 is also linked to the maintenance of S6RP phosphorylation in 148R-N cells, it is unclear why ERK 1/2 inhibition did not sensitise 148R-N cells to AT13148. In 148R-N cells, it could be possible that both ERK 1/2 and SGK (directly or via upstream regulators) act as drivers of AT13148 resistance, and that inhibition of both ERK 1/2 and SGK is required to sensitise 148R-N cells to AT13148 (Figure 7.4). This should be considered when interpreting the results of combination assays with AT13148 and an SGK inhibitor, such as GSK650394.

7.3. Future studies

Much of the future work discussed thus far in this chapter, has been focused on answering questions that have arisen during this PhD project, that as of yet, have not been satisfactorily answered, e.g. what is the mechanism of ROCK cross-resistance and its relevance to AT13148 resistance? Whilst these questions will be important to answer, they are mostly confined within the narrow focus of this project, i.e. investigating AT13148 resistance using A2780-148R and 148R clones, alone, as a model. Any future studies should also focus upon asking, and attempting to answer, new questions regarding AT13148 resistance and its future clinical use, thus further facilitating the clinical development of AT13148

One such question that is immediately prompted by the work presented in this thesis is: are the findings of this thesis, regarding AT13148 resistance, relevant to other cell line models/tissue types, i.e. is AT13148 resistance always driven, in part, by increased activation of ERK 1/2? To answer this question, acquired resistance to AT13148 would have to be generated in other cell line models representing different tissue types. Since it has been suggested that AT13148 could be used as an adjuvant therapy in pancreatic cancer, it would prudent to generate and investigate AT13148 resistance in PDAC cell lines, such as PANC-1 and Bx-PC3 (Deer *et al.*, 2010; Rath *et al.*, 2018). Furthermore, AT13148 may have a clinical use in the treatment of RCC, since ROCK inhibition has been shown to be synthetically lethal with *VHL* loss in RCC (Thompson *et al.*, 2017). Therefore, AT13148 resistance should also be generated and investigated in *VHL*-null RCC cell lines, such as RCC4 and 786-O (Thompson *et al.*, 2017). Investigating resistance in these cell

lines would gain insight into the potential use, and resistance, of AT13148 in cancers in which the PAM pathway is not dysregulated.

When investigating resistance in these cell lines, a candidate approach should initially be undertaken, based on the findings of this thesis. Initially, the basal expression of markers of the MAPK pathway should be assessed, such as ERK 1/2 phosphorylation. If ERK 1/2 phosphorylation is also increased in these resistant cell lines, ERK 1/2 should be validated as a driver of AT13148 resistance by using combination assays with AT13148 and an ERK inhibitor, as shown in Figure 5.5 & Figure 5.8. If increased ERK 1/2 phosphorylation is shown to be acting as a driver of AT13148 resistance, then the expression of DUSP6, as well as the response of ERK 1/2 phosphorylation to FGFR inhibition, should also be evaluated.

However, if ERK 1/2 was not shown to be a driver of AT13148 resistance in these resistant cell lines, then unbiased approaches such as global genomic analysis could be used to identify candidate drivers of resistance. For example, whole exome sequencing could be used to compare resistant cell lines to their respective parental counterparts, from which they were derived, to identify resistance conferring mutations. In addition, RNA sequencing could be used to compare gene expression profiles, and identify altered gene expression, which might gain insight into AT13148 resistance.

In the above examples of how resistance should be investigated, it has been assumed a similar approach, to the one presented in this thesis, will be undertaken, whereby AT13148 resistance is studied by using resistant cell lines generated by dose-escalation. However, alternative approaches should also be considered to model AT13148 resistance in future studies, such as the use of functional genetic screens. In these screens, parental cell lines would be submitted to systematic loss-of-function (e.g. by RNA interference) or gain-of-function (e.g. by lentiviral open reading frame [ORF] libraries) of the entire genome, to identify genes associated with AT13148 resistance (Garraway and Jänne, 2012). Using these approaches offers several advantages as they are unbiased, high-throughput and may enable the identification of several mechanisms of resistance to a single therapy (Garraway and Jänne, 2012). For example, Wilson and colleagues (Wilson *et al.*, 2015) used a lentiviral ORF library to identify several drivers of ALK inhibitor resistance in NSCLC, including several previously established resistance

drivers such as KRAS and COT, as well novel drivers, such as the P2Y subfamily of P2 purinergic receptors.

In addition, one the limitations of the work presented in this thesis, due to the potent inhibition of PKA by AT13148, is the lack of understanding of the status of PKA signalling in A2780, A2780-148R and 148R clones. As discussed in section 3.3, an attempt was made to determine the phosphorylation level of VASP, a PKA substrate, via western blotting, so as to have a biological readout of PKA activation in A2780 and A2780-148R cells, but VASP was undetectable. Furthermore, it was also considered that a PKA inhibitor could be used in cross-resistance profiling, however, there aren't many marketed PKA inhibitors that are commercially available, and the PKA inhibitors that are most frequently used for research, H 89 and KT 5720, have been shown to lack selectivity for PKA, inhibiting several other kinases more potently (Davies *et al.*, 2000; Lochner and Moolman, 2006; Murray, 2008).

In future studies, the use of functional genetic screens may also be able to elucidate the role of PKA, if any, in AT13148 resistance. This approach was used by Johannessen and colleagues (Johannessen *et al.*, 2013), where a functional genetic screen identified that *PRKACA*, a catalytic subunit of PKA, could convey resistance against MAPK pathway inhibitors in *BRAF* mutant melanoma. Alternatively, a candidate approach could be undertaken; cell-permeable cAMP derivatives, such as bucladesine and 8-Br-cAMP, or the adenylate cyclase stimulator forskolin, could be used to increase PKA activation in A2780 cells (and other AT13148 sensitive parental cell lines), to evaluate if this could recapitulate the resistance phenotype.

Future studies should also focus on investigating the clinical relevance of the insight gained into AT13148 resistance, presented in this thesis. This would be undertaken by using patient data and tumour biopsies obtained from clinical trials conducted on AT13148. Currently, only one phase 1 clinical trial has been completed for AT13148, of which the results have not been fully published; only an abstract from the ASCO annual meeting is publicly available (Papadatos-Pastos *et al.*, 2015). Therefore, patient data and samples might be limited and difficult to gain access to. However, the inclusion criteria from the phase 1 clinical trial, states that paraffin embedded tumour tissue from patients must be available (*clinicaltrials.gov – identifier: NCT01585701*). Therefore, one

could envisage a future study in which immunohistochemical staining is used to detect ERK 1/2 phosphorylation and DUSP6 expression, in tumour samples from patients that took part in the phase 1 clinical trial for AT13148. The data from this could be compared to the response evaluation criteria in solid tumours (RECIST) from patients, to see if phosphorylation of ERK 1/2 or DUSP6 expression correlated with a lack of response to AT13148. Alternatively, if more clinical trials are conducted, it might be possible obtain pre-treatment and post-relapse samples from AT13148 treated patients, and again, investigate the phosphorylation of ERK 1/2 and DUSP6 using immunohistochemistry. A similar approach was used by Hrustanovic and colleagues (Hrustanovic *et al.*, 2015), where it was demonstrated that DUSP6 expression was lower in post-ALK inhibitor-resistance tumour samples vs treatment naïve samples, validating their *in vitro* findings of loss of DUSP6 expression as a mechanism of acquired resistance to ALK inhibitors in NSCLC.

7.4. Potential therapeutic strategies to treat AT13148 resistance

As well as gaining insight into the drivers and mechanisms of AT13148 resistance, the work presented in this thesis has also identified several potential therapeutic strategies to overcome AT13148 resistance, should it emerge in the clinic. As has been discussed, the combination of AT13148 with ERK inhibitors was synergistic and was able to re-sensitise 148R-K and 148R-S to AT13148 (Figure 5.5, Figure 5.6 & Figure 5.8). Since several ERK inhibitors are currently in clinical trials, including GDC-0994 and SCH772984, AT13148 resistance could potentially be treated by the combination of AT13148 and, for example, GDC-0994. The efficacy of this combination would be based upon increased ERK 1/2 phosphorylation driving AT13148 resistance, therefore, increased ERK 1/2 phosphorylation could be used as a potential biomarker when selecting patients that would best benefit from this combination. However, it should also be considered that increased ERK 1/2 phosphorylation didn't always correlated with the efficacy of this combination, as shown by the lack of response in 148R-N (Figure 4.17 & Figure 5.5).

In addition, AT13148 resistant patients might also benefit from the combination of AT13148 and a MEK inhibitor, since the combination of AT13148 and PD0325901 (MEK inhibitor), was also shown to be synergistic and re-sensitised 148R-S cells to AT13148

(Figure 5.9). This might be more immediately applicable to AT13148 resistant patients, since several MEK inhibitors are clinically approved, such as trametinib and cobimetinib (Cheng and Tian, 2017). However, unacceptable toxicities might develop when using AT13148 in combination with a MEK inhibitor in patients, due the inhibition of AKT by AT13148, as the combination of MEK and AKT inhibitors has been shown to be prohibitively toxic in several clinical trials (Chung *et al.*, 2017; Cao *et al.*, 2019).

It should also be considered that the combination of AT13148 with a MEK or ERK inhibitor, might have improved efficacy in treatment-naïve patients, when compared to AT13148 monotherapy. This is because the combination of AT13148 with a MEK or ERK inhibitor was also shown to sensitise parental A2780 cells to AT13148, in a synergistic manner (Figure 5.5, Figure 5.6, Figure 5.8 & Figure 5.9). The sensitivity to these combinations was likely due to the response of ERK phosphorylation to AT13148, which upon review of the literature published on AT13148, has only been described in this thesis. The ERK 1/2 response to AT13148 would therefore need be validated in additional cell lines/tissue types, before the combination of AT13148 with MAPK pathway inhibitors could be considered as a genuine therapeutic option in treatment naïve patients.

Another potential therapeutic option for AT13148 resistant patients would be to treat them with an FGFR inhibitor, as A2780-148R and all 148R clones, with the exception of 148R-N, were shown to be highly sensitive to the FGFR inhibitor AZD4547 (Figure 3.7, Figure 4.5 & Figure 4.11). Furthermore, there are several FGFR inhibitors currently in clinical development, including AZD4547 in which a phase 1/2 clinical trial was recently completed (Dai *et al.*, 2019; *clinicaltrials.gov – identifier: NCT02824133*). Therefore, targeting FGFR in AT13148 resistant patients may be a realistic option in the future. However, a biomarker of FGFR inhibitor sensitivity was not identified in this thesis, which would therefore make it difficult to select AT13148 resistant patients that would most benefit from FGFR inhibitor treatment. Accordingly, the identification of a biomarker of FGFR sensitivity should be a focus of any future work conducted. In doing so, it will be important to assess the expression and phosphorylation of FGFR1-4, which might be best achieved by using a phospho-RTK array. The discovery of a biomarker of FGFR

sensitivity might also help further understand the role of FGFR signalling in AT13148 resistance, as previously discussed in section 7.2.3.

7.5. Concluding remarks

The AGC family of serine/threonine kinases contains multiple members that can drive cancer progression and survival and are therefore attractive therapeutic targets. In targeting multiple AGC kinases, AT13148 represents a novel therapeutic strategy, that may provide improved efficacy over other, more selective inhibitors of AGC kinases. For these reasons, AT13148 is currently in clinical development having recently completed a phase 1 clinical trial. However, the acquisition of drug resistance to targeted agents is a frequent problem encountered in the clinic, and likely to occur with AT13148.

In this thesis, acquired resistance to AT13148 was generated in the A2780 human ovarian carcinoma cell line and it was demonstrated that upregulated ERK 1/2 phosphorylation could act as a driver of AT13148 resistance. It is likely that the ability of ERK 1/2 to act as a key signalling node, with over 160 recognised substrates, enables the compensation of the inhibition of several targets of AT13148, either via direct pathway reactivation, as was shown with the AT13148 target p70S6K, or pathway bypass. It was also shown that other drivers of AT13148 resistance are likely to exist, which appear proximal to the PAM pathway but independent of AKT, which warrants further investigation. The exact mechanism(s) by which ERK 1/2 phosphorylation had been increased was not identified, but was linked, in part, to a loss of DUSP6 expression. Nonetheless, the clinical relevance of increased ERK 1/2 phosphorylation to AT13148 resistance should be the subject of future studies.

In conclusion, the work presented in this thesis has gained invaluable insight into acquired AT13148 resistance. This has provided a firm foundation on which future studies will be conducted and identified therapeutic strategies to improve the efficacy of AT13148 treatment and overcome AT13148 resistance. Therefore, the work presented in this thesis, will aid the future clinical development of AT13148, and should AT13148 advance to the clinic, potentially improve the outcome of patients treated with AT13148.

References

References

Acosta-Martínez, M. (2012) 'PI3K: An attractive candidate for the central integration of metabolism and reproduction', *Frontiers in Endocrinology*. doi: 10.3389/fendo.2011.00110.

Afify, S. M. and Seno, M. (2019) 'Conversion of stem cells to cancer stem cells: Undercurrent of cancer initiation', *Cancers*. MDPI AG, 11(3). doi: 10.3390/cancers11030345.

Ahmad, A. S., Ormiston-Smith, N. and Sasieni, P. D. (2015) 'Trends in the lifetime risk of developing cancer in Great Britain: Comparison of risk for those born from 1930 to 1960', *British Journal of Cancer*. Nature Publishing Group, 112(5), pp. 943–947. doi: 10.1038/bjc.2014.606.

Akan, D. T. (2015) *'Investigating mechanisms of acquired resistance to AKT inhibitors'*. PhD thesis, Institute of Cancer Research, London.

Van Allen, E. M. *et al.* (2014) 'The Genetic Landscape of Clinical Resistance to RAF Inhibition in Metastatic Melanoma', *Cancer Discovery*. American Association for Cancer Research, 4(1), pp. 94–109. doi: 10.1158/2159-8290.CD-13-0617.

Alzahrani, A. S. (2019) 'PI3K/Akt/mTOR inhibitors in cancer: At the bench and bedside', *Seminars in Cancer Biology*. Academic Press. doi: 10.1016/j.semcancer.2019.07.009.

Amano, M., Nakayama, M. and Kaibuchi, K. (2010) 'Rho-kinase/ROCK: A key regulator of the cytoskeleton and cell polarity', *Cytoskeleton*, pp. 545–554. doi: 10.1002/cm.20472.

Amin, E. *et al.* (2013) 'Rho-kinase: Regulation, (dys)function, and inhibition', *Biological Chemistry*, pp. 1399–1410. doi: 10.1515/hsz-2013-0181.

Anand, P. *et al.* (2008) 'Cancer is a preventable disease that requires major lifestyle changes', *Pharmaceutical Research*. Springer New York LLC, pp. 2097–2116. doi: 10.1007/s11095-008-9661-9.

André, F. *et al.* (2019) 'Alpelisib for PIK3CA-mutated, hormone receptor-positive advanced breast cancer', *New England Journal of Medicine*, 380(20), pp. 1929–1940. doi: 10.1056/NEJMoa1813904.

Anjum, R. and Blenis, J. (2008) 'The RSK family of kinases: Emerging roles in cellular signalling', *Nature Reviews Molecular Cell Biology*, pp. 747–758. doi: 10.1038/nrm2509.

Aoki, K. *et al.* (1997) 'Suppression of Ki-ras p21 levels leading to growth inhibition of pancreatic cancer cell lines with Ki-ras mutation but not those without Ki- ras mutation', *Molecular Carcinogenesis*, 20(2), pp. 251–258. doi: 10.1002/(SICI)1098-2744(199710)20:2<251::AID-MC12>3.0.CO;2-9.

Arencibia, J. M., Pastor-Flores, D., Bauer, A. F., Schulze, J. O. and Biondi, R. M. (2013) 'AGC protein kinases: From structural mechanism of regulation to allosteric drug development for the treatment of human diseases', *Biochimica et Biophysica Acta - Proteins and Proteomics*, pp. 1302–1321. doi: 10.1016/j.bbapap.2013.03.010.

Arozarena, I. and Wellbrock, C. (2017) 'Overcoming resistance to BRAF inhibitors', *Annals of Translational Medicine*. AME Publishing Company, 5(19), pp. 1–12. doi: 10.21037/atm.2017.06.09.

Ascierto, P. A. *et al.* (2016) 'Cobimetinib combined with vemurafenib in advanced BRAFV600-mutant melanoma (coBRIM): updated efficacy results from a randomised, double-blind, phase 3 trial', *The Lancet Oncology*. Elsevier, 17(9), pp. 1248–1260. doi: 10.1016/S1470-2045(16)30122-X.

Baker, S. G. (2015) 'A cancer theory kerfuffle can lead to new lines of research', *Journal of the National Cancer Institute*. Oxford University Press. doi: 10.1093/jnci/dju405.

Balendran, A. *et al.* (1999) 'PDK1 acquires PDK2 activity in the presence of a synthetic peptide derived from the carboxyl terminus of PRK2', *Current Biology*. Current Biology Ltd, 9(8), pp. 393–404. doi: 10.1016/S0960-9822(99)80186-9.

Balzano, D. *et al.* (2015) 'Alternative activation mechanisms of protein kinase B trigger distinct downstream signaling responses', *Journal of Biological Chemistry*. American Society for Biochemistry and Molecular Biology Inc., 290(41), pp. 24975–24985. doi: 10.1074/jbc.M115.651570.

Barber, L. J. *et al.* (2013) 'Secondary mutations in BRCA2 associated with clinical resistance to a PARP inhibitor', *Journal of Pathology*, 229(3), pp. 422–429. doi: 10.1002/path.4140.

Barrett, S. D. *et al.* (2008) 'The discovery of the benzhydroxamate MEK inhibitors CI-1040 and PD 0325901', *Bioorganic & Medicinal Chemistry Letters*, 18(24), pp. 6501–6504. doi: 10.1016/j.bmcl.2008.10.054.

Ben-David, U. *et al.* (2018) 'Genetic and transcriptional evolution alters cancer cell line drug response', *Nature*. Nature Publishing Group, 560(7718), pp. 325–330. doi: 10.1038/s41586-018-0409-3.

Beurel, E., Grieco, S. F. and Jope, R. S. (2015) 'Glycogen synthase kinase-3 (GSK3): regulation, actions, and diseases.', *Pharmacology & therapeutics*. NIH Public Access, 148, pp. 114–31. doi: 10.1016/j.pharmthera.2014.11.016.

Bhullar, K. S. *et al.* (2018) 'Kinase-targeted cancer therapies: Progress, challenges and future directions', *Molecular Cancer*. BioMed Central Ltd. doi: 10.1186/s12943-018-0804-2.

Biondi, R. M., Kieloch, A., Currie, R. A., Deak, M. and Alessi, D. R. (2001) 'The PIF-binding pocket in PDK1 is essential for activation of S6K and SGK, but not PKB', *EMBO Journal*, 20(16), pp. 4380–4390. doi: 10.1093/emboj/20.16.4380.

Blagden, S. P. (2015) 'Harnessing Pandemonium: The Clinical Implications of Tumor Heterogeneity in Ovarian Cancer', *Frontiers in Oncology*. Frontiers, 5, p. 149. doi: 10.3389/fonc.2015.00149.

Blagosklonny, M. V (2005) 'Molecular theory of cancer', *Cancer Biology & Therapy*, 621(6), pp. 621–627. doi: 10.4161/cbt.4.6.1818.

Blake, J. F. *et al.* (2016) 'Discovery of (*S*)-1-(1-(4-Chloro-3-fluorophenyl)-2-hydroxyethyl)-4-(2-((1-methyl-1 *H* -pyrazol-5-yl)amino)pyrimidin-4-yl)pyridin-2(1 *H*)-one (GDC-0994), an Extracellular Signal-Regulated Kinase 1/2 (ERK1/2) Inhibitor in Early Clinical Development', *Journal of Medicinal Chemistry*. American Chemical Society, 59(12), pp. 5650–5660. doi: 10.1021/acs.jmedchem.6b00389.

Blüthgen, N. *et al.* (2009) 'A systems biological approach suggests that transcriptional feedback regulation by dual-specificity phosphatase 6 shapes extracellular signal-related kinase activity in RAS-transformed fibroblasts', *FEBS Journal*, 276(4), pp. 1024–1035. doi: 10.1111/j.1742-4658.2008.06846.x.

Bozulic, L., Surucu, B., Hynx, D. and Hemmings, B. A. (2008) 'PKBα/Akt1 Acts Downstream of DNA-PK in the DNA Double-Strand Break Response and Promotes Survival', *Molecular Cell*, 30(2), pp. 203–213. doi: 10.1016/j.molcel.2008.02.024.

Bray, F. *et al.* (2018) 'Global cancer statistics 2018: GLOBOCAN estimates of incidence and mortality worldwide for 36 cancers in 185 countries', *CA: A Cancer Journal for Clinicians*, 68(6), pp. 394–424. doi: 10.3322/caac.21492.

Bridgeman, V. L. *et al.* (2017) 'Vessel co-option is common in human lung metastases and mediates resistance to anti-angiogenic therapy in preclinical lung metastasis models', *Journal of Pathology*. John Wiley and Sons Ltd, 241(3), pp. 362–374. doi: 10.1002/path.4845.

Bromann, P. A., Korkaya, H. and Courtneidge, S. A. (2004) 'The interplay between Src family kinases and receptor tyrosine kinases', *Oncogene*. Nature Publishing Group, 23(48), pp. 7957–7968. doi: 10.1038/sj.onc.1208079.

ter Brugge, P. *et al.* (2016) 'Mechanisms of Therapy Resistance in Patient-Derived Xenograft Models of BRCA1-Deficient Breast Cancer', *Journal of the National Cancer Institute*, 108(11), p. djw148. doi: 10.1093/jnci/djw148.

Bruhn, M. A., Pearson, R. B., Hannan, R. D. and Sheppard, K. E. (2010) 'Second AKT: The rise of SGK in cancer signalling', *Growth Factors*. Taylor & Francis, 28(6), pp. 394–408. doi: 10.3109/08977194.2010.518616.

Bruhn, M. A., Pearson, R. B., Hannan, R. D. and Sheppard, K. E. (2013) 'AKT-independent PI3-K signaling in cancer - emerging role for SGK3.', *Cancer management and research*. Dove Press, 5, pp. 281–92. doi: 10.2147/CMAR.S35178.

Brunet, A. *et al.* (2001) 'Protein kinase SGK mediates survival signals by phosphorylating the forkhead transcription factor FKHRL1 (FOXO3a).', *Molecular and cellular biology*. American Society for Microbiology Journals, 21(3), pp. 952–65. doi: 10.1128/MCB.21.3.952-965.2001.

Buffet, C. *et al.* (2017) 'DUSP5 and DUSP6, two ERK specific phosphatases, are markers of a higher MAPK signaling activation in BRAF mutated thyroid cancers', *PLoS ONE*. Public Library of Science, 12(9). doi: 10.1371/journal.pone.0184861.

Burnette, W. N. (1981) '"Western Blotting": Electrophoretic transfer of proteins from sodium dodecyl sulfate-polyacrylamide gels to unmodified nitrocellulose and radiographic detection with antibody and radioiodinated protein A', *Analytical Biochemistry*, 112(2), pp. 195–203. doi: 10.1016/0003-2697(81)90281-5.

Burrell, R. A. and Swanton, C. (2014) 'Tumour heterogeneity and the evolution of polyclonal drug resistance.', *Molecular oncology*. Wiley-Blackwell, 8(6), pp. 1095–111. doi: 10.1016/j.molonc.2014.06.005.

Campbell, L. J. *et al.* (2002) 'BCR/ABL amplification in chronic myelocytic leukemia blast crisis following imatinib mesylate administration.', *Cancer genetics and cytogenetics*, 139(1), pp. 30–3. doi: 10.1016/s0165-4608(02)00615-5.

Cao, Z. *et al.* (2019) 'AKT and ERK dual inhibitors: The way forward?', *Cancer Letters*. Elsevier Ireland Ltd, pp. 30–40. doi: 10.1016/j.canlet.2019.05.025.

Caretta, A. and Mucignat-Caretta, C. (2011) 'Protein kinase a in cancer', *Cancers*, pp. 913–926. doi: 10.3390/cancers3010913.

Cargnello, M., Tcherkezian, J. and Roux, P. P. (2015) 'The expanding role of mTOR in cancer cell growth and proliferation', *Mutagenesis*. Oxford University Press, pp. 169–176. doi: 10.1093/mutage/geu045.

Carpten, J. D. *et al.* (2007) 'A transforming mutation in the pleckstrin homology domain of AKT1 in cancer', *Nature*. Nature Publishing Group, 448(7152), pp. 439–444. doi: 10.1038/nature05933.

Carracedo, A., Alimonti, A. and Pandolfi, P. P. (2011) 'PTEN level in tumor suppression: How much is too little?', *Cancer Research*, pp. 629–633. doi: 10.1158/0008-5472.CAN-10-2488.

Casamayor, A., Morrice, N. A. and Alessi, D. R. (1999) 'Phosphorylation of Ser-241 is essential for the activity of 3-phosphoinositide-dependent protein kinase-1: Identification of five sites of phosphorylation in vivo', *Biochemical Journal*, 342(2), pp. 287–292. doi: 10.1042/0264-6021:3420287.

Caunt, C. J., Rivers, C. A., Conway-Campbell, B. L., Norman, M. R. and McArdle, C. A. (2008) 'Epidermal growth factor receptor and protein kinase C signaling to ERK2: Spatiotemporal regulation of ERK2 by dual specificity phosphatases', *Journal of Biological Chemistry*, 283(10), pp. 6241–6252. doi: 10.1074/jbc.M706624200.

Chandarlapaty, S. *et al.* (2011) 'AKT inhibition relieves feedback suppression of receptor tyrosine kinase expression and activity.', *Cancer cell*. Elsevier, 19(1), pp. 58–71. doi: 10.1016/j.ccr.2010.10.031.

Chang, F. *et al.* (2003) 'Involvement of PI3K/Akt pathway in cell cycle progression, apoptosis, and neoplastic transformation: A target for cancer chemotherapy', *Leukemia*. Nature Publishing Group, pp. 590–603. doi: 10.1038/sj.leu.2402824.

Chang, F. *et al.* (2018) 'ROCK inhibitor enhances the growth and migration of BRAF-mutant skin melanoma cells', *Cancer Science*. Wiley-Blackwell, 109(11), pp. 3428–3437. doi: 10.1111/cas.13786.

Chapman, P. B. *et al.* (2011) 'Improved Survival with Vemurafenib in Melanoma with BRAF V600E Mutation', *New England Journal of Medicine*, 364(26), pp. 2507–2516. doi: 10.1056/NEJMoa1103782.

Chen, C. Y., Chen, J., He, L. and Stiles, B. L. (2018) 'PTEN: Tumor suppressor and metabolic regulator', *Frontiers in Endocrinology*. Frontiers Media S.A. doi: 10.3389/fendo.2018.00338.

Chen, W., Mao, K., Liu, Z. and Dinh-Xuan, A. T. (2014) 'The role of the RhoA/Rho kinase pathway in angiogenesis and its potential value in prostate cancer (review)', *Oncology Letters*. Spandidos Publications, 8(5), pp. 1907–1911. doi: 10.3892/ol.2014.2471.

Cheng, X., Ma, Y., Moore, M., Hemmings, B. A. and Taylor, S. S. (1998) 'Phosphorylation and activation of cAMP-dependent protein kinase by phosphoinositide-dependent protein kinase', *Proceedings of the National Academy of Sciences of the United States of America*, 95(17), pp. 9849–9854. doi: 10.1073/pnas.95.17.9849.

Cheng, Y. and Tian, H. (2017) 'Current Development Status of MEK Inhibitors.', *Molecules (Basel, Switzerland)*. Multidisciplinary Digital Publishing Institute (MDPI), 22(10). doi: 10.3390/molecules22101551.

Cherrin, C. *et al.* (2010) 'An allosteric Akt inhibitor effectively blocks Akt signaling and tumor growth with only transient effects on glucose and insulin levels in vivo', *Cancer Biology and Therapy*. Landes Bioscience, 9(7), pp. 493–503. doi: 10.4161/cbt.9.7.11100.

Chiarini, F., Evangelisti, C., McCubrey, J. A. and Martelli, A. M. (2015) 'Current treatment strategies for inhibiting mTOR in cancer', *Trends in Pharmacological Sciences*. Elsevier Ltd, pp. 124–135. doi: 10.1016/j.tips.2014.11.004.

Chung, V. *et al.* (2017) 'Effect of selumetinib and MK-2206 vs oxaliplatin and fluorouracil in patients with metastatic pancreatic cancer after prior therapy: SWOG S1115 study randomized clinical trial', *JAMA Oncology*. American Medical Association, 3(4), pp. 516–522. doi: 10.1001/jamaoncol.2016.5383.

Cole, P. A., Chu, N., Salguero, A. L. and Bae, H. (2019) 'AKTivation mechanisms', *Current Opinion in Structural Biology*. Elsevier Ltd, pp. 47–53. doi: 10.1016/j.sbi.2019.02.004.

Colomer, R., Lupu, R., Bacus, S. S. and Gelmann, E. P. (1994) 'erbB-2 antisense oligonucleotides inhibit the proliferation of breast carcinoma cells with erbB-2 oncogene amplification', *British Journal of Cancer*, 70(5), pp. 819–825. doi: 10.1038/bjc.1994.405.

Cree, I. A. and Charlton, P. (2017) 'Molecular chess? Hallmarks of anti-cancer drug resistance', *BMC Cancer*, 17(1), p. 10. doi: 10.1186/s12885-016-2999-1.

Croft, D. R. and Olson, M. F. (2006) 'The Rho GTPase effector ROCK regulates cyclin A, cyclin D1, and p27Kip1 levels by distinct mechanisms.', *Molecular and cellular biology*. American Society for Microbiology, 26(12), pp. 4612–27. doi: 10.1128/MCB.02061-05.

Dai, S., Zhou, Z., Chen, Z., Xu, G. and Chen, Y. (2019) 'Fibroblast Growth Factor Receptors (FGFRs): Structures and Small Molecule Inhibitors', *Cells*. MDPI AG, 8(6), p. 614. doi: 10.3390/cells8060614.

Daley, G. Q., Van Etten, R. A. and Baltimore, D. (1990) 'Induction of chronic myelogenous leukemia in mice by the P210 bcr/abl gene of the Philadelphia chromosome', *Science*, 247(4944), pp. 824–830. doi: 10.1126/science.2406902.

Daly, C. *et al.* (2017) 'FGFR3-TACC3 fusion proteins act as naturally occurring drivers of tumor resistance by functionally substituting for EGFR/ERK signaling', *Oncogene*. Nature Publishing Group, 36(4), pp. 471–481. doi: 10.1038/onc.2016.216.

Dasi, S. *et al.* (2005) 'Tp12/Cot signals activate ERK, JNK, and NF-κB in a cell-type and stimulus-specific manner', *Journal of Biological Chemistry*, 280(25), pp. 23748–23757. doi: 10.1074/jbc.M412837200.

Davies, B. R. *et al.* (2012) 'Preclinical pharmacology of AZD5363, an inhibitor of AKT: Pharmacodynamics, antitumor activity, and correlation of monotherapy activity with genetic background', *Molecular Cancer Therapeutics*. American Association for Cancer Research, 11(4), pp. 873–887. doi: 10.1158/1535-7163.MCT-11-0824-T.

Davies, M. A. *et al.* (2008) 'A novel AKT3 mutation in melanoma tumours and cell lines', *British Journal of Cancer*, 99(8), pp. 1265–1268. doi: 10.1038/sj.bjc.6604637.

Davies, S. P., Reddy, H., Caivano, M. and Cohen, P. (2000) 'Specificity and mechanism of action of some commonly used protein kinase inhibitors', *Biochemical Journal*, 351(1), pp. 95–105. doi: 10.1042/0264-6021:3510095.

Davis, H. E., Rosinski, M., Morgan, J. R. and Yarmush, M. L. (2004) 'Charged Polymers Modulate Retrovirus Transduction via Membrane Charge Neutralization and Virus Aggregation', *Biophysical Journal*. Biophysical Society, 86(2), pp. 1234–1242. doi: 10.1016/S0006-3495(04)74197-1.

Deer, E. L. *et al.* (2010) 'Phenotype and genotype of pancreatic cancer cell lines', *Pancreas*. Lippincott Williams and Wilkins, pp. 425–435. doi: 10.1097/MPA.0b013e3181c15963.

Desai, A. and Adjei, A. A. (2016) 'FGFR Signaling as a Target for Lung Cancer Therapy', *Journal of Thoracic Oncology*. Elsevier, 11(1), pp. 9–20. doi: 10.1016/J.JTHO.2015.08.003.

Dickinson, R. J. and Keyse, S. M. (2006) 'Diverse physiological functions for dual-specificity MAP kinase phosphatases.', *Journal of cell science*. The Company of Biologists Ltd, 119(Pt 22), pp. 4607–15. doi: 10.1242/jcs.03266.

Diehl, J. A., Cheng, M., Roussel, M. F. and Sherr, C. J. (1998) 'Glycogen synthase kinase-3β regulates cyclin D1 proteolysis and subcellular localization', *Genes and Development*. Cold Spring Harbor Laboratory Press, 12(22), pp. 3499–3511. doi: 10.1101/gad.12.22.3499.

Donnem, T. *et al.* (2018) 'Non-angiogenic tumours and their influence on cancer biology', *Nature Reviews Cancer*. Nature Publishing Group, pp. 323–336. doi: 10.1038/nrc.2018.14.

Dorard, C. *et al.* (2017) 'RAF proteins exert both specific and compensatory functions during tumour progression of NRAS-driven melanoma', *Nature Communications*. Nature Publishing Group, 8. doi: 10.1038/ncomms15262.

Dougherty, M. K. *et al.* (2005) 'Regulation of Raf-1 by Direct Feedback Phosphorylation', *Molecular Cell*. Cell Press, 17(2), pp. 215–224. doi: 10.1016/J.MOLCEL.2004.11.055.

Dowd, S., Sneddon, A. A. and Keyse, S. M. (1998) 'Isolation of the human genes encoding the Pyst1 and Pyst2 phosphatases: Characterisation of Pyst2 as a cytosolic dual-specificity MAP kinase phosphatase and its catalytic activation by both MAP and SAP kinases', *Journal of Cell Science*, 111(22), pp. 3389–3399.

Du, Z. and Lovly, C. M. (2018) 'Mechanisms of receptor tyrosine kinase activation in cancer', *Molecular Cancer*. BioMed Central Ltd. doi: 10.1186/s12943-018-0782-4.

Dumaz, N. *et al.* (2006) 'In melanoma, RAS mutations are accompanied by switching signaling from BRAF to CRAF and disrupted cyclic AMP signaling', *Cancer Research*, 66(19), pp. 9483–9491. doi: 10.1158/0008-5472.CAN-05-4227.

Dumaz, N. (2011) 'Mechanism of RAF isoform switching induced by oncogenic RAS in melanoma', *Small GTPases*, 2(5), pp. 289–292. doi: 10.4161/sgtp.2.5.17814.

Eblen, S. T. *et al.* (2004) 'Mitogen-Activated Protein Kinase Feedback Phosphorylation Regulates MEK1 Complex Formation and Activation during Cellular Adhesion', *Molecular and Cellular Biology*. American Society for Microbiology Journals, 24(6), pp. 2308–2317. doi: 10.1128/MCB.24.6.2308-2317.2004.

Ekerot, M. *et al.* (2008) 'Negative-feedback regulation of FGF signalling by DUSP6/MKP-3 is driven by ERK1/2 and mediated by Ets factor binding to a conserved site within the DUSP6/MKP-3 gene promoter.', *The Biochemical journal*. Portland Press Ltd, 412(2), pp. 287–98. doi: 10.1042/BJ20071512.

Engelman, J. A. *et al.* (2007) 'MET amplification leads to gefitinib resistance in lung cancer by activating ERBB3 signaling.', *Science (New York, N.Y.)*. American Association for the Advancement of Science, 316(5827), pp. 1039–43. doi: 10.1126/science.1141478.

Ercan, D. *et al.* (2012) 'Reactivation of ERK signaling causes resistance to EGFR Kinase inhibitors', *Cancer Discovery*. American Association for Cancer Research Inc., 2(10), pp. 934–947. doi: 10.1158/2159-8290.CD-12-0103.

Fallahi-Sichani, M., Honarnejad, S., Heiser, L. M., Gray, J. W. and Sorger, P. K. (2013) 'Metrics other than potency reveal systematic variation in responses to cancer drugs.', *Nature chemical biology*. NIH Public Access, 9(11), pp. 708–14. doi: 10.1038/nchembio.1337.

Feng, J. *et al.* (1999) 'Rho-associated kinase of chicken gizzard smooth muscle', *Journal of Biological Chemistry*, 274(6), pp. 3744–3752. doi: 10.1074/jbc.274.6.3744.

Fenton, T. R. and Gout, I. T. (2011) 'Functions and regulation of the 70 kDa ribosomal S6 kinases', *International Journal of Biochemistry and Cell Biology*, pp. 47–59. doi: 10.1016/j.biocel.2010.09.018.

Fincham, V. J., Chudleigh, A. and Frame, M. C. (1999) 'Regulation of p190 Rho-GAP by v-Src is linked to cytoskeletal disruption during transformation', *Journal of Cell Science*, 112(6), pp. 947–956.

Flaherty, K. T. *et al.* (2010) 'Inhibition of Mutated, Activated BRAF in Metastatic Melanoma', *New England Journal of Medicine*, 363(9), pp. 809–819. doi: 10.1056/NEJMoa1002011.

Flinn, I. W. *et al.* (2018) 'The phase 3 DUO trial: Duvelisib vs ofatumumab in relapsed and refractory CLL/SLL', *Blood*. American Society of Hematology, 132(23), pp. 2446–2455. doi: 10.1182/blood-2018-05-850461.

Foucquier, J. and Guedj, M. (2015) 'Analysis of drug combinations: current methodological landscape.', *Pharmacology research & perspectives*. Wiley-Blackwell, 3(3), p. e00149. doi: 10.1002/prp2.149.

Fritsch, R. *et al.* (2013) 'RAS and RHO families of GTPases directly regulate distinct phosphoinositide 3-kinase isoforms', *Cell*. Cell Press, 153(5), p. 1050. doi: 10.1016/j.cell.2013.04.031.

Fruman, D. A. *et al.* (2017) 'The PI3K Pathway in Human Disease', *Cell*. Cell Press, pp. 605–635. doi: 10.1016/j.cell.2017.07.029.

Furman, R. R. *et al.* (2014) 'Idelalisib and Rituximab in Relapsed Chronic Lymphocytic Leukemia', *New England Journal of Medicine*, 370(11), pp. 997–1007. doi: 10.1056/NEJMoa1315226.

Furukawa, T., Sunamura, M., Motoi, F., Matsuno, S. and Horii, A. (2003) 'Potential tumor suppressive pathway involving DUSP6/MKP-3 in pancreatic cancer.', *The American journal of pathology*. American Society for Investigative Pathology, 162(6), pp. 1807–15. doi: 10.1016/S0002-9440(10)64315-5.

Gagliardi, P. A. *et al.* (2012) '3-phosphoinositide-dependent kinase 1 controls breast tumor growth in a kinase-dependent but Akt-independent manner.', *Neoplasia (New York, N.Y.)*. Neoplasia Press, 14(8), pp. 719–31. doi: 10.1593/neo.12856.

García-Martínez, J. M. and Alessi, D. R. (2008) 'mTOR complex 2 (mTORC2) controls hydrophobic motif phosphorylation and activation of serum- and glucocorticoid-induced protein kinase 1 (SGK1)', *Biochemical Journal*, 416(3), pp. 375–385. doi: 10.1042/BJ20081668.

Garnock-Jones, K. P. (2016) 'Osimertinib: First Global Approval', *Drugs*. Springer International Publishing, pp. 1–7. doi: 10.1007/s40265-015-0537-0.

Garraway, L. A. and Jänne, P. A. (2012) 'Circumventing cancer drug resistance in the era of personalized medicine', *Cancer Discovery*, pp. 214–226. doi: 10.1158/2159-8290.CD-12-0012.

Gerlinger, M. *et al.* (2012) 'Intratumor heterogeneity and branched evolution revealed by multiregion sequencing.', *The New England journal of medicine*. Europe PMC Funders, 366(10), pp. 883–892. doi: 10.1056/NEJMoa1113205.

Gerlinger, M. and Swanton, C. (2010) 'How Darwinian models inform therapeutic failure initiated by clonal heterogeneity in cancer medicine', *British Journal of Cancer*. Nature Publishing Group, 103(8), pp. 1139–1143. doi: 10.1038/sj.bjc.6605912.

Gogola, E., Rottenberg, S. and Jonkers, J. (2019) 'Resistance to PARP Inhibitors: Lessons from Preclinical Models of BRCA-Associated Cancer', *Annual Review of Cancer Biology*, 3(1), pp. 235–254. doi: 10.1146/annurev-cancerbio-030617-050232.

Gorre, M. E. *et al.* (2001) 'Clinical resistance to STI-571 cancer therapy caused by BCR-ABL gene mutation or amplification', *Science*, 293(5531), pp. 876–880. doi: 10.1126/science.1062538.

Gowrishankar, K. *et al.* (2012) 'Acquired Resistance to BRAF Inhibition Can Confer Cross-Resistance to Combined BRAF/MEK Inhibition', *Journal of Investigative Dermatology*. Elsevier, 132(7), pp. 1850–1859. doi: 10.1038/JID.2012.63.

Grabiner, B. C. *et al.* (2014) 'A diverse array of cancer-associated MTOR mutations are hyperactivating and can predict rapamycin sensitivity', *Cancer Discovery*. American Association for Cancer Research Inc., 4(5), pp. 554–563. doi: 10.1158/2159-8290.CD-13-0929.

Griffin, M. *et al.* (2017) 'BRAF inhibitors: Resistance and the promise of combination treatments for melanoma', *Oncotarget*. Impact Journals LLC, pp. 78174–78192. doi: 10.18632/oncotarget.19836.

Gross, S., Rahal, R., Stransky, N., Lengauer, C. and Hoeflich, K. P. (2015) 'Targeting cancer with kinase inhibitors', *Journal of Clinical Investigation*. American Society for Clinical Investigation, pp. 1780–1789. doi: 10.1172/JCI76094.

Grzmil, M. and Hemmings, B. A. (2012) 'Translation regulation as a therapeutic target in cancer.', *Cancer research*. American Association for Cancer Research, 72(16), pp. 3891–900. doi: 10.1158/0008-5472.CAN-12-0026.

Guan, K. L. *et al.* (2000) 'Negative regulation of the serine/threonine kinase B-Raf by Akt', *Journal of Biological Chemistry*, 275(35), pp. 27354–27359. doi: 10.1074/jbc.M004371200.

Gupta, S. *et al.* (2007) 'Binding of Ras to Phosphoinositide 3-Kinase p110α Is Required for Ras-Driven Tumorigenesis in Mice', *Cell*, 129(5), pp. 957–968. doi: 10.1016/j.cell.2007.03.051.

Gurkar, A. U. *et al.* (2013) 'Identification of ROCK1 kinase as a critical regulator of Beclin1-mediated autophagy during metabolic stress', *Nature Communications*, 4. doi: 10.1038/ncomms3189.

Hanahan, D. and Weinberg, R. A. (2011) 'Hallmarks of cancer: The next generation', *Cell*, pp. 646–674.

Hanrahan, A. J. *et al.* (2012) 'Genomic complexity and AKT dependence in serous ovarian cancer', *Cancer Discovery*, 2(1), pp. 57–67. doi: 10.1158/2159-8290.CD-11-0170.

Harada, H., Andersen, J. S., Mann, M., Terada, N. and Korsmeyer, S. J. (2001) 'p70S6 kinase signals cell survival as well as growth, inactivating the pro-apoptotic molecule BAD', *Proceedings of the National Academy of Sciences of the United States of America*, 98(17), pp. 9666–9670. doi: 10.1073/pnas.171301998.

Haslehurst, A. M. *et al.* (2012) 'EMT transcription factors snail and slug directly contribute to cisplatin resistance in ovarian cancer.', *BMC cancer*. BioMed Central, 12, p. 91. doi: 10.1186/1471-2407-12-91.

Hassan, B., Akcakanat, A., Holder, A. M. and Meric-Bernstam, F. (2013) 'Targeting the PI3-Kinase/Akt/mTOR Signaling Pathway', *Surgical Oncology Clinics of North America*, pp. 641–664. doi: 10.1016/j.soc.2013.06.008.

Heinonen, H. *et al.* (2008) 'Deciphering downstream gene targets of PI3K/mTOR/p70S6K pathway in breast cancer', *BMC Genomics*, 9. doi: 10.1186/1471-2164-9-348.

Henkes, M., van der Kuip, H. and Aulitzky, W. E. (2008) 'Therapeutic options for chronic myeloid leukemia', *Therapeutics and Clinical Risk Management*, 4(1), pp. 163–187.

Heppner, G. H. (1984) *Tumor Heterogeneity*, CANCER RESEARCH.

Hirai, H. *et al.* (2010) 'MK-2206, an Allosteric Akt Inhibitor, Enhances Antitumor Efficacy by Standard Chemotherapeutic Agents or Molecular Targeted Drugs In vitro and In vivo', *Molecular Cancer Therapeutics*. American Association for Cancer Research, 9(7), pp. 1956–1967. doi: 10.1158/1535-7163.mct-09-1012.

Hobbs, G. A., Der, C. J. and Rossman, K. L. (2016) 'RAS isoforms and mutations in cancer at a glance', *Journal of Cell Science*. Company of Biologists Ltd, 129(7), pp. 1287–1292. doi: 10.1242/jcs.182873.

Hrustanovic, G. *et al.* (2015) 'RAS-MAPK dependence underlies a rational polytherapy strategy in EML4-ALK-positive lung cancer.', *Nature medicine*. NIH Public Access, 21(9), pp. 1038–47. doi: 10.1038/nm.3930.

Hua, H. *et al.* (2019) 'Targeting mTOR for cancer therapy', *Journal of Hematology and Oncology*. BioMed Central Ltd. doi: 10.1186/s13045-019-0754-1.

Huettner, C. S., Zhang, P., Van Etten, R. A. and Tenen, D. G. (2000) 'Reversibility of acute B-cell leukaemia induced by BCR-ABL1', *Nature Genetics*, 24(1), pp. 57–60. doi: 10.1038/71691.

Inoki, K., Li, Y., Xu, T. and Guan, K. L. (2003) 'Rheb GTpase is a direct target of TSC2 GAP activity and regulates mTOR signaling', *Genes and Development*, 17(15), pp. 1829–1834. doi: 10.1101/gad.1110003.

Inoki, K., Li, Y., Zhu, T., Wu, J. and Guan, K. L. (2002) 'TSC2 is phosphorylated and inhibited by Akt and suppresses mTOR signalling', *Nature Cell Biology*, 4(9), pp. 648–657. doi: 10.1038/ncb839.

Iqbal, Nida and Iqbal, Naveed (2014) 'Human Epidermal Growth Factor Receptor 2 (HER2) in Cancers: Overexpression and Therapeutic Implications', *Molecular Biology International*. Hindawi Limited, 2014, pp. 1–9. doi: 10.1155/2014/852748.

Jabbour, E., Kantarjian, H. and Cortes, J. (2015) 'Use of second- and third-generation tyrosine kinase inhibitors in the treatment of chronic myeloid leukemia: An evolving treatment paradigm', *Clinical Lymphoma, Myeloma and Leukemia*. Elsevier Inc., pp. 323–334. doi: 10.1016/j.clml.2015.03.006.

Jackson, A. L. *et al.* (2003) 'Expression profiling reveals off-target gene regulation by RNAi.', *Nature biotechnology*, 21(6), pp. 635–7. doi: 10.1038/nbt831.

Jamalzadeh, L. *et al.* (2016) 'Cytotoxic Effects of Some Common Organic Solvents on MCF-7, RAW-264.7 and Human Umbilical Vein Endothelial Cells', *Avicenna Journal of Medical Biochemistry*. Hamadan University of Medical Sciences., In press(In press), pp. 10–33453. doi: 10.17795/ajmb-33453.

Johannessen, C. M. *et al.* (2010) 'COT drives resistance to RAF inhibition through MAP kinase pathway reactivation', *Nature*, 468(7326), pp. 968–972. doi: 10.1038/nature09627.

Johannessen, C. M. *et al.* (2013) 'A melanocyte lineage program confers resistance to MAP kinase pathway inhibition', *Nature*, 504(7478), pp. 138–142. doi: 10.1038/nature12688.

Johnson, D. B. *et al.* (2015) 'Acquired BRAF inhibitor resistance: A multicenter meta-analysis of the spectrum and frequencies, clinical behaviour, and phenotypic associations of resistance mechanisms', *European Journal of Cancer*. Elsevier Ltd, 51(18), pp. 2792–2799. doi: 10.1016/j.ejca.2015.08.022.

Julian, L. and Olson, M. F. (2014) 'Rho-associated coiled-coil containing kinases (ROCK): Structure, regulation, and functions', *Small GTPases*. Taylor & Francis, 5. doi: 10.4161/SGTP.29846.

Kaelin, W. G. (2006) 'Cell biology: Divining cancer cell weaknesses', *Nature*. Nature Publishing Group, pp. 32–34. doi: 10.1038/441032a.

Karlsson, M., Mathers, J., Dickinson, R. J., Mandl, M. and Keyse, S. M. (2004) 'Both nuclear-cytoplasmic shuttling of the dual specificity phosphatase MKP-3 and its ability to anchor MAP kinase in the cytoplasm are mediated by a conserved nuclear export signal.', *The Journal of biological chemistry*. American Society for Biochemistry and Molecular Biology, 279(40), pp. 41882–91. doi: 10.1074/jbc.M406720200.

Katayama, R. *et al.* (2011) 'Therapeutic strategies to overcome crizotinib resistance in non-small cell lung cancers harboring the fusion oncogene EML4-ALK', *Proceedings of the National Academy of Sciences*. National Academy of Sciences, 108(18), pp. 7535–7540. doi: 10.1073/PNAS.1019559108.

Keisell, D. P., Black, D. M., Bishop, D. T. and Spurr, N. K. (1993) 'Genetic analysis of the BRCA1 region in a large breast/ovarian family: Refinement of the minimal region containing BRCA1', *Human Molecular Genetics*, 2(11), pp. 1823–1828. doi: 10.1093/hmg/2.11.1823.

Kern, S. E. and Winter, J. M. (2006) 'Elegance, silence and nonsense in the mutations literature for solid tumors', *Cancer Biology and Therapy*. Landes Bioscience, pp. 349–359. doi: 10.4161/cbt.5.4.2551.

Keyse, S. M. (2000) 'Protein phosphatases and the regulation of mitogen-activated protein kinase signalling.', *Current opinion in cell biology*, 12(2), pp. 186–92. doi: 10.1016/s0955-0674(99)00075-7.

Kidger, A. M. and Cook, S. J. (2018) 'De-RSKing ERK – regulation of ERK1/2-RSK dissociation by phosphorylation within a disordered motif', *The FEBS Journal*. John Wiley & Sons, Ltd (10.1111), 285(1), pp. 42–45. doi: 10.1111/febs.14344.

Kidger, A. M. and Keyse, S. M. (2016) 'The regulation of oncogenic Ras/ERK signalling by dual-specificity mitogen activated protein kinase phosphatases (MKPs).', *Seminars in cell & developmental biology*. Elsevier, 50, pp. 125–32. doi: 10.1016/j.semcdb.2016.01.009.

Kidger, A. M., Sipthorp, J. and Cook, S. J. (2018) 'ERK1/2 inhibitors: New weapons to inhibit the RAS-regulated RAF-MEK1/2-ERK1/2 pathway', *Pharmacology & Therapeutics*, 187, pp. 45–60. doi: 10.1016/j.pharmthera.2018.02.007.

Kim, S. B. *et al.* (2017) 'Ipatasertib plus paclitaxel versus placebo plus paclitaxel as first-line therapy for metastatic triple-negative breast cancer (LOTUS): a multicentre, randomised, double-blind, placebo-controlled, phase 2 trial', *The Lancet Oncology*. Lancet Publishing Group, 18(10), pp. 1360–1372. doi: 10.1016/S1470-2045(17)30450-3.

Kirouac, D. C. *et al.* (2016) 'HER2+ Cancer Cell Dependence on PI3K vs. MAPK Signaling Axes Is Determined by Expression of EGFR, ERBB3 and CDKN1B', *PLoS Computational Biology*. Public Library of Science, 12(4). doi: 10.1371/journal.pcbi.1004827.

Kitano, H. (2007) 'A robustness-based approach to systems-oriented drug design', *Nature Reviews Drug Discovery*, 6(3), pp. 202–210. doi: 10.1038/nrd2195.

Klemke, R. L. *et al.* (1997) 'Regulation of cell motility by mitogen-activated protein kinase', *Journal of Cell Biology*, 137(2), pp. 481–492. doi: 10.1083/jcb.137.2.481.

Klug, L. R., Kent, J. D. and Heinrich, M. C. (2018) 'Structural and clinical consequences of activation loop mutations in class III receptor tyrosine kinases', *Pharmacology and Therapeutics*. Elsevier Inc., pp. 123–134. doi: 10.1016/j.pharmthera.2018.06.016.

Konieczkowski, D. J., Johannessen, C. M. and Garraway, L. A. (2018) 'A Convergence-Based Framework for Cancer Drug Resistance', *Cancer Cell*. Cell Press, 33(5), pp. 801–815. doi: 10.1016/J.CCELL.2018.03.025.

Kopetz, S. *et al.* (2015) 'Phase II pilot study of vemurafenib in patients with metastatic BRAF-mutated colorectal cancer', *Journal of Clinical Oncology*. American Society of Clinical Oncology, 33(34), pp. 4032–4038. doi: 10.1200/JCO.2015.63.2497.

Korotchenko, V. N. *et al.* (2014) 'In vivo structure-activity relationship studies support allosteric targeting of a dual specificity phosphatase.', *Chembiochem : a European journal of chemical biology*. NIH Public Access, 15(10), pp. 1436–45. doi: 10.1002/cbic.201402000.

Krakhmal, N. V., Zavyalova, M. V., Denisov, E. V., Vtorushin, S. V. and Perelmuter, V. M. (2015) 'Cancer invasion: Patterns and mechanisms', *Acta Naturae*. Acta Naturae, pp. 17–28. doi: 10.32607/20758251-2015-7-2-17-28.

Kucharska, A., Rushworth, L. K., Staples, C., Morrice, N. A. and Keyse, S. M. (2009) 'Regulation of the inducible nuclear dual-specificity phosphatase DUSP5 by ERK MAPK', *Cellular Signalling*, 21(12), pp. 1794–1805. doi: 10.1016/j.cellsig.2009.07.015.

Kumar, M. S. *et al.* (2012) 'The GATA2 Transcriptional Network Is Requisite for RAS Oncogene-Driven Non-Small Cell Lung Cancer', *Cell*. Cell Press, 149(3), pp. 642–655. doi: 10.1016/J.CELL.2012.02.059.

Kümper, S. *et al.* (2016) 'Rho-associated kinase (ROCK) function is essential for cell cycle progression, senescence and tumorigenesis.', *eLife*. eLife Sciences Publications, Ltd, 5, p. e12994. doi: 10.7554/eLife.12203.

Kutner, R. H., Zhang, X.-Y. and Reiser, J. (2009) 'Production, concentration and titration of pseudotyped HIV-1-based lentiviral vectors', *Nature Protocols*. Nature Publishing Group, 4(4), pp. 495–505. doi: 10.1038/nprot.2009.22.

Kwon, M. J. and Shin, Y. K. (2011) 'Epigenetic regulation of cancer-associated genes in ovarian cancer', *International Journal of Molecular Sciences*. MDPI AG, pp. 983–1008. doi: 10.3390/ijms12020983.

Laemmli, U. K. (1970) 'Cleavage of structural proteins during the assembly of the head of bacteriophage T4', *Nature*, 227(5259), pp. 680–685. doi: 10.1038/227680a0.

Lake, D., Corrêa, S. A. L. and Müller, J. (2016) 'Negative feedback regulation of the ERK1/2 MAPK pathway.', *Cellular and molecular life sciences : CMLS*. Springer, 73(23), pp. 4397–4413. doi: 10.1007/s00018-016-2297-8.

Laplante, M. and Sabatini, D. M. (2012) 'MTOR signaling in growth control and disease', *Cell*, pp. 274–293. doi: 10.1016/j.cell.2012.03.017.

Larsson, E., Sander, C. and Marks, D. (2010) 'mRNA turnover rate limits siRNA and microRNA efficacy.', *Molecular systems biology*. European Molecular Biology Organization, 6, p. 433. doi: 10.1038/msb.2010.89.

Lawrence, M. S. *et al.* (2014) 'Discovery and saturation analysis of cancer genes across 21 tumour types', *Nature*, 505(7484), pp. 495–501. doi: 10.1038/nature12912.

Lee, H. H. *et al.* (2010) 'Src-dependent phosphorylation of ROCK participates in regulation of focal adhesion dynamics', *Journal of Cell Science*, 123(19), pp. 3368–3377. doi: 10.1242/jcs.071555.

Lehmann, B. D. *et al.* (2019) 'Identification of Targetable Recurrent MAP3K8 Rearrangements in Melanomas Lacking Known Driver Mutations', *Molecular cancer research : MCR*. NLM (Medline), 17(9), pp. 1842–1853. doi: 10.1158/1541-7786.MCR-19-0257.

Li, C., Scott, D. A., Hatch, E., Tian, X. and Mansour, S. L. (2007) 'Dusp6 (Mkp3) is a negative feedback regulator of FgF-stimulated ERK signaling during mouse development', *Development*, 134(1), pp. 167–176. doi: 10.1242/dev.02701.

Liegl, B. *et al.* (2008) 'Heterogeneity of kinase inhibitor resistance mechanisms in GIST', *The Journal of Pathology*. NIH Public Access, 216(1), pp. 64–74. doi: 10.1002/path.2382.

Liu, P. *et al.* (2015) 'Ptdins(3,4,5) P3 -dependent activation of the mTORC2 kinase complex', *Cancer Discovery*. American Association for Cancer Research, 5(11), pp. 1194–11209. doi: 10.1158/2159-8290.CD-15-0460.

Liu, P., Cheng, H., Roberts, Thomas M and Zhao, J. J. (2009) 'Targeting the phosphoinositide 3-kinase pathway in cancer.', *Nature reviews. Drug discovery*. NIH Public Access, 8(8), pp. 627–44. doi: 10.1038/nrd2926.

Liu, P., Cheng, H., Roberts, Thomas M. and Zhao, J. J. (2009) 'Targeting the phosphoinositide 3-kinase pathway in cancer', *Nature Reviews Drug Discovery*, pp. 627–644. doi: 10.1038/nrd2926.

Liu, S., Knapp, S. and Ahmed, A. A. (2014) 'The structural basis of PI3K cancer mutations: From mechanism to therapy', *Cancer Research*, pp. 641–646. doi: 10.1158/0008-5472.CAN-13-2319.

Liu, T. *et al.* (2018) 'The suppression of DUSP5 expression correlates with paclitaxel resistance and poor prognosis in basal-like breast cancer', *International Journal of Medical Sciences*. Ivyspring International Publisher, 15(7), pp. 738–747. doi: 10.7150/ijms.24981.

Lochner, A. and Moolman, J. A. (2006) 'The many faces of H89: A review', *Cardiovascular Drug Reviews*, pp. 261–274. doi: 10.1111/j.1527-3466.2006.00261.x.

Lord, C. J. and Ashworth, A. (2017) 'PARP inhibitors: Synthetic lethality in the clinic', *Science*. American Association for the Advancement of Science, pp. 1152–1158. doi: 10.1126/science.aam7344.

Lotz-Jenne, C. *et al.* (2016) 'A high-content EMT screen identifies multiple receptor tyrosine kinase inhibitors with activity on TGFβ receptor.', *Oncotarget*. Impact Journals, LLC, 7(18), pp. 25983–6002. doi: 10.18632/oncotarget.8418.

Lugo, T. G., Pendergast, A. M., Muller, A. J. and Witte, O. N. (1990) 'Tyrosine kinase activity and transformation potency of bcr-abl oncogene products', *Science*, 247(4946), pp. 1079–1082. doi: 10.1126/science.2408149.

Maillet, M. *et al.* (2008) 'DUSP6 (MKP3) null mice show enhanced ERK1/2 phosphorylation at baseline and increased myocyte proliferation in the heart affecting disease susceptibility', *Journal of Biological Chemistry*, 283(45), pp. 31246–31255. doi: 10.1074/jbc.M806085200.

Manning, B. D. and Cantley, L. C. (2007) 'AKT/PKB Signaling: Navigating Downstream', *Cell*, pp. 1261–1274. doi: 10.1016/j.cell.2007.06.009.

Manning, B. D. and Toker, A. (2017) 'Leading Edge Review AKT/PKB Signaling: Navigating the Network'. doi: 10.1016/j.cell.2017.04.001.

Manning, G., Whyte, D. B., Martinez, R., Hunter, T. and Sudarsanam, S. (2002) 'The protein kinase complement of the human genome', *Science*, pp. 1912–1934. doi: 10.1126/science.1075762.

Marchetti, S. *et al.* (2005) 'Extracellular signal-regulated kinases phosphorylate mitogen-activated protein kinase phosphatase 3/DUSP6 at serines 159 and 197, two sites critical for its proteasomal degradation.', *Molecular and cellular biology*. American Society for Microbiology (ASM), 25(2), pp. 854–64. doi: 10.1128/MCB.25.2.854-864.2005.

Marone, R., Cmiljanovic, V., Giese, B. and Wymann, M. P. (2008) 'Targeting phosphoinositide 3-kinase-Moving towards therapy', *Biochimica et Biophysica Acta - Proteins and Proteomics*, pp. 159–185. doi: 10.1016/j.bbapap.2007.10.003.

Martini, M., Ciraolo, E., Gulluni, F. and Hirsch, E. (2013) 'Targeting PI3K in cancer: Any good news?', *Frontiers in Oncology*. doi: 10.3389/fonc.2013.00108.

Mason, J. M., Morrison, D. J., Basson, M. A. and Licht, J. D. (2006) 'Sprouty proteins: Multifaceted negative-feedback regulators of receptor tyrosine kinase signaling', *Trends in Cell Biology*, pp. 45–54. doi: 10.1016/j.tcb.2005.11.004.

Matsumura, F. (2005) 'Regulation of myosin II during cytokinesis in higher eukaryotes', *Trends in Cell Biology*, pp. 371–377. doi: 10.1016/j.tcb.2005.05.004.

Matsumura, F. and Hartshorne, D. J. (2008) 'Myosin phosphatase target subunit: Many roles in cell function', *Biochemical and Biophysical Research Communications*, 369(1), pp. 149–156. doi: 10.1016/j.bbrc.2007.12.090.

Mendoza, M. C., Er, E. E. and Blenis, J. (2011) 'The Ras-ERK and PI3K-mTOR pathways: cross-talk and compensation.', *Trends in biochemical sciences*. NIH Public Access, 36(6), pp. 320–8. doi: 10.1016/j.tibs.2011.03.006.

Meng, L. H. and Zheng, X. S. (2015) 'Toward rapamycin analog (rapalog)-based precision cancer therapy', *Acta Pharmacologica Sinica*. Nature Publishing Group, pp. 1163–1169. doi: 10.1038/aps.2015.68.

Menon, S. and Manning, B. D. (2008) 'Common corruption of the mTOR signaling network in human tumors', *Oncogene*, pp. S43–S51. doi: 10.1038/onc.2009.352.

Menyhart, O. *et al.* (2017) 'DUSP4 is associated with increased resistance against anti-HER2 therapy in breast cancer.', *Oncotarget*, 8(44), pp. 77207–77218. doi: 10.18632/oncotarget.20430.

Milojkovic, D. and Apperley, J. (2009) 'Mechanisms of Resistance to Imatinib and Second-Generation Tyrosine Inhibitors in Chronic Myeloid Leukemia.', *Clinical cancer research : an official journal of the American Association for Cancer Research*. American Association for Cancer Research, 15(24), pp. 7519–7527. doi: 10.1158/1078-0432.CCR-09-1068.

Molina, G. *et al.* (2009) 'Zebrafish chemical screening reveals an inhibitor of Dusp6 that expands cardiac cell lineages.', *Nature chemical biology*. NIH Public Access, 5(9), pp. 680–7. doi: 10.1038/nchembio.190.

Molinari, F. and Frattini, M. (2014) 'Functions and Regulation of the PTEN Gene in Colorectal Cancer', *Frontiers in Oncology*, 3. doi: 10.3389/fonc.2013.00326.

Moore, M. J., Kanter, J. R., Jones, K. C. and Taylor, S. S. (2002) 'Phosphorylation of the catalytic subunit of protein kinase A: Autophosphorylation versus phosphorylation by phosphoinositide-dependent kinase-1', *Journal of Biological Chemistry*, 277(49), pp. 47878–47884. doi: 10.1074/jbc.M204970200.

Mora, A., Komander, D., Van Aalten, D. M. F. and Alessi, D. R. (2004) 'PDK1, the master regulator of AGC kinase signal transduction', *Seminars in Cell and Developmental Biology*. Elsevier Ltd, 15(2), pp. 161–170. doi: 10.1016/j.semcdb.2003.12.022.

Morris, E. J. *et al.* (2013) 'Discovery of a Novel ERK Inhibitor with Activity in Models of Acquired Resistance to BRAF and MEK Inhibitors', *Cancer Discovery*. American Association for Cancer Research, 3(7), pp. 742–750. doi: 10.1158/2159-8290.CD-13-0070.

Morrison, D. K. (2012) 'MAP kinase pathways', *Cold Spring Harbour Persepectives in Biology*, 4(11), pp. 1–5. doi: 10.1101/cshperspect.a011254.

Motzer, R. J. *et al.* (2010) 'Phase 3 trial of everolimus for metastatic renal cell carcinoma: Final results and analysis of prognostic factors', *Cancer*. John Wiley and Sons Inc., 116(18), pp. 4256–4265. doi: 10.1002/cncr.25219.

Murray, A. J. P. P. inhibition: A. may not be what it seems (2008) 'Pharmacological PKA inhibition: All may not be what it seems', *Science Signaling*. doi: 10.1126/scisignal.122re4.

Murray, J. T. *et al.* (2004) 'Exploitation of KESTREL to identify NDRG family members as physiological substrates for SGK1 and GSK3.', *The Biochemical journal*. Portland Press Ltd, 384(Pt 3), pp. 477–88. doi: 10.1042/BJ20041057.

Murugan, A. K., Liu, R. and Xing, M. (2019) 'Identification and characterization of two novel oncogenic mTOR mutations', *Oncogene*. Nature Publishing Group, 38(26), pp. 5211–5226. doi: 10.1038/s41388-019-0787-5.

Nakanishi, Y., Mizuno, H., *et al.* (2015) 'ERK Signal Suppression and Sensitivity to CH5183284/Debio 1347, a Selective FGFR Inhibitor.', *Molecular cancer therapeutics*. American Association for Cancer Research, 14(12), pp. 2831–9. doi: 10.1158/1535-7163.MCT-15-0497.

Nakanishi, Y., Akiyama, N., *et al.* (2015) 'Mechanism of oncogenic signal activation by the novel fusion kinase FGFR3-BAIAP2L1', *Molecular Cancer Therapeutics*. American Association for Cancer Research Inc., 14(3), pp. 704–712. doi: 10.1158/1535-7163.MCT-14-0927-T.

Navin, N. *et al.* (2011) 'Tumour evolution inferred by single-cell sequencing.', *Nature*. NIH Public Access, 472(7341), pp. 90–4. doi: 10.1038/nature09807.

Nazarian, R. *et al.* (2010) 'Melanomas acquire resistance to B-RAF(V600E) inhibition by RTK or N-RAS upregulation.', *Nature*. NIH Public Access, 468(7326), pp. 973–7. doi: 10.1038/nature09626.

Negrini, S., Gorgoulis, V. G. and Halazonetis, T. D. (2010) 'Genomic instability an evolving hallmark of cancer', *Nature Reviews Molecular Cell Biology*, pp. 220–228. doi: 10.1038/nrm2858.

Nelson, M. L. *et al.* (2010) 'Ras signaling requires dynamic properties of Ets1 for phosphorylation-enhanced binding to coactivator CBP', *Proceedings of the National Academy of Sciences of the United States of America*, 107(22), pp. 10026–10031. doi: 10.1073/pnas.0915137107.

O'Reilly, K. E. *et al.* (2006) 'mTOR inhibition induces upstream receptor tyrosine kinase signaling and activates Akt', *Cancer Research*, 66(3), pp. 1500–1508. doi: 10.1158/0008-5472.CAN-05-2925.

O'Reilly, L. A. *et al.* (2009) 'MEK/ERK-Mediated Phosphorylation of Bim Is Required to Ensure Survival of T and B Lymphocytes during Mitogenic Stimulation', *The Journal of Immunology*. The American Association of Immunologists, 183(1), pp. 261–269. doi: 10.4049/jimmunol.0803853.

Ohashi, K. *et al.* (2000) 'Rho-associated kinase ROCK activates LIM-kinase 1 by phosphorylation at threonine 508 within the activation loop', *Journal of Biological Chemistry*, 275(5), pp. 3577–3582. doi: 10.1074/jbc.275.5.3577.

Okudela, K. *et al.* (2009) 'Down-regulation of DUSP6 expression in lung cancer: its mechanism and potential role in carcinogenesis.', *The American journal of pathology*. American Society for Investigative Pathology, 175(2), pp. 867–81. doi: 10.2353/ajpath.2009.080489.

Okuzumi, T. *et al.* (2009) 'Inhibitor hijacking of Akt activation.', *Nature chemical biology*. NIH Public Access, 5(7), pp. 484–93. doi: 10.1038/nchembio.183.

Pagliarini, R., Shao, W. and Sellers, W. R. (2015) 'Oncogene addiction: pathways of therapeutic response, resistance, and road maps toward a cure', *EMBO reports*. EMBO, 16(3), pp. 280–296. doi: 10.15252/embr.201439949.

Pandya, P., Orgaz, J. L. and Sanz-Moreno, V. (2017) 'Modes of invasion during tumour dissemination', *Molecular oncology*, pp. 5–27. doi: 10.1002/1878-0261.12019.

Papadatos-Pastos, D. *et al.* (2015) 'A first-in-human study of the dual ROCK I/II inhibitor, AT13148, in patients with advanced cancers.', *Journal of Clinical Oncology*. American Society of Clinical Oncology , 33(15_suppl), pp. 2566–2566. doi: 10.1200/jco.2015.33.15_suppl.2566.

Pavlovsky, C., Chan, O., Talati, C. and Pinilla-Ibarz, J. (2019) 'Ponatinib in the treatment of chronic myeloid leukemia and philadelphia chromosome positive acute lymphoblastic leukemia', *Future Oncology*. Future Medicine Ltd., 15(3), pp. 257–269. doi: 10.2217/fon-2018-0371.

Pearce, Laura R., Komander, D. and Alessi, D. R. (2010a) 'The nuts and bolts of AGC protein kinases', *Nature Reviews Molecular Cell Biology*. Nature Publishing Group, pp. 9–22. doi: 10.1038/nrm2822.

Pearce, Laura R. *et al.* (2010b) 'Characterization of PF-4708671, a novel and highly specific inhibitor of p70 ribosomal S6 kinase (S6K1)', *Biochemical Journal*, 431(2), pp. 245–255. doi: 10.1042/BJ20101024.

Pedrero, J. M. *et al.* (2005) 'Frequent genetic and biochemical alterations of the PI 3-K/AKT/PTEN pathway in head and neck squamous cell carcinoma', *International Journal of Cancer*, 114(2), pp. 242–248.

Perri, F., Pisconti, S. and Vittoria Scarpati, G. Della (2016) 'P53 mutations and cancer: A tight linkage', *Annals of Translational Medicine*. AME Publishing Company, 4(24). doi: 10.21037/atm.2016.12.40.

Peterson, J. E. *et al.* (1996) 'Src phosphorylates the insulin-like growth factor type I receptor on the autophosphorylation sites. Requirement for transformation by src.', *The Journal of biological chemistry*. American Society for Biochemistry and Molecular Biology, 271(49), pp. 31562–71. doi: 10.1074/jbc.271.49.31562.

Phuchareon, J., McCormick, F., Eisele, D. W. and Tetsu, O. (2015) 'EGFR inhibition evokes innate drug resistance in lung cancer cells by preventing Akt activity and thus inactivating Ets-1 function.', *Proceedings of the National Academy of Sciences of the United States of America*. National Academy of Sciences, 112(29), pp. E3855-63. doi: 10.1073/pnas.1510733112.

Pinner, S. and Sahai, E. (2008) 'PDK1 regulates cancer cell motility by antagonising inhibition of ROCK1 by RhoE', *Nature Cell Biology*, 10(2), pp. 127–137. doi: 10.1038/ncb1675.

Piotrowska, Z. *et al.* (2015) 'Heterogeneity underlies the emergence of EGFRT790wild-type clones following treatment of T790M-positive cancers with a third-generation EGFR inhibitor', *Cancer Discovery*. American Association for Cancer Research Inc., 5(7), pp. 713–723. doi: 10.1158/2159-8290.CD-15-0399.

Piya, S. *et al.* (2012) 'DUSP6 is a novel transcriptional target of p53 and regulates p53-mediated apoptosis by modulating expression levels of Bcl-2 family proteins', *FEBS Letters*. Wiley-Blackwell, 586(23), pp. 4233–4240. doi: 10.1016/j.febslet.2012.10.031.

Pon, J. R. and Marra, M. A. (2015) 'Driver and Passenger Mutations in Cancer', *Annual Review of Pathology: Mechanisms of Disease*. Annual Reviews, 10(1), pp. 25–50. doi: 10.1146/annurev-pathol-012414-040312.

Prabhakar, C. N. (2015) 'Epidermal growth factor receptor in non-small cell lung cancer', *Translational Lung Cancer Research*. AME Publishing Company, pp. 110–118. doi: 10.3978/j.issn.2218-6751.2015.01.01.

Prêtre, V. and Wicki, A. (2018) 'Inhibition of Akt and other AGC kinases: A target for clinical cancer therapy?', *Seminars in Cancer Biology*. Academic Press, pp. 70–77. doi: 10.1016/j.semcancer.2017.04.011.

Prior, I. A., Lewis, P. D. and Mattos, C. (2012) 'A comprehensive survey of ras mutations in cancer', *Cancer Research*, pp. 2457–2467. doi: 10.1158/0008-5472.CAN-11-2612.

Prunier, C., Prudent, R., Kapur, R., Sadoul, K. and Lafanechère, L. (2017) 'LIM kinases: Cofilin and beyond', *Oncotarget*. Impact Journals LLC, pp. 41749–41763. doi: 10.18632/oncotarget.16978.

Pursiheimo, J.-P., Kieksi, A., Jalkanen, M. and Salmivirta, M. (2002) 'Protein kinase A balances the growth factor-induced Ras/ERK signaling', *FEBS Letters*, 521(1–3), pp. 157–164. doi: 10.1016/S0014-5793(02)02864-8.

Qi, X. J., Wildey, G. M. and Howe, P. H. (2006) 'Evidence that Ser87 of BimEL is phosphorylated by Akt and regulates BimEL apoptotic function', *Journal of Biological Chemistry*, 281(2), pp. 813–823. doi: 10.1074/jbc.M505546200.

Rath, N. *et al.* (2018) 'Rho Kinase Inhibition by AT13148 Blocks Pancreatic Ductal Adenocarcinoma Invasion and Tumor Growth.', *Cancer research*. American Association for Cancer Research, 78(12), pp. 3321–3336. doi: 10.1158/0008-5472.CAN-17-1339.

Rath, N. and Olson, M. F. (2012) 'Rho-associated kinases in tumorigenesis: re-considering ROCK inhibition for cancer therapy', *EMBO reports*. John Wiley & Sons, Ltd, 13(10), pp. 900–908. doi: 10.1038/embor.2012.127.

Revathidevi, S. and Munirajan, A. K. (2019) 'Akt in cancer: Mediator and more', *Seminars in Cancer Biology*. Academic Press. doi: 10.1016/j.semcancer.2019.06.002.

Reynolds, A. R. (2010) 'Potential Relevance of Bell-Shaped and U-Shaped Dose-Responses for the Therapeutic Targeting of Angiogenesis in Cancer', *Dose-Response*. SAGE PublicationsSage CA: Los Angeles, CA, 8(3), p. dose-response.0. doi: 10.2203/dose-response.09-049.Reynolds.

Riento, K., Guasch, R. M., Garg, R., Jin, B. and Ridley, A. J. (2003) 'RhoE Binds to ROCK I and Inhibits Downstream Signaling', *Molecular and Cellular Biology*. American Society for Microbiology, 23(12), pp. 4219–4229. doi: 10.1128/mcb.23.12.4219-4229.2003.

Riento, K. and Ridley, A. J. (2003) 'Rocks: Multifunctional kinases in cell behaviour', *Nature Reviews Molecular Cell Biology*, pp. 446–456. doi: 10.1038/nrm1128.

Ritt, D. A., Monson, D. M., Specht, S. I. and Morrison, D. K. (2010) 'Impact of feedback phosphorylation and Raf heterodimerization on normal and mutant B-Raf signaling.', *Molecular and cellular biology*. American Society for Microbiology Journals, 30(3), pp. 806–19. doi: 10.1128/MCB.00569-09.

Rivlin, N., Brosh, R., Oren, M. and Rotter, V. (2011) 'Mutations in the p53 tumor suppressor gene: Important milestones at the various steps of tumorigenesis', *Genes and Cancer*, pp. 466–474. doi: 10.1177/1947601911408889.

Rodríguez, J. *et al.* (2010) 'ERK1/2 MAP kinases promote cell cycle entry by rapid, kinase-independent disruption of retinoblastoma-lamin A complexes.', *The Journal of cell biology*. Rockefeller University Press, 191(5), pp. 967–79. doi: 10.1083/jcb.201004067.

Roskoski, R. (2016) 'Classification of small molecule protein kinase inhibitors based upon the structures of their drug-enzyme complexes', *Pharmacological Research*. Academic Press, pp. 26–48. doi: 10.1016/j.phrs.2015.10.021.

Roskoski, R. (2019) 'Properties of FDA-approved small molecule protein kinase inhibitors', *Pharmacological Research*. Academic Press, pp. 19–50. doi: 10.1016/j.phrs.2019.03.006.

Roux, P. P., Richards, S. A. and Blenis, J. (2003) 'Phosphorylation of p90 ribosomal S6 kinase (RSK) regulates extracellular signal-regulated kinase docking and RSK activity.', *Molecular and cellular biology*. American Society for Microbiology Journals, 23(14), pp. 4796–804. doi: 10.1128/mcb.23.14.4796-4804.2003.

Roux, P. P. and Topisirovic, I. (2018) 'Signaling Pathways Involved in the Regulation of mRNA Translation', *Molecular and Cellular Biology*. American Society for Microbiology, 38(12). doi: 10.1128/mcb.00070-18.

Sadok, A. *et al.* (2015) 'Rho Kinase Inhibitors Block Melanoma Cell Migration and Inhibit Metastasis', *Cancer Research*. American Association for Cancer Research, 75(11), pp. 2272–2284. doi: 10.1158/0008-5472.CAN-14-2156.

Saito, M. *et al.* (2000) 'Allelic imbalance and mutations of thePTEN gene in ovarian cancer', *International Journal of Cancer*. John Wiley & Sons, Ltd, 85(2), pp. 160–165. doi: 10.1002/(SICI)1097-0215(20000115)85:2<160::AID-IJC2>3.0.CO;2-5.

Sakamoto, K. M. and Frank, D. A. (2009) 'CREB in the pathophysiology of cancer: Implications for targeting transcription factors for cancer therapy', *Clinical Cancer Research*, pp. 2583–2587. doi: 10.1158/1078-0432.CCR-08-1137.

Salk, J. J., Fox, E. J. and Loeb, L. A. (2010) 'Mutational Heterogeneity in Human Cancers: Origin and Consequences', *Annual Review of Pathology: Mechanisms of Disease*. Annual Reviews, 5(1), pp. 51–75. doi: 10.1146/annurev-pathol-121808-102113.

Sancak, Y. *et al.* (2007) 'PRAS40 Is an Insulin-Regulated Inhibitor of the mTORC1 Protein Kinase', *Molecular Cell*, 25(6), pp. 903–915. doi: 10.1016/j.molcel.2007.03.003.

Sanchez-Vega, F. *et al.* (2018) 'Oncogenic Signaling Pathways in The Cancer Genome Atlas Article Oncogenic Signaling Pathways in The Cancer Genome Atlas', *Cell*, 173, pp. 321–337. doi: 10.1016/j.cell.2018.03.035.

Sapio, L. *et al.* (2014) 'Targeting protein kinase a in cancer therapy: An update', *EXCLI Journal*. Leibniz Research Centre for Working Environment and Human Factors, pp. 843–855. doi: 10.17877/DE290R-6736.

Saraste, A. and Pulkki, K. (2000) 'Morphologic and biochemical hallmarks of apoptosis', *Cardiovascular Research*. Narnia, 45(3), pp. 528–537. doi: 10.1016/S0008-6363(99)00384-3.

Schenone, S., Brullo, C., Musumeci, F., Radi, M. and Botta, M. (2011) 'ATP-Competitive Inhibitors of mTOR: An Update', *Current Medicinal Chemistry*. Bentham Science Publishers Ltd., 18(20), pp. 2995–3014. doi: 10.2174/092986711796391651.

Schmid, P. *et al.* (2018) 'AZD5363 plus paclitaxel versus placebo plus paclitaxel as first-line therapy for metastatic triple-negative breast cancer (PAKT): A randomised, double-blind, placebo-controlled, phase II trial.', *Journal of Clinical Oncology*. American Society of Clinical Oncology (ASCO), 36(15_suppl), pp. 1007–1007. doi: 10.1200/jco.2018.36.15_suppl.1007.

Sebbagh, M. *et al.* (2001) 'Caspase-3-mediated cleavage of ROCK I induces MLC phosphorylation and apoptotic membrane blebbing', *Nature Cell Biology*. Macmillan Magazines Ltd, 3(4), pp. 346–352. doi: 10.1038/35070019.

Sebbagh, M., Hamelin, J., Bertoglio, J., Solary, E. and Bréard, J. (2005) 'Direct cleavage of ROCK II by granzyme B induces target cell membrane blebbing in a caspase-independent manner', *Journal of Experimental Medicine*. Rockefeller University Press, 201(3), pp. 465–471. doi: 10.1084/jem.20031877.

Sequist, L. V. *et al.* (2011) 'Genotypic and histological evolution of lung cancers acquiring resistance to EGFR inhibitors', *Science Translational Medicine*, 3(75). doi: 10.1126/scitranslmed.3002003.

Serra, V. *et al.* (2011) 'PI3K inhibition results in enhanced HER signaling and acquired ERK dependency in HER2-overexpressing breast cancer', *Oncogene*, 30(22), pp. 2547–2557. doi: 10.1038/onc.2010.626.

Seyfried, T. N. (2015) 'Cancer as a mitochondrial metabolic disease', *Frontiers in Cell and Developmental Biology*. Frontiers Media S.A., 3(JUL). doi: 10.3389/fcell.2015.00043.

Sherk, A. B. *et al.* (2008) 'Development of a small-molecule serum- and glucocorticoid-regulated kinase-1 antagonist and its evaluation as a prostate cancer therapeutic', *Cancer Research*, 68(18), pp. 7475–7483. doi: 10.1158/0008-5472.CAN-08-1047.

Shojaee, S. *et al.* (2015) 'Erk Negative Feedback Control Enables Pre-B Cell Transformation and Represents a Therapeutic Target in Acute Lymphoblastic Leukemia', *Cancer Cell*. Cell Press, 28(1), pp. 114–128. doi: 10.1016/J.CCELL.2015.05.008.

Siegel, R. L., Miller, K. D. and Jemal, A. (2019) 'Cancer statistics, 2019', *CA: A Cancer Journal for Clinicians*, 69(1), pp. 7–34. doi: 10.3322/caac.21551.

Skehan, P. *et al.* (1990) 'New colorimetric cytotoxicity assay for anticancer-drug screening', *Journal of the National Cancer Institute*, 82(13), pp. 1107–1112. doi: 10.1093/jnci/82.13.1107.

Smit, M. A. *et al.* (2014) 'ROCK1 is a potential combinatorial drug target for BRAF mutant melanoma.', *Molecular systems biology*. European Molecular Biology Organization, 10(12), p. 772. doi: 10.15252/MSB.20145450.

Smith, P. K. *et al.* (1985) 'Measurement of protein using bicinchoninic acid', *Analytical Biochemistry*, 150(1), pp. 76–85. doi: 10.1016/0003-2697(85)90442-7.

Sommer, E. M. *et al.* (2013) 'Elevated SGK1 predicts resistance of breast cancer cells to Akt inhibitors.', *The Biochemical journal*. Portland Press Ltd, 452(3), pp. 499–508. doi: 10.1042/BJ20130342.

Soverini, S. *et al.* (2014) 'Drug resistance and BCR-ABL kinase domain mutations in Philadelphia chromosome-positive acute lymphoblastic leukemia from the imatinib to the second-generation tyrosine kinase inhibitor era: The main changes are in the type of mutations, but not in the fr', *Cancer*, 120(7), pp. 1002–1009. doi: 10.1002/cncr.28522.

Stella, A. *et al.* (1992) 'Familial adenomatous polyposis: Identification of a new frameshift mutation of the APC gene in an Italian family', *Biochemical and Biophysical Research Communications*, 184(3), pp. 1357–1363. doi: 10.1016/S0006-291X(05)80032-4.

Stokoe, D. *et al.* (1997) 'Dual role of phosphatidylinositol-3,4,5-trisphosphate in the activation of protein kinase B', *Science*, 277(5325), pp. 567–570. doi: 10.1126/science.277.5325.567.

Stoletov, K. *et al.* (2010) 'Visualizing extravasation dynamics of metastatic tumor cells', *Journal of Cell Science*, 123(13), pp. 2332–2341. doi: 10.1242/jcs.069443.

Stottrup, C., Tsang, T. and Chin, Y. R. (2016) 'Upregulation of AKT3 Confers Resistance to the AKT Inhibitor MK2206 in Breast Cancer', *Molecular Cancer Therapeutics*. American Association for Cancer Research, 15(8), pp. 1964–1974. doi: 10.1158/1535-7163.MCT-15-0748.

Street, C. A. and Bryan, B. A. (2011) 'Rho kinase proteins--pleiotropic modulators of cell survival and apoptosis.', *Anticancer research*. International Institute of Anticancer Research, 31(11), pp. 3645–57.

Su, K.-Y. *et al.* (2012) 'Pretreatment epidermal growth factor receptor (EGFR) T790M mutation predicts shorter EGFR tyrosine kinase inhibitor response duration in patients with non-small-cell lung cancer.', *Journal of clinical oncology : official journal of the American Society of Clinical Oncology*. American Society of Clinical Oncology, 30(4), pp. 433–40. doi: 10.1200/JCO.2011.38.3224.

Sutherland, C., Leighton, I. A. and Cohen, P. (1993) 'Inactivation of glycogen synthase kinase-3β by phosphorylation: New kinase connections in insulin and growth-factor signalling', *Biochemical Journal*, 296(1), pp. 15–19. doi: 10.1042/bj2960015.

Swanton, C. (2012) 'Intratumor Heterogeneity: Evolution through Space and Time', *Cancer Research*. American Association for Cancer Research, 72(19), pp. 4875–4882. doi: 10.1158/0008-5472.CAN-12-2217.

Tanimura, S. and Takeda, K. (2017) 'ERK signalling as a regulator of cell motility', *The Journal of Biochemistry*, 162(3), pp. 145–154. doi: 10.1093/jb/mvx048.

Taylor, S. S. and Kornev, A. P. (2011) 'Protein kinases: Evolution of dynamic regulatory proteins', *Trends in Biochemical Sciences*, pp. 65–77. doi: 10.1016/j.tibs.2010.09.006.

Tessier, M. and Woodgett, J. R. (2006) 'Serum and glucocorticoid-regulated protein kinases: Variations on a theme', *Journal of Cellular Biochemistry*, pp. 1391–1407. doi: 10.1002/jcb.20894.

Tetsu, O. and McCormick, F. (2017) 'ETS-targeted therapy: can it substitute for MEK inhibitors?', *Clinical and Translational Medicine*. SpringerOpen, 6(1), p. 16. doi: 10.1186/s40169-017-0147-4.

Thompson, J. M. *et al.* (2017) 'Rho-associated kinase 1 inhibition is synthetically lethal with von Hippel-Lindau deficiency in clear cell renal cell carcinoma', *Oncogene*. Nature Publishing Group, 36(8), pp. 1080–1089. doi: 10.1038/onc.2016.272.

Thumkeo, D., Shimizu, Y., Sakamoto, S., Yamada, S. and Narumiya, S. (2005) 'ROCK-I and ROCK-II cooperatively regulate closure of eyelid and ventral body wall in mouse embryo', *Genes to Cells*, 10(8), pp. 825–834. doi: 10.1111/j.1365-2443.2005.00882.x.

Tomasetti, C. and Vogelstein, B. (2015) 'Variation in cancer risk among tissues can be explained by the number of stem cell divisions', *Science*. American Association for the Advancement of Science, 347(6217), pp. 78–81. doi: 10.1126/science.1260825.

Torii, S., Yamamoto, T., Tsuchiya, Y. and Nishida, E. (2006) 'ERK MAP kinase in G1 cell cycle progression and cancer', *Cancer Science*, 97(8), pp. 697–702. doi: 10.1111/j.1349-7006.2006.00244.x.

Towbin, H., Staehelin, T. and Gordon, J. (1979) 'Electrophoretic transfer of proteins from polyacrylamide gels to nitrocellulose sheets: Procedure and some applications', *Proceedings of the National Academy of Sciences of the United States of America*, 76(9), pp. 4350–4354. doi: 10.1073/pnas.76.9.4350.

Trojaniello, C., Festino, L., Vanella, V. and Ascierto, P. A. (2019) 'Encorafenib in combination with binimetinib for unresectable or metastatic melanoma with BRAF mutations', *Expert Review of Clinical Pharmacology*, 12(3), pp. 259–266. doi: 10.1080/17512433.2019.1570847.

Unni, A. M. *et al.* (2018) 'Hyperactivation of ERK by multiple mechanisms is toxic to RTK-RAS mutation-driven lung adenocarcinoma cells', *eLife*, 7. doi: 10.7554/eLife.33718.

Ursan, I. D. *et al.* (2015) 'Emergence of BCR-ABL Kinase Domain Mutations Associated with Newly Diagnosed Chronic Myeloid Leukemia: A Meta-Analysis of Clinical Trials of Tyrosine Kinase Inhibitors', *Journal of Managed Care & Specialty Pharmacy*, 21(2), pp. 114–122. doi: 10.18553/jmcp.2015.21.2.114.

Vasan, N., Baselga, J. and Hyman, D. M. (2019) 'A view on drug resistance in cancer', *Nature*. Nature Publishing Group, pp. 299–309. doi: 10.1038/s41586-019-1730-1.

Vasudevan, K. M. *et al.* (2009) 'AKT-independent signaling downstream of oncogenic PIK3CA mutations in human cancer.', *Cancer cell*. NIH Public Access, 16(1), pp. 21–32. doi: 10.1016/j.ccr.2009.04.012.

Villanueva, J. *et al.* (2010) 'Acquired resistance to BRAF inhibitors mediated by a RAF kinase switch in melanoma can be overcome by cotargeting MEK and IGF-1R/PI3K.', *Cancer cell*. Elsevier, 18(6), pp. 683–95. doi: 10.1016/j.ccr.2010.11.023.

Vogelstein, B. *et al.* (2013) 'Cancer genome landscapes', *Science*. American Association for the Advancement of Science, pp. 1546–1558. doi: 10.1126/science.1235122.

Wagle, M.-C. *et al.* (2018) 'A transcriptional MAPK Pathway Activity Score (MPAS) is a clinically relevant biomarker in multiple cancer types', *npj Precision Oncology*. Springer Nature, 2(1). doi: 10.1038/s41698-018-0051-4.

Wagle, N. *et al.* (2011) 'Dissecting therapeutic resistance to RAF inhibition in melanoma by tumor genomic profiling', *Journal of Clinical Oncology*, 29(22), pp. 3085–3096. doi: 10.1200/JCO.2010.33.2312.

Wang, H. *et al.* (2019) 'Feedback Activation of SGK3 and AKT Contributes to Rapamycin Resistance by Reactivating mTORC1/4EBP1 Axis via TSC2 in Breast Cancer', *International journal of biological sciences*. NLM (Medline), 15(5), pp. 929–941. doi: 10.7150/ijbs.32489.

Wang, X., Hu, S. and Liu, L. (2017) 'Phosphorylation and acetylation modifications of FOXO3a: Independently or synergistically?', *Oncology letters*. Spandidos Publications, 13(5), pp. 2867–2872. doi: 10.3892/ol.2017.5851.

Wee, S. *et al.* (2008) 'PTEN-deficient cancers depend on PIK3CB', *Proceedings of the National Academy of Sciences of the United States of America*, 105(35), pp. 13057–13062. doi: 10.1073/pnas.0802655105.

Weinstein, I. B. (2000) 'Disorders in cell circuitry during multistage carcinogenesis: the role of homeostasis', *Carcinogenesis*, 21(5), pp. 857–864. doi: 10.1093/carcin/21.5.857.

Weinstein, I. B. (2002) 'Cancer: Addiction to oncogenes - The Achilles heal of cancer', *Science*, pp. 63–64. doi: 10.1126/science.1073096.

Weinstein, I. B. and Joe, A. (2008) 'Oncogene addiction', *Cancer Research*, pp. 3077–3080. doi: 10.1158/0008-5472.CAN-07-3293.

Weinstein, I. B. and Joe, A. K. (2006) 'Mechanisms of Disease: Oncogene addiction - A rationale for molecular targeting in cancer therapy', *Nature Clinical Practice Oncology*, pp. 448–457. doi: 10.1038/ncponc0558.

Welch, D. R. (2016) 'Tumor Heterogeneity--A 'Contemporary Concept Founded on Historical Insights and Predictions', *Cancer Research*. American Association for Cancer Research, 76(1), pp. 4–6. doi: 10.1158/0008-5472.CAN-15-3024.

Wen, Y., Liu, W., Yan, J. and Zhang, M. (2008) 'Structure basis and unconventional lipid membrane binding properties of the PH-C1 tandem of Rho kinases', *Journal of Biological Chemistry*, 283(38), pp. 26263–26273. doi: 10.1074/jbc.M803417200.

Wilkinson, S., Paterson, H. F. and Marshall, C. J. (2005) 'Cdc42–MRCK and Rho–ROCK signalling cooperate in myosin phosphorylation and cell invasion', *Nature Cell Biology*, 7(3), pp. 255–261. doi: 10.1038/ncb1230.

Wilson, F. H. *et al.* (2015) 'A functional landscape of resistance to ALK inhibition in lung cancer.', *Cancer cell*. Elsevier, 27(3), pp. 397–408. doi: 10.1016/j.ccell.2015.02.005.

Wittig-Blaich, S. *et al.* (2017) 'Systematic screening of isogenic cancer cells identifies DUSP6 as context-specific synthetic lethal target in melanoma.', *Oncotarget*. Impact Journals, LLC, 8(14), pp. 23760–23774. doi: 10.18632/oncotarget.15863.

Wu, J. J. *et al.* (2006) 'Mice lacking MAP kinase phosphatase-1 have enhanced MAP kinase activity and resistance to diet-induced obesity', *Cell Metabolism*, 4(1), pp. 61–73. doi: 10.1016/j.cmet.2006.05.010.

Wu, P. K. and Park, J. I. (2015) 'MEK1/2 Inhibitors: Molecular Activity and Resistance Mechanisms', *Seminars in Oncology*. W.B. Saunders, pp. 849–862. doi: 10.1053/j.seminoncol.2015.09.023.

Wu, Y. L. *et al.* (2018) 'Phase Ib/II Study of Capmatinib (INC280) Plus Gefitinib after Failure of Epidermal Growth Factor Receptor (EGFR) Inhibitor Therapy in Patients with EGFR-Mutated, MET Factor-Dysregulated Non-Small-Cell Lung Cancer', *Journal of Clinical Oncology*. American Society of Clinical Oncology, 36(31), pp. 3101–3109. doi: 10.1200/JCO.2018.77.7326.

Wyckoff, J. B., Pinner, S. E., Gschmeissner, S., Condeelis, J. S. and Sahai, E. (2006) 'ROCK- and Myosin-Dependent Matrix Deformation Enables Protease-Independent Tumor-Cell Invasion In Vivo', *Current Biology*, 16(15), pp. 1515–1523. doi: 10.1016/j.cub.2006.05.065.

Xing, Y. *et al.* (2019) 'Phase II trial of AKT inhibitor MK-2206 in patients with advanced breast cancer who have tumors with PIK3CA or AKT mutations, and/or PTEN loss/PTEN mutation', *Breast Cancer Research*, 21(1), p. 78. doi: 10.1186/s13058-019-1154-8.

Xu, S., Furukawa, T., Kanai, N., Sunamura, M. and Horii, A. (2005) 'Abrogation of DUSP6 by hypermethylation in human pancreatic cancer', *Journal of Human Genetics*. Nature Publishing Group, 50(4), pp. 159–167. doi: 10.1007/s10038-005-0235-y.

Yadav, V. *et al.* (2012) 'Reactivation of mitogen-activated protein kinase (MAPK) pathway by FGF receptor 3 (FGFR3)/Ras mediates resistance to vemurafenib in human B-RAF V600E mutant melanoma.', *The Journal of biological chemistry*. American Society for Biochemistry and Molecular Biology, 287(33), pp. 28087–98. doi: 10.1074/jbc.M112.377218.

Yang, B. S. *et al.* (1996) 'Ras-mediated phosphorylation of a conserved threonine residue enhances the transactivation activities of c-Ets1 and c-Ets2.', *Molecular and Cellular Biology*. American Society for Microbiology, 16(2), pp. 538–547. doi: 10.1128/mcb.16.2.538.

Yang, E. *et al.* (1995) 'Bad, a heterodimeric partner for Bcl-x L and Bcl-2, displaces bax and promotes cell death', *Cell*, 80(2), pp. 285–291. doi: 10.1016/0092-8674(95)90411-5.

Yang, J. *et al.* (2002) 'Crystal structure of an activated Akt/Protein Kinase B ternary complex with GSK3-peptide and AMP-PNP', *Nature Structural Biology*, 9(12), pp. 940–944. doi: 10.1038/nsb870.

Yang, J. *et al.* (2019) 'Targeting PI3K in cancer: Mechanisms and advances in clinical trials', *Molecular Cancer*. BioMed Central Ltd. doi: 10.1186/s12943-019-0954-x.

Yap, T. A. *et al.* (2012) 'AT13148 is a novel, oral multi-AGC kinase inhibitor with potent pharmacodynamic and antitumor activity', *Clinical Cancer Research*, 18(14), pp. 3912–3923. doi: 10.1158/1078-0432.CCR-11-3313.

Yeh, T. C. *et al.* (2007) 'Biological Characterization of ARRY-142886 (AZD6244), a Potent, Highly Selective Mitogen-Activated Protein Kinase Kinase 1/2 Inhibitor', *Clinical Cancer Research*. American Association for Cancer Research, 13(5), pp. 1576–1583. doi: 10.1158/1078-0432.CCR-06-1150.

Yi, K. H. and Lauring, J. (2016) 'Recurrent AKT mutations in human cancers: Functional consequences and effects on drug sensitivity', *Oncotarget*. Impact Journals LLC, 7(4), pp. 4241–4251. doi: 10.18632/oncotarget.6648.

Yokoyama, N. *et al.* (2017) 'Activation of ERK1/2 Causes Pazopanib Resistance via Downregulation of DUSP6 in Synovial Sarcoma Cells.', *Scientific reports*. Nature Publishing Group, 7, p. 45332. doi: 10.1038/srep45332.

Yoon, S. and Seger, R. (2006) 'The extracellular signal-regulated kinase: Multiple substrates regulate diverse cellular functions', *Growth Factors*. Taylor & Francis, 24(1), pp. 21–44. doi: 10.1080/02699050500284218.

Yu, H. A. *et al.* (2013) 'Analysis of tumor specimens at the time of acquired resistance to EGFR-TKI therapy in 155 patients with EGFR-mutant lung cancers', *Clinical Cancer Research*, 19(8), pp. 2240–2247. doi: 10.1158/1078-0432.CCR-12-2246.

Yuan, H. X. and Guan, K. L. (2015) 'The SIN1-PH domain connects mTORC2 to PI3K', *Cancer Discovery*. American Association for Cancer Research Inc., 5(11), pp. 1127–1129. doi: 10.1158/2159-8290.CD-15-1125.

Zhang, X., Tang, N., Hadden, T. J. and Rishi, A. K. (2011) 'Akt, FoxO and regulation of apoptosis', *Biochimica et Biophysica Acta - Molecular Cell Research*, pp. 1978–1986. doi: 10.1016/j.bbamcr.2011.03.010.

Zhang, Y. *et al.* (2017) 'A Pan-Cancer Proteogenomic Atlas of PI3K/AKT/ mTOR Pathway Alterations', *Cancer Cell*, 31, pp. 820-832.e3. doi: 10.1016/j.ccell.2017.04.013.

Zhang, Y. L. *et al.* (2016) 'The prevalence of EGFR mutation in patients with non-small cell lung cancer: A systematic review and meta-analysis', *Oncotarget*. Impact Journals LLC, 7(48), pp. 78985–78993. doi: 10.18632/oncotarget.12587.

Zhang, Z. *et al.* (2010) 'Dual specificity phosphatase 6 (DUSP6) is an ETS-regulated negative feedback mediator of oncogenic ERK signaling in lung cancer cells', *Carcinogenesis*. Oxford University Press, 31(4), pp. 577–586. doi: 10.1093/carcin/bgq020.

Zhao, B. *et al.* (2017) 'Mechanisms of resistance to anti-EGFR therapy in colorectal cancer', *Oncotarget*. Impact Journals LLC, 8(3), pp. 3980–4000. doi: 10.18632/oncotarget.14012.

Zheng, X. *et al.* (2008) 'Proteomic Analysis for the Assessment of Different Lots of Fetal Bovine Serum as a Raw Material for Cell Culture. Part IV. Application of Proteomics to the Manufacture of Biological Drugs', *Biotechnology Progress*, 22(5), pp. 1294–1300. doi: 10.1021/bp060121o.

Zimmermann, S. and Moelling, K. (1999) 'Phosphorylation and regulation of Raf by Akt (protein kinase B)', *Science*, 286(5445), pp. 1741–1744. doi: 10.1126/science.286.5445.1741.

Zorea, J. *et al.* (2018) 'IGF1R upregulation confers resistance to isoform-specific inhibitors of PI3K in PIK3CA-driven ovarian cancer.', *Cell death & disease*. Nature Publishing Group, 9(10), p. 944. doi: 10.1038/s41419-018-1025-8.